UNIVERSITY OF BIRMINGHAM

Characterisation of PD1-expressing CMV-specific $CD8^+$ T-cells in healthy donors and cancer patients.

By

Megan Sangita Butler

A thesis submitted to the

University of Birmingham for the degree of

Doctor of Philosophy

School of Infection, Inflammation & Immunology

College of Medicine and Health

University of Birmingham

November 2024

ABSTRACT

Cytomegalovirus (CMV) is a prevalent herpesvirus that establishes lifelong infection and is highly immunogenic. Viral replication is controlled by persistent immune surveillance that includes the establishment of a large virus-specific $CD8^+$ T-cell response that can comprise up to 20% of the total systemic $CD8^+$ T-cell repertoire. As such there is considerable interest in how viral replication is controlled whilst minimising potential inflammatory tissue damage.

An important protein that is expressed on CMV-specific $CD8^+$ T-cells is the immune checkpoint regulator PD1. Due to the remarkable success of antibody-mediated PD1 inhibition in the treatment of cancer this is one of the most important proteins in medical research at the current time. These therapeutic successes have arisen due to the presence of PD1 on tumour-specific T-cells that undergo chronic antigen stimulation from cancer cells but become functionally exhausted within the tumour microenvironment. However, this success is only present in a subset of patients, and it is vital to define determining factors in treatment success.

Despite the expression of PD1 on many CMV-specific $CD8^+$ T-cells, the functional profile of $PD1^+$ $CD8^+$ T-cells and their broader profile of checkpoint co-expression are unknown. Furthermore, the profile of PD1 expression on CMV-specific T-cells within the tumour microenvironment and their response to therapeutic PD1 inhibition are uncertain.

Using MHC-I tetramer technology, I identified CMV-specific $CD8^+$ T-cells in blood samples from healthy donors, within the tumour microenvironment of patients with ovarian cancer, and in blood of patients undergoing PD1 blockade for the treatment of lung cancer. EBV is another prevalent herpesvirus that leads to lifelong infection, and in many of these setting I was able to compare my findings in CMV-specific $CD8^+$ T-cells to EBV-specific $CD8^+$ T-cells.

These studies show that PD1 is expressed on a significant portion of CMV-specific T-cells and is often co-expressed with the checkpoint proteins 2B4 and TIGIT. Unexpectedly, $PD1^+$ CMV-specific $CD8^+$ T-cells showed enhanced cytokine production in response to antigen

presentation revealing little evidence of functional exhaustion. Despite this, cytokine responses increased further in the setting of PD1 inhibition, indicating that the function of the $PD1^+$ cells is somewhat constrained by this inhibitory interaction.

$PD1^+$ CMV-specific T-cells were the dominant viral phenotype in the tissue of ovarian cancer patients. However, in this setting I identified two distinct cellular subsets based on the relative intensity of PD1 expression. In particular, a $PD1_{MID}$ population which corresponded with cells seen in peripheral blood whilst a $PD1_{HIGH}$ subset was only seen within tumour. Importantly, $PD1_{HIGH}$ cells exhibited higher expression of the checkpoint proteins TIM3, LAG3 and the ectoenzyme CD39 in comparison to the $PD1_{MID}$ subset. This work suggests that $PD1_{MID}$ cells within tumour are unlikely to be functionally exhausted, possibly increasing interest in their potential to be 'redirected' against tumour. In contrast, $PD1_{HIGH}$ subsets may have undergone localised functional exhaustion but it is now critical that experiments are undertaken to assess this using cells isolated directly from tissue samples.

In my final studies I was able to assess how CMV-specific T-cells were modulated by in vivo PD1 checkpoint blockade. Overall, rather minimal changes were observed over several months of therapy although a transient modulation was seen with the first cycle, with CMV-specific $CD8^+$ T-cells exhibiting increased expression of TIGIT and granzyme B.

The efficacy of PD1 blockade in the treatment of cancer is suboptimal due to the small subset of patients it affects and needs further optimisation. The study of PD1 function in the setting of persistent viral infection will be helpful in uncovering insights into the physiological function of this protein. My work has uncovered a range of novel observations relating to the pattern and functional correlates of PD1. These findings emphasise the need for further research in this area. One important aim of this will be to guide the use of checkpoint blockade in the management of malignant disease and other clinical settings.

ACKNOWLEDGEMENTS

Firstly, I wish to thank my supervisor, Professor Paul Moss, for the opportunity to undertake this PhD within your group and for the enthusiasm in my project over the last three years.

I would also like to thank my supervisors Dr Jianmin Zuo and Dr Alex Dowell for your day-to-day guidance and scientific knowledge throughout my PhD.

Thank you to my colleagues within the Moss Group for all your advice and support. A special thank you to Jusnara Begum, who's technical advice and experimental wisdom has guided me throughout my PhD, to David Bone, who put up with my constant questions about high dimensional analysis, and to Dr Rachel Bruton, for being able to answer, quite literally, any question known to man.

Thank you to Eliška, my bestie, for the endless laughs and friendship, you truly made the last three years enjoyable, and I can't wait to celebrate when you also finish your PhD.

Thank you, Mum and Dad, for your limitless support, encouragement and love, despite not understanding what I am talking about! Thank you to Devika, for never failing to cheer me up and always being on-hand for a Hannah Montana sing-a-long session.

Thank you to Nanima and Nanabapa, who always encouraged my academic achievements and whose work ethic continues to inspire me.

For Yasmin.

CONTRIBUTIONS

Patient samples and data were kindly provided from the PePS2 clinical trial; an investigator-initiated and investigator-led trial funded by Merck, Sharp & Dohme and sponsored by the University of Birmingham. Thank you to all the patients and their families who participated in this trial, and the NHS trusts & staff and members of the trial management group/trial steering committee who have supported it. The Cancer Research UK Clinical Trials Unit at the University of Birmingham is supported by funding from CRUK. PePS2 was supported by Experimental Cancer Medicine Centres (ECMC) funding and by the ECMC Network.

Thank you to Victoria Homer (Trial Statistician) for providing the PePS2 patient data and to Professor Gary Middleton who conducted the trial.

Ovarian tissue samples and peripheral blood were collected at City Hospital, Birmingham and New Cross Hospital, Wolverhampton. I am so grateful to the patients who so generously consented to be part of the research.

A huge thank you to Dr Rachel Pounds and Dr Dani O'Neill for helping with tissue collection.

Finally, thank you to all the donors from the institute who contributed to this study, without whom this would have not been possible.

ABBREVIATIONS

Abbreviation	*Meaning*
APC	antigen presenting cell
CAFs	cancer associated fibroblasts
CAR	chimeric antigen receptor
CMV	Cytomegalovirus
CTL	cytotoxic T lymphocyte
CTLA-4	cytotoxic T lymphocyte associated protein 4
DAMP	damage-associated molecular patterns
DC	Dendritic cell
EBV	Epstein-Barr Virus
EOC	epithelial ovarian cancer
HBV	Hepatitis B virus
HCV	Hepatitis C virus
HGSOC	high-grade serous ovarian cancer
HLA	human leukocyte antigen
HPV	Human Papillomavirus
IE	immediate-early
LAG-3	lymphocyte activating 3
LCMV	Lymphocytic Choriomeningitis Virus
MDSCs	myeloid-derived suppressor cells
MHC	major histocompatibility complexes
NK	Natural killer
OvCa	Ovarian Cancer
PAMP	pathogen-associated molecular patterns
PD-1	Programmed Cell Death protein 1
pp65	phosphoprotein 65
PRR	pattern recognition receptors
PS	performance status
TAA	Tumour-associated antigen
TAMs	tumour associated macrophages
TCR	T-cell receptor
TIGIT	T-cell immunoreceptor with Ig and ITIM domains
TIL	tumour infiltrating lymphocyte
TILs	tumour infiltrating lymphocyte
TIM-3	T-cell immunoglobulin and mucin domain-containing protein 3

TLR	toll like receptors
TME	Tumour microenvironment
TME	Tumour microenvironment
Tregs	regulatory T-cells
V(D)J	variable (diversity) joining

TABLE OF CONTENTS

LIST OF FIGURES

CHAPTER 1: INTRODUCTION

CHAPTER 2: Materials and Methods

CHAPTER 3: Phenotypic and functional analysis of $PD1^{+}$ CMV-specific $CD8^{+}$ T-cells in healthy donors

LIST OF TABLES

CHAPTER 1: Introduction

1.1 The human immune system

1.1.1 The immune system

1.1.1.1 The innate immune response

The immune system is an incredibly complex and vital network which has evolved to protect the host from pathogens and other toxic substances which may threaten homeostasis. In humans the innate and adaptive components of the immune response work together. The innate response provides an immediate and rapid response, and includes physical barriers such as mucus in the respiratory tract, whereas the adaptive response provides a long-term and specific memory (Chaplin, 2010). The innate immune system has a number of functions including recognising pathogenic structures as well as producing regulatory cytokines and effector components such as complement (Pradeu et al., 2024). Initiation of the immune response occurs through a range of diverse mechanisms, for example in response to microbial infection pathogen-associated molecular patterns (PAMPs) such microbial nucleic acids are recognised by pattern recognition receptors (PRRs), including toll like receptors (TLRs), on antigen presenting cells (APCs). APCs can also recognise damage-associated molecular patterns (DAMPs), which initiate immunity in the setting of tissue damage. PRR activation leads to the activation of signalling pathways and the production of proinflammatory cytokines and interferons which in turn further initiate the innate immune response, inducing responses such as autophagy, phagocytosis and cell death (Brubaker et al., 2015).

The innate immune response is composed of a range of cellular components that are essential for the first line of defence against pathogens. Phagocytic cells, including granulocytes, Natural Killer (NK) cells and monocytes, play a key role in recognition and opsonisation of foreign pathogens. These cells are enlisted in various ways, for example the stimulation of

TLRs can activate signalling pathways that trigger the transcription factor NFκB. This leads to the rapid expression of costimulatory molecules such as CD80 and CD86 on the surface of antigen-presenting cells (APCs), particularly DCs. DCs are crucial in both the innate and adaptive immune responses, serving as a bridge between the two by capturing antigens and presenting them to T-cells, thus initiating a tailored immune response against pathogens (Janeway and Medzhitov, 2002)

APC are essential components of the immune system that continuously monitor their environment, capturing foreign materials such as pathogens or abnormal cells. Once these materials are internalised, they are processed into smaller fragments. These are antigenic peptides derived from the degradation of proteins which are presented on their surface by major histocompatibility complex (MHC) molecules. This presentation allows antigen-specific lymphocytes, particularly T-cells, to recognise and respond, triggering an immune response (Mantegazza et al., 2013).

APCs utilise various methods to capture antigens. Receptor-mediated endocytosis involves the selective uptake of specific molecules bound to receptors on the cell surface. Phagocytosis is the process by which APCs engulf large particles, such as bacteria, whilst pinocytosis allows them to take in extracellular fluids and solutes (Joffre et al., 2012, Trombetta and Mellman, 2005). These diverse methods of antigen uptake ensure APCs can effectively capture and present a wide range of potential threats to the immune system.

NK cells are critical components of both the innate and adaptive immune systems. They are cytotoxic lymphocytes that have an innate ability to recognise and eliminate virally infected and malignantly transformed cells. NK cells can be activated in multiple ways. One such way,

through the lack of MHC-I recognition. This downregulation can occur with viral infection such as cytomegalovirus infection or in tumours (Gabor et al., 2020, Cristiani et al., 2020). Furthermore, they can also be activated when activating receptors outweigh inhibitory receptors. Activating receptor ligands are not typically expressed on healthy cells. An example of this is the NKG2D receptor, which binds to stress-induced ligands that are frequently upregulated on cancer cells and virus-infected cells but are minimally expressed on healthy host-cells. This receptor-ligand interaction enables NK cells to distinguish non-self from self and effectively target and clear tumours (Yang et al., 2006, Iannello and Raulet, 2013). Finally, NKs can mediate antibody-dependent cell-mediated cytotoxicity (ADCC) (Lo Nigro et al., 2019).

1.1.1.2 The innate immune response: Complement

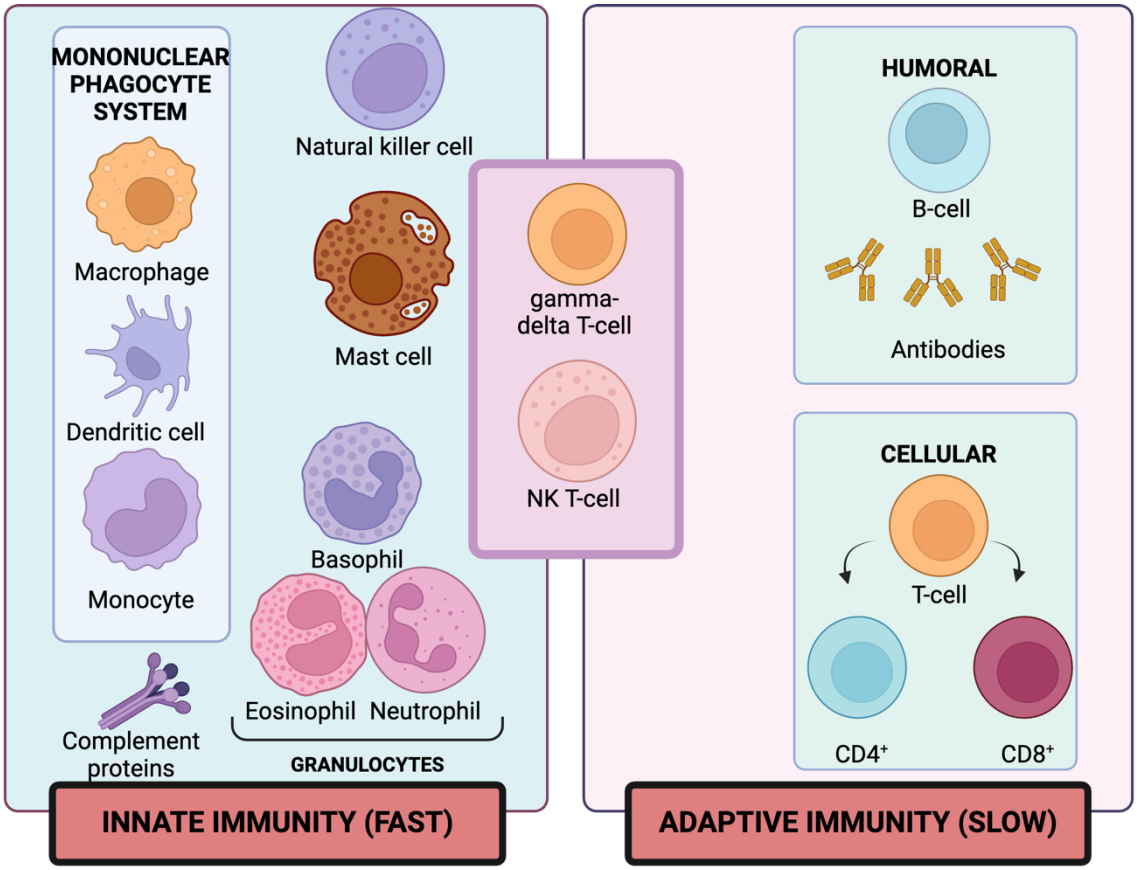

Figure 1: Innate and Adaptive Immunity

The innate immune response occurs rapidly and is made up of NK cells, granulocytes (basophils, eosinophils and neutrophils), macrophages, dendritic cells and mast cells. The adaptive immune system takes longer to come into effect however demonstrates antigen specificity and memory. This system comprises the humoral immunity of B-cells and antibodies, and cellular components including $CD4^+$ and $CD8^+$ T-cells. Gamma delta and NK T-cells provide overlap between the two systems. Created with biorender.com.

The complement system is a crucial part of the innate immune response, consisting of a series of more than 30 proteins that circulate in the plasma and on cell surfaces in an inactive form. Upon activation by pathogens, these proteins initiate a cascade of reactions that enhance the ability of antibodies and phagocytic cells to clear microbes, promote inflammation and attack the pathogen's cell membrane (Dunkelberger and Song, 2010).

The complement system can be activated by three pathways: the classical, lectin and alternative pathways. Each pathway converges on the activation of C3, a central protein in the complement cascade, leading to the formation of the membrane attack complex that lyses target cells (Ricklin et al., 2010). Whilst initially thought to play a major role in the innate immune response, emerging evidence indicates that complement also plays an important role in adaptive immunity, with C3 binding to B-cells and a depletion of the protein causing impaired humoral immune responses (Dunkelberger and Song, 2010, Sarma and Ward, 2011).

1.1.1.3 The adaptive immune response

Unlike the rapid response of the innate system, the adaptive immune response is generated within days following recognition of foreign pathogens and can be an ongoing process in which the specificity of the immune response is optimised in the presence of chronic antigen persistence (Bonilla and Oettgen, 2010). It is initiated when APCs interact with cells of the adaptive immune system, primarily B cells and T-cells. APC present antigen in the form of peptides to T-cell effector cells whilst B cells recognise conformational protein structures (Pennock et al., 2013, Ivanisenko et al., 2024). The adaptive response consists of $CD4^+$ T-cells, $CD8^+$ T-cells and B-cells and is vital for controlling and clearing viral infections. Whilst naive T-cells are generated in the thymus and exert their roles through a range of helper and effector

functions, B-cells are generated in the bone marrow and produce antibodies (Sette and Crotty, 2021).

Humoral immunity is a key component of the adaptive immune system and is primarily mediated by antibodies. These antibodies are produced by plasma cells which originate from B-cells. The development of plasma cells from B-cells is facilitated by signalling from other immune cells, particularly T-helper cells. B-cells acquire their antigen specificity during their development in the bone marrow which results in them expressing a unique B-cell receptor on their surface. Once B-cells encounter their specific antigen in the periphery, typically with help from T-cells, they can differentiate into antibody-secreting plasma cells or memory B-cells, thus contributing to long-term immunity (Bonilla and Oettgen, 2010, Nutt et al., 2015).

Historically, NK cells were considered to have been part of the innate immune system. However, research over the past two decades has revealed that NK cells can also exhibit adaptive memory-like phenotypes. This adaptive response is often triggered by stress signals in infected cells, such as during acute cytomegalovirus (CMV) infection, where there is a notable expansion and increased cytotoxicity of circulating NK cells (Pierce et al., 2020, Newhook et al., 2017). NKs can also regulate immune responses by targeting DCs which can affect quality of the T-cell response (Pierce et al., 2020). Two major subsets of NK cells can be distinguished on the basis of the expression of CD56 on the cell surface with $CD56^{dim}$ NK cells being more cytotoxic in nature whilst $CD56^{bright}$ NK cells demonstrate higher levels of cytokine secretion and play a regulatory role (Vivier et al., 2008).

T-cell recognition is mediated through the T-cell receptor (TCR). The TCRs is a heterodimeric protein composed of an α and β chain or a γ and δ chain pairing. Through a process termed

variable (diversity) joining (V(D)J) recombination, the V and J regions in α and γ chains, or the V, D and J regions in the β and δ chains, undergo rearrangement. This process, which is mediated randomly within a developing T-cell, acts to generate a varied TCR repertoire capable of recognising a wide spectrum of antigens (Rosati et al., 2017). In humans, around 90-99% of $CD8^+$ T-cells contain a TCR comprising of $\alpha\beta$ chains with the remaining T-cells being formed with $\gamma\delta$ chains (Adams et al., 2015). The work in my thesis is focussed on $\alpha\beta$ $CD8^+$ T-cells.

1.1.2 T-cell activation

Three signals are essential for T-cell activation. Initially, TCRs recognise and bind to antigenic peptides presented on major histocompatibility complexes (MHCs), also known as the human leukocyte antigen (HLA), on the surface of antigen presenting cells. Peptides derived from protein cleavage are presented by two MHC classes: MHC class I (MHC-I) which presents internally cleaved peptides (proteins degraded by the proteosome into small peptides) for $CD8^+$ T-cell recognition, whilst MHC class II (MHC-II) presents peptide predominantly derived from proteins that have been taken up by the APC for $CD4^+$ T-cell recognition. The three classical MHC-I genes are HLA-A, HLA-B and HLA-C whilst the three are MHC-II genes, HLA-DR, HLA-DQ and HLA-DP, which are predominant in $CD4^+$ biology (Blum et al., 2013, Hutchison and Pritchard, 2018). A costimulatory signal is needed as the second signal during T-cell activation, whilst its absence can lead to T-cell anergy. Cytokine signalling is also required to promote effector functions including T-cell differentiation and effector mechanisms (Goral, 2011).

T-cell activation relies on co-inhibitory and co-stimulatory receptors such as CD27 and CD28 to regulate effector function and survival (Chen and Flies, 2013). Upon recognition of peptide

antigen presented on the MHC by the $CD8^+$ TCRs, clonal expansion and differentiation into cytotoxic T lymphocytes (CTLs) occurs. Thereafter, CTLs produce cytokines such as IFN-γ, IL-2 and TNF- α to directly kill target cells that are infected by the pathogen (Rha and Shin, 2021). Following the acute infection, most CTLs die, whilst a fraction become mature memory $CD8^+$ T-cells (Kaech and Cui, 2012).

T-cells can be categorised into five main memory subsets using the markers CD45RA and CCR7 (Figure 2). Naïve T-cells, which have not previously encountered antigens, respond rapidly to pathogens and express high levels of CD45RA and CCR7. Upon encountering their specific antigens, T-cells differentiate into distinct memory subsets. The least differentiated memory T-cell subset is stem like memory T-cells (T_{SCM}). These cells retain expression of both CD45RA and CCR7 that is seen in naïve T-cells, however begin to express some markers that are characteristic of memory cells such as CD95 (Wang et al., 2022). Central memory T-cells (T_{CM}) express CCR7 but lack CD45RA, instead expressing CD45RO. These cells have high proliferative capacity but lack immediate effector functions. This contrasts with effector memory T-cells (T_{EM}); these cells lack both CCR7 and CD45RA and can rapidly respond upon stimulation with their cognate antigen, making them crucial for immediate immune responses. Terminal effector memory T-cells (T_{EMRA}) re-expressing CD45RA, are CCR7 negative. T_{EMRA} cells typically do not express CD27 or CD28 and have the shortest telomeres among the four subsets. These cells also express markers of senescence and exhibit low proliferative and functional capacity, indicating terminal differentiation (Mahnke et al., 2013, Kumar et al., 2018, Larbi and Fulop, 2014, Wang et al., 2022). The distant roles and characteristics of these subsets are critical for the adaptive immune system's ability to effectively combat infections.

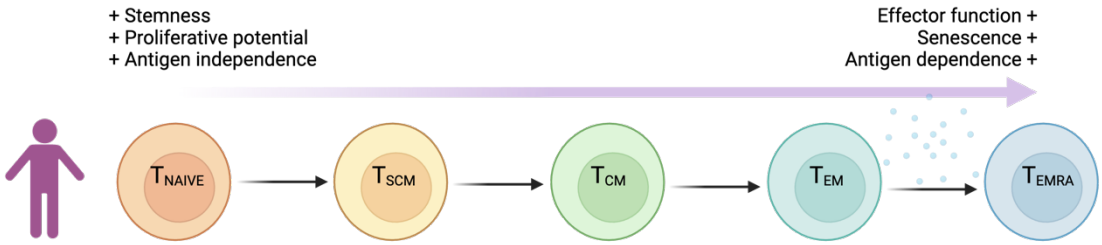

	T_{NAIVE}	T_{SCM}	T_{CM}	T_{EM}	T_{EMRA}
CCR7	+	+	+	-	-
CD45RA	+	+	-	-	+
CD27	+	+	+	+/-	-
CD28	+	+	+	+/-	-
CD95	-	+	+	+	+

Figure 2: T-cell memory subsets

Naïve T-cells are double positive for CCR7 and CD45RA. These differentiate into stem-cell like memory T-cells, central memory T-cells, effector memory T-cells and effector T-cells which retain CD45RA expression. As cells progress, they lose their stemness, proliferative potential and lack of antigen specificity, becoming effector cells with markers of terminal differentiation and antigen dependence. Figure created with BioRender.com.

1.1.3 Immune Checkpoints

Persistent antigen stimulation through the TCR can lead to impairment of CTL function and development of a state of 'exhaustion'. Initially observed in 1993 in response to lymphocytic choriomeningitis virus (LCMV) infection in mice, exhausted T-cells demonstrate constrained immune responses, consisting of reduced proliferation, impaired cytokine release and impaired cytotoxicity (Gallimore et al., 1998, Moskophidis et al., 1993). Since then, multiple studies have published the same findings in the context of chronic viral infections in humans, and within the tumour microenvironment of solid cancers.

Notably, exhausted T-cells often display an upregulation of immune checkpoint molecules (Figure 3). Immune checkpoints play pivotal roles in regulating T-cell activation across various phases of the immune response to prevent auto-immune disorders. However, their overexpression can also restrict T-cell-mediated immune responses (Chauvin et al., 2015a, He et al., 2018, Fourcade et al., 2010).

Prominent checkpoint proteins such as Programmed Cell Death Protein 1 (PD1) and Cytotoxic T-lymphocyte associated protein 4 (CTLA4) have been studied extensively and are major targets for cancer immunotherapy. Additional proteins such as T-cell immunoglobulin and mucin domain-containing protein 3 (TIM3), T-cell immunoglobulin and ITIM domain (TIGIT), lymphocyte-activation gene 3 (LAG3) and 2B4 are also recognised as important regulators of T-cell function. These proteins modulate T-cell activation throughout the immune response to maintain immune tolerance and minimise tissue damage during effector responses (Anderson et al., 2016, Dyck and Mills, 2017). Each checkpoint protein interacts with specific ligands, for example PD-1 has two main immunoregulatory ligands termed programmed cell death ligand

1 and 2 (PD-L1 and PD-L2). When PD1 binds to its ligands, it results in the recruitment of phosphatases SHP-1 and SHP-2, which dephosphorylate key signalling molecules leading to reduced TCR signalling and diminished T-cell proliferation and cytokine production. PDL-1 is widely expressed by APCs and tumour cells whilst PD-1 is expressed on other activated cells including B-cells, NK cells and T-cells (Topalian et al., 2012). The ligands for CTLA4 are CD80 and CD86, for TIGIT are CD155 and CD112, and CD48 for 2B4. The ligands for LAG-3 are MHC-II, Galectin-3 (Gal-3), lymph node sinusoidal endothelial cell C-type lectin (LSECtin) and Fibronigen-like protein 1 (FGL1). There are multiple ligands for TIM3 with two main ones being galectin 9 (Gal-9) and the adhesion molecule carcinoembryonic antigen-related cell adhesion molecule 1 (CEACAM1). Checkpoint-ligand binding results in decreased T-cell activation by inhibiting proliferation, TCR signalling and cytokine production (Joller and Kuchroo, 2017, Dyck and Mills, 2017, Wolf et al., 2020, Ahmad et al., 2017, Rowshanravan et al., 2018, Burnell et al., 2021).

T-cells exhibit a diverse array of these inhibitory receptors whose expression varies depending on the context of the cellular environment and activation status. (Thommen and Schumacher, 2018). The receptors are not exclusive to T-cells but can also be found on other cell types including NKs, where their expression limits functional response, as well as antigen presenting cell populations (Cao et al., 2020).

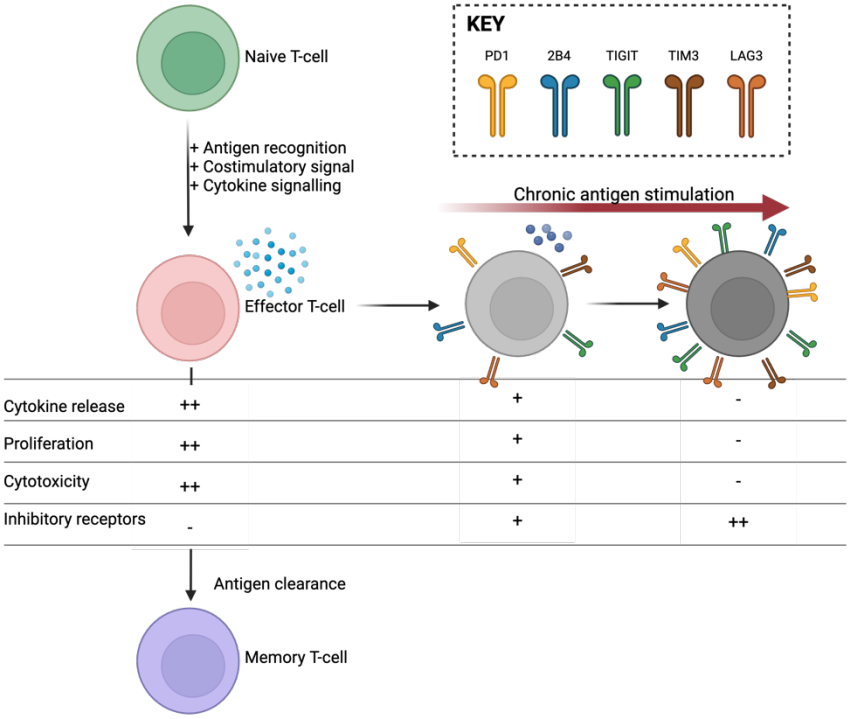

Figure 3: Stages in the development of CD8+ T-cell exhaustion

Naïve T-cells differentiate into effector T-cells in the presence of antigen stimulation and co-stimulation. Effector T-cells can become exhausted if chronic antigen stimulation occurs. Exhausted T-cells in cancer express high levels of inhibitory receptors together with functional impairment including a decrease in cytokine release, proliferation and cytotoxic capacity (Figure adapted from (He et al., 2018)). Figure made with BioRender.com

1.1.4 PD1 on T-cells

It was initially thought that PD1 expressing T-cells were terminally differentiated cells with no capacity for further proliferation. However, further research indicates that a memory pool of PD-1$^+$ cells have the ability to regain function and can proliferate when exposed to checkpoint blockade therapies (Utzschneider et al., 2016).

Several studies have delineated PD1$^+$ cells into distinct categories: stem-like, transitional, and terminally differentiated. These cells were categorised using human papillomavirus (HPV)-specific T-cells from patients with head and neck cancer. The stem-like cluster exhibited heightened mRNA expression of *TCF7,* the gene encoding the TCF1 transcription factor which is crucial for the genesis of stem-like CD8$^+$ T-cells during chronic viral infection. Additionally, this cluster displayed high levels of CD127 and CCR7, alongside a lack of effector molecules. The transitional subset displayed certain stem-like characteristics but also the upregulation of some effector markers such as *GZMB* and *PRF1*. Conversely, the terminally differentiated population exhibited an increase in inhibitory markers with decreased expression of costimulatory molecules. These subsets have been observed consistently across multiple studies.

TCF-1 expression, often used to identify the stem-like population, closely correlates with the expression of the chemokine receptor, CXCR5, suggesting CXCR5 also as a defining marker for this population (Utzschneider et al., 2016, Im et al., 2020). This CXCR5$^+$ population has been shown to be one of the key viral specific T-cell populations which could response to checkpoint blockade. In LCMV-infected mouse models, distinct gene signatures were observed in PD1$^+$ CXCR5$^+$ and PD1$^+$ CXCR5$^-$ CD8$^+$ T-cell populations. The CXCR5$^+$ population displayed higher

levels of costimulatory markers such as CD28 and lower levels of inhibitory markers such as 2B4, TIM-3 and CD39. PD1 blockade led to significant increase in the $CXCR5^+$ population, while no significant increase was observed in the $CXCR5^-$ population (Im et al., 2016).

1.2 T-cells in cancer immunology

1.2.1 Non-small cell lung cancer

Two cohorts of cancer patients were used in my thesis: Non-small cell lung cancer (NSCLC) and ovarian cancer (OvCa). Lung cancer remains a significant health challenge globally, characterised by a high mortality rate among both men and women, with over 50% of patients succumbing to the disease within one year of diagnosis. NSCLC is the predominant type of lung cancer, an epithelial cancer comprising the majority of lung cancer cases. Risk factors are primarily linked to cigarette smoking, although other environmental factors also play a role (Zappa and Mousa, 2016).

Despite the availability of several treatment options, the five year survival rate for NSCLC in 2017 remained low at 17% (Khanna et al., 2017). However, the introduction of PD-1 and PD-L1 blockade has helped to transform treatment outcomes. Numerous clinical trials investigating different immunotherapies have been conducted, culminating in the approval of pembrolizumab as a first-line treatment for patients with metastatic NSCLC (Middleton et al., 2020).

Initial clinical trials demonstrated that in patients with PD-L1 expression on over 50% of tumour cells, both overall and progression-free survival were significantly improved. More recent trials have indicated that even patients with PD-L1 expression on just 1% of their

tumour cells may derive benefit from these therapies (Khanna et al., 2017). This highlights the remarkable potential of PD-1 and PD-L1 blockade to improve outcomes for a broader spectrum of NSCLC patients, offering hope for increased survival.

Despite this significant improvement, a notable proportion of patients still do not respond to therapy and may experience adverse events. In a study where patients received pembrolizumab alongside chemotherapy, 39% experienced treatment-related adverse events, with some patients even experiencing treatment-related mortality (Langer et al., 2016). This underscores the importance of identifying biomarkers that can predict which patients are likely to respond favourably to treatment. Such biomarkers could aid clinicians in selecting the appropriate therapeutic strategies for patients, thereby minimising adverse events and optimising patient outcomes. Therefore, ongoing research into identifying predictive biomarkers hold immense promise for further improving the management of NSCLC.

1.2.2 Ovarian cancer

Ovarian cancer is one of the most prevalent and lethal gynaecological malignancies, with poor prognosis and a high mortality rate worldwide. The poor outcomes associated with the disease stem from the lack of symptoms in early stage disease, resulting in delayed diagnosis with most patients presenting at an already advanced stage, with metastatic legions within the peritoneal cavity (Coburn et al., 2017, Momenimovahed et al., 2019). Approximately 75% of women are diagnosed at advanced stage disease with only 45% surviving beyond five years post-diagnosis. When ovarian cancer is detected at stage I, the five-year survival rate is significantly increased at 92% however, this figure drops to 17-28% for individuals diagnosed

with late stage tumours (Doubeni et al., 2016). These statistics underscore the urgent need for improved therapeutic interventions and understanding the TME of ovarian cancer patients will provide significant insight towards this.

In patients with advanced-stage epithelial ovarian cancer (EOC), the standard treatment approach typically involves debulking surgery followed by chemotherapy. However, for patients presenting at even more advanced stages, neoadjuvant chemotherapy followed by interval debulking surgery is employed (Armstrong et al., 2021). Despite these treatment strategies, tumour recurrence from residual disease remains a significant challenge, affecting approximately 70% of patients. Moreover, as the disease progresses, there is often an increase in chemotherapy resistance, further complicating treatment efforts (Borley et al., 2012).

Ovarian cancer exhibits remarkable heterogeneity, particularly in the TME. Evidence suggests that the TME plays a pivotal role in the pathogenesis of high-grade serous ovarian cancer (HGSOC), underscoring the potential significance of immunological therapies in the management of this disease (Bell et al., 2011, Ghoneum et al., 2018).

Whilst there have been several trials investigating PD-1 and PD-L1 inhibitors in ovarian cancer, the response rates have been generally poor, with less than 15% of patients demonstrating positive responses and short-term progression-free survival of less than 3.4 months. Recognising these limitations, ongoing research is exploring combination strategies, such as PD-1 and PD-L1 blockade in conjunction with chemotherapy, in an effort to enhance treatment efficacy (Leary et al., 2021). Given the relatively small subset of patients who respond to immunotherapy, it is crucial to identify predictive biomarkers that can help guide

treatment decisions and provide a more informed understanding of prognosis and treatment outcomes.

1.2.3 The tumour microenvironment

One of the key challenges encountered by the immune system is its ability to detect and eliminate carcinogenic cells. A fundamental role of the immune system is distinguishing between 'self' and 'non-self'; as cancer develops from host cells, one of the reasons it does not generate an immune response is the lower affinity of TCRs for self-antigens compared to foreign antigens. Additionally, cancer can actively evade immune surveillance by modifying tumour immunogenicity and enabling immunosuppressive mechanisms in a process called immunoediting. Immunoediting encompasses three main phases: elimination, equilibrium and escape (Figure 4). The first phase, elimination, is evidenced by numerous mouse studies where mice with varying degrees of immunodeficiency show a higher susceptibility to induced and spontaneous cancers compared to immunocompetent mice (Mittal et al., 2014, Diamond et al., 2011). In this immunosurveillance phase, the adaptive and innate immune responses work cohesively to identify and eliminate transformed cells that have evaded tumour suppressor mechanisms before they progress and become clinically detectable. If malignant cells reach a large enough size, they secrete cytokines which recruit macrophages, T-cells, natural killer (NKs) cells or dendritic cells (DCs) which then engulf the cells and cross-present the tumour antigens to T-cells (Miliotou and Papadopoulou, 2018). The release of IFN- ɣ by these effector cells plays a crucial role in regulating anti-tumour effects by inhibiting angiogenesis and proliferation of malignant T-cells. Activated $CD8^+$ T-cells can then induce apoptosis with the secretion of perforin and granzymes, or by interacting with death receptors

on tumour cells (Mittal et al., 2014). During the equilibrium phase, net tumour growth is restricted, but not eliminated entirely. Tumour cell immunogenicity is altered due to pressure from the immune system, along with genetic instability, resulting in progression to the escape phase where less immunogenic cells can proliferate unchecked and evade the immune system (McCoach and Bivona, 2018).

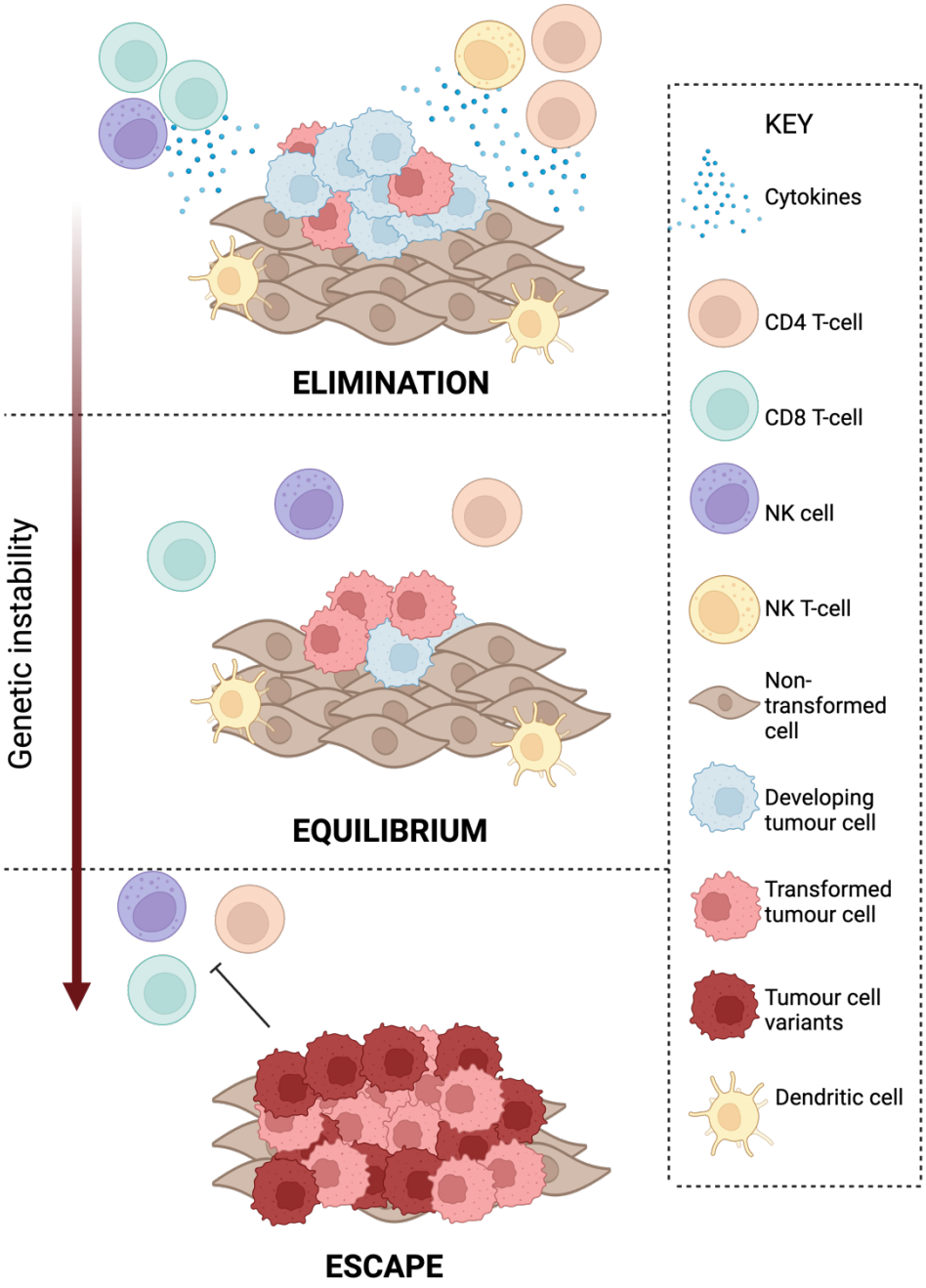

Figure 4: Cancer immunoediting

Cancer immunoediting consists of three stages and describes the transformation process of normal cells to tumour cells. In the elimination phase, immune surveillance cells detect malignant cells and rapidly act to eliminate them. In the equilibrium phase the immune system promotes the generation of tumour cell variants capable of resisting the immune responses. Finally, in the escape phase, the transformed tumour cell variants expand in an uncontrollable manner. Figure created with Biorender.com

The interaction between tumour cells and their surrounding environment is crucial for tumour growth, dissemination and signalling (Tesi, 2019). The tumour microenvironment (TME) comprises a complex network of various components, including cancer-killing cells, and those that actively protect the tumour from immune surveillance (Figure 5). These cells encompass regulatory T-cells (T_{REGS}), cancer-associated fibroblasts (CAFs), immune lymphocytes (T, B and NK cells), myeloid-derived suppressor cells (MDSCs), and tumour-associated macrophages (TAMs) (Ariztia et al., 2006). These cells, under healthy conditions, would protect the host against tumours, however, now play active roles in supporting the microenvironment for the tumour to grow.

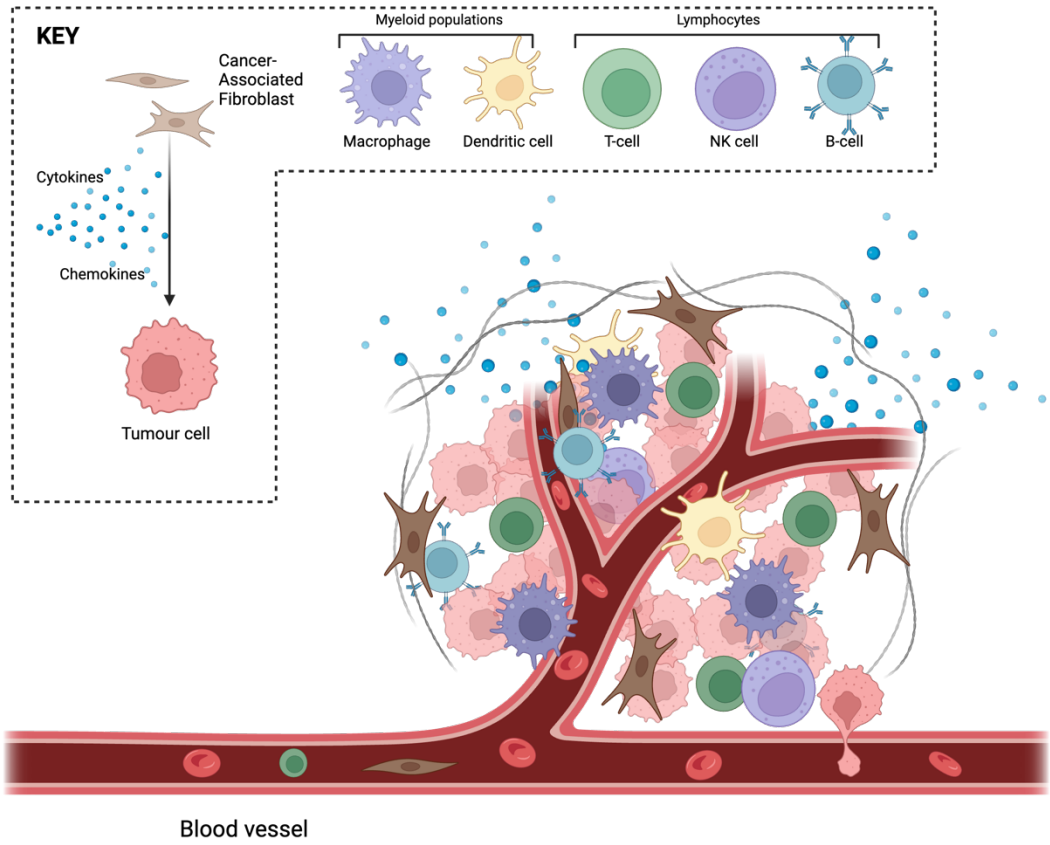

Figure 5: The tumour microenvironment.

The tumour microenvironment is a network comprised of many components such as tumour cells, cancer associated fibroblasts (CAFS), myeloid populations (macrophages, dendritic cells) and lymphocytes (B-cells, natural killer cells and T-cells). Cytokines and chemokines all affect the microenvironment to promote an immunosuppressive environment, whilst blood vessels supply oxygen and nutrients. (Figure adapted from (Kinan Drak and Didier, 2018, Stefanski and Prosperi, 2020)). Figure created with BioRender.com.

The immune infiltrate plays a significant role in cancer and treatment, with the presence of tumour-infiltrating lymphocytes (TILs) in some solid tumours correlating with improved survival (Westergaard et al., 2019). The accumulation of cytotoxic $CD8^+$ T-cells as a prognostic marker in malignancies such as ovarian tumours was first described in 1991 (Santoiemma and Powell, 2015). It has since been consistently associated with progression-free and disease-free survival in subsequent studies, establishing them as a biomarker for overall survival (Hwang et al., 2012).

However, cytotoxic T lymphocytes are subject to immunosuppression within the microenvironment through mechanisms such as immune checkpoint engagement, cytokine release, and CD4+ T_{REGS} (Lieber et al., 2018). Whilst T_{REGS} play a crucial role in maintaining immune system homeostasis by regulating excessive responses and preventing immune reactions against self-antigens, within the TME they suppress the function of $CD8^+$ T-cells. This suppression occurs through the secretion of inhibitory cytokines such as IL-10, and via cell-to-cell contact mechanisms, limiting cytotoxicity (Wefers et al., 2018). An expansion of T_{REG} populations is observed in patients with late-stage ovarian cancer, with higher proportions of these cells at treatment onset associated with poorer outcomes (Dutsch-Wicherek et al., 2019).

The infiltrating $CD8^+$ T-cells within cancer tissues often exhibit functional impairments due to T-cell 'exhaustion'. This state arises from sustained exposure to their cognate antigen, leading to a reduction in cytotoxicity, compromised cell viability and impaired proliferative capacity. Consequently, the presence of these exhausted T-cells impedes the successful elimination of

cancer (Jiang et al., 2015). One of the earliest papers linking exhausted T-cells with the TME was published in 2002, where it was discovered that mouse mastocytoma P815 cells overexpressed PDL-1, leading them to be less susceptible to cytotoxicity and have increased tumorigenesis and invasiveness (Iwai et al., 2002). Since then, copious research has been done, and it is now well established that PD1 is upregulated in $CD8^+$ TILs in several cancers, contributing to the immunosuppressive microenvironment seen in myriad tumour subtypes (Yamamoto et al., 2008, Fourcade et al., 2009, Gehring et al., 2009). Co-expression of PD1 with other checkpoints such as TIM3 and LAG3 has been shown to be indicative of a more exhausted phenotype, leading to more dysfunctional T-cells in cancer patients and an impaired prognosis (Jiang et al., 2015).

1.2.4 Neoantigens

In the last couple of decades, there has been a significant shift in cancer treatment towards immunotherapy and harnessing the immune system to treat malignancies (Houghton and Guevara-Patiño, 2004, Vonderheide and June, 2014). One approach involves targeting tumour-associated antigens (TAAs), a class of proteins that encompass antigens displaying high tumour specificity. This can be achieved through various methods, for example prophylactic vaccine based therapy such as a HPV-16 vaccine to elicit immune responses and prevent viral infection, or by harnessing T-cells through Chimeric Antigen Receptor (CAR) technology to genetically modify and redirect T-cells to target tumour antigens (Kenter et al., 2009, Miliotou and Papadopoulou, 2018). However, it is important to note that many important tumour antigens are self-proteins, and arise from proteins that are aberrantly or

overexpressed in tumour cells so whilst targeting these cells is feasible, it can lead to dangerous side effects due to off-target expression (Lee et al., 2018).

The identification of markers exclusive to cancerous cells is therefore incredibly important. When cancer-associated genes undergo mutations, they lead to changes in the corresponding proteins. These altered proteins, known as neoantigens, are subsequently presented on the MHC. Since these neoantigens are not typically presented on healthy somatic tissues, they are perceived as foreign by the immune system and can be recognised by T-cells (Lee et al., 2018). Importantly, the mutational burden, which refers to the total number of mutations present in a cancerous genome, varies across different types of cancers. Consequently, the level of neoantigen production also fluctuates amongst malignancies.

As neoantigens are tumour specific, they provide a target for personalised cancer immunotherapies whilst also serving as potential predictors of response to other treatments. Neoantigen-based therapies typically involve the identification of these unique antigens by sequencing of patient tumour DNA, followed by the development of personalised vaccines or adoptive T-cell therapies that are designed to elicit a robust immune response specifically against these neoantigens (Xie et al., 2023).

Clinical trials have shown that neoantigen vaccines can induce strong T-cell responses and have demonstrated potential in shrinking tumours and prevention of recurrence in cancers such as melanoma. Ott *et al.* demonstrated that a vaccine that can target up to 20 predicted personal neoantigens can be safely administered. This targeted patients with melanoma-associated mutations such as in *BRAF* and *NRAS*, with 4/6 vaccinated patients demonstrating no recurrence 25 months post-vaccination, and the remaining two successfully treated with

checkpoint blockade (Ott et al., 2017). Some of the challenges with this approach include effective neoantigen target discovery and the delivery platform of the vaccines. One emerging method of interest is the use of chemically synthesised minimal mRNA (CmRNA). CmRNA, which has been optimised for coding efficiency, is encapsulated in lipid polymer particles. This amongst with its reduced size due to lack of non-coding sequences, improves its stability and offers a promising strategy for the further development of neoantigen vaccines (Imani et al., 2024).

Whilst neoantigen-specific TILs are often present within the TME, the population of TILs in general is extremely heterogenous. The prognostic value of TIL suggests that they have an important physiological function, but their exact contribution remains unclear, particularly in the context of diseases such as ovarian cancer, which often exhibit poor responses to immunotherapy such as PD1 inhibitors. It has been hypothesised that tumour-reactive TILs could lead to an upregulation of PD1 and PD-L1, making them potential targets for anti-PD1/PD-L1 therapies. However, it is also plausible that TILs are attracted to tumours that inherently have a better response to therapy, rather than actively exerting effector mechanisms on the tumour itself. Further investigation is imperative to unravel the exact mechanisms of how TILs are functioning within the microenvironment.

1.2.5 Checkpoint Blockade

TILs which have infiltrated the cancer tissue often become exhausted, leading them to be functionally impaired and preventing effective elimination of cancer. Various studies have shown a wide range of cancers exhibit impaired $CD8^+$ TILs with upregulation of these co-

inhibitory receptors including ovarian cancer (Matsuzaki et al., 2010), non-small cell lung carcinoma (Thommen et al., 2015) and melanoma (Ahmadzadeh et al., 2009).

A study by Dong et al. in 2002 showed that immunosuppression could be eliminated by inhibiting the binding of PD-1 and PD-L1 in mouse models (Dong et al., 2002). Since then, treatment has been developed which inhibits these checkpoint pathways in order to augment the immunological response against cancers, with these becoming standard of care in several tumours (Zhang et al., 2024, Brahmer et al., 2021).

The first immune checkpoint inhibitor to be approved was ipilimumab, an anti-CTLA-4 monoclonal antibody, followed by several anti-PD-1 and anti-PD-L1 therapies. CTLA-4 is an inhibitory receptor expressed on T-cells, which downregulates immune responses by competing with the stimulatory receptor CD28 when binding to CD80 on APCs, and delivering opposing inhibitory signals compared to the stimulatory signals of CD28 (Krummel and Allison, 1995).

Currently, checkpoint therapy is approved for 14 cancer types, representing almost 39% of all cancer patients to be eligible for this treatment. Although this has led to an improvement in treatment outcomes and responses, treatment is only successful in a small subset of patients, although durable responses are observed in responsive patients. (Marin-Acevedo et al., 2021, Schillebeeckx et al., 2022, Shiravand et al., 2022). A summary of trials involving checkpoint blockade can be seen in Table 1. Many patients experience immune-related adverse events and as such it is important for biomarkers to be established in order to indicate who will benefit from this treatment and to expand its therapeutic reach so further patients can benefit.

Table 1: FDA approved checkpoint inhibitor drugs

Product	Target	Year	Cancers (not comprehensive)
YERVOY (Ipilimumab)	CTLA-4	2011	Melanoma, RCC, CRC, NSCLC
KEYTRUDA (Pembrolizumab)	PD-1	2014	Melanoma, NSCLC, CRC, EC
OPDIVO (Nivolumab)	PD-1	2014	Melanoma, NSCLC, CRC, EC
TECENTRIQ (Atezolizumab)	PD-L1	2016	UC, NSCLC, HCC, melanoma
BAVENCIO (Avelumab)	PD-L1	2017	MCC, UC, RCC
IMFINZI (Durvalumab)	PD-L1	2017	UC. NSCLC, BTC
LIBTAYO (Cemiplimab)	PD-1	2018	SCC, BCC, NSCLC
JEMPERLI (Dostarlimab)	PD-1	2021	dMMR, EMC
OPDUALAG (Nivolumab and Relatlimab)	PD-1 & LAG-3	2022	Melanoma

FDA approved checkpoint inhibitors up to 2023 with their commercial name, target, year of first trials and examples of cancers they have been trialled in.

Key: RCC- renal cell carcinoma, CRC- colorectal cancer, NSCLC- non-small cell lung cancer, EC- oesophageal cancer, BTC- biliary tract cancer, UC- urothelial carcinoma, MCC- Merkel cell carcinoma, EMC- endometrial carcinoma

Table adapted from (Sun et al., 2023).

Pembrolizumab, a humanized IgG4κ monoclonal antibody targeting PD-1, is approved for treatment of several solid tumours. It blocks the PD-1/PD-L1 pathway by binding to the PD-1 receptor, inhibiting TCR/CD28 signalling, thereby restoring T-cell anti-tumour responses (Ai et al., 2020). This drug has been approved by the FDA for adult and paediatric patients with tumour mutational burden-high unresectable or metastatic tumours. In the UK this is now standard of care for non-small cell lung carcinoma (NSLC) patients with a tumour proportion score of over 50% (Marcus et al., 2021, Middleton et al., 2020). With a half-life of 26 days regardless of age or gender, Pembrolizumab demonstrated a 19.4% overall response rate in the KEYNOTE-001 trial in patients with NSCLC, with a median overall survival (OS) of 12 months (Dang et al., 2016).

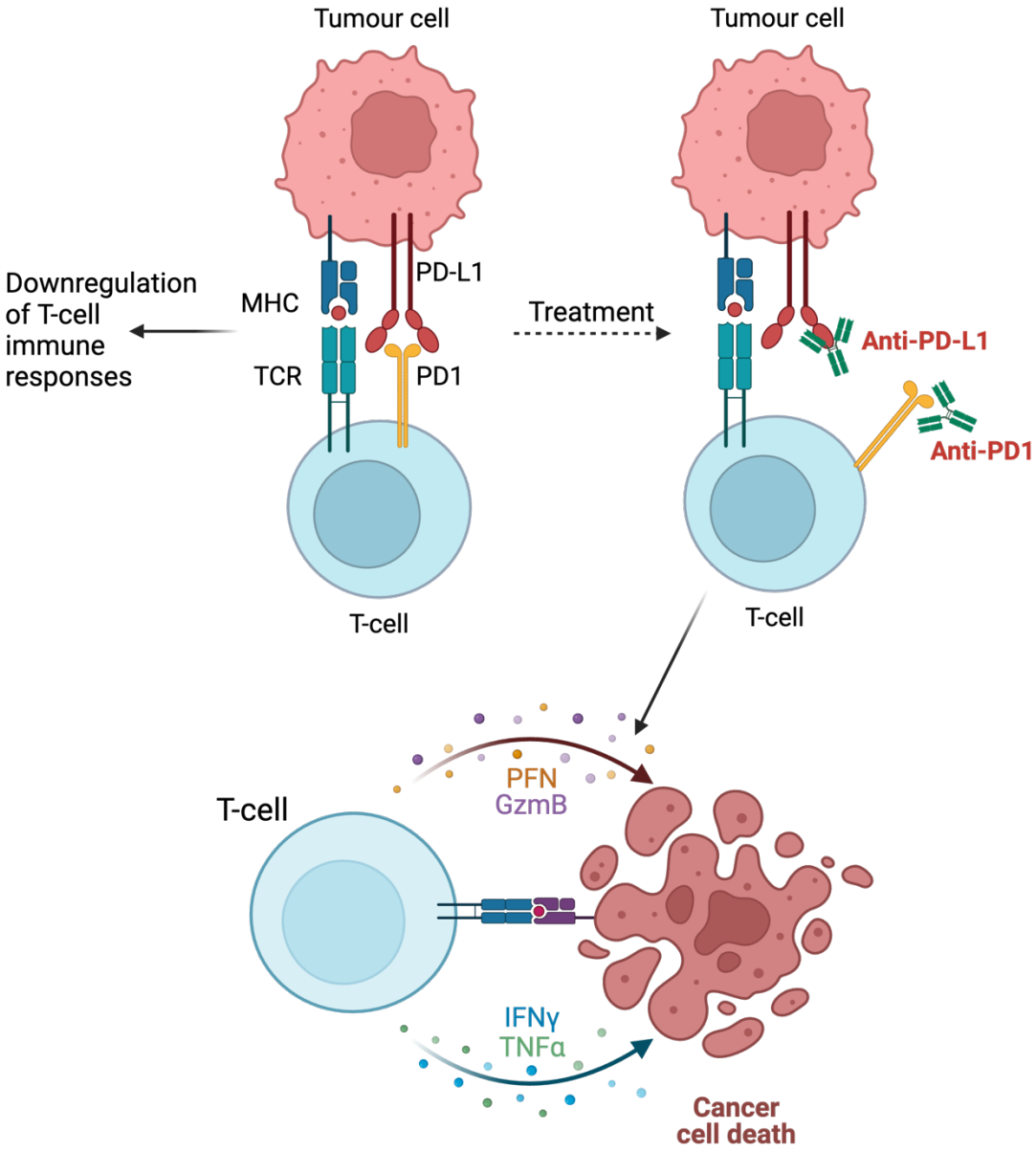

Figure 6: PD1 and PDL1 blockade

Activated T-cell will upregulate the expression of PD-1. As PD1 binds to it's ligand PD-L1 or PD-L2, found on the surface of tumour cells, downstream TCR signalling will be inhibited leading to downregulation of T-cell activity. Upon treatment with an anti-PD1 or anti-PDL1 blockade, the antibody binds to the respective protein and reinvigorates exhausted T-cells, increasing the T-cell activity, resulting in cancer cell death. Figure created with Biorender.com.

One population of cells which are proving to be important in the success of checkpoint blockade is the aforementioned $TCF1^+$ cells. These cells maintain proliferative capacity and give rise to more differentiated exhausted T-cells. As such, these cells have been termed progenitor or precursors of exhausted T-cells (T_{PEX}). Despite exhibiting features of exhaustion such as increased PD1 expression and impaired cytokine production, it has been found that these cells, with their proliferative capacity, are vital in the therapeutic success of PD1/PDL-1 inhibition. The presence of T_{PEX} cells in tumours has been correlated with better responses to immunotherapy, as literature suggests they are responsible for the proliferative burst post anti-PD1/PDL1 therapy, which leads to the generation of functional effector cells. This highlights their importance in the overall immune landscape of cancer (Im et al., 2016, He et al., 2016, Kallies et al., 2020).

Whilst recent studies have shown that checkpoint blockade therapies, particularly ones targeting the PD1/PDL-1 pathway, have become integral in the standard of care for various cancers, their effectiveness varies. The treatment offers significant promise however their application must be tailored to individual patient needs, and ongoing research is essential to optimise their use and manage associated risks effectively.

Chronic antigen exposure caused by the presence of tumours or chronic viral infections can lead to an upregulation of these checkpoints and promote a state of T-cell differentiation that severely limits its ability to carry out its effector functions.

In contrast, certain chronic infections, such as CMV or EBV, exhibit a distinct lack of T-cell exhaustion despite persistent antigen exposure. Notably, CMV expression is characterised by a robust expansion of $CD8^+$ and $CD4^+$ T-cell populations during latent phases, resulting in

expanded populations in the peripheral tissue (Tovar-Salazar and Weinberg, 2020). Given the prevalence and immunogenicity of CMV, it serves as an ideal model for studying the dynamics and characteristics of antigen specific T-cells and tumour infiltrating lymphocytes (TILs).

1.3 Immunity against herpesviruses

1.3.1 Cytomegalovirus

1.3.1.1 The Lifecycle of CMV

Cytomegalovirus (CMV), a β-herpesvirus, infects a significant portion of the population (40-90%), and infection prevalence is dependent on age, geographical and socioeconomic status. The virus establishes lifelong latent infection due to its ability to evade the immune system.

CMV infection occurs when the virus comes into contact with a mucosal surface, allowing it to spread within the host (Zanghellini et al., 1999). It establishes life-long latency and undergoes periodic reactivation, resulting in lytic viral replication (Cohen, 2020). As a virus, it exhibits remarkably high species-specificity, a characteristic that has evolved over time through long-term co-evolution and adaptation to its host. Comparison of the human CMV (HCMV) genome with those of non-human primate- cytomegaloviruses has revealed that duplication and gene copy number variation of non-core genes were frequently observed during CMV evolution, likely playing a significant role in allowing the virus to better exploit and adapt to its specific host environment (Mozzi et al., 2020). Although CMV infection is generally asymptomatic, in immunocompromised individuals the virus can cause significant clinical problems, for example in transplant recipients or HIV/AIDS patients CMV can be the cause of life-threatening disease (Sager et al., 2015).

The complex structure of a CMV virion is typical of herpesviruses and has four main components: the core, capsid, tegument and envelope (Figure 7). The nucleocapsid contains the core in which there is the linear double stranded DNA genome of approximately 230 kilobase pairs, therefore, CMV has the largest genome of human herpesviruses (Dolan et al., 2004). Between the envelope, which is a cellularly derived lipid membrane containing viral glycoproteins, and the nucleocapsid, there is a protein layer called the tegument (Kalejta, 2008).

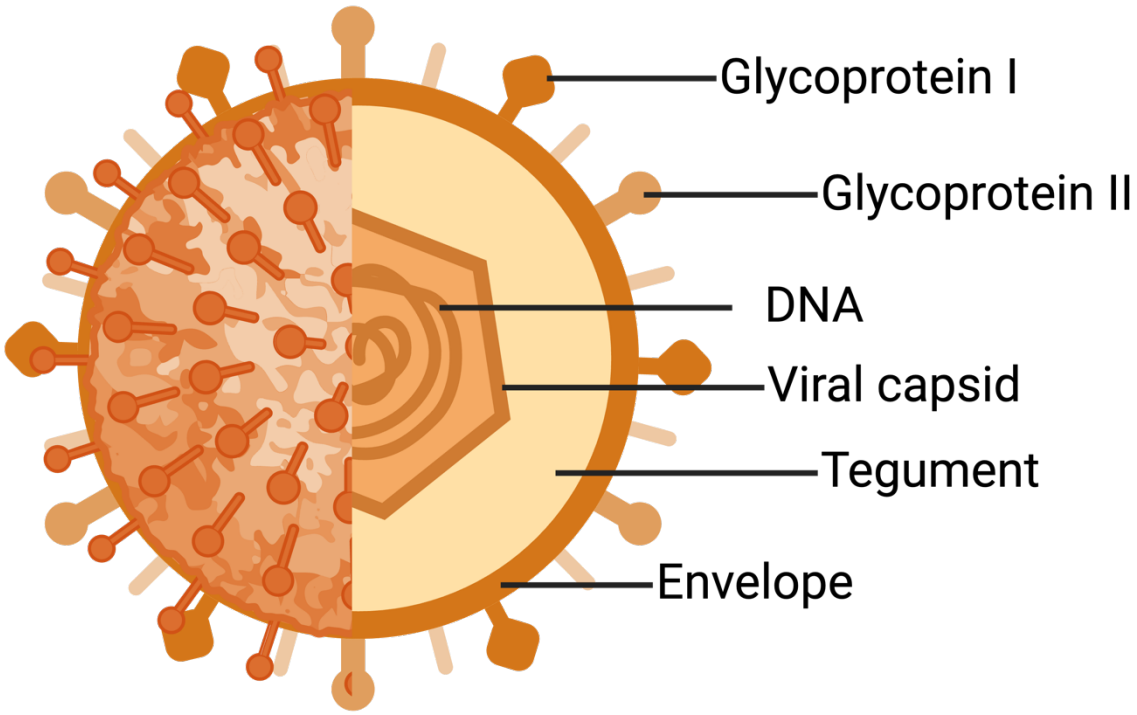

Figure 7: The structure of human cytomegalovirus

Representation of CMV virion. Virions contain a double-stranded DNA genome enclosed within a viral capsid. This is surrounded by the tegument and coated by an envelope which presents glycoproteins. Created with Biorender.com.

CMV encodes 166 viral genes and can undergo lytic and latent phases of survival and replication. CMV can infect host cells by binding to cellular receptors and fusing with the cell membrane in order to facilitate entry, mediated by glycoproteins in the viral envelope. The glycoprotein gB binds epidermal growth factor receptor (EGFR) or platelet-derived growth factor receptor α (PDGFRα) and the glycoprotein gH binds integrin β1 to induce cellular

signalling required for entry of CMV into monocytes (Mahmud et al., 2020). This releases the DNA-containing capsid, and the tegument proteins into the cell (Ye et al., 2020).

The outcome of CMV infection depends on the expression of the immediate-early (IE) genes. The IE genes are vital for progression into the early phase of the lytic cycle, leading to the replication of viral DNA (Kalejta, 2008). Two of the most abundant IE proteins are IE1, a 71-kDa protein encoded by UL123, and IE2, an 86-kDa protein encoded by UL122 (Nevels et al., 2004). The IE1 protein is expressed at the onset of infection and is necessary for early gene expression whilst also antagonising the host's antiviral responses, including upregulating pro-inflammatory and immune stimulatory genes, typically induced by IFNγ signalling. Cells which express IE1 have also been shown to repress the hosts defences by downregulating cytokines such as IL6 (Knoblach et al., 2011, Adamson and Nevels, 2020). It has also been associated with condensed chromatin during mitosis, with this first being described over 30 years ago (Lafemina et al., 1989). Subsequent research elucidated that this happens via the IE1 protein attaching to mitotic chromosomes through a chromatin tethering domain at the carboxy terminus. (Mücke et al., 2014). This promotes the transcription of viral genes and disrupts antiviral defences. Unlike IE1, IE2 binds with DNA. It also interacts with histones and histone-associated proteins. By directly binding to the promoters of early CMV genes, it enhances their transcription and ensures the progression of the viral life cycle (Adamson and Nevels, 2020). Together, IE1 and IE2 are essential for overcoming host antiviral defences, activating viral gene expression, and ensuring the successful replication and persistence of CMV within the host.

One protein which is abundant throughout CMV infection is the lower matrix protein 65 (pp65), encoded by the gene UL83 (Biolatti et al., 2018). This major tegument protein is a

structural protein that is widely recognised as the immune-dominant target of the $CD8^+$ T-cell response against CMV making it a significant focus of CMV research (Hyun et al., 2017). pp65 is responsible for modulating both the innate and adaptive host immune responses during CMV infection (Tomtishen, 2012). It not only prevents immediate-early proteins from being recognised by components of the immune system, by blocking their presentation to MHC class I molecules, but disrupts the host cell immune response via mechanisms such as downregulation of HLA-DR, impairment of IFN-β release, and interference with signalling pathways such as cGAS/STRING (Odeberg et al., 2003, Biolatti et al., 2018, Tomtishen, 2012).

The pp50 protein, also known as UL44, is predominantly found in the nucleus. This non-structural phosphoprotein is an accessory protein which acts as a processivity factor for DNA polymerase by binding with high affinity to DNA and stimulating long-chain DNA synthesis (Loregian et al., 2004, Sinigalia et al., 2008).

Once DNA replication has occurred, viral late genes are expressed. These proteins are primarily structural components of the virion, playing crucial roles in the assembly and egress of new viral particles. During the latent phase, viral gene expression is minimised to evade immune detection, and no viral progeny are released. This is regulated by the viral major immediate early promoter (MIEP), with suppression of the MIEP required for latency. Furthermore, the viral genes US28, UL138 and viral IL-10 have been identified during latent infection (Poole et al., 2023). However, CMV infections periodically reactivate, transitioning into the lytic phases where viral reactivation and spread can occur once again (Kalejta, 2008).

Once in the latent phase, CMV persists in a dormant state within the host's monocytes, myeloid progenitors or endothelial cells, evading immune detection. Reactivation can occur

in states of immunosuppression, leading to recurrent infection. The ability of CMV to switch between the lytic and latent phases ensures its persistence and lifelong infection in the host (Dupont and Reeves, 2016).

1.3.1.2 The immune response to CMV

CMV is one of the most immunogenic human pathogens, engaging both the innate and adaptive immune responses. Upon infection, CMV triggers the release of inflammatory cytokines and the production of neutralising antibodies, which help to control the viral spread. The antibodies are specific for a variety of CMV proteins including structural proteins such as pp65 and non-structural proteins such as IE1 (Jackson et al., 2011).

The virus also activates NK cells, which play a crucial role in the early defence by targeting infected cells. Moreover, the adaptive immune system responds vigorously, with CMV-specific $CD4^+$ and, in particular, $CD8^+$ T-cells becoming highly activated and often dominating the T-cell repertoire in infected individuals (Klenerman and Oxenius, 2016).

CMV employs a variety of strategies to evade the immune system, dedicating a significant portion of its genome to immune modulation. One such mechanism is interfering with MHC-I presentation, with CMV genes such as US2, US3, US6, and US11 causing a decrease in CMV antigen presentation to $CD8^+$ T-cells (Hanley and Bollard, 2014). However, this can leave the virus vulnerable to detection by NKs due to “missing self” recognition. Therefore, the virus can suppress the NK response using genes such as UL18 which mimics the MHC-I molecule on the cell surface, triggering the NK cell inhibitory receptors, or UL40 which stabilises HLA-E

expression on the cell surface (Forrest et al., 2020). Amongst others, these tactics are critical for the virus to establish lifelong latency.

1.3.1.3 CMV in cancer

While CMV infection has been associated with the development of some cancer subtypes such as glioblastoma and nasopharyngeal carcinoma, there is conflicting evidence regarding its role in the pathogenesis of malignant disease. Indeed, it is unclear whether CMV contributes to cancer development or if it is simply reactivated due to the immunosuppressive cancer microenvironment (Yu et al., 2023, Mitchell et al., 2008).

There is also conflicting literature regarding the presence of CMV in tumours with some studies being able to detect CMV DNA in tumours and others not. The data supporting the presence of CMV in glioblastoma is particularly controversial. For example, one study using immunohistochemistry (IHC) in order to detect the pp65 and IE1 proteins, and in-situ hybridization (ISH) to detect CMV nucleic acids, detected the presence of IE1 in 27/27 of malignant glioma samples and was able to identify CMV DNA in the tumours (Cobbs et al., 2002). This is supported with several other studies who have also been able to detect CMV within glioblastoma samples using similar methods (Scheurer et al., 2008, Mitchell et al., 2008). However, there are also studies who have failed to detect CMV with one study detecting CMV-positive cells by IHC in only 9/81 glioblastoma cases and very little detection of IE1 in tumour cells (Sabatier et al., 2005). Again, this is supported with several other studies failing to readily detect CMV in brain tumours (Lau et al., 2005, Poltermann et al., 2006). Furthermore, viral detection was observed a much lower rate in lower grade tumours which could also contribute to the conflicting evidence (Scheurer et al., 2008, Cobbs et al., 2002).

There was also the use of different methodological approaches with studies emphasising that the sample preparation and detection techniques need to be optimised to adjust for low level infections (Dziurzynski et al., 2012).

The virus has also been investigated in other tumours. Baryawno, N. *et al* (2011) investigated the presence of CMV in medulloblastoma using immunohistochemistry (IHC) and in-situ hybridization and detected 92% of primary samples expressed IE proteins, with 73% expressing late proteins. This was then confirmed with the detection of CMV DNA in medulloblastoma cell lines (Baryawno et al., 2011).

1.3.2 Epstein-Barr Virus

Epstein-Barr Virus (EBV) is also a member of the herpesvirus family and is widely prevalent, infecting more than 90% of the global population. EBV establishes lifelong latency in B-cells (Yu and Robertson, 2023) and during this latent phase the virus persists in a dormant state with minimal gene expression, evading the immune system. Periodically the virus can reactivate, transitioning into the lytic phase where it replicates actively and produces viral particles that can infect other cells. The lytic phase involves the expression of early, intermediate and late genes, leading to the production of viral proteins necessary for replication, assembly and release of new virions. This sophisticated life cycle allows it to evade the immune system and persist within the host undetected for such a long period of time (Murata, 2014, Young and Rickinson, 2004).

There are several key proteins involved in the lytic cycle of EBV. BHRF1 helps the virus to evade apoptosis, BALF4 and BALF5 play a role in the replication of viral DNA and BZLF1 and BRLF1 are IE proteins which activate lytic gene expression, switching the virus from latent to lytic

state (Dorothea et al., 2023). In the latent phase, EBNA1 and EBNA2 are involved in ensuring the viral episome is maintained and replicated in the host nucleus during cell division and also help to promote proliferation. EBNA3A, EBNA3B and EBNA3C help to regulate viral gene expression and assist in immune evasion whilst LMP1, LMP2A and LMP2B promote B-cell proliferation and survival via signalling pathways. During this phase, the virus does not produce new virions, allowing it to persist in the host for a lifetime (Damania et al., 2022, Dorothea et al., 2023).

Unlike CMV, EBV is an oncogenic virus, known to be implicated in the pathogenesis of several cancers, as well as other non-malignant diseases such as infectious mononucleosis (Zanella et al., 2019). It was initially discovered in Burkitt lymphoma, however is now associated with a variety of other malignancies including nasopharyngeal carcinoma and post-transplant lymphoproliferative diseases (Smatti et al., 2018, Thompson and Kurzrock, 2004). The presence of EBV DNA has been shown to be present in Burkitt's lymphoma and EBV nucleic acids found to be present in nasopharyngeal carcinoma (Yu and Robertson, 2023).

1.3.3 The CMV-specific T-cell response

Virus-specific T-cells play a crucial role in controlling viral infections by recognising viral peptides presented by MHC molecules, leading to elimination of infected cells. Research has highlighted the importance of these T-cells in chronic infections, such as CMV and EBV, where they contribute to immune surveillance and long-term viral control (Schmidt et al., 2023).

Upon stimulation of the TCR, naïve T-cells proliferate and differentiate into activated effector cells. Following elimination of the target cells, a small portion of antigen-experienced T-cells will differentiate into a heterogenous memory T-cell population (Mahnke et al., 2013).

Unlike typical viral infections where memory T-cell populations stabilise post-infection, CMV drives a continuous accumulation of these cells, this leads to one of the hallmarks of the virus, memory inflation. This refers to the phenomenon where the CD8 and CD4 T-cell subsets undergo a sustained expansion in response to CMV antigens over time, leading to expanded populations of CMV-specific T-cells in the peripheral blood. As this increases over time it can be particularly observed in the elderly with up to 20% of their total T-cell repertoire being specific for CMV, and in particular the pp65 protein (Kim et al., 2015, Karrer et al., 2003, Khan et al., 2002). This effect is due to the ability of CMV to establish lifelong infection with periodic reactivation, continuously stimulating the immune system and resulting in functional memory T-cells dominating the T-cell repertoire. This effect is mainly seen in the CD8 repertoire, although has been observed to a lesser extent in the CD4 T-cell compartment (Kim et al., 2015).

CMV-specific T-cells often display markers of effector memory EMRA T-cells, along with other characteristics of T-cell maturation including downregulation of the co-receptors CD27 and CD28 and upregulation of CD57 and KLRG1. Whilst displaying markers of maturation and indicating highly differentiated T-cells, they do not express markers of exhaustion but retain functionality and produce Granzyme B and perforin (Appay et al., 2002, Klenerman and Oxenius, 2016).

However, CMV-specific T-cells do display a range of varied phenotypes, including $CD103^{+}CD69^{+}$ tissue resident memory (T^{RM}) populations within tissue (Klenerman and Oxenius, 2016).

Two of the most common immunodominant targets recognised by CMV-specific $CD8^+$ T-cells are epitopes from the pp65 and IE1 proteins. The pp65 protein, a major tegument protein, is particularly immunodominant and is targeted by a large portion of the CMV-specific $CD8^+$ T-cell population (Sylwester et al., 2005, García-Ríos et al., 2021). The antigen specificity of these $CD8^+$ T-cells is determined by the peptide sequences presented by the MHC class I molecules on the surface of infected cells. The specificity and effectiveness of these T-cells are also influenced by the host HLA type, as this determines the repertoire of CMV peptides that can be presented and recognised by the immune system (Jackson et al., 2014, Sylwester et al., 2005). For this reason, part of this study looks at epitope-specific T-cell responses in order to elucidate if there are any differences between the different T-cell epitopes present amongst the most common HLA types.

1.3.4 PD-1 on viral specific T-cells

Parry, H. *et al.* conducted an extensive analysis of PD-1 on CMV-specific CD4+ T-cells during latent infection, revealing a wide variability in expression levels among patients (ranging from 10-85%). Interestingly, this expression level was not linked to the activation or exhaustion state of the cell, but rather correlated with the viral load at the time of infection, remaining stable over time. PD-1 emerged as the most commonly expressed checkpoint, with 60% of $tetramer^+$ cells expressing PD-1 exclusively (Parry et al., 2021). Whilst there are few studies into the phenotype and functionality of CMV-specific T-cells in cancer, there are several studies investigating other viral-specific T-cells including human papillomavirus (HPV) and LCMV. Interestingly, studies have found that the expression of inhibitory receptors on other viral-specific T-cells, such as those against hepatitis B virus (HBV) and hepatitis C virus (HCV),

is higher than that specific for CMV, indicating they may play a different function in the immune control of these viruses (van den Berg et al., 2019, Sauce et al., 2007).

Some studies have started to characterise the expression of PD1 on $CD8^+$ CMV-specific T-cells, often using them as controls in research focussing on other viruses. However, those that have examined PD-1 expression levels on CD8 T-cells have reported a wide variation in relative expression, ranging from 0.44%-65.4% in one study, with expression decreasing with age, and from 15.9-87% in another (Hosie et al., 2017, Dirks et al., 2013). High PD-1 expression on $CD8^+$ CMV-specific T-cells has been associated with reduced cytokine release, whilst PD-1 blockade restored expression of some cytokines (IL2, IFNγ and TNFα) on cells with high PD-1 expression, but had no effect on those with PD-1 low expression (Dirks et al., 2013). PD-1 expression on CMV-specific T-cells has also been used as a control in comparing levels to other viral-specific T-cells, revealing lower median PD-1 expression on $CD8^+$ CMV-specific T-cells (median of 49%), compared to HIV-specific T-cells (median of 67%), and similar findings were observed when comparing CMV-specific T-cells (0-40% PD-1 expression) to HCV-specific T-cells which expressed significantly more PD-1 (Gabriele et al., 2012, Pettersen et al., 2010).

Studies have also shown expression of other checkpoints on CMV-specific T-cells, including TIGIT (Chauvin et al., 2015a), 2B4 (Buggert et al., 2014), LAG3 and TIM3 (Ogando-Rivas et al., 2022). Similarly to PD1, some of these checkpoints are expressed at lower levels on CMV-specific T-cells compared to other virus-specific populations such as those specific for EBV, flu and HIV (Hertoghs et al., 2010, Sauce et al., 2007, Buggert et al., 2014, Schmidt et al., 2023). However, there is limited research focusing on concurrent expression of multiple checkpoints,

along with other phenotypic markers, in order to comprehensively phenotype and understand the function of these cells.

It has been established in the literature that viral specific T-cells can proliferate after PD1 blockade. In lymphocytic choriomeningitis (LCMV)-infected mice, dextramer-specific T-cells increase post PD-1 blockade, and are associated with a trend towards enhanced IFN-γ production following peptide stimulation, indicating heightened LCMV-specific T-cell responses. Moreover, the LCMV-infected mice treated with anti-PD-1 therapy exhibited reduced viral loads compared to the untreated group, suggesting reinvigoration of LCMV-specific CD8+ T-cells by the treatment (Klein et al., 2020). The reactivation of viral specific T-cells in response to checkpoint blockade has also been demonstrated in people living with HIV, where latent infection poses a challenge to treatment efficacy due to minimal antigen expression. PD-1 is upregulated on T-cells in HIV-positive individuals and a study has indicated that anti-PD-1 therapy reverses HIV-infected cell latency, suggesting that combining this therapy with the current anti-retroviral therapy may be beneficial (Uldrick et al., 2022). Whilst these findings suggest that the blockade “removes the brakes” from these cells, it could also be hypothesised that the positive outcome of this therapy stems from the proliferation of a stem-like pool of cells, which further differentiate into effector cells, rather than solely reactivating previously “exhausted” cells.

CMV reactivation commonly occurs during periods of immunosuppression, such as after transplantation or during other viral infections, and can lead to tissue-invasive diseases such as hepatitis and colitis. A previous study investigating anti-PD-1 therapy in metastatic melanoma found that CMV reactivation post combined PD1 and CTLA4 therapy resulted in

hepatitis in CMV-seropositive patients. This CMV reactivation suggests that PD1 inhibition may downregulate PD1 on CMV-specific T-cells, allowing these cells to regain function from a previously latent state. It was found that high levels of CD4 effector memory T-cell expansion before therapy, particularly in patients with high CMV titres, was predictive of this effect (Hutchinson et al., 2021). Whilst this study did not extensively phenotype CMV-specific T-cells, the current study aims to conduct a more detailed analysis to explore whether co-expression of other markers with PD-1 could indicate the function of the cells, which could provide useful in the consideration of therapeutic outcomes.

1.3.5 Bystander T-cells in TILs

Whilst cancer specific TILs play a central role in immunotherapies, there is emerging evidence that 'bystander' TILs, which do not target cancer-related antigens, are also present within the tumour microenvironment, although their function is not completely understood. This subset of T-cells are specific for unrelated epitopes such as viruses. Simoni, *et al.* carried out a study investigating T-cell specificity in colorectal and lung cancer patients and identified $CD8^+$ TILs specific for CMV, EBV and influenza epitopes. Using mass cytometry (CyTOF) technology, they carried out in-depth phenotyping of these cells and identified that these 'bystander' TILs possessed diverse phenotypes which possess similarities with tumour-specific cells, however notably, do not express CD39. (Simoni et al., 2018). Further work by the same group included in-depth phenotyping of CMV specific CD4+ cells and found these to also lack the exhaustion marker, CD39 (Li et al., 2022).

The presence of virus specific T-cells in the blood has been found to be predictive of the same population being present in tumours such as ovarian cancer, breast cancer and head and neck

cancer. Importantly, within tumour tissues, these T-cells have been shown to express varying levels of the tissue resident T-cell markers CD103 and CD69, suggesting that at least some of these cells are not transiently passing through the tumours, but rather residing within them. This is in contract to tumour specific T-cells, whereby most of the T-cells display a $CD69^+$ $CD103^+$ phenotype (Rosato et al., 2019, Simoni et al., 2018). These studies consistently highlight that a variety of human cancers contain virus specific $CD8^+$ T-cells.

Research has indicated that the frequency of $CD103^+$ $CD8^+$ TILs correlate positively with favourable outcomes in several tumour times, including lung and ovarian cancer (Djenidi et al., 2015, Ganesan et al., 2017, Webb et al., 2014). Since a subset of virus specific T-cells have been shown to express CD103, and CMV-specific T-cells can contribute a significant proportion of the $CD8^+$ T-cell compartment, the presence of viral-specific T-cells within the TME could potentially confer favourable clinical outcomes.

1.3.6 Viral peptide-based vaccines

Antigen-based therapies, such as those targeting neoantigens, often face challenges due to the low density of antigen presentation on MHC-I complexes. This can make treatment less effective, as it may not be sufficient to elicit a strong immune response (Nobuoka et al., 2013). In contract, virus specific $CD8^+$ T-cells, particularly those targeting well-characterised peptides such as those from CMV, are highly immunogenic. This reduces the need for the sequencing and personalisation required in neoantigen based approaches, meaning they are a promising target for offering more consistent treatment options.

Research has shown that reactivating virus-specific T-cells within tumours can significantly impact the growth of tumours. For instance, Rosato *et al.* (2019) demonstrated that

intertumoral injection of viral peptides in combination with checkpoint blockade in mouse models led to the complete eradication of melanoma tumours in 34% of cases. This is due to the fact that the expression of PD-L1 is induced after peptide therapy, leading to the PD1 blockade being more effective (Rosato et al., 2019). Similarly, Nobuoka *et al.* (2013), found that injecting the CMV NLVPMVATV peptide into tumours resulted in robust CTL responses against peptide-loaded cells. This response was effective even in tumours that did not naturally express the antigen, as the intratumoral injections enhanced the loading of additional peptides onto MHC-I complexes, improving tumour recognition by antigen-specific CTLs (Nobuoka et al., 2013).

These findings suggest that viral peptide-based therapies could enhance the efficacy of immunotherapies, particularly in cases where tumour antigens are scarce or not adequately or not adequately recognised by the immune system.

1.3.7 Harnessing viral-specific T-cells in cancer

A major limitation of CAR-T-cell therapy lies in its ability to infiltrate solid tumours. Therefore, the capacity of these bystander cells to penetrate tumours could be informative, or exploited, in order to enhance therapy effectiveness. This highlights the potential of leveraging viral specific T-cells as a therapeutic strategy, particularly in tumours resistant to conventional treatments. Further research into the mechanisms underlying the tumour-killing activity of virus-specific T-cells holds promise for advancing cancer immunotherapy.

Conversely, a recent study examining the T-cell repertoire in lung cancer patients revealed contrasting findings. It found that patients with a higher proportion of viral-specific T-cells in the lung experience poorer treatment outcomes compared to those with a more focussed T-

cell repertoire targeting the tumour (Reuben et al., 2020). This highlights the complex interplay between different T-cell populations within the TME and underscores the need for further investigation to elucidate their precise roles in cancer progression and treatment response.

Given the challenges associated with studying TAA and neoantigen-specific TILs, due to their potential rarity or uniqueness to the individual, investigating viral antigen specific T-cells presents a promising alternative for understanding TIL function within the TME. Viruses such as CMV and EBV, which are highly immunogenic, offer valuable opportunities for such investigations, with CMV eliciting particularly robust immune responses. These virus-specific TILs could not only provide insight into the behaviour of TILs in general, but also serve as a model for studying TILs exposed to chronic antigen stimulation, in a way similar to tumour specific TILs. Therefore, these viral antigen-specific T-cells can significantly enhance our understanding of TIL dynamics and function within the TME.

Furthermore, studying these T-cell populations could provide insights into potential immune-related side effects associated with CMV reactivation. By identifying specific T-cell subsets it may be possible to gain information about which patients are more likely to experience side effects. This knowledge can inform personalized treatment strategies, minimizing adverse reactions and improving overall patient outcomes. Therefore, understanding the behaviour and function of bystander TILs holds promise for refining cancer therapies and optimising patient care.

1.4 Aims and objectives

CMV-specific T-cells have been identified within the tumour microenvironment, yet their presence, comprehensive phenotype and potential therapeutic role in cancer treatment remain poorly understood. Whilst PD1 is expressed on a substantial proportion of CMV-specific T-cells, the phenotypic and functional correlates of this, within blood and tissue, have not been identified. PD1 is a negative regulator of T-cell function and antibodies that block PD1 are highly effective in cancer immunotherapy. Therefore, this project hypothesises that PD1 expression on CMV-specific $CD8^+$ T-cells would act as a negative regulator of T-cell function following engagement with PDL1/2, and that the phenotype of $PD1^+$ cells would show differential features between blood and tissue. Given the limited research surrounding PD1 on CMV^+ $CD8^+$ T-cells, this project aims to address this gap by:

1) Analysing the extensive phenotype of checkpoint expression on CMV- and EBV-specific $CD8^+$ T-cells in healthy donors using high-dimensional flow cytometry.

2) In depth characterisation of the expression of checkpoint proteins on viral-specific T-cells in ovarian cancer.

3) Determination of how systemic treatment with anti-PD1 therapy affects the phenotype and function of antigen specific T-cells in patients with cancer, using CMV as a model.

These findings have the potential to increase understanding of the physiological role of checkpoint protein expression on virus-specific T-cells. Furthermore, they may provide insight into the relative impact of the suppressive immune environment within tumours on the phenotype of virus-specific cells and reveal the relative potential of PD-1 blockade therapy to modulate antigen-specific T-cell populations in relation to prior phenotypic profile.

CHAPTER 2: MATERIALS AND METHODS

2.1 Materials and reagents

2.1.1 Materials

The materials used in this study are outlined in Table 2, the kits used in this study are outlined in Table 3.

Table 2: A list of materials used in this study

Materials	Manufacturer	Catalogue Number
BD heparin vacutainer tubes	BD Biosciences	202605
0.5ml microcentrifuge tubes	Sarstedt, Inc. Fisher Scientific	72.699
1.5ml microcentrifuge tubes	Sarstedt, Inc. Fisher Scientific	72.690
1ml Cryovial	Nunc, Thermo Fisher Scientific	347597K
1.8ml Cryovials	Nunc, Thermo Fisher Scientific	375418K
15ml falcon tubes	Sarstedt, Inc. Fisher Scientific	62.554.502
50ml conical tubes	Sarstedt, Inc. Fisher Scientific	62.547.254
Haemocytometer	Biosigma S.R.L	BVS100
Mr. Frosty™ Freezing Container	Thermo Fisher Scientific	5100-0001
MAXISORP ELISA plate	Nunc, Thermo Fisher Scientific	439454
Multiwell plates (6, 12, 24 and 48 wells)	Corning, Sigma-Aldrich	3516, 3513, 3526, 3548
96 well round bottom microtitre plates	Thermo Fisher Scientific	249570
96-well round bottom tissue-culture treated plate with lid	Corning, Sigma-Aldrich	3799
96 well V-bottom microtitre plates	Corning, Sigma-Aldrich	249570
Reagent reservoir	Corning, Sigma-Aldrich	4870
5mL polystyrene FACS tubes	Corning, Sigma-Aldrich	352054

5mL polystyrene FACS tubes with cell strainer cap	Corning, Sigma-Aldrich	352235
Tissue culture flasks (25, 75 and 150 cm)	Corning, Sigma-Aldrich	430168
gentleMACS C Tubes	Miltenyi Biotec	130-093-237
MACS SmartStrainers (70µm)	Miltenyi Biotec	130-098-463

Table 3: A list of kits used in this study

Kits	Manufacturer	Catalogue Number
DNeasy Blood & Tissue Kit (50)	Qiagen	69504
Human FoxP3 buffer set	BD Biosciences	560098
Human anti-cytomegalovirus IgG ELISA kit	Abcam	AB108724
Human Anti-Epstein Barr Virus Nuclear Antigen 1 (EBNA-1) IgG ELISA Kit	Alpha Diagnostic International	510-205-HEG
CD8/NK LEGENDplex™	BioLegend	741187
EasySep™ Human CD8 Enrichment Kit	Stemcell Technologies	19053
PECy5 Lightning-Link Conjugation Kit	Abcam	ab102893
Human Tumour Dissociation Kit	Miltenyi Biotec	130-095-929

2.1.2 Buffers and Reagents

The reagents used in this study are outlined in Table 4. The culture media and individual components are listed in Table 5. Buffers and components are listed in Table 6 and cell lines used are listed in Table 7.

Table 4: A list of reagents used in this study

Reagent	Manufacturer	Catalogue Number
1X Phosphate-buffered saline (PBS)	Gibco, Thermo Fisher Scientific	14190-094
Roswell Park Memorial Institute 1640 (RPMI)	Gibco, Thermo Fisher Scientific	21875-034
Fetal calf serum (FCS)	Gibco, Thermo Fisher Scientific	10500-064
Penicillin/Streptomycin (P/S)	Sigma-Aldrich	P4458
3% Acetic Acid with Methylene Blue	StemCell Technologies	07060
Saponin	Sigma-Aldrich	SAE0073-25G
Human Serum (HS)	Sigma-Aldrich	H3667
Lymphoprep	StemCell Technologies	07851
Dimethyl Sulfoxide (DMSO)	Sigma-Aldrich	D2650-100ML
BioTAQ DNA polymerase	Bioline	BIO-21060
100bp ladder	Life Technologies	15628019
SYBR Safe	Invitrogen, Thermo Fisher Scientific	533102
Nuclease-free water	New England Biolabs	B1500S

Carbonate bicarbonate coating buffer	Sigma-Aldrich	C3041-100CAP
Tween 20	Sigma-Aldrich	P9416-100ML
Bovine Serum Albumin (BSA)	Merck, Sigma-Aldrich	AF906
IgG-HRP conjugate	Southern Biotech	2040-05
IFNγ monoclonal antibody, biotin	Invitrogen, Thermo Fisher Scientific	M701B
IFNγ monoclonal antibody	Invitrogen, Thermo Fisher Scientific	M700A
ExtrAvidin peroxidase	Sgima-Aldrich	EZ886
TMB substrate	Thermo Fisher Scientific	34029
Hydrochloric Acid (HCl) 6M	Thermo Fisher Scientific	11915506
EDTA	PluriSelect	60-00030-12
Fixation Buffer	Invitrogen	FB001
TNFα Processing Inhibitor 0 (TAPI-0)	Sigma-Aldrich	51017
Pan-select peptides	JPT	54347
Peptides	Peptide 2.0	
Cell Stimulation Cocktail (50X)	eBioscience, Invitrogen	00-4970-93
Benzonase	Sigma-Aldrich	E1014-25KU
Red Blood Cell Lysis Solution (10X)	Miltenyi Biotec	130-094-183
Pembrolizumab	Medchem Express	HY-P9902
Agarose	Bioline	BIO-41026

Table 5: A list of culture media and individual components used in this study

Culture Media	Components
R10	RPMI- 1640 10% Fetal Calf Serum (FCS) 1% Penicillin/streptomycin
Freezing medium	FCS 10% Dimethyl sulfoxide (DMSO)
Polyclonal T-cell culture medium	R10 (as above: RPMI + 10% FCS + 1% PS) 1% Human Serum 10,000 IU/ml IL-2

Table 6: A list of buffers and individual components used in this study

Buffer	Components
Wash Buffer	PBS 0.1% Tween® 20
Carbonate coating buffer (0.05M)	1 Carbonate-Bicarbonate Buffer capsule 100ml dH_2O
Blocking Buffer	PBS 3% BSA
Dilution Buffer	PBS 0.05% Tween® 20 1% BSA
MACS buffer	PBS 0.5% BSA 2mM EDTA

Table 7: Cell lines used and their source throughout the study

Cell lines used	Source
Lymphoblastoid cell lines (LCLs)	In house

2.2 Methods

2.2.1 Research study ethics statements and recruitment of donors

2.2.1.1 Healthy volunteer cohort

Healthy donors used in Chapter 3, and used as controls for flow cytometry staining were recruited for the study among the staff and students at the Institute of Immunology and Immunotherapy, University of Birmingham. Up to 60mL of blood was collected by a trained phlebotomist. (Ethics details: Cellular immunity to herpesvirus infection: Studies with EBV & CMV; REC ref: 14/WM/1254; REC: NRES Committee West Midlands- South Birmingham). Further donor PBMC with known CMV-status and HLA-type were purchased from STEMCELL with $1x10^8$ cells / cryovial.

2.2.1.2 Leucocyte cones

Leucocyte cones were obtained from platelet donors from the NHS Blood and Transport Services Birmingham Donor Centre. Studies were carried out under approved ethics: Cellular immunity to herpesvirus infection: Studies with EBV & CMV; REC ref: 14/WM/1254; REC: NRES Committee West Midlands- South Birmingham.

2.2.1.3 Ovarian Cancer cohort

Up to 50ml of peripheral blood and ovarian tumour samples from the ovary or metastatic sites were collected in sodium heparin tubes from ovarian cancer patients at City Hospital, Birmingham and New Cross Hospital, Wolverhampton following full written informed consent (Ethics details: Investigation into new biomarkers for diagnosing and treating ovarian cancer; REC ref 18/NE/001; protocol number: RG 17-225). The samples were either collected during

cytoreductive debulking surgery pre-chemotherapy, or during interval debulking surgery after three rounds of chemotherapy, before being followed up with more chemotherapy up to six cycles.

2.2.1.4 PePS2 cohort

Patients with non-small cell lung cancer (NSCLC) enrolled in a multicentre, single-arm, open-label, phase 2 trial in ten hospitals were given 200mg pembrolizumab every 3 weeks and recruited into the PePS2 trial. Up to 10ml of peripheral blood was obtained from patients following full written informed consent. (Ethics details: A phase II trial of pembrolizumab in patients with non-small cell lung cancer and performance status of 2; IRAS ID: 169512; REC ref: 16/WM/0010; protocol number: RG_14_172). These samples were analysed under the ethics: Cellular immunity to herpesvirus infection: Studies with EBV & CMV; REC ref: 14/WM/1254; REC: NRES Committee West Midlands- South Birmingham.

All samples used throughout the study were transported to the laboratory as per the ethical requirements and once processed, were stored in compliance with the Human Tissue Act (2004).

2.2.2 Methods used across Chapters

2.2.2.1 Preparation of plasma and Peripheral blood Mononuclear Cells (PBMCs) from healthy donors and patient samples

PBMCs were isolated by density gradient centrifugation of whole blood. Blood was collected in 'BD Heparin Vacutainer Tubes' (BD Biosciences) and spun at 233g for 5 minutes before 1ml of plasma was removed from the top. This was centrifuged in a microcentrifuge at 7400g for 10 minutes and the supernatant collected and stored in a cryovial at -70^{o}C. The remaining blood was diluted with RPMI at a 1:1 ratio and layered onto 15ml of Ficoll-Pacque (Cedarlane), a cell separation media. This was centrifuged at 755g for 25 minutes with the brake off. The PBMC at the plasma-Ficoll interface were washed twice with RPMI (Gibco) at 755g for 10 minutes to remove excess lymphoprep. The cell count was determined by mixing cells with 3% Acetic Acid with Methylene Blue (Stemcell) at a 1:1 ratio and counted using a haematocytometer. Cells were resuspended in freezing medium (FCS and 10% DMSO) and frozen at up to 10x10^{6}/ml in a cryovial. Cryovials were stored overnight in a -80^{o}C freezer in a 'Mr Frosty Freezing Container' (Thermo Fisher Scientific) to control the cooling rate, before being transferring to liquid nitrogen for long term storage.

2.2.2.2 Determination of CMV serological status by in house ELISA

Serum or plasma from donors recruited to the investigation were tested by an enzyme-linked immunosorbent assay (ELISA) to determine the CMV serology of the patients by presence of anti-CMV IgG. Mock and HCMV lysate was used as the positive and negative fractions for the serum IgG to bind to. These were generated prior to the start of this study by Miss Jusnara Begum.

Day 1:

CMV-lysate (in-house) was diluted 1:5000 in carbonate coating buffer (Sigma), 50µl was added into wells of a 96 well NUNC MAXISORP ELISA plate (Thermoscientific). As a control, the same was done with a mock-lysate solution. The plate was incubated overnight at 4^{o}C.

Day 2:

Standard curve preparation: in a spare 96 well plate, 80µl of dilution buffer was added into well A1, and 75µl into the remaining wells in column A. 20µl of standard (three seropositive CMV patients) was added to well A1 and pipetted up and down to mix. 25µl from well A1 was transferred to well A2 and repeated until well A7 where 25µl was removed, leaving well A8 blank.

Sample preparation: Plasma samples were diluted 1/60. Known CMV-seropositive and negative control samples were also diluted.

The ELISA plate was washed with wash buffer (Table 6) and 90µl of dilution buffer (Table 6) and 10µl of either the standard or diluted plasma samples were added to each well; the final dilution of samples was 1/600. Following incubation for one hour at room temperature (RT), the plate was washed a further three times with wash buffer. The IgG conjugate (Southern Biotech) was diluted 1:8000 and 100µl of this added to the plate before incubation for an hour at RT followed by three further washes with wash buffer. The plate was incubated for 15 minutes after the addition of 100µl TMB substrate (Thermo Fisher Scientific) followed by the addition of 100µl 1M HCl (Thermo Fisher Scientific) to stop the colour reaction. The plate absorbance was read at 450nm and results calculated in Graphpad Prism 10. Donors with an

IgG titre of over 10 arbitrary units were considered positive for CMV infection. Donors close to the threshold were repeated.

Figure 8 shows an example of the IgG titre of 6 donors as assessed by CMV ELISA with the positive control showing a titre of over 10 and the negative control not detectable. In this case, donors 1, 5 and 6 were determined to be positive for CMV IgG antibodies.

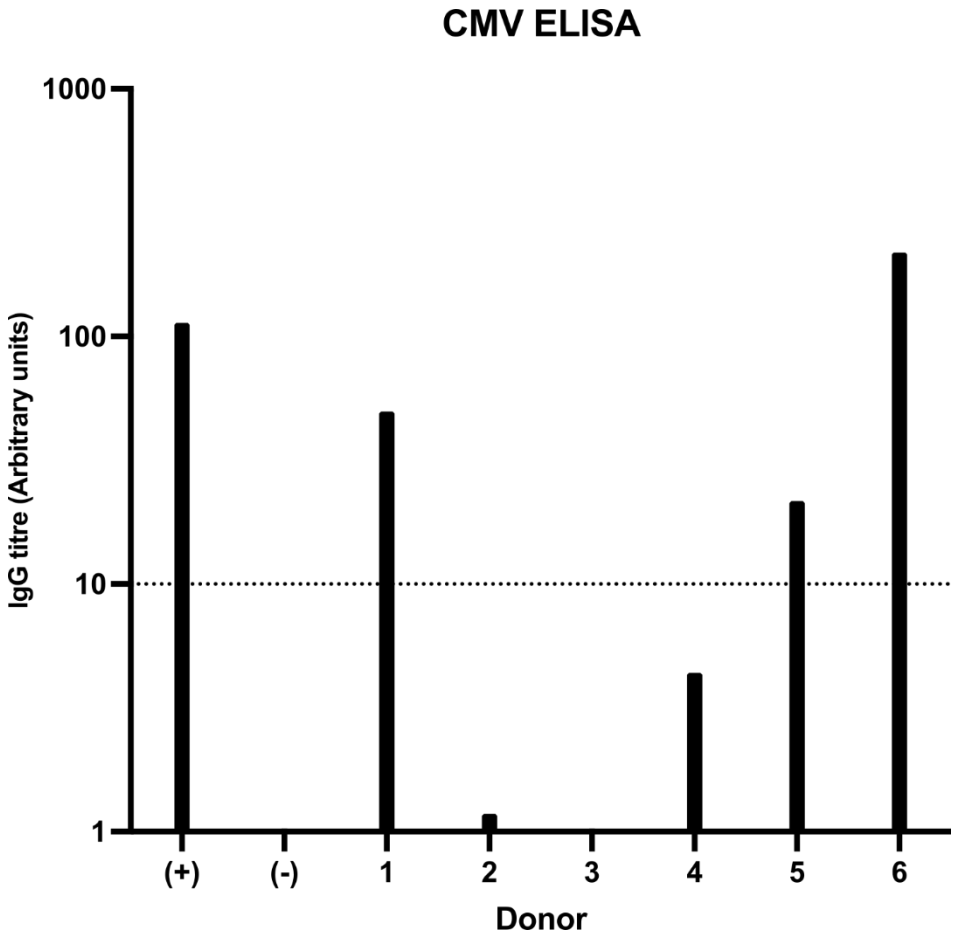

Figure 8: CMV titres as identified by ELISA

Representative example of the IgG titre (Arbitrary units) as detected by CMV ELISA with a positive control, negative control and n = 6 donor samples. Samples with a titre of under 10 were considered negative. Any samples with a titre of 8-12 were repeated. Samples 1, 5 and 6 were considered positive for CMV infection.

2.2.2.3 Determination of CMV serological status by abcam ELISA

When it was critical to assess the CMV serostatus of donors in a time sensitive manner, the Human Anti-Cytomegalovirus IgG ELISA kit (abcam) was used as per the manufacturers protocol. Briefly, plasma was diluted 1:100 and added to precoated plates before addition of an IgG-HRP conjugate and TMB and the absorbance read at 450nm.

2.2.2.4 DNA extraction and HLA typing by PCR

DNA extraction was carried out using the GenElute™ Mammalian Genomic DNA Miniprep kit (Sigma Aldrich) as per the manufacturer protocol. DNA concentration was measured using a Nanodrop microvolume spectrophotometer in ng/µl. The polymerase chain reaction (PCR) was used to identify the HLA types of the patients using a set of eleven primer pairs as per Table 9, specific for various class 1 and class 2 HLA antigens (Bunce et al., 1995). A mastermix was made up so there would be one reaction per patient, per primer set, with the components set out in Table 8.

Table 8: Summary of DNA mastermix used for 14 tubes of PCR reaction mix

Reagent	**Amount (µL)**
TDMH	70.9
Nuclease-free water	49
Control primer mix	3.5
BIOTAQ DNA polymerase (Bioline)	0.75
DNA at 28ng/µL	5 (140ng DNA)

The control primer mix consisted of the primers:

63F: TGCCAAGTGGAGCACCCAA

64R: GCATCTTGCTCTGTGCAGAT

Primer mixes were made up with nuclease free water as per Bunce et al. (1995), and 9µL of the DNA containing mastermix and 4µL of the relevant primermix were added per well on a PCR plate. The primers used can be found in Table 9.

Table 9: Summary of forward (F) and reverse (R) primers used for specific HLA types

Primer pair	Antigen	Alleles	Primer	Sequence
1	A1	A*0101, 0102	286F	CGACGCCGCGAGCCAGAA
			431R	AGCCCGTCCACGCACCG
2	A2	A*0201-17	296F	GTGGATAGAGCAGGAGGGT
			302R	CCAAGAGCGCAGGTCCTCT
3	B7 (inc. B703), B8101	B*0702-0705, 8101	193F	GGAGTATTGGGACCGGAAC
			221R	TACCAGCGCGCTCCAGCT
4	B703	B*0703	312F	ACACAGATCTACAAGACCAAC
			221R	TACCAGCGCGCTCCAGCT
5	B8, B51GAC, B*4406	B*0801, 0802, B51GAC, B*4406	195F	GACCGGAACACACAGATCTT
			212R	CCTCCAGGTAGGCTCTGTC
6	B8	B*0801, 0802	195F	GACCGGAACACACAGATCTT
			220R	CCGCGCGCTCCAGCGTG
7	DR7	DRB1*0701	48F	CCTGTGGCAGGGTAAGTATA
			49R	CCCGTAGTTGTGTCTGCACAC
8	DR52b	DRB3*0201, 0202, 0203	76F	GGA GTA CCG GGC GGT GAG
			151-1R	CGT AGT TGT GTC TGC AGT AAT TG
9	DR52c (and b)	DRB3*0201, 0301	70F	GTT TCT TGG AGC TGC TTA AGT C
			38R	CTG CAC TGT GAA GCT CTC CA
10	DQ6	DQB1*0601/2/3	347F	TTT CGT GCT CCA GTT TAA GGC

			348F	GAC GTG GGG GTG TAC CGC
			111R	CCG CGG AAC GCC ACC TC
11	DQ6	DQB1*0603-9	349F	GGA GCG CGT GCG TCT TGT A
			350R	TGC ACA CCG TGT CCA ACT C
			351R	TGC ACA CCC TGT CCA CCG

The conditions set up on the thermocycler for the PCR reaction are set out in Table 10.

Table 10: PCR cycling conditions for HLA typing

Temperature	Time		Cycles
96°C	1 minute		
96°C		25 seconds	5 Cycles
70°C		45 seconds	
72°C		45 seconds	
96°C		25 seconds	21 Cycles
65°C		50 seconds	
72°C		45 seconds	
96°C		25 seconds	4 Cycles
55°C		60 seconds	
72°C		120 seconds	
4°C	∞		

After PCR, 1% agarose gel electrophoresis using 13µl of the nucleic acid stain SYBR Safe (Invitrogen) in a 130ml gel, was conducted on the PCR DNA products, running at 90V for 75 minutes. The gel images were captured using UV imagine, and the bands were identified based on the DNA base pair sizes outlined in Bunce, *et al.* (1995).

Figure 9 shows an example of HLA-typing for a patient sample, with control primer bands visible in each lane. There are bands indicating positivity for HLA-types detected in lane 2 (A1), lanes 6 and 7 (B8), lane 10 (DR52C) and lane 12 (DQ6).

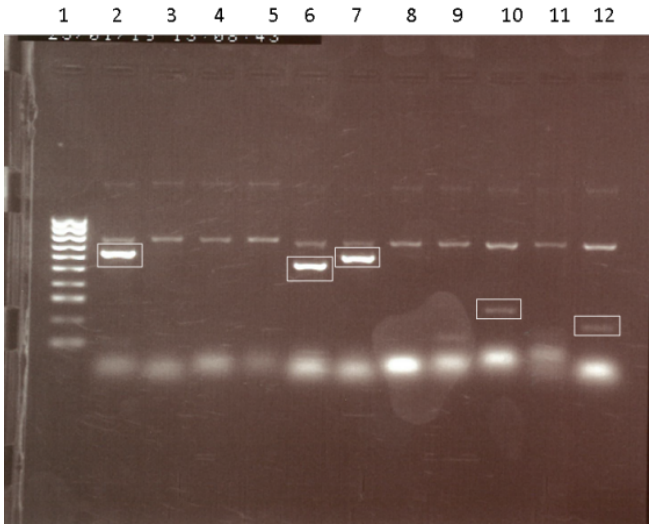

Figure 9: HLA typing of one representative patient sample

1% agarose gel with SYBR Safe to test for HLA types. Lane 1: Bioline HyperLadder™ 100bp; Lanes 2-12: patient 139, primers 1-11. The control primer bands are present in all lanes. Boxes indicate the presence of bands of the relevant size (bp). This patient example exhibits a band in lane 2 (629bp, HLA-A1), lane 6 (543bp, HLA-B8), lane 7 (606bp, HLA-B8), lane 10 (259bp, HLA-DR52C) and lane 12 (140bp, HLA-DQ6).

2.2.2.5 HLA-typing by flow cytometry

HLA typing was carried out using HLA-A2, HLA-B7 and HLA-B8 antibodies and assessed using flow cytometry. The red blood cells from an aliquot of whole blood were lysed using 10X RBC lysis solution (miltenyi). This is diluted 1:10 with dH2O and added to the sample for 10 minutes before being washed off with MACS buffer. Once resuspended in MACS buffer the samples were split in two, and antibodies listed in Table 13 (OvCa- CMV and HLA panel) were added to one tube for 20 minutes at room temperature, protected from light. No antibodies were added to the second tube to act as a negative control. Samples were washed and acquired using a BD Symphony A3 flow cytometer.

2.2.2.6 Tetramer conjugation

Monomers in 20µl aliquots (supplied by the Protein Expression Facility, University of Birmingham), were thawed on ice protected from light. For the PE-conjugated tetramers, 1.58µl of 0.2mg/ml streptavidin conjugated anti-PE (BioLegend) is added per 1µg of monomer. A total of 10µl of streptavidin-PE diluted in PBS was made up, and one-fifth (2µl) added every 20 minutes before vortexing whilst keeping the tetramers protected from light. A summary of the tetramers can be found in Table 11.

The same protocol was followed for the APC-conjugated EBV-specific antibodies except 0.87µl of 0.2mg/ml streptavidin-APC is added per 1µg of monomer, diluted to a final volume of 10µl with PBS, and one-fifth (2µl) of the streptavidin-APC / PBS mix was added once an hour. A summary of the tetramers can be found in Table 11. Throughout the study, tetramers are referred to by the first three letters of the monomer sequence as underlined in the tables.

Tetramers were stored at 4^{o}C and used within two weeks.

Table 11: Summary of Class I CMV monomers and fractions used to make up CMV tetramers conjugated to PE

Monomer	Protein	Concentration (µg/ml)	Quantity per 20µl aliquot (µg)	Streptavidin-PE (µL) (0.2mg/ml)	PBS (µL)
YSEHPTFTSQY	PP65	162	3.25	5.13	4.87
NLVPMVATV	PP65	58	1.16	1.84	8.16
RPHERNGFTVL	PP65	95	1.90	2.99	7.01
TPRVTGGGAM	PP65	378	7.56	11.95	0
VLEETSVML	IE1	64	1.29	2.03	7.97
QIKVRVDMV	IE1	120	2.40	3.80	6.20
ELRRKMMYM	IE1	586	11.72	18.52	0.00
ELKRKMMYM	IE1	436	8.71	13.77	0
VTEHDTTLY	PP50	209	4.18	6.60	3.40

Table 12: Summary of Class I EBV monomers and fractions used to make up EBV tetramers conjugated to APC

Monomer	Protein	Concentration (µg/ml)	Quantity per 20µl aliquot (µg)	Streptavidin-APC (µL) (0.2mg/ml)	PBS (µL)
GLCTLVAML	BMFL1	130	2.60	2.26	7.74
YVLDHLIVV	BRFL1	15	0.30	0.26	9.74
RAKFKQLL	BZLF1	975	19.51	16.97	0.00
CLGGLLTMV	LMP2	115	2.29	2.00	8.00
FLRGRAYGL	EBNA3A	93	1.85	1.61	8.39

2.2.3 Chapter 3: Phenotypic and functional analysis of PD1$^+$ CMV-specific CD8$^+$ T-cells in healthy donors

2.2.3.1 Tetramer screen and phenotyping

R10 media was warmed to 37^{o}C in a water bath. Cryopreserved PBMC vials were thawed for 1-2 minutes at 37^{o}C. Cells were diluted with 10ml R10 and spun at 335g for 10 minutes to wash the freezing media off. Cells were resuspended in MACS and split between the relevant amount of FACS tubes in order to allow individual staining of all tetramers for the matched HLA types of the donor. Tubes were topped up with 2ml of MACS buffer and washed for 5 minutes at 525g before supernatant discarded. For class I staining, 1µl of tetramer was added to all relevant tubes, leaving one without as a no tetramer control. Cells were incubated for 20 minutes at 37^{o}C. Cells were washed in 2ml MACS and the supernatant discarded before the addition of the antibodies in Table 13 (Healthy Donors- surface panel), with one control tube

per patient only being stained with the core control antibodies. Cells were incubated for 30 minutes at RT, protected from light before being washed in 2ml MACS and the supernatant discarded. Cells were topped up with 100µl MACS buffer and acquired on BD Symphony A3 flow cytometer.

2.2.3.2 Ex vivo selection of $PD1^{+/-}$ CMV-specific $CD8^{+}$ T-cells and Cytokine assay

Day 1:

Leukocyte cones were obtained from the NHS Blood and Transplant Service. The blood was drained into a 15ml falcon tube and spun at 335g for 5 minutes, before as much plasma as possible was collected from the top (<100ul) into a microcentrifuge tube. The remaining blood was transferring into a 75cm tissue culture flask containing 120ml RPMI and pipetted up and down to mix and prevent clotting. 500ul of this then taken separately into a 5ml FACS tube in order to HLA type. The remaining blood and RPMI mixture were processed as per section 2.2.2.1 to extract PBMC.

CMV serostatus was determined using a Human Anti-Cytomegalovirus IgG ELISA kit (abcam) as described in section 2.2.2.3..

HLA typing was carried out using by flow cytometry as described in section 2.2.2.5.

$CD8^{+}$ T-cells from CMV positive patients with an A2, B7 or B8 HLA type were negatively selected using the EasySep™ Human CD8 Enrichment Kit (StemCell Technologies) before being washed, and rested at 2-5x10^6/ml overnight in R10 at 37°C in 6 well plates. Remaining samples were frozen down using freezing media.

Alternative Day 1:

Cryopreserved human PBMC were sourced from StemCell Technologies. These cells had predetermined HLA, and CMV positive donors were selected. Three vials containing $1x10^8$ cells each were thawed for 2-3 minutes in a water bath at 37°C. The cells were resuspended in 30ml R10 in a 50ml conical tube and spun at 335g for 10 minutes. Cells were resuspended in 31ml R10, 1ml ($9.6x10^6$) was taken into a FACS tube for phenotyping. Whilst CD8s were negatively selected out of the remaining cells using the EasySep™ Human CD8 Enrichment Kit (StemCell Technologies) as per the manufacturers protocol. Cells were washed and resuspended in R10 before being incubated at 37°C overnight at $2\text{-}5x10^6$ / ml in a 6 well plate.

The cells taken for phenotyping were split amongst the relevant number of FACS tube in order to test the individual tetramer responses to determine the largest response for the sorting. This was done using the same method as outlined in 2.2.3.1 using the panel in Table 13 (Healthy Donor- surface panel).

Day 2:

LCLs from donors who were matched on one allele for the HLA-restriction of the specific epitope, were aliquoted into a flask. Half were set aside to be the non-peptide pulsed control. Peptide, at a final concentration of 1µg/ml, was added to the cells, and the cells were incubated at 37°C for an hour, resuspending every 15 minutes. LCLs were washed with R10 and resuspended at 1x10^6/ml.

The cells from the leukocyte cone were tetramer and antibody stained using the antibodies in Table 13 (Healthy Donor- sorting panel) with some cells set aside and used as a PD1 and tetramer negative control. The negative control was run first through a BD FACS Melody cell

sorter, and the gates were set in order to identify the tetramer positive and PD1 positive and negative. As many cells were acquired as possible.

If cell numbers allowed, 1000 T-cells and 10,000 LCLs were plated per well with the following conditions set up in duplicate:

- T-cells + peptide pulsed LCLs
- T-cells + peptide pulsed LCLs + pembrolizumab
- T-cells + LCL
- T-cells + LCL + pembrolizumab
- T-cells + anti CD3 (1/1000)
- LCLs only

If there were insufficient cells, the cell numbers were dropped to 500 T-cells and 5000 LCLs per well. Pembrolizumab (a PD1 inhibitor) was added at a concentration of 1µg/ml. The anti-CD3 antibody was added at a final concentration of 1µg/ml. Spare cells were used to set up polyclonal T-cell cultures as described below. Cells were incubated at 37^{o}C for 18 hours and the supernatant harvested the next day before being stored at -80C.

Cytokine production was analysed using the CD8/NK LEGENDplex^{TM} (BioLegend) kit. The manufacturers protocol was followed but briefly, it is a bead-based assay whereby beads are added to cell culture supernatant, which bind to analytes. These can then be detected by flow cytometry using detection antibodies and a streptavidin conjugated PE fluorophore. By producing a standard curve using controls of known concentrations, the software is able to determine the concentration of cytokines by quantifying the amount of PE bound to the relevant detection beads for each cytokine. This allowed quantification of the following

cytokines: IL-17A, IL-2, IL-4, IL-10, IL-6, TNF-α, Fas, FasL, IFN-γ, Granzyme A, Granzyme B, Perforin, Granulysin.

A summary of this protocol can be seen in Figure 10.

.

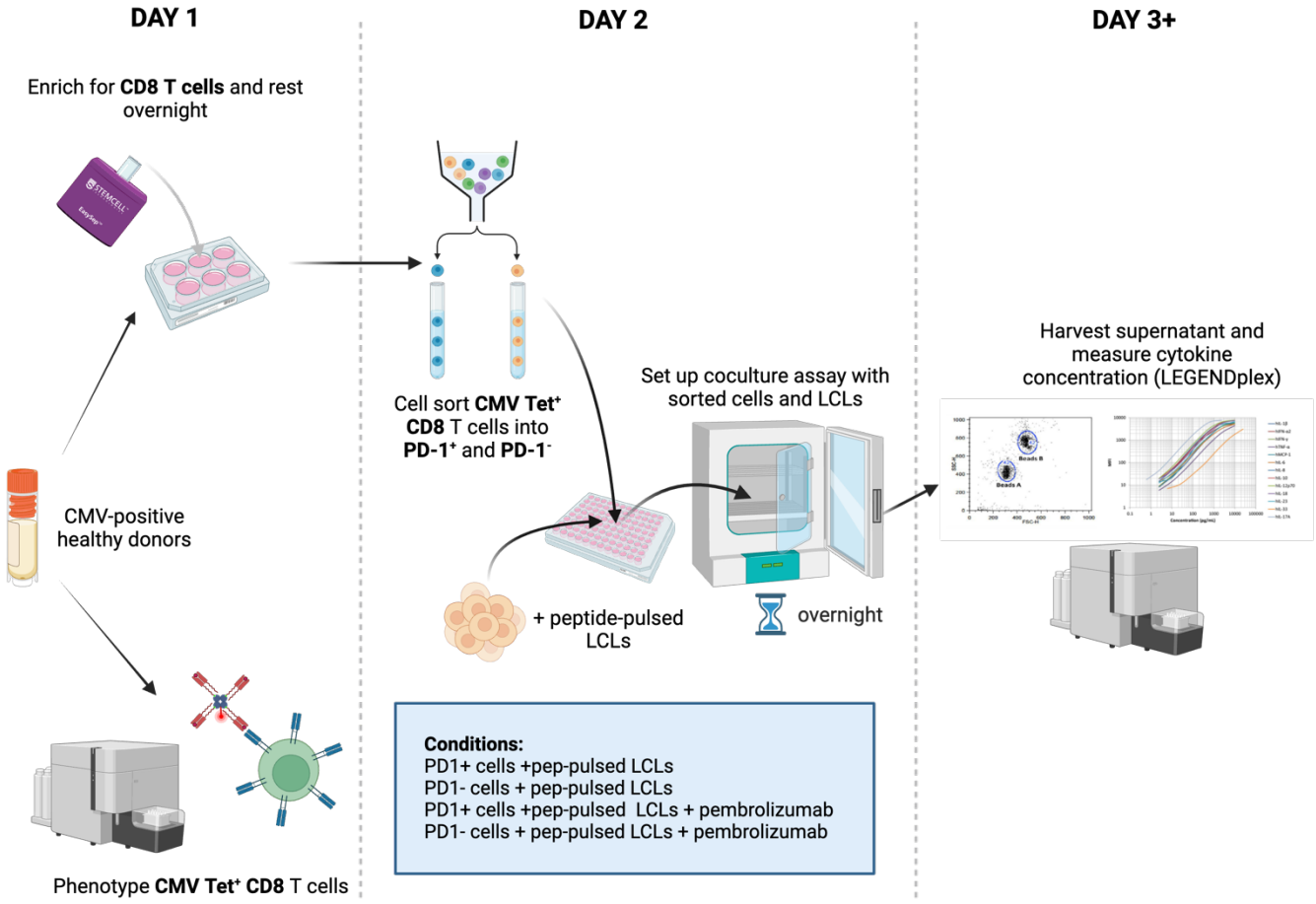

Figure 10: Ex vivo selection of PD1$^{+/-}$ CMV-specific CD8^{+} T-cells and cytokine assay

On day 1, a small aliquot of cells was taken for phenotyping whilst most were enriched for CD8^{+} T-cells and rested overnight at 37°C. The following day the CD8^{+} cells were sorted into PD1^{+} and PD1^{-} CMV-specific T-cells and incubated overnight at 37°C with peptide-pulsed LCLs with and without pembrolizumab. The following day, supernatant was harvested and frozen for future use to measure the cytokine concentrations using the LEGENDPlex kit (BioLegend). Figure created with BioRender.com

2.2.3.3 Culturing polyclonal cells

For samples who had more than the number of $PD1^+$ and $PD1^-$ CMV tetramer-specific T-cells than was required for the co-culture assay, the spare cells were used to set up polyclonal T-cell cultures.

LCLs were peptide pulsed with 1µg/ml for 1-2 hours with the peptide that matched the specificity of the $tetramer^+$ cells that were being sorted. The cells were irradiated at 40Gys, washed twice with RPMI and resuspended at a concentration of $1x10^6$/ml in polyclonal T-cell culture medium.

The remaining $PD1^+$ and $PD1^-$ cells were added into one well each of a 48 well plate, with the addition of $1x10^6$ irradiated LCLs and topped up to 1ml with polyclonal T-cell culture medium and incubated at 37^oC.

The media was changed twice a week by removing the top 500µl without disturbing the cells, and adding fresh media.

After 2 weeks (to allow for the PD1 level to reduce after the stimulation with the peptide pulsed LCLs), the cells were counted and the PD1 levels of the cells were phenotyped using the panel Healthy Donors- sorting in Table 13. If there were sufficient cells, they were then measured every week to track the levels of PD1 on the T-cells, if there were not sufficient cells, the whole well was used to get reliable phenotypes at the 2-week timepoint.

2.2.4 Chapter 4: CMV-specific $CD8^+$ T-cell phenotype within Ovarian Cancer tissue and its relationship to PD1 expression

2.2.4.1 Determining CMV-status and HLA-typing

For donors with available plasma and DNA, CMV status was determined by in-house CMV ELISA, and HLAs-status was assessed using PCR, both methods as described above.

For patients without available plasma, the CMV specific T-cell responses were analysed using a stimulation assay in the presence of TAPI-0. Unlike most cytokines, upon production, TNFα is produced in a membrane bound form before being cleaved by the TNFα converting enzyme (TACE). The TNFα Processing Inhibitor 0 (TAPI-0) enzyme prevents this cleavage step from occurring, allowing the detection of TNFα on the cell surface of cells.

Patient and healthy donor samples (used for controls) were thawed in a water bath for 2 minutes before being resuspended in 10ml R10 buffer and spun for 10 minutes at 335g. Cells were resuspended in 5ml R10 and rested in a 6 well plate at 37^{o}C overnight. The next day cells were counted using Methylene Blue dye (Stem Cell) on a haematocytometer. Cells were then split into Unstimulated and CMV-stim tubes (aiming for at least 1.5x10^6 cells per tube). Cells were spun at 525g for 5 minutes and supernatant discarded. Either CMV pan-select peptides (JPT) or DMSO were added at a final concentration of 1µg/ml. A positive control was included for the healthy donor control by stimulating with Cell Stimulation Cocktail 500X (ebioscience). TAPI:0 enzyme was added at a final concentration of 1µg/ml and 5µl TNFα-APC antibody (clone Mab11) was added. Cells were incubated for 4 hours at 37^{o}C, resuspending cells every hour to keep in suspension. Stimulated cells were washed in MACS buffer before staining for

25 minutes at RT protected from light with the antibodies listed in Table 13 (OvCa- CMV and HLA panel). Cells were washed in MACS, resuspended in 150µl MACS buffer and acquired on a Symphony A3 flow cytometer.

This panel also contained HLA-antibodies to identify the HLA types of patients. This allowed identification of the HLA-types simultaneously with the CMV-status. As there was no antibody for HLA-A1, PCR was used to HLA-type donors for HLA-A1.

2.2.4.2 Extracting cells from tumour tissue

The cohort of samples used in this study specifically had been historically collected and processed with the cells isolated either by tissue digestion or the 'grow out' method:

The overnight grow out method involved manually lacerating the samples in a six well plate and resuspending the tissues in a volume of R10 appropriate for the size of the tissue, ensuring it was covered. The samples were then left overnight at 37^{o}C, and the media collected the next day.

The digestion method comprised of manually lacerating the tissue in a six well plate before using the Tumour Dissociation Kit (Miltenyi) as per the manufacturer's instructions. Briefly, enzymes were added before vortexing and heating on a gentleMACS Octo Dissociator with Heater. This method allows for gentle and rapid single cell suspensions to be generated whilst preserving the cell surface epitopes.

Following either method, cells were passed through a 70µm MACS SmartStrainer (Miltenyi) to collect lymphocytes, then washed with R10 by centrifuging for 5 minutes at 525g and discarding supernatant. The cells were topped up with R10 and counted using Methylene Blue

Dye (StemCell) on a haemocytometer. After being centrifuged again for a further 5 minutes at 525g, the supernatant was discarded and the pellet suspended in freezing media for freezing at 10 x 10^6 per ml in 1ml cryovials. Samples were stored in a Mr Frosty™ at -70°C for 24 hours before being moved to liquid nitrogen.

2.2.4.3 Phenotyping viral-specific T-cells in tissue

Once the CMV-status and HLA-type of patients were identified, surface phenotyping of the cells was carried out of the CMV-positive donors for who there was HLA-matched tetramers.

Patient PBMC and tissue samples, and healthy donor samples (used for controls), were thawed in a water bath for 2 minutes before being resuspended in 10ml R10 buffer and spun for 10 minutes at 335g. As this cohort contained tissue samples it was important to minimise cell clumping for optimal running on the flow cytometer. Therefore, nuclease was diluted 1/8000 with PBS and 1ml added to cells before incubation for 15 minutes at 37°C, resuspending every 5 minutes to keep cells in suspension. Cells were washed in R10 and counted on a haemocytometer using Methylene Blue dye (Stem Cell). Cells were resuspended in MACS buffer and transferred into 5ml polystyrene FACS tubes. The healthy donor control was split between two tubes into to have a 'core' panel of fewer antibodies to control for setting the gates. A master mix of HLA-matched Class I tetramers were then added to the tube before incubation for 20 minutes at 37°C. Cells were washed and stained with the antibodies in Table 13 (OvCa- surface panel) before being incubated at 4°C for 20 minutes protected from light. Cells were washed and topped up with 150µl MACS buffer before acquisition on a Symphony A3 flow cytometer.

2.2.5 Chapter 5: Prospective analysis of the CMV-specific T-cell phenotype during PD1 inhibition therapy in patients with lung cancer

2.2.5.1 Assessing CMV and EBV status of patients

Assessment of CMV status and HLA-type was carried out prior to this study taking place by Miss Jusnara Begum using the in-house CMV ELISA and PCR as described in sections 2.2.2.2 and 2.2.2.4.

EBV analysis was carried out using the Human Anti-Epstein Barr (EBNA-1) IgG ELISA Kit (alpha-diagnostic international) as per the manufacturer's instructions. Briefly, patient plasma is incubated on plate-bound EBNA-1 antigen for any IgG in the plasma to bind. Enzyme-conjugate is added to bind to any bound IgG which is then detected by addition of a substrate and read using a plate reader.

2.2.5.2 Assessing the T-cell response to pembrolizumab

Due to the limited fluorophores that IgG4 antibodies were available from, it was necessary to conjugate it to PE-Cy5 so it would fit into the panel around the tetramers, whilst being on a sufficiently bright marker to provide good resolution. The anti-human IgG4 antibody was conjugated to PE-Cy5 using the PE/Cy5® Conjugation Kit- Lightning Link (abcam), as per the manufacturer's instructions.

Patient and healthy donor samples (used for controls) were thawed in a water bath for 2 minutes before being resuspended in 10ml MACS buffer and spun for 10 minutes at 335g. The cells were resuspended in 4ml MACS and counted using Methylene Blue dye (Stem Cell) on a haematocytometer. If there were over 2 million viable cells, both the surface and intranuclear

panels were run on the sample. The cells were spun down, and the supernatant discarded with residual buffer removed. A master mix of HLA-matched Class I tetramers were added to the relevant samples before incubation for 20 minutes. The cells were split between two tubes if both panels were being run (a surface and an intranuclear tube), all tubes were topped up to 2ml and spun down with supernatant discarded. The relevant panel surface antibody master mix was added to the sample tubes whilst the healthy donor controls were stained with a full surface and core control master mix and samples were incubated for 25 minutes at RT protected from light. Cells were washed and supernatant discarded. The surface panel samples were resuspended in 150µl fixation buffer (eBioscience) and stored at 4^{o}C overnight. The intranuclear samples were washed once more in MACS and resuspended in the residual volume. The Human FoxP3 buffer set (BD) was used for the intranuclear staining as per the kit instructions. Briefly, the cells were fixed for 10 minutes protected from light at RT then permeabilised for 30 minutes at RT. Cells were washed twice in wash buffer and intranuclear antibodies were added at the appropriate volumes to the residual liquid. Cells were resuspended and incubated for 30 minutes at RT protected from light. Cells were washed in MACS and resuspended in 150ul fixation buffer (eBioscience) and stored at 4^{o}C overnight.

The following day all cells were washed in 2ml MACS and resuspended in 150µl of MACS buffer before acquisition on a Symphony A3 flow cytometer (BD).

Details of the surface panel can be found in Table 13 (PEPS2- surface panel) and details of the intracellular panel can be found in Table 13 (PEPS2- intranuclear panel).

Table 13: Details of antibodies used for panels across the study. Ticks indicate the antibody was used within that panel.

					Panel					
Marker	**Clone**	**Conjugate**	**Supplier**	**Cat. No.**	**Healthy Donors-surface**	**Healthy Donors-sorting**	**OvCa-CMV and HLA**	**OvCa-surface**	**PEPS2-surface**	**PEPS2-Intranuclear**
Tetramer	-	PE	BioLegend	405204	✓	✓		✓	✓	✓
Tetramer	-	APC	BioLegend	405207				✓	✓	✓
Viability dye	-	FVS575	BD	565694	✓		✓	✓	✓	✓
CD14	M5E2	BV650	Biolegend	301836	✓		✓	✓	✓	✓
CD19	HIB19	BV650	Biolegend	302238	✓		✓	✓	✓	✓
CD3	SK7	APC-R700	Biolegend	344822	✓		✓	✓	✓	✓
CD4	SK3	BUV496	BD	612936	✓		✓	✓	✓	✓
CD8	SK1	BUV805	BD	612889	✓		✓	✓	✓	✓
CD45RA	HI100	BV510	BioLegend	304142	✓			✓	✓	✓
CCR7	2-L1-A	APC-Cy7	Biolegend	353212	✓			✓	✓	✓
CD39	TU66	BV750	BD	747079	✓			✓	✓	✓
CD38	HB7	BUV615	BD	752351	✓			✓	✓	✓
CD28	CD28.2	BUV661	BD	741635	✓				✓	✓
CD27	L128	BUV563	BD	748705	✓			✓	✓	✓
TIGIT	741182	BV421	BD	747844	✓			✓	✓	✓
HLA-DR	G46-6	BUV737	BD	748339	✓			✓	✓	✓
Tim-3	7D3	BB700	BD	746178	✓			✓	✓	✓
Lag-3	11C3C65	BV605	BioLegend	369324	✓			✓	✓	✓

PD1	EH12.2H7	PE-Cy7	Biolegend	329918	✓	✓		✓	✓	✓
2B4	Feb-69	PE-Dazzle	Biolegend	393506	✓				✓	
CLTA4	BNI3	BB515 (FITC)	BD	566917	✓					
CD160	BY55	AF647 (APC)	BioLegend	341208	✓					
CD137	4B4-1	PE-Cy5	BioLegend	309808	✓					
CD69	FN50	BV785	BioLegend	310932	✓		✓	✓		
Viability dye	-	FVS780	BD	565388		✓				
CD14	63D3	BV421	BioLegend	367144		✓				
CD19	HIB19	BV421	BioLegend	302234		✓				
CD3	Hit3a	FITC	BioLegend	300306		✓				
CD4	OKT4	PerCPCy5.5	BioLegend	317428		✓				
CD8	SK1	BV510	BioLegend	344732		✓				
HLA-A2	BB7.2	PE-Dazzle	BioLegend	343333			✓			
HLA-B7	BB7.1	PE	BioLegend	372403			✓			
HLA-B8	REAfinity	FITC	Miltenyi	130-118-502			✓			
TNFa	Mab11	APC	BioLegend	502912			✓			
CXCR5	J252D4	BV711	BioLegend	356934				✓	✓	✓
CCR5	2D7/CCR5	BUV661	BD	741644				✓		
GITR	V27-580	BB515	BD	567782				✓		
CD95	DX2	BUV395	BD	740306				✓		
CD103	Ber-ACT8	PE-Dazzle	Biolegend	350224				✓		
IgG4	QA16A15	PECy5	BioLegend	403702					✓	✓

T-bet	04-46	BV786	BD	564141						✓
GRZB	GB11	PE-CF594	BD	562462						✓
TCF-1	S33-966	AF488	BD	567018						✓
Ki-67	B56	BUV395	BD	564071						✓

CHAPTER 3: PHENOTYPIC AND FUNCTIONAL ANALYSIS OF $PD1^+$ CMV-SPECIFIC $CD8^+$ T-CELLS IN HEALTHY DONORS

3.1 Introduction

The T-cell response is crucial in controlling CMV infection. CMV-specific $CD8^+$ T-cells play a major role in controlling viral reactivation and cellular immunodeficiency is associated with a range of CMV-associated complications (Agrawal et al., 2019, van der Heiden et al., 2018). However, CMV has evolved a range of mechanisms to limit the efficacy of immune detection, and this has likely been critical in its ability to establish a persistent lifelong infection.

A further notable feature is that the magnitude of the CMV-specific T-cell response is considerable and comprises a significant portion of the T-cell repertoire in CMV-seropositive people (Gillespie et al., 2000, Khan et al., 2010). Furthermore, this can increase with age in a process that has been termed 'memory inflation' (Sylwester et al., 2005, Varani and Landini, 2011).

The magnitude of the CMV specific $CD8^+$ T-cell response within the vascular system is remarkable, larger than that documented against any other pathogen, and can occupy a significant portion of the $CD8^+$ T-cell repertoire, often comprising >10% of cells (Khan et al., 2004). Indeed, this response is often oligoclonal with T-cell responses against individual peptide epitopes often representing over 2% of the repertoire (Gillespie et al., 2000). Memory inflation may see this proportion increase to over 20% of the total $CD8^+$ T-cell pool and is believed to represent an immune response to intermittent viral reactivation (Khan et al., 2002, Snyder et al., 2008, Lang et al., 2002).

Murine CMV (MCMV) recapitulates many of the features of human CMV infection and mouse studies are often used to analyse viral-specific T-cell responses. Interestingly, *Sierro et al.* observed that only a subset of MCMV-specific T-cells, with specific antigenic specificity, were

enriched in the periphery, indicating that not all CMV-specific T-cells undergo memory inflation (Sierro et al., 2005).

CMV-specific $CD8^+$ T-cells typically exhibit a unique and highly differentiated phenotype that is believed to represent a response to the chronic nature of CMV infection and episodes of intermittent viral reactivation. These cells often express markers associated with late-stage differentiation such as CD57, which has been linked to reduced proliferative capacity but high cytotoxic potential (Kared et al., 2016). They also typically lack the costimulatory molecules CD28 and CD27 and the lymphoid tissue homing receptor CCR7, instead expressing adhesion molecules such as CD44 and CX3CR1 which facilitate their migration to peripheral tissues (van den Berg et al., 2019). Despite their highly differentiated phenotype, these cells remain functionally active and capable of responding to CMV reactivation. This distinct phenotype sets them apart from T-cells specific to other chronic infections such as EBV or HIV (van den Berg et al., 2019, Klenerman and Oxenius, 2016, Snyder et al., 2008).

In healthy individuals CMV-specific $CD8^+$ T-cells often exhibit high levels of PD1 expression. Expression of this immune checkpoint protein is heterogeneous on CMV-specific T-cells, with values ranging from 0.44% to 87% in different studies (Dirks et al., 2013, Hosie et al., 2017).

Despite the remarkable expansion of CMV-specific T-cells in healthy people, and a further increment associated with aging, T-cells appear to remain largely functional across the life course. CMV-specific $CD8^+$ T-cells can maintain strong effector functions including broad cytokine production and proliferative capacity (Hertoghs et al., 2010, Klenerman and Hill, 2005). Nevertheless, few studies have characterised the profile of PD1 expression on CMV-specific $CD8^+$ T-cells or assessed how this might relate to functional capacity.

This study aims to address this gap by providing an in-depth phenotypic characterisation of CMV-specific $CD8^+$ T-cells against a range of immunodominant CMV epitopes. A focus was on the detailed assessment of the relative membrane phenotype of PD1+ or $PD1^-$ virus-specific cells. As a comparison, a thorough characterisation of relative expression of PD-1 on EBV specific T-cells, and its associated extended phenotype, was also undertaken. As another herpesvirus that leads to life-long infection and is periodically reactivated within the body, EBV also leads to detectable frequencies of EBV-specific $CD8^+$ T-cells (Lanfermeijer et al., 2021). This makes it a good comparison as it is possible to determine whether phenotypes are characteristic of CMV in particular or are observed in multiple herpesvirus.

The major immediate early protein (IE-1) and the phosphoprotein 65 (pp65) are well characterised as highly immunodominant viral proteins for generation of T-cell responses (Alp et al., 1991, Kern et al., 2002, Gibson et al., 2004). As such, T-cell responses against epitopes from these proteins was a primary focus of the work, whilst immunity against a single immunodominant peptide from pp50 was also investigated. One of the major advantages of this approach was the ability to compare and contrast the phenotype of virus-specific T-cells against a range of epitopes from the pp65, pp50 and IE1 proteins.

Historically, many studies of virus-specific T-cells have relied on stimulation assays with viral protein or peptide in order to elicit virus-specific responses. However, the use of MHC-tetramers, which were used in my study, enables the identification and characterisation of unstimulated T-cells, providing insights into their natural state without artificial activation (Altman et al., 1996). This method allows for precise phenotyping of cellular state as it focuses

on proteins expressed on the cell surface in the 'resting' state and is therefore not influenced by the dynamic up- or downregulation of proteins following T-cell activation.

My phenotypic studies incorporated a combination of manual flow cytometry 'gating' together with high-dimensional clustering analysis. This allowed for a nuanced and unsupervised insight into the heterogeneity within the CMV-specific T-cell compartment.

Furthermore, to gain insight into how PD1 expression might act to regulate the functional response of CMV specific T-cells, I undertook a range of studies to assess cellular response to antigen stimulation in the presence or absence of PD1 engagement.

3.2 Results

3.2.1 Flow cytometric staining of virus-specific T-cells

Samples were comprised of phlebotomy aliquots from healthy laboratory donors and leukocyte cones supplied by the NHS Blood and Transplant service. Donors were tested for CMV serostatus by CMV ELISA and HLA genotype determined by PCR. As seroprevalence for EBV is >95% of the adult population, donors were assumed to have experienced prior EBV infection.

PBMC from CMV-seropositive donors with appropriate HLA genotype for HLA-peptide tetramer staining (HLA-A*0101 (A1), HLA-A*0201 (A2), HLA-B*0702 (B7) and HLA-B*0801 (B8)) were stained with appropriate tetramer reagents. In order to confirm positive tetramer staining, a negative control was also included which did not include the tetramer stain. $CD8^+$ T-cells were selected by gating on singlet cells; lymphocytes according to forward and side

scatter; live cells; cells negative for the dump channel markers CD14 and CD19 which would indicate monocytes and B-cells; $CD3^+$ cells, and finally $CD8^+$ $CD4^-$ cells to establish the $CD8^+$ population (Figure 11a). This gating strategy was used for all future analysis throughout the chapter to identify $CD8^+$ cells.

Figure 11b shows representative examples of the tetramer staining for the class I CMV-specific T-cell epitopes. The responses encompass three different proteins (IE1, pp65 and pp50) and four HLA types (A1, A2, B7 and B8).

Figure 11c shows representative examples of staining with HLA class I tetramer containing EBV peptides from six proteins (BRFL1, LMP2, BMLF1, EBNA3A, BaRF1 and BZLF1) across three different HLA types (A2, B7 and B8).

Details of the tetramers can be found in Table 14 (CMV) and Table 15 (EBV).

a)

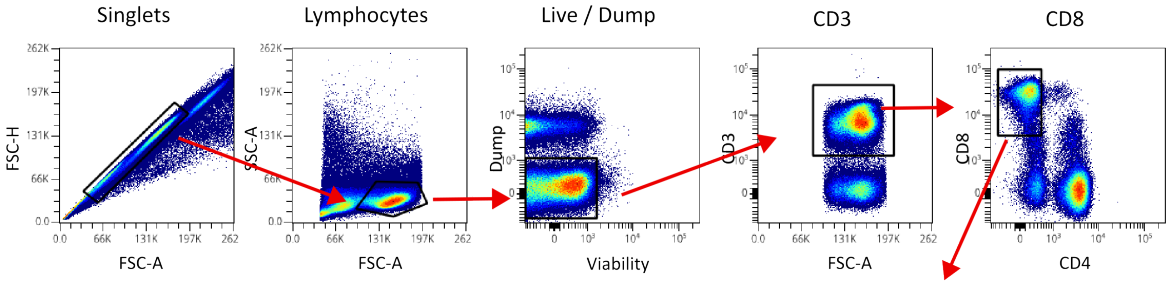
Singlets
Lymphocytes
Live / Dump
CD3
CD8
FSC-H
FSC-A
SSC-A
FSC-A
Dump
Viability
CD3
FSC-A
CD8
CD4

b)

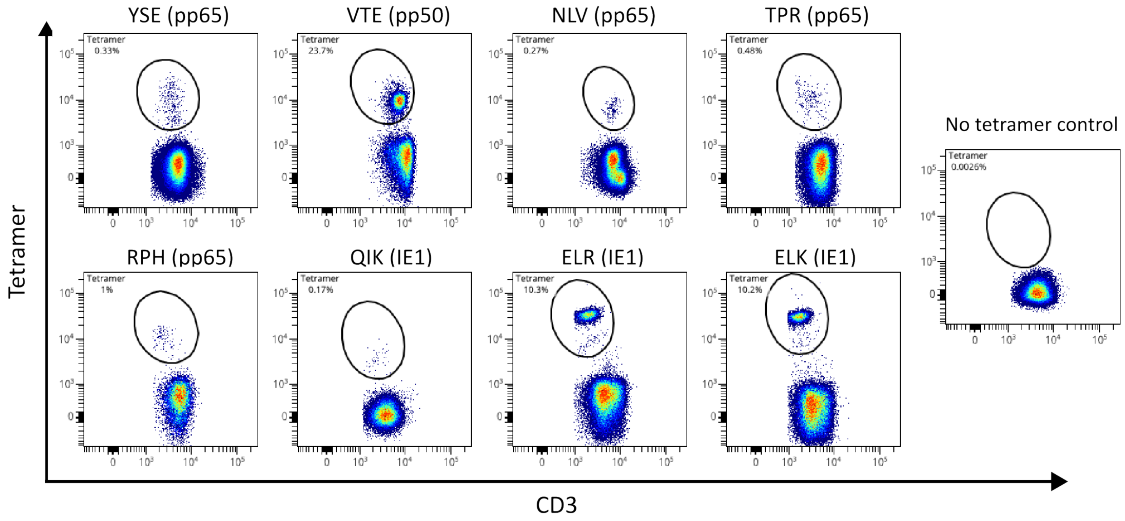
YSE (pp65)
VTE (pp50)
NLV (pp65)
TPR (pp65)
No tetramer control
RPH (pp65)
QIK (IE1)
ELR (IE1)
ELK (IE1)
Tetramer
CD3

c)

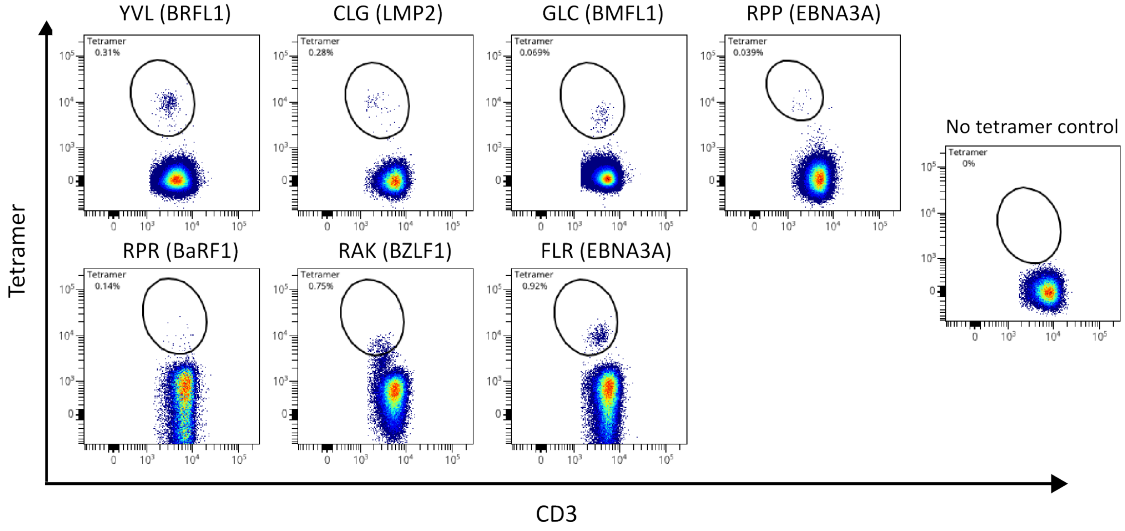
YVL (BRFL1)
CLG (LMP2)
GLC (BMFL1)
RPP (EBNA3A)
No tetramer control
RPR (BaRF1)
RAK (BZLF1)
FLR (EBNA3A)
Tetramer
CD3

Figure 11: Representative gating strategy to identify tetramer$^+$ cells

a) Gating strategy to identify CD8$^+$ T-cells. Samples were stained with the antibody panel (Healthy Donors- Surface Table 13) before flow cytometric analysis. From left to right: singlet discrimination, lymphocytes, live/ dump negative cells, T-cells and CD8$^+$ cells. This gating strategy was used throughout all CD8$^+$ T-cell analysis.

b) Representative examples of tetramer staining on CD8$^+$ T-cells across the different epitopes with the associated protein for CMV-specific CD8$^+$ T-cells with a no-tetramer control.

c) Representative examples of tetramer staining on CD8$^+$ T-cells across the different epitopes with the associated protein for EBV-specific CD8$^+$ T-cells with a no-tetramer control.

3.2.2 Healthy donor cohorts

Tetramer-specific T-cell responses are often of low magnitude whilst the relative intensity of staining can also be modest. As such, a negative control stain was included, which excluded tetramer in the staining mix. Table 14 shows a summary of the number of CMV-specific tetramer responses that showed a distinct population with good resolution across all donors with 89 responses to 8 CMV epitopes being observed across 33 donors.

Table 14: Summary of number of positive tetramer responses out of total donors assessed across CMV+ donors with details of the protein the epitope is expressed on.

Epitope	Protein	Stage expressed	HLA type	Donors (n/ total n)
YSE	Pp65	Lytic	A1	10/18 (56%)
VTE	Pp50	Lytic	A1	17/17 (100%)
NLV	Pp65	Lytic	A2	15/23 (65%)
RPH	Pp65	Lytic	B7	11/12 (92%)
TPR	Pp65	Lytic	B7	11/12 (92%)
QIK	IE1	Lytic	B8	9/11 (82%)
ELR	IE1	Lytic	B8	7/9 (78%)
ELK	IE1	Lytic	B8	9/11 (82%)
			Total Responses	**89**
			Individual donors	**33**

Similarly, EBV tetramer responses were analysed and patients showing distinct responses with good resolution were used in the final analysis. Table 15 shows the details of the EBV-responses observed in the healthy donors, with a total of 50 epitope responses in 21 donors.

Table 15: Summary of number of positive tetramer responses out of total donors assessed across EBV+ donors with details of the protein the epitope is expressed on.

Epitope	Protein	Stage expressed	HLA type	Donors (n/total n)
YVL	BRFL1	Lytic	A2	11/14 (79%)
CLG	LMP2	Latent	A2	9/14 (64%)
GLC	BMLF1	Lytic	A2	13/14 (93%)
RPP	EBNA3A	Latent	B7	6/8 (75%)
RPR	BaRF1	Lytic	B7	4/9 (44%)
RAK	BZLF1	Lytic	B8	4/6 (67%)
FLR	EBNA3A	Latent	B8	4/6 (67%)
			Total Responses	**51**
			Individual donors	**21**

3.2.3 Initial phenotyping of virus-specific T-cells

The percentage of the total $CD8^+$ T-cell repertoire that was specific for each epitope was quantified initially (Figure 12). As a large amount of the donors were from anonymised leukocyte cones it was not possible to get demographic information such as age therefore this was unable to be considered. This value was fairly consistent across all epitopes with typical ranges between 0.1% and 10% of the CD8+ T-cell pool. Of note, one donor exhibited a T-cell response of 24% against a single epitope (VTE). A significantly higher T-cell response against the pp50 VTE-epitope was seen in comparison to that against the pp65 YSE-epitope ($p = 0.0203$) (Figure 12a).

The $CD8^+$ T-cell responses against EBV epitopes were also compared to each other with the key also identifying the target proteins as either a lytic or a latent epitope (Figure 12b). An increase in T-cell response against several of the lytic epitopes was seen in comparison to recognition of latent epitopes. This was notable in the RAK-specific T-cell response, which was notably increased in comparison to that seen against two of the latent epitopes, RPP ($p = 0.0203$) and CLG ($p= 0.0046$). This is in line with the literature which indicates that $CD8^+$ responses to lytic cycle antigens occur at a higher frequency (Long et al., 2019). T-cells specific for the BMLF1 epitope GLC were also significantly upregulated in comparison to CLG-specific T-cells ($p = 0.019$). There was also a much smaller range in the percentage of cells specific for EBV epitopes, from 0.001-2.3%, indicating that the EBV-specific $CD8^+$ T-cell response in general is much smaller than the CMV-specific pool.

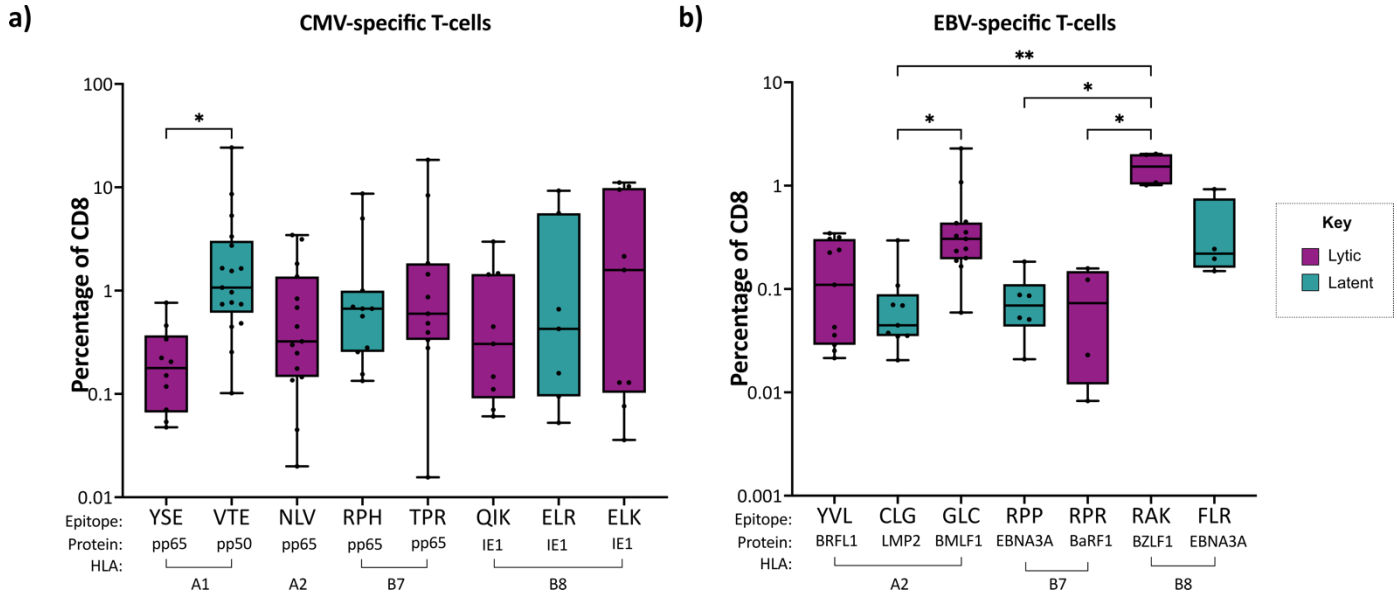

Figure 12: Summary of virus-specific T-cells for individual CMV and EBV epitopes

a) Summary of the percentage of $CD8^+$ T-cells specific for different CMV epitopes with details of the protein they originate from and which HLA-type they cover. Statistical analysis performed with Kruskal-Wallis test with Dunn's multiple comparisons test to compare all epitopes against each other with * $p < 0.05$; ** $p < 0.01$; *** $p < 0.001$; **** $p < 0.0001$.

b) Summary of the percentage of $CD8^+$ T-cells specific for different EBV epitopes with details of the protein they originate from and which HLA-type they cover. Statistical analysis performed with Kruskal-Wallis test with Dunn's multiple comparisons test to compare all epitopes against each other with * $p < 0.05$; ** $p < 0.01$; *** $p < 0.001$; **** $p < 0.0001$.

3.2.4 Memory phenotype of viral specific T-cells in healthy donors

I next went on to comprehensively phenotype CMV and EBV-specific T-cell responses using 21-colour flow cytometry as per the 'Healthy Donors- surface' panel outlined in Table 13. By combining this with tetramer staining this approach allowed substantial characterisation of the phenotype of virus-specific T-cells without the effects of stimulation on the cells.

Initial studies determined the memory phenotype of the virus-specific T-cell pool. This was done using CCR7 and CD45RA which allowed discrimination of T-cells that are Naïve ($CCR7^+$ $CD45RA^+$); central memory (T_{CM}) ($CCR7^+$ $CD45RA^-$); effector memory (T_{EM}) ($CCR7^-$ $CD45RA^-$) or effector memory with CD45RA expression (T_{EMRA}) ($CCR7^-$ $CD45RA^+$). Figure 13a shows the gating strategy applied to the $tetramer^-$ population. As there were often relatively few cells within the $tetramer^+$ population, flow cytometry gating was done within the tetramer negative population to accurately identify the memory populations with confidence and then these gates were applied to the $tetramer^+$ cells.

The data in Figure 13b summarises the memory phenotypes of the CMV-specific $CD8^+$ tetramer responses, the EBV tetramer responses, and the tetramer-negative compartment. As expected, naïve cells are found predominantly within the tetramer-negative pool, and this was markedly different to the CMV-specific T-cell profile ($p = 0.006$). In relation to the EBV-specific T-cell response, a significant increase was seen in the T_{CM} compartment in comparison to both the CMV ($p < 0.0001$) and tetramer-negative cells ($p = 0.0006$). A similar trend is shown in the T_{EM} populations, $p = 0.032$ and $p = 0.027$ respectively. However, there were significantly more CMV-specific and tetramer-negative T_{EMRA} cells in comparison to EBV-specific subsets (both $p < 0.0001$).

Together the data show significant differences in the memory profile of virus-specific CD8+ T-cell populations with T_{EM} and T_{CM} dominating the EBV-specific response whilst CMV-specific T-cells comprise a large T_{EMRA} component.

a)

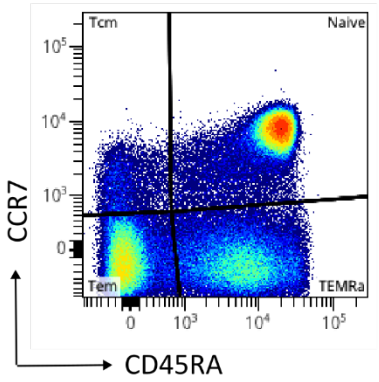
Tcm
Naive
Tem
TEMRa
CCR7
CD45RA

b)

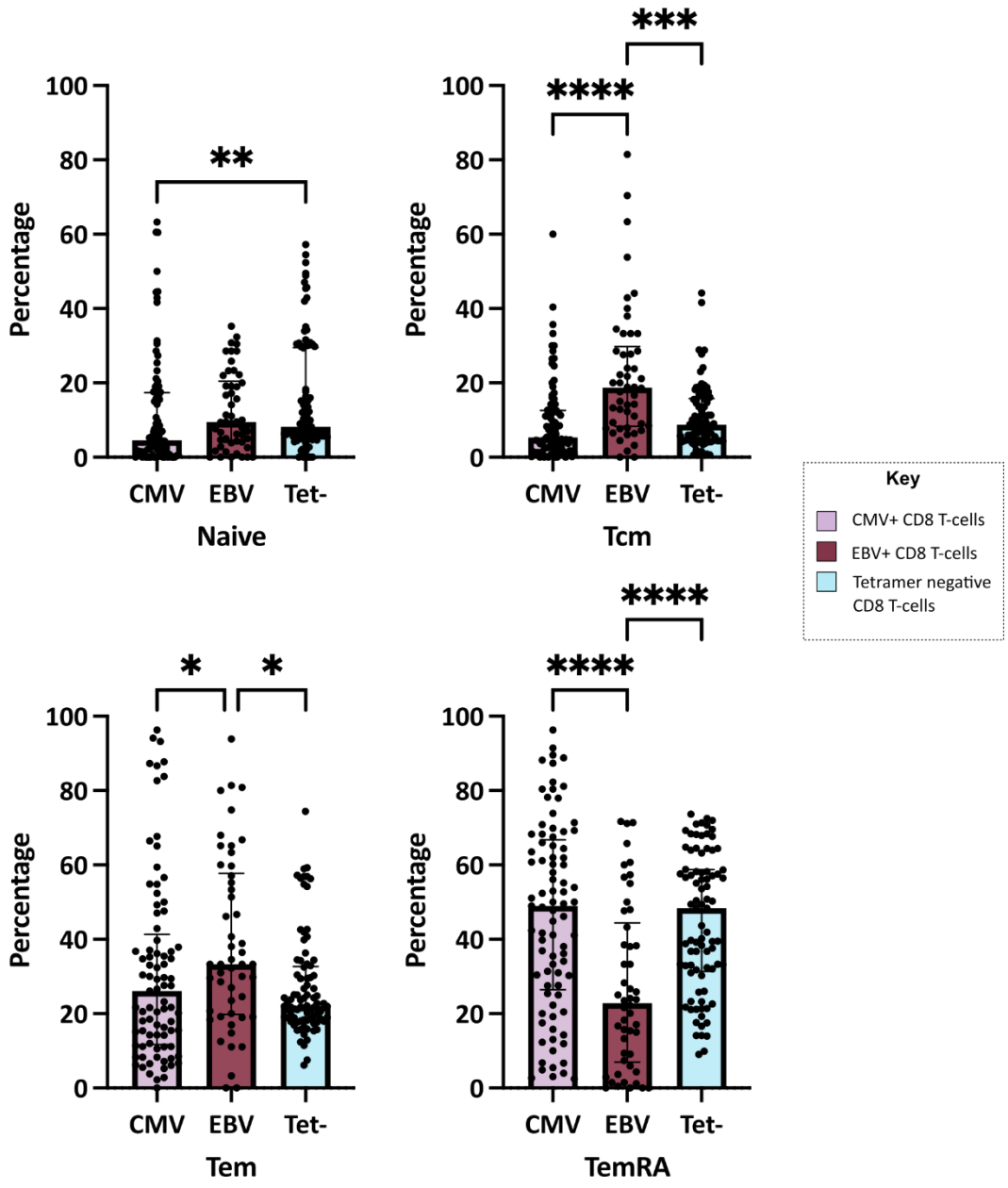
Percentage
CMV
EBV
Tet-
Naive
Tcm
Tem
TemRA
Key
CMV+ CD8 T-cells
EBV+ CD8 T-cells
Tetramer negative CD8 T-cells

Figure 13: Memory phenotyping of virus-specific T-cells

a) Representative gating strategy showing the four memory phenotypes on the tetramer$^-$ CD8$^+$ T-cells and tetramer$^+$ CD8$^+$ T-cells. Naïve T-cells (T_N), (CCR7$^+$ CD45RA$^+$), central memory (T_{CM}) (CCR7$^+$ CD45RA$^-$), effector memory (T_{EM}) (CCR7$^-$ CD45RA$^-$) and effector memory with CD45RA expression (T_{EMRA}) (CCR7$^-$ CD45RA$^+$).

b) Summary of the percentage distribution of T-cell memory phenotypes within CMV-specific, EBV-specific and tetramer negative T-cells in healthy donors. Each dot represents one tetramer response. Bars represent the percentage median of each phenotype (± interquartile range). Statistical analysis performed with Kruskal-Wallis test with Dunn's multiple comparisons test * $p < 0.05$; ** $p < 0.01$; *** $p < 0.001$; **** $p < 0.0001$.

Next, as the staining was done on individual epitopes, the memory phenotypes across the different tetramer responses were analysed. The data in Figure 14 shows that, whilst some variation in the range of memory subtype was seen between responses, there were no significant changes or trends between the different proteins and epitopes.

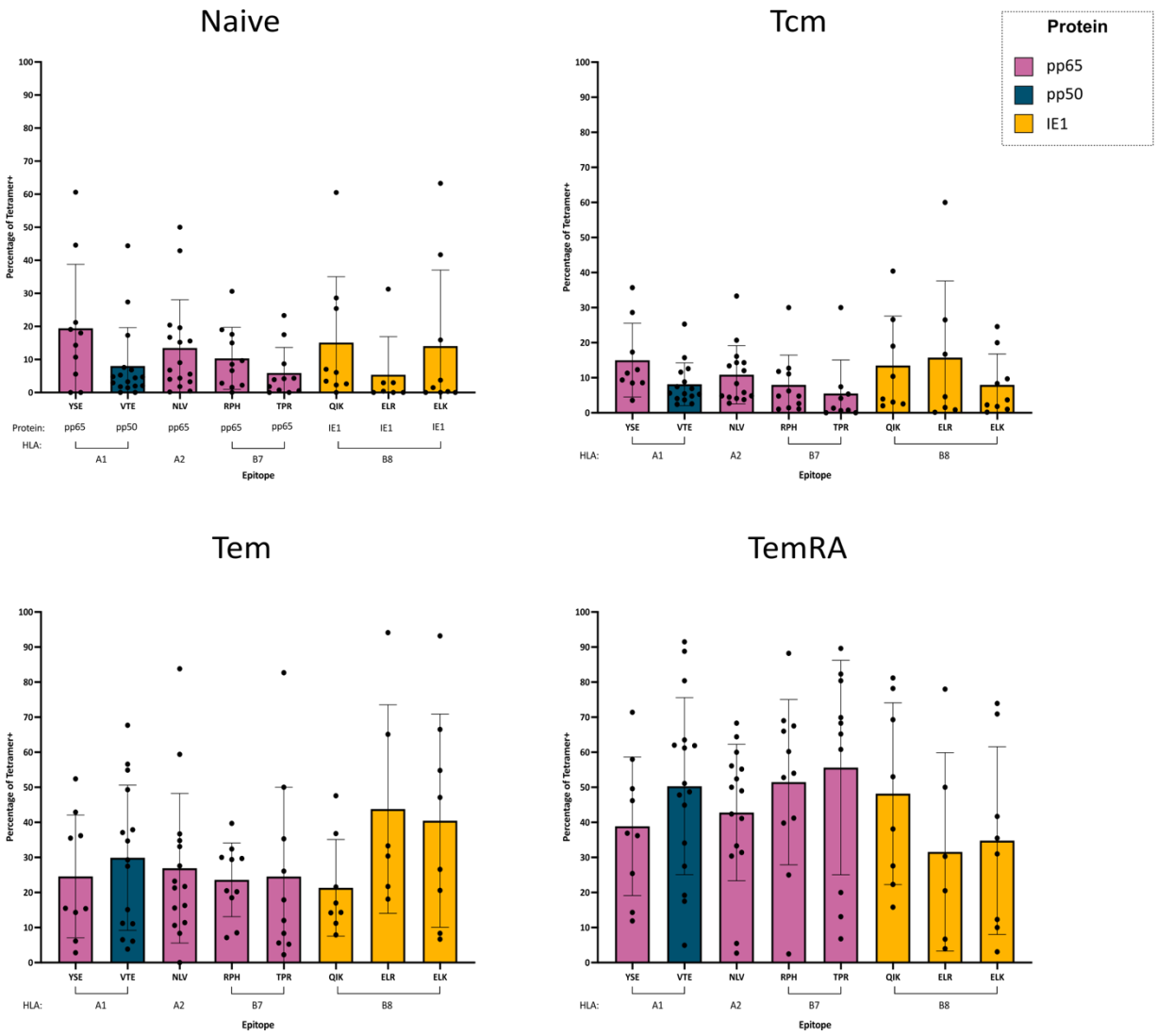

Figure 14: Memory phenotype by CMV epitope

Summary of the percentages of T-cell memory phenotypes across the different class I CMV epitopes in healthy donors. Each dot represents one tetramer response. Bars represent the percentage median of each phenotype (± interquartile range). Statistical analysis performed with Kruskal-Wallis test with Dunn's multiple comparisons test. There were no statistical differences between the populations.

Similarly, the memory phenotype of T-cells specific for EBV epitopes was next determined (Figure 15). As EBV has a defined latent and lytic life cycle, allowing confident allocation of individual proteins into a latent or lytic subgroups, I was also able to assess EBV-specific immunity against lytic and latent epitopes (Figure 15b). The T-cells which are responding to proteins in the lytic cycle are specific for the tetramers YVL, GLC, RPR and RAK, and the latent tetramers are CLG, RPP and FLR. Of note, there was an increase in cells expressing the T_{CM} phenotype ($CCR7^{+}$ $CD45RA^{-}$) within latent protein-specific responses in comparison to the lytic-specific response ($p < 0.0001$). A higher expression of T_{EMRA} cells ($CCR7^{-}$ $CD45RA^{+}$) was also seen within lytic-specific T-cells compared to the latent-specific subgroup ($p = 0.0043$).

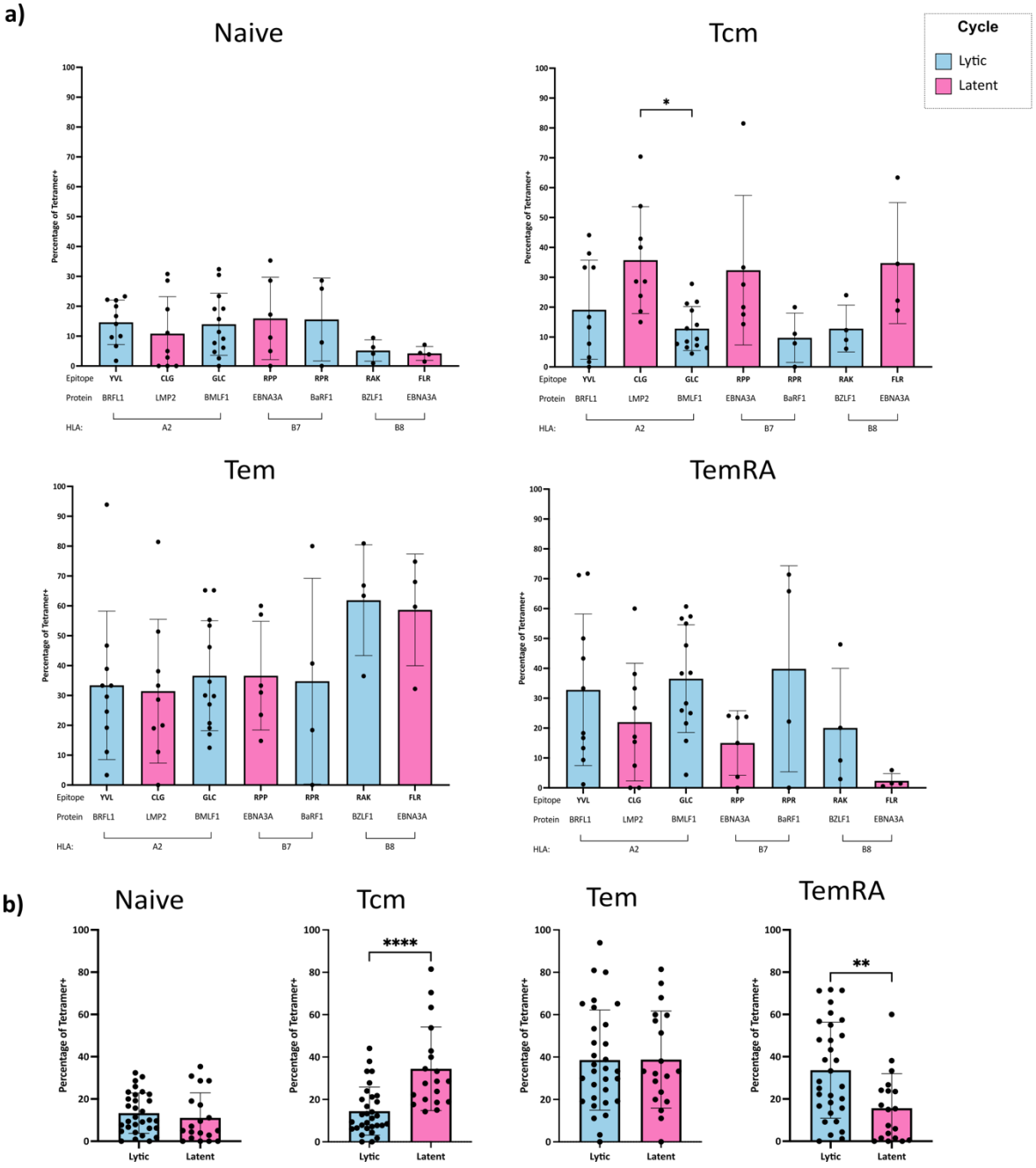

Figure 15: Memory phenotypes by EBV epitope and virus replication cycle

a) Summary of the percentages of T-cell memory phenotypes on T-cells specific for different HLA class I-restricted EBV epitopes in healthy donors. Statistical analysis performed with Kruskal-Wallis test with Dunn's multiple comparisons test.

b) Summary of the percentages of T-cell memory phenotypes on T-cells responding to proteins in the lytic and latent cycles of EBV. Statistical analysis performed with Mann-Whitney test.

Each dot represents one tetramer response. Bars represent the percentage median of each phenotype (± interquartile range), with * p <0.05; ** p <0.01; *** p <0.001; **** p <0.0001..

3.2.5 Checkpoint protein expression profile on virus-specific T-cells

PD1 is a critical negative checkpoint regulator on leucocytes and its expression has been shown on subpopulations of EBV or CMV-specific T-cells (gating shown in Figure 16a). As such, the percentage expression and relative fluorescence intensity of PD1 expression was next determined on CMV-specific, EBV-specific and tetramer-negative $CD8^+$ cells. The gating analysis is shown in Figure 16a. Of note, an increase in the percentage of $PD1^+$ $CD8^+$ T-cells was observed on the CMV-specific populations, with a median value of 60% compared to 40% on the tetramer-negative pool ($p = 0.0012$). This value was further increased to reach 80% on EBV-specific cells ($p < 0.0001$).

It was important to investigate the relative level of PD-1 expression on these cell subsets. As such the median-fluorescence intensity (MFI) was measured on PD1 positive populations as this reflects the relative amount of PD1 protein on the cell membrane. Interestingly, expression was slightly reduced on CMV-specific cells (median = 1955) in comparison to the $tetramer^-$ (median = 2398) ($p = 0.03$) but was somewhat higher on the EBV-specific pool (median = 2640) in comparison to the CMV-specific cells ($p < 0.0001$) and slightly in comparison to the $tetramer^-$ ($p = 0.08$).

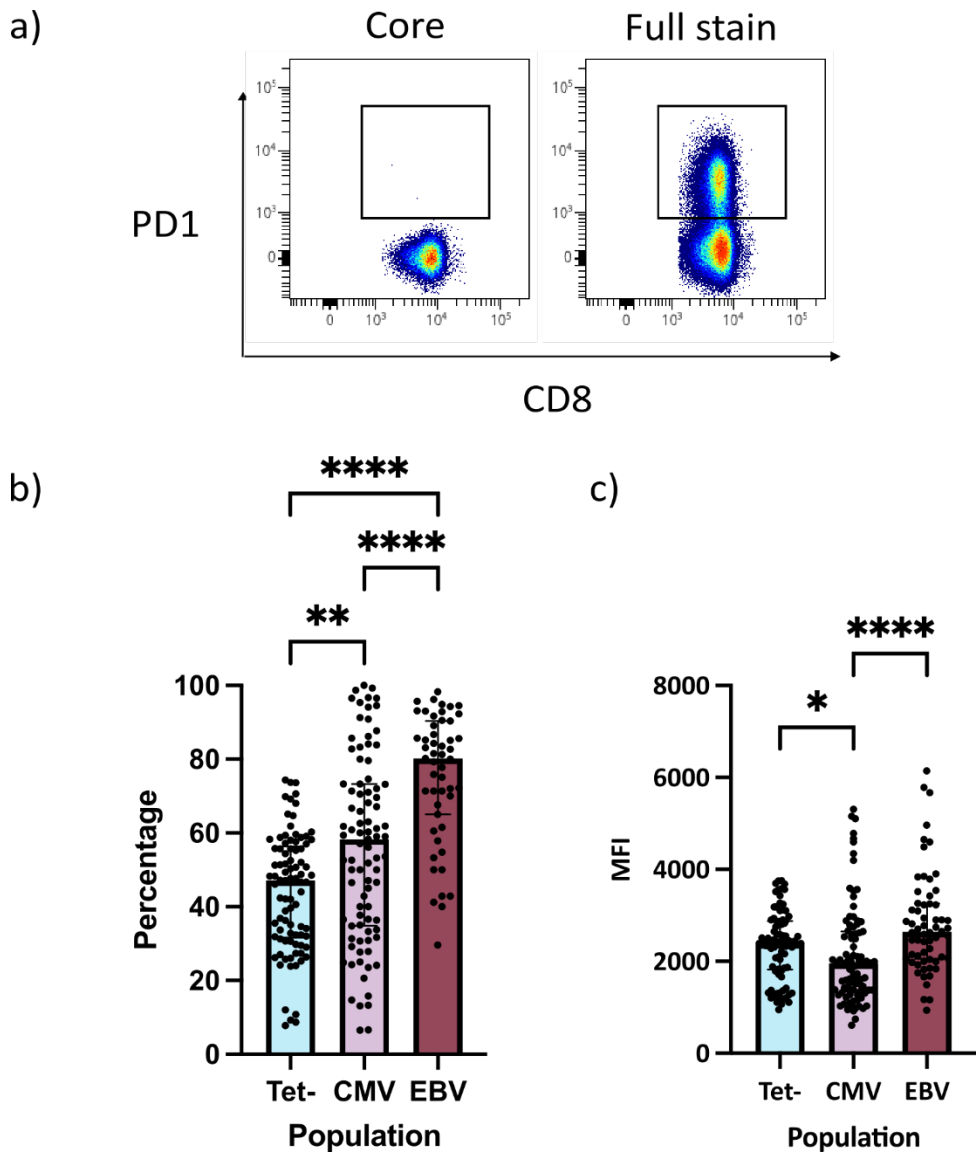

Figure 16: PD1 expression across T-cells populations

- **a)** Representative dot plots of PD1 staining and gating with the negative core control.
- **b)** Summary of the percentage of PD1 expression on CMV^+ T-cells, EBV^+ T-cells and tetramer negative T-cells.
- **c)** Summary of the median fluorescence intensity (MFI) of PD1 on CMV^+ T-cells, EBV^+ T-cells and tetramer negative T-cells.

Each dot indicates data from one donor. Bars represent the percentage median of PD1. Statistical analysis performed with Kruskal-Wallis test with Dunn's multiple comparisons test with * $p < 0.05$; ** $p < 0.01$; *** $p < 0.001$; **** $p < 0.0001$.

I next went on to assess the relative expression of other checkpoint proteins in relation to PD1 profile. In particular, my flow cytometry panel included antibodies against TIGIT, 2B4, TIM3 and LAG3.

The relative expression of each of these was determined and is shown in Figure 17. A striking observation was that TIGIT expression was markedly increased on the EBV-specific T-cell pool, seen on a median of 68% of cells in comparison to 40% and 38% specifically of the CMV-specific ($p < 0.0001$) and tetramer-negative pool ($p < 0.0001$).

In contrast, the proportion of virus-specific cells expressing 2B4 was slightly increased on the CMV-specific population compared to the tetramer-negative pool, with median values of 55.1% and 48.3% respectively ($p = 0.0035$). A trend was observed toward higher expression compared to EBV-specific cells, but this was not significant. In relation to TIM3, the number of positive cells was overall small but increased incrementally on CMV- and EBV-specific pools (medians of 2.4%, 3.3% and 5.5% respectively; $p = 0.015$ and $p = 0.0049$). Expression of LAG3 was uncommon on all CD8+ T-cells although it was notable that some donors showed very high expression on virus-specific populations, sometimes representing over 20% of the CMV- or EBV-specific compartments.

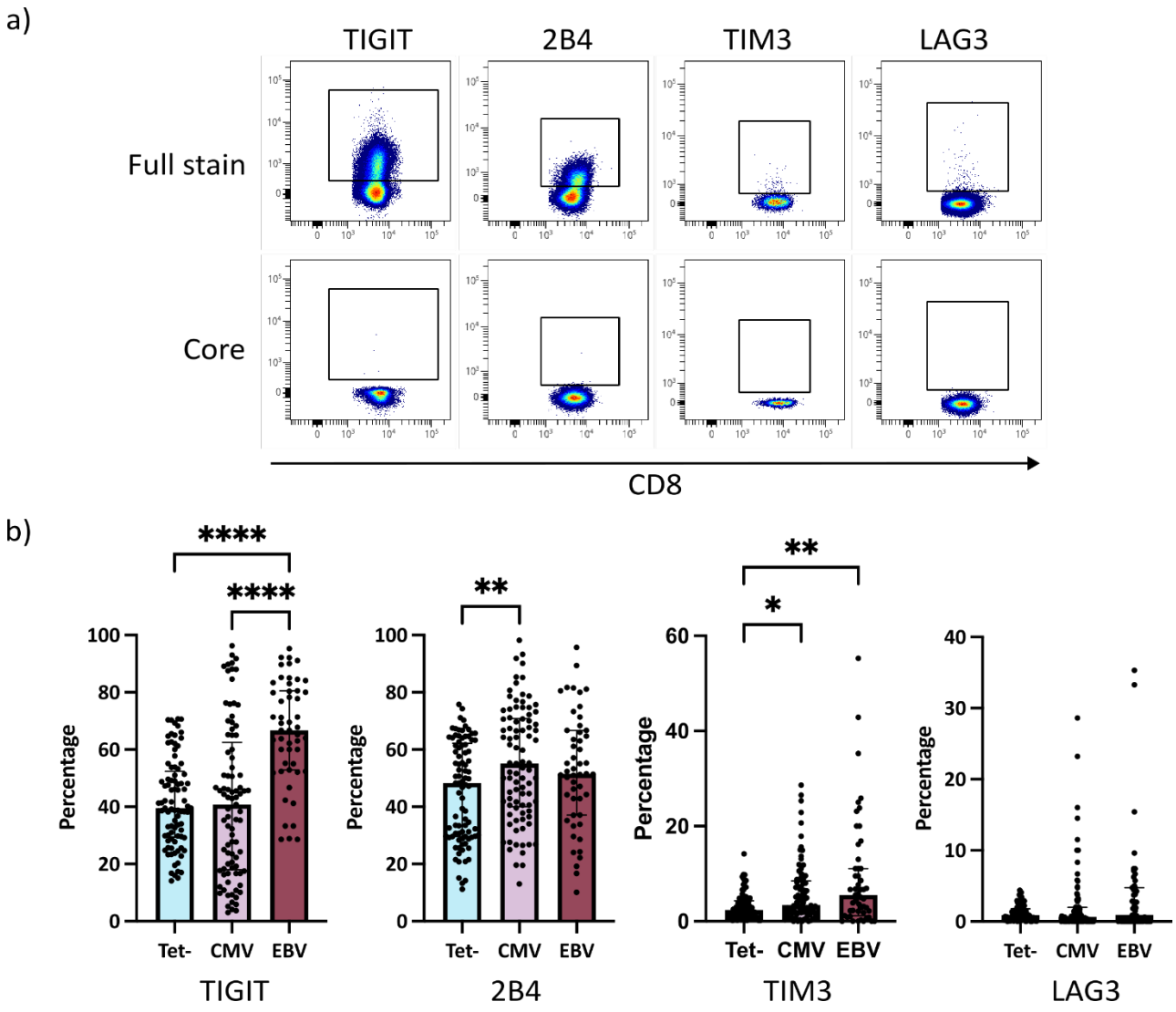

Figure 17: Expression of TIGIT, 2B4, TIM3 and LAG3 on viral specific T-cells

a) Representative dot plots of TIGIT, 2B4, TIM3 and LAG3 staining and gating with the negative core control.

b) Summary of the percentage of TIGIT, 2B4, TIM3 and LAG3 expression on CMV^+ T-cells, EBV^+ T-cells and tetramer negative T-cells. Each dot indicates data from one donor. Bars represent the percentage median of PD1. Statistical analysis performed with Kruskal-Wallis test with Dunn's multiple comparisons test with * $p < 0.05$; ** $p < 0.01$; *** $p < 0.001$; **** $p < 0.0001$.

A summary of the percentage of cells expressing each checkpoint can be found in Table 16.

Table 16: Summary of median checkpoint expression percentage from CMV-specific, EBV-specific and tetramer- cells in the PBMC of healthy donors

	Checkpoint median expression (%)				
Population	**PD1**	**TIGIT**	**2B4**	**TIM3**	**LAG3**
CMV-tetramer+	58.3	40.8	55.1	3.4	0.6
EBV-tetramer^{+}	80.2	66.7	51.5	5.5	0.9
Tetramer^{-}	47.1	39.5	48.3	2.4	0.9

Given these differences in relative cellular expression of checkpoints, it was considered important to analyse the MFI of expression (Figure 18). This comparison was much more stable and comparable across the study groups compared to relative cellular expression. However, 2B4 was seen to be more highly expressed on CMV-specific T-cells in comparison to EBV-specific cells ($p = 0.049$). LAG3 was also expressed more highly on CMV-specific T-cells in comparison to the tetramer^{-} population ($p = 0.0032$).

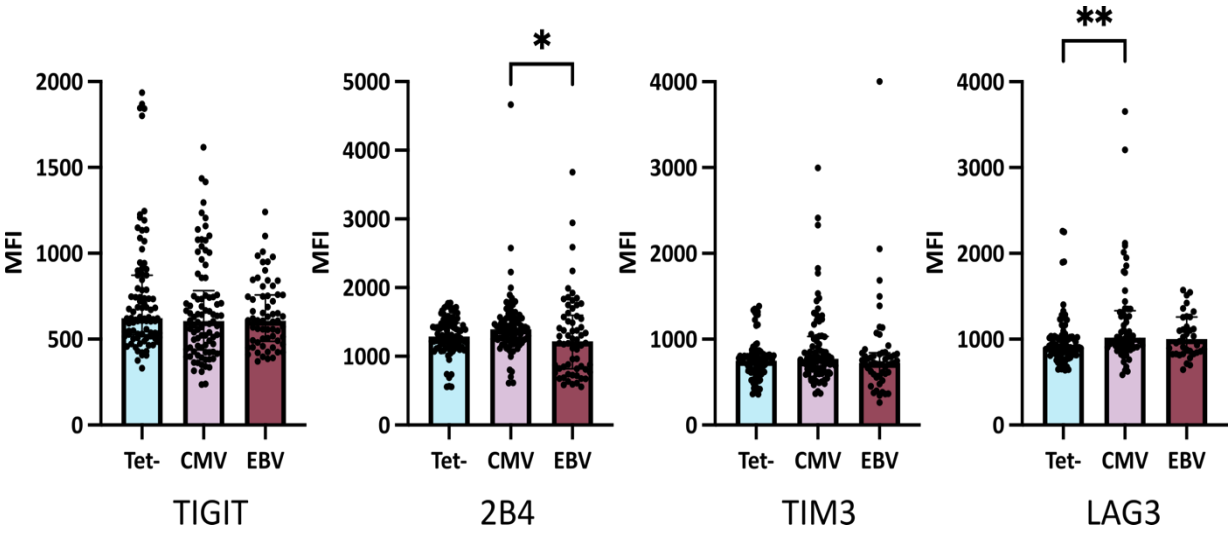

Figure 18: MFI of checkpoint expression across cell populations

Summary of the median fluorescence intensity (MFI) of TIGIT, 2B4, TIM3 and LAG3 expression on CMV-specific CD8+ cells, EBV-specific cells and tetramer-negative T-cells. Each dot indicates data from one donor. Bars represent the MFI median of the checkpoints. Statistical analysis performed with Kruskal-Wallis test with Dunn's multiple comparisons test with * p <0.05; ** p <0.01; *** p <0.001; **** p <0.0001.

A summary of the MFI data can be found in Table 17.

Table 17: Summary of median MFI of positive populations from CMV-specific, EBV-specific and tetramer- cells in the PBMC of healthy donors

	Checkpoint median MFI				
Population	**PD1**	**TIGIT**	**2B4**	**TIM3**	**LAG3**
CMV-tetramer+	1955	607	1396	772	1020
EBV-tetramer^{+}	2640	608	1220	724	1001
Tetramer^{-}	2398	622	1289	748	906

Given that my work had shown that the major differences in the relative expression of checkpoint proteins on virus-specific T-cells was seen in relation to the proportion of checkpoint-expressing cells, I next assessed this further by assessing the profile in relation to the epitope-specificity of the cell populations. PD1, TIGIT and 2B4 had been seen to be expressed on many CMV-specific T-cells and their relative distribution on epitope-specific populations was assessed initially (Figure 19).

Expression of PD1 and 2B4 was stable across all cells with different epitope specificities. In contrast, some differences were seen in relation to TIGIT expression, where expression had been documented at 40% on the total CMV-specific T-cell pool. Here expression was notably high at 66% and 50% on the NLV-specific and RPH-specific T-cell pools, with both peptides derived from the pp65 structural protein. In contrast, expression was low on T-cells specific for the QIK, ELR and ELK peptides from the IE1 protein.

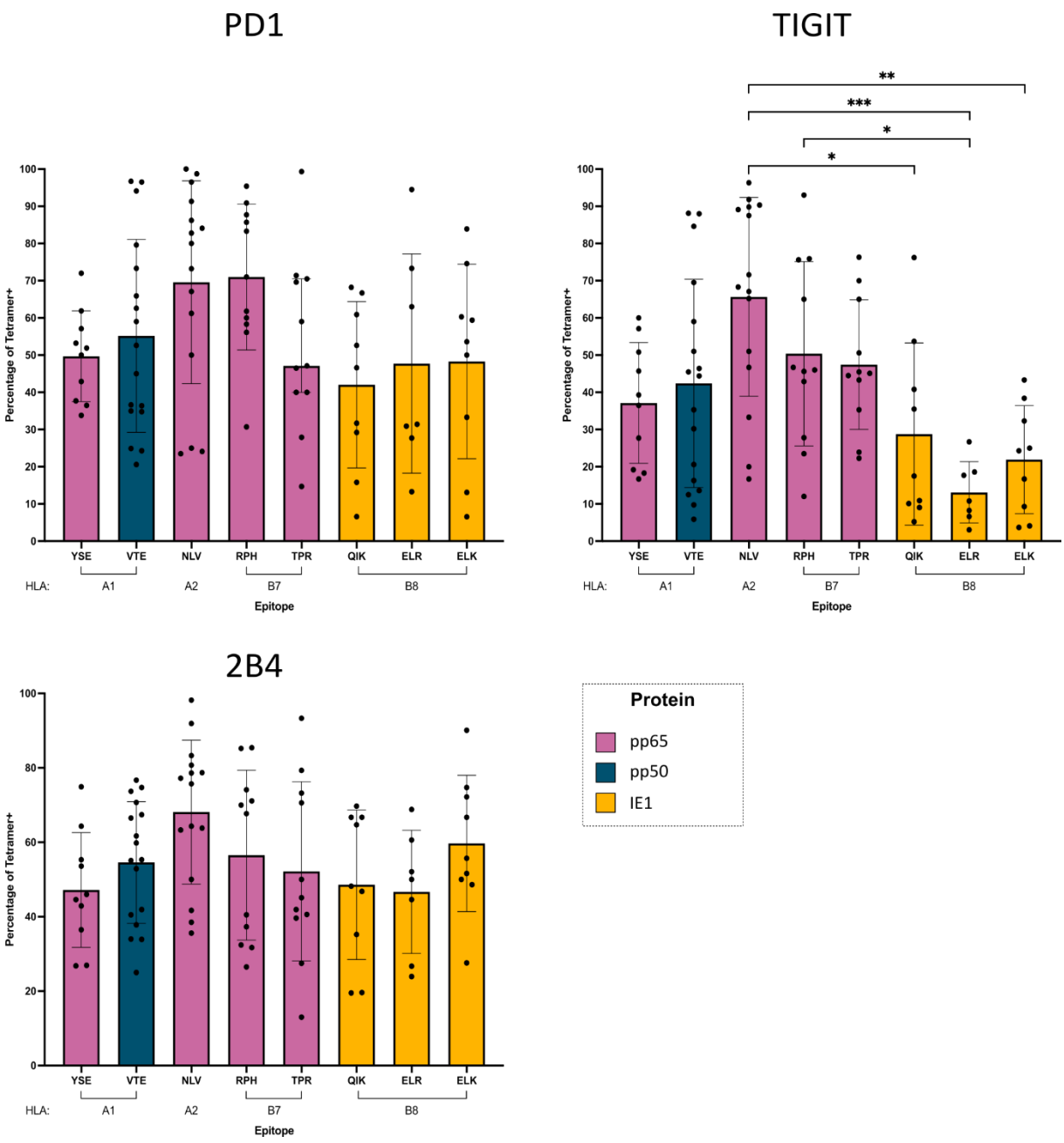

Figure 19: PD1, TIGIT and 2B4 by epitope specific CMV⁺ T-cells

Summary of the percentage cellular expression of checkpoint proteins PD1, TIGIT and 2B4 on CMV-specific CD8+ T-cells specific for peptide epitopes from three different proteins in healthy donors. Each dot represents one tetramer response. Bars represent the percentage median of each phenotype (± interquartile range). Statistical analysis performed with Kruskal-Wallis test with Dunn's multiple comparisons test with * p <0.05; ** p <0.01; *** p <0.001; **** p <0.0001.

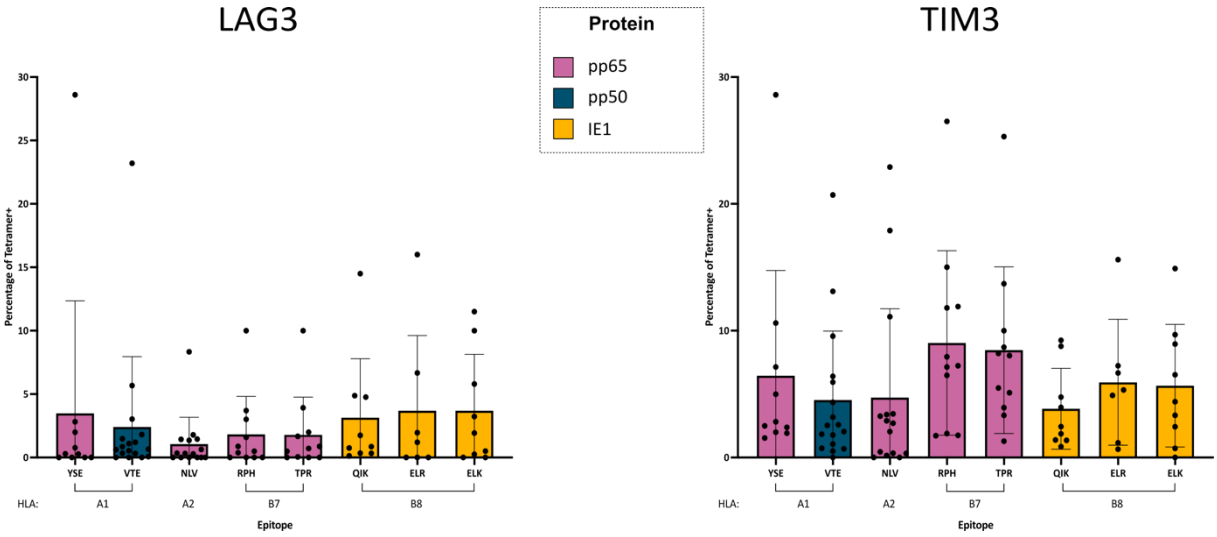

Figure 20: LAG3 and TIM3 expression by epitope specific CMV^{+} T-cells

Summary of the percentage of checkpoints LAG3 and TIM3 expression on CMV-specific CD8+ T-cells specific for peptide epitopes from three different proteins in healthy donors. Each dot represents one tetramer response. Bars represent the percentage median of each phenotype (± interquartile range). Statistical analysis performed with Kruskal-Wallis test with Dunn's multiple comparisons test with $p < 0.05$.

Expression of LAG3 and TIM3 were low on T-cells of all peptide-specificity and no significant changes were observed across epitope-specificity.

As EBV has tetramers that fall under the lytic and latent cycles, the checkpoints for EBV were analysed based on what stage of the viral replication cycle the epitope was expressed in. Here a major difference was observed in relation to TIM3 expression, which was expressed on 14.3% of CD8+ T-cells specific for peptides from latency-associated proteins compared to 6.3% on peptides from lytic-associated proteins ($p = 0.001$). A trend was also seen towards an increase in PD1 expression on the lytic cycle-specific T-cells (median = 80%) in comparison to the latent pool (median = 68%; $p = 0.12$). Relative expression of TIGIT, 2B4 and LAG3 was stable on both populations.

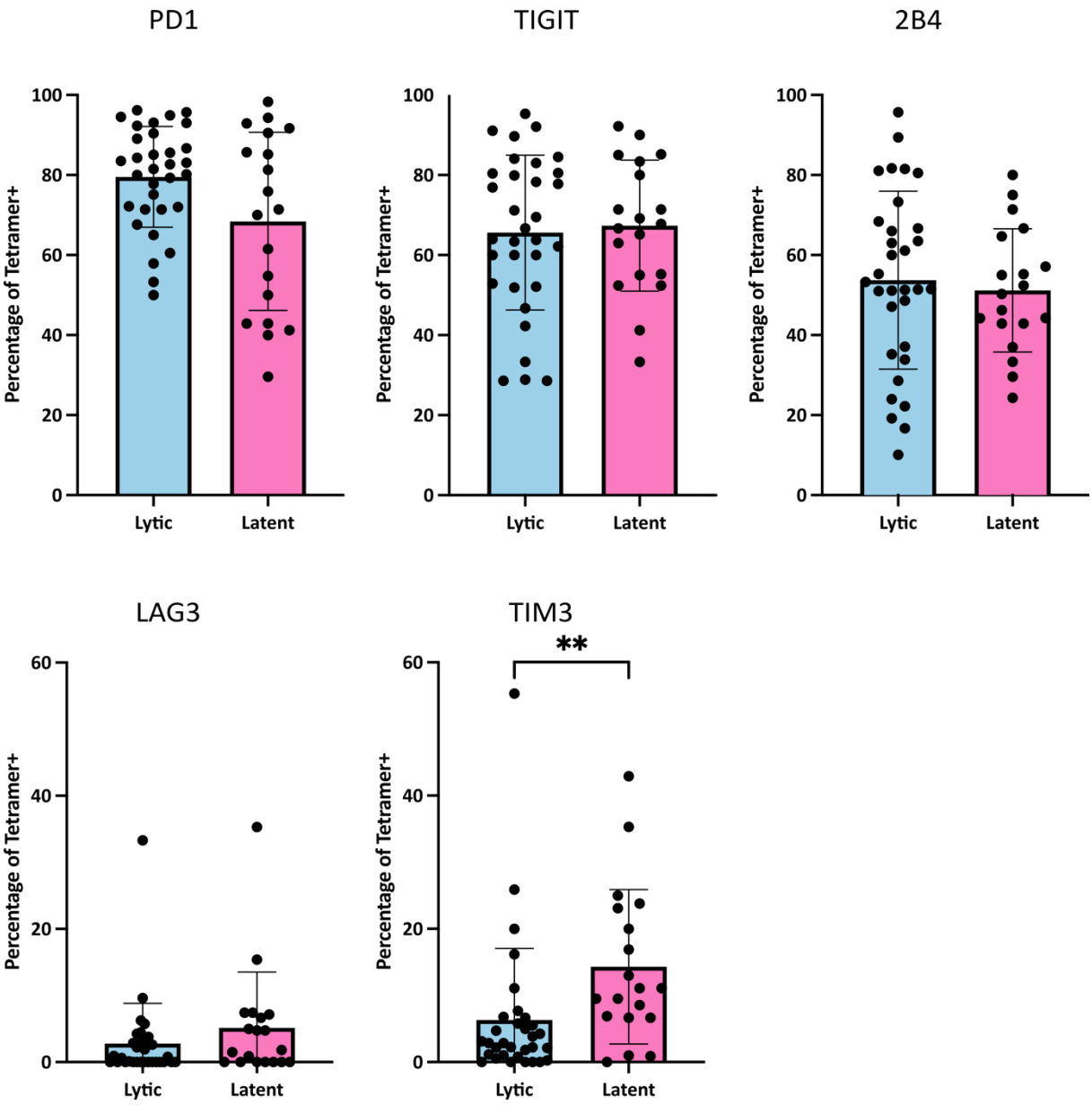

Figure 21: Checkpoint expression from T-cells specific for lytic and latent proteins

Summary of the percentage cellular expression of checkpoint proteins PD1, TIGIT, 2B4, LAG3 and TIM3 on EBV-specific CD8+ T-cells specific for peptide epitopes from the lytic or latent cycle in healthy donors. Each dot represents one tetramer response. Bars represent the percentage median of each phenotype (± interquartile range). Statistical analysis performed with Mann-Whitney test with * p <0.05; ** p <0.01; *** p <0.001; **** p <0.0001..

3.2.5.1 The pattern of checkpoint protein co-expression on virus-specific T-cells

I next undertook an assessment of the pattern of checkpoint protein co-expression.

Initial work assessed the proportion of cells with expression of a single checkpoint protein. For example, cells were identified that expressed PD1 but were negative for 2B4, TIGIT, TIM3 and LAG3 (Figure 22).

Populations that uniquely express PD1 were common in both CMV- and EBV-specific T-cell subsets and were markedly higher than single expression of TIGIT ($p = 0.0051$ and $p < 0.0001$ respectively) or TIM3 ($p < 0.0001$ in both cases). Single PD1 expression was also a more common phenotype than single 2B4 expression within EBV-specific T-cells ($p = 0.0130$). Notably, however, cells uniquely expressing 2B4 were a common subtype within the CMV-specific pool. Interestingly, in the EBV-specific cell subset there was also a high percentage of cells with sole expression of LAG3, which was higher than the 2B4 ($p = 0.013$), TIGIT ($p < 0.0001$) and TIM3 populations ($p < 0.0001$).

However, a key takeaway from this data is that the majority of $CD8^+$ T-cells specific for CMV or EBV express more than one checkpoint proteins, with this pattern showing a significant increase with a p-value of < 0.0001 in all comparisons for both viruses.

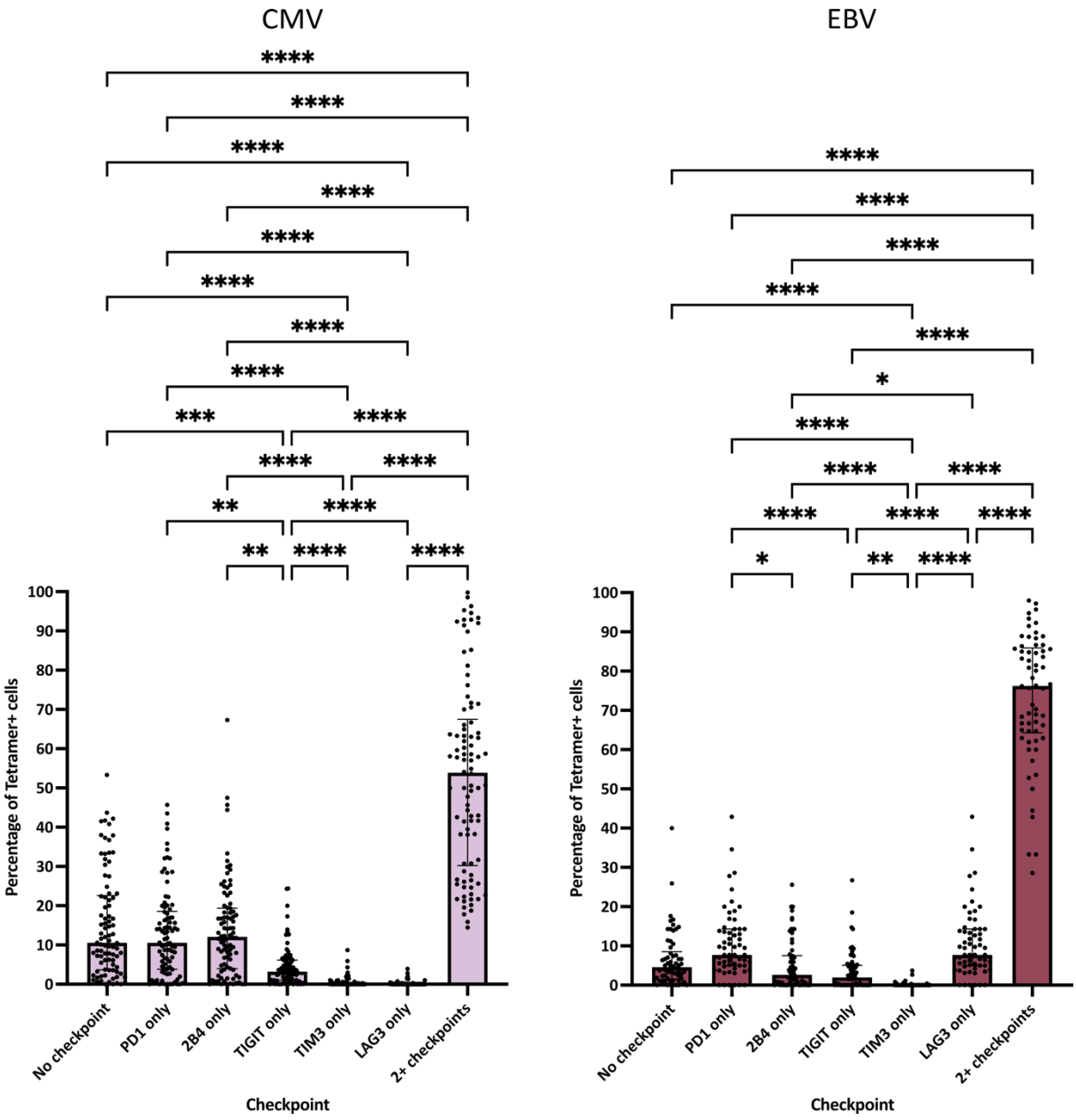

Figure 22: Phenotypic distribution of CMV- or EBV-specific CD8+ cells expressing only one checkpoint protein

Summary of expression of checkpoint expression on CMV or EBV-specific $CD8^+$ T-cells which express only one checkpoint protein. Each dot represents one tetramer response. Bars represent the percentage median of each phenotype (± interquartile range). Statistical analysis performed with Kruskal-Wallis test with Dunn's multiple comparisons test with * p <0.05; ** p <0.01; *** p <0.001; **** p <0.0001.

As PD1 expression is a major focus of my thesis, the co-expression of PD1 with an additional checkpoint protein was next analysed (Figure 23). In the CMV-specific cohort, PD1 and 2B4 co-expression was the most common phenotype (median = 9.7%), with these cells significantly increased compared to the $PD1^+$ $TIM3^+$ phenotype (median = 0.01%) and the $PD1^+$ $LAG3^+$ phenotype (median = 0%; $p < 0.0001$ in both cases). Conversely, in relation to EBV-specific T-cells, PD1 and TIGIT co-expression was the most common phenotype (median = 20.9%), with this phenotype significantly increased in comparison to $PD1^+2B4^+$, $PD1^+$ $TIM3^+$ and $PD1^+$ $LAG3^+$ populations (median = 6%, 0%, 0% respectively; $p < 0.0001$ in all cases). These findings are consistent with the data in Figure 17 which also shows TIGIT to be highly expressed on the EBV-specific CD8+ T-cell population, whilst 2B4 is more present on CMV-specific cells.

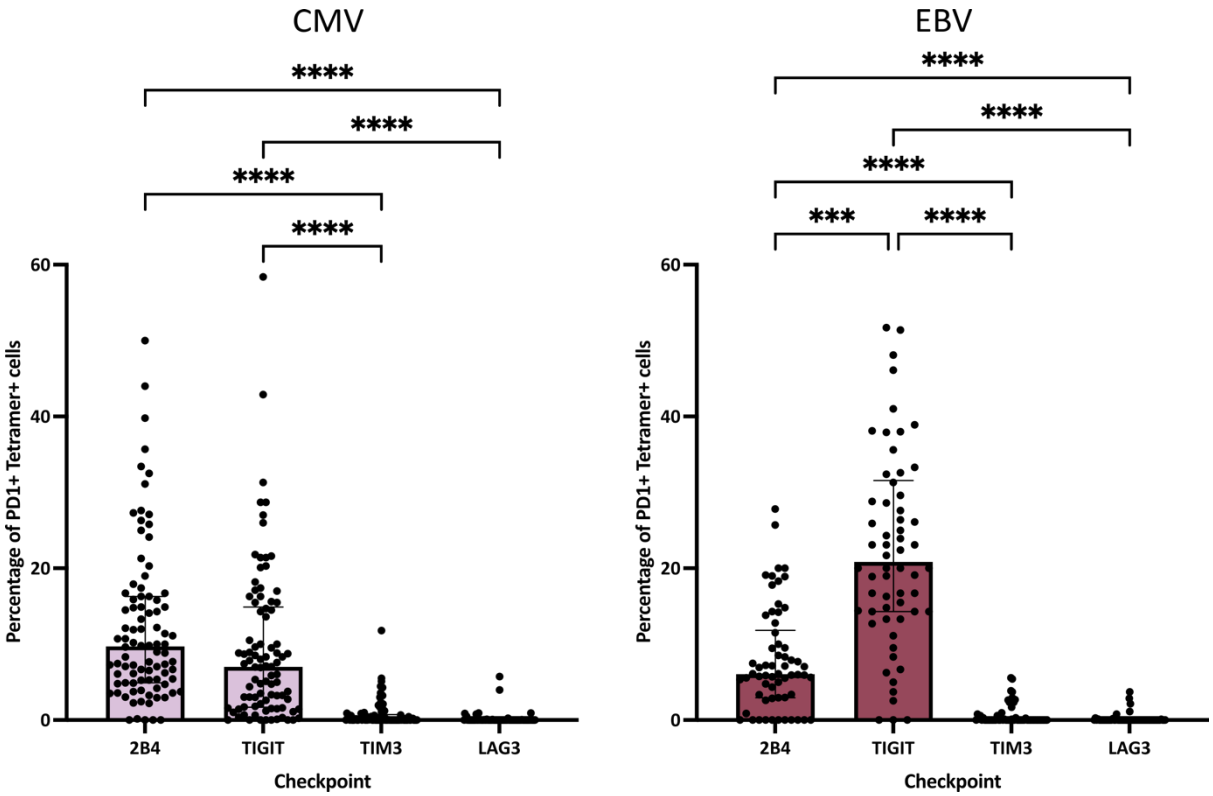

Figure 23: Co-expression of PD1 with other checkpoint proteins

Summary of checkpoint protein co-expression with PD1 on CMV- and EBV-specific $CD8^+$ T-cells. Each dot represents one tetramer response. Bars represent the percentage median of each phenotype (± interquartile range). Statistical analysis performed with Kruskal-Wallis test with Dunn's multiple comparisons test with * $p < 0.05$; ** $p < 0.01$; *** $p < 0.001$; **** $p < 0.0001$.

As the presence of PD1 on T-cells can indicate recent activation, or associate with functional exhaustion when chronically expressed, PD1 expression was also analysed with the activation markers HLA-DR and CD38 (Figure 24). Whilst no difference was seen between the tetramer^{-} and CMV-tetramer^{+} populations, the proportion of HLA-DR+CD38+ cells within the EBV-tetramer^{+} population was significantly increased in comparison to both ($p = 0.039$ and $p = 0.003$ respectively), indicating a more activated phenotype for EBV-specific PD1+ T-cells.

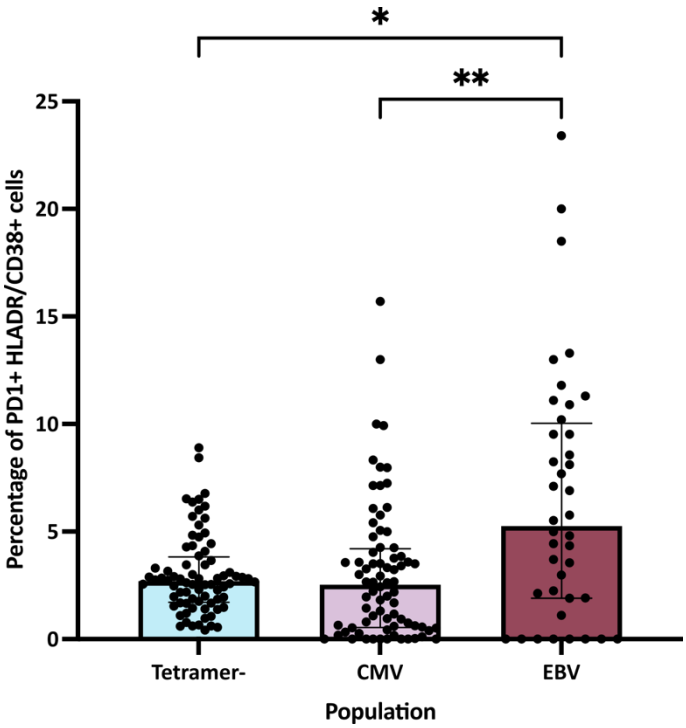

Figure 24: Co-expression of PD1 and HLA-DR+CD38+ on T-cell populations

Summary of co-expression of the activation markers HLA-DR and CD38 being co-expressed with PD1 on tetramer^{-}, CMV-specific and EBV-specific CD8^{+} T-cells. Each dot represents one tetramer response. Bars represent the percentage median of each phenotype (± interquartile range). Statistical analysis performed with Kruskal-Wallis test with Dunn's multiple comparisons test with * p <0.05; ** p <0.01; *** p <0.001; **** p <0.0001.

3.2.6 High dimensional analysis of checkpoint protein expression

3.2.6.1 Clustering of flow cytometry data

In order to carry out unsupervised assessment of checkpoint protein expression I next undertook high dimensional analysis using the OMIQ software (Dotmatics).

In flow cytometry, each event corresponds to one cell recorded by the cytometer and the intensity of marker expression detected for each event provides detailed phenotypic

information about that cell which can be used to classify cells into cell subsets based on their characteristics.

The traditional method of analysis used in flow cytometry is manual gating, where researchers visually inspect and analyse bi-axial plots (scatter plots of two markers), to identify and classify cell populations based on known marker expressions. This method relies heavily on the researchers' prior knowledge and experience to set the sequence of gates and marker thresholds. Whilst it can be precise, it is also inherently subjective and can introduce bias into the analysis.

Unsupervised clustering is an alternative approach in flow cytometry data analysis, particularly useful in large-scale or exploratory studies. Unlike manual gating, this method does not require predefined markers or prior knowledge and instead leverages algorithms to automatically identify structures or patterns within the data, grouping cells into similar clusters. Over the years the number of variables measured by flow cytometry has increased exponentially, making standard bi-axial gating a time consuming and labour-intensive method to see an overview of how the many populations of cells interact in large cohorts. Unsupervised clustering can also help to find rare and unknown cell populations (den Braanker et al., 2021, Quintelier et al., 2021).

Due to the exploratory nature of this cohort and the high number of markers being analysed, an unsupervised clustering approach was selected to identify clusters of tetramer-specific cells with phenotypes of interest that may vary between the populations before more in-depth statistical analysis of these populations using bi-axial gating.

Several clustering algorithms have been developed to analyse high-dimensional flow cytometry data, such as FlowSOM, PhenoGraph and X-shift, each offering unique advantages. FlowSOM leverages self-organising maps to organise data into clusters and is particularly notable for its fast runtimes, making it a popular choice for exploratory analysis in high-dimensional data (Weber and Robinson, 2016). First developed in 2015, the algorithm works by creating a map of nodes, where each node represents a cluster of similar cells (Van Gassen et al., 2015). For this reason, FlowSOM was selected to use for this data.

All files were uploaded to OMIQ with compensation applied and after scaling and following the gating strategy Figure 11b and c, samples were subsampled and up to 1000 tetramer$^+$ CD8$^+$ T-cells from each donor was selected. The FlowSOM algorithm was then used to cluster the cells. This was done by clustering on every marker in the panel with the exception of markers that had already been utilised or gated out in the pre-gating, such as CD3, viability dye, CD4, CD8, the dump channel and PE as this was conjugated to the preselected tetramer populations.

In the FlowSOM algorithm, determining the optimal number of metaclusters (*k*) is crucial for effective analysis. Since the exact number of expected cell types might be unknown, particularly when working with a specific subset like CD8$^+$ cells, the elbow metaclustering method is a robust approach. This method evaluates how the variance between clusters changes as *k* increases. Initially, with a low number of clusters, the variance is high because dissimilar cells are grouped together. As *k* increases, the variance decreases as clusters become more refined. The elbow criterion helps identify the optimal *k* by finding the point where the rate of variance reduction sharply declines, where adding more clusters provides

minimal further variance reduction. This method offers a data-driven way to determine *k,* especially in exploratory analyses (Van Gassen et al., 2015). For this study, the algorithm detected the optimum *k* to be 25 (Figure 25a). The star plot in Figure 25b also gives an overview of the different clusters identified and the markers they are expressing.

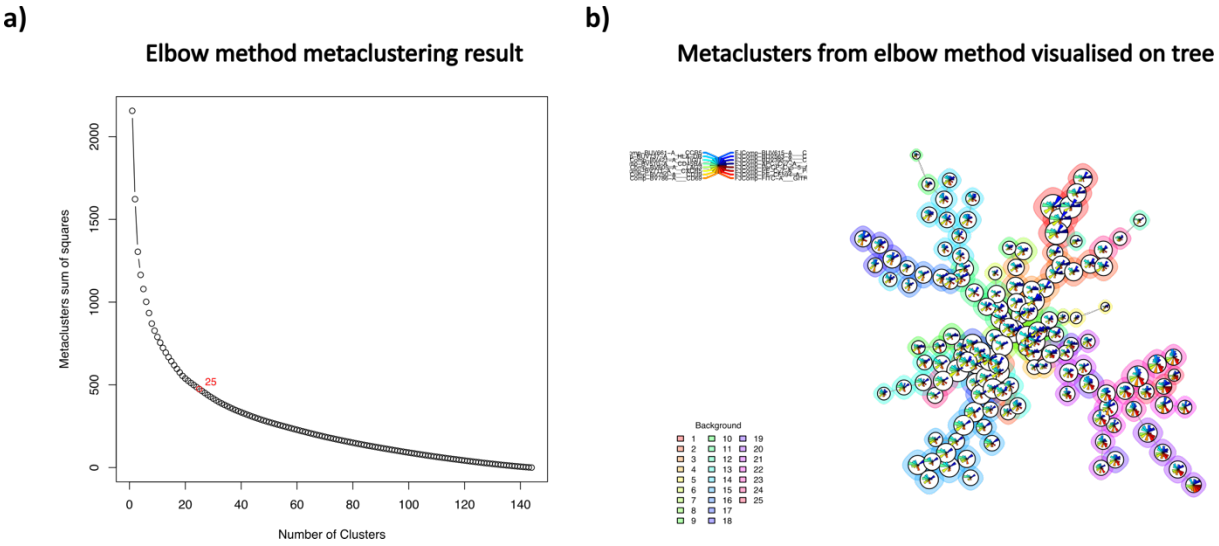

Figure 25: FlowSOM output

a) Elbow method metaclustering result. Plot showing the 25 clusters was selected as the optimal *k* as this is where the rate of reduction sharply declines, the "elbow".

b) Starplot showing the 25 metaclusters from the elbow method visualised on a tree to show an overview of the different clusters identified and how they interact with each other.

3.2.6.2 Dimension reduction

To visualise high-dimensional data, such as the results from FlowSOM clustering, dimension reduction (DR) algorithms are essential. These algorithms project the data onto a two-dimensional landscape, allowing for the visualising of complex, multi-parameter datasets in a more intuitive form. By plotting the data in two dimensions, researchers can observe how similar, or dissimilar, cell populations are spatially arranged, with cells with similar multidimensional phenotypes positioned close together on the plot and distinct populations placed further apart. This visualisation retains single-cell resolution, meaning that individual cells can still be distinguished, which is crucial for detailed analysis and understanding of the underlying biological structures (Amir el et al., 2013).

There are several DR methods available, including Isomap, t-distributed stochastic neighbour embedding (t-SNE) and uniform manifold approximation and projection (UMAP). Each method has its advantages and drawbacks. For example, t-SNE is effective at separating clusters but often loses information about the relationships between the clusters, and also requires significant computational time. UMAP preserves more of the overall data structure, such as the global relationships between clusters, while also being computationally efficient. (Becht et al., 2019). Due to these advantages, UMAP was selected for this analysis. After some initial assessment, the settings used to run the UMAPs were as follows: Neighbours: 15, Minimum Distance: 0.4, Components: 2, Metric: Euclidean, Learning Rate: 1, Epochs: 200, Random Seed: 3680, embedding initialisation: spectral. These allowed good resolution of clusters without over-clustering.

One of the problems with clustering and DR is they can often identify too many clusters with cells that display minimal or no differences in characteristics (Huang et al., 2022). As this was already a specific subset of cells (Tetramer^{+} CD8^{+}), this appeared to have happened with this dataset, with several of the clusters displaying minimal biological variance. Clusters were analysed using a combination of a heatmap and histograms to determine the expression of markers within each cluster, alongside visually inspecting where the clusters sat on the UMAP plot. This way several clusters were merged leaving a total of 12 distinct clusters as shown in UMAP plots in Figure 26.

Whilst less EBV tetramer^{+} T-cells were available for analysis, meaning the clusters are not as visually dense as the CMV tetramer^{+} populations, it was apparent that the general outline of the UMAPs were broadly similar, although clear differences were seen in relation to cell clustering.

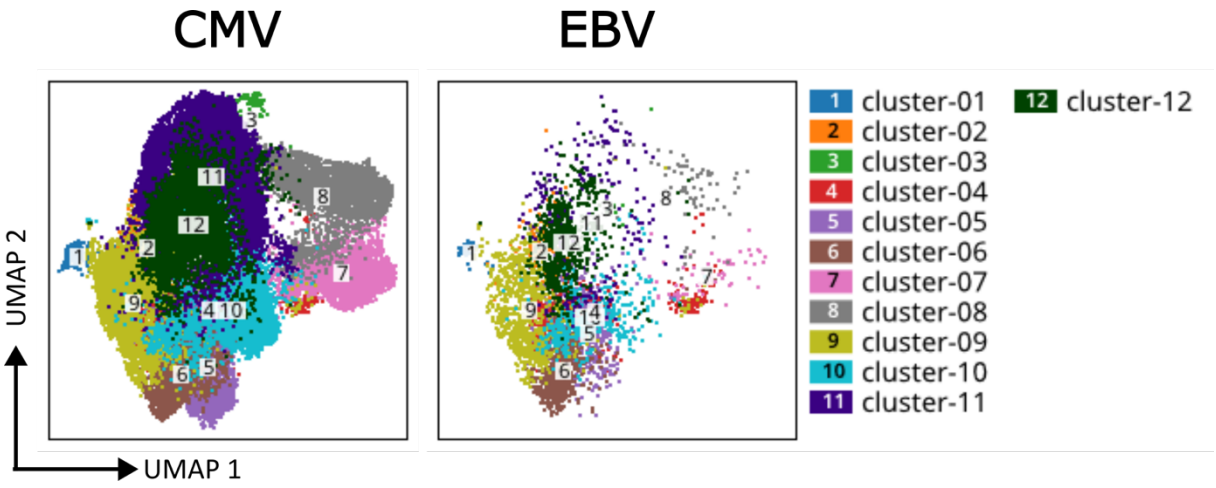

Figure 26: UMAPs of virus-specific T-cells based on checkpoint protein expression

UMAPs showing the concatenated CMV and EBV tetramer^{+} T-cells with the 12 identified clusters overlaid.

To get an overview of the expression of individual membrane proteins in each cluster, a heatmap was generated (Figure 27). This showed the distribution of the different markers across each cluster to aid further analysis.

PD1	TIGIT	2B4	LAG3	TIM3	CCR7	CD45RA	CD27	CD28	HLA-DR	CD38	CD39	CD69	
0.84	-1.88	1.31	0.12	0.25	0.29	2.14	0.17	0.42	-1.7	0.89	3.32	0.87	Cluster 3
0.27	-0.17	0.61	0.11	0.11	3.62	4.1	2.62	1.7	0.63	1.03	-0.07	0.84	Cluster 1
1.33	-0.01	1.37	-0.04	0.24	-1.02	-0.64	0.1	0.34	0.51	0.74	-2.14	5.12	Cluster 7
1.47	-0.04	1.25	-0.03	0.17	-0.56	2.56	0.26	0.23	0.23	0.59	-1.54	4.52	Cluster 8
0.62	0.44	1.39	0.15	0.17	-0.42	2.61	0.38	0.42	0.73	0.68	-0.17	0.96	Cluster 11
2.55	1.12	1.4	0.05	0.15	-0.48	2.56	0.84	0.53	0.51	0.72	-0.46	1.5	Cluster 12
2.43	0.82	1.16	0.09	0.12	-0.67	2.47	2.18	1.84	0.82	0.46	-0.39	1.45	Cluster 2
1.89	1.39	1.36	0	0.06	0.65	-0.08	2.31	1.35	1.82	0.75	-0.7	1.98	Cluster 4
1.9	0.74	1.01	0.05	0.08	1.48	1.03	2.41	2.04	0.84	0.5	-0.3	1.32	Cluster 9
2.76	0.85	1.16	0.03	0.09	-0.46	0.01	0.41	0.47	0.86	0.77	-0.37	1.42	Cluster 10
3	1.29	1.44	0.06	0.06	0.06	0	2.33	0.47	0.57	0.38	-0.63	1.8	Cluster 5
3.18	1.3	1.05	0.01	0.07	-0.79	-0.31	2.38	1.65	1.36	0.46	-0.42	1.37	Cluster 6

Figure 27: Heatmap of membrane phenotype of cells within each cluster

Heatmap showing the expression of the markers across the 12 different clusters. The shade of colour corresponds to the cell value with a darker shade indicating higher expression. The cell values for each marker are median ArcSinH values and are scaled individually to allow relative comparison between each cluster.

To further evaluate the co-expression of the checkpoints, density UMAPs were used to help assess the distribution of the markers on CMV-tetramer$^+$ CD8$^+$ T-cells (Figure 28). In line with the manual gating data, it shows a strong expression of PD1 in certain subsets of cells, and a weaker but higher percentage of cells that are positive for 2B4. There is also some strong expression of TIGIT in a smaller number of cells. Due to the low expression, the LAG3 and TIM3 populations are difficult to assess.

Overall, the UMAPs and heatmap show that the cells in clusters 5 and 6 are positive for PD1, TIGIT and 2B4 expression, however there is also a population of cells in clusters 7 and 8 that are PD1 and 2B4 positive but do not express TIGIT (with cell values of -0.01 and -0.04 on the heatmap). From the density UMAPs, only the subsets strongly expressing PD1 are positive for further checkpoints, indicating this may be an exhausted population.

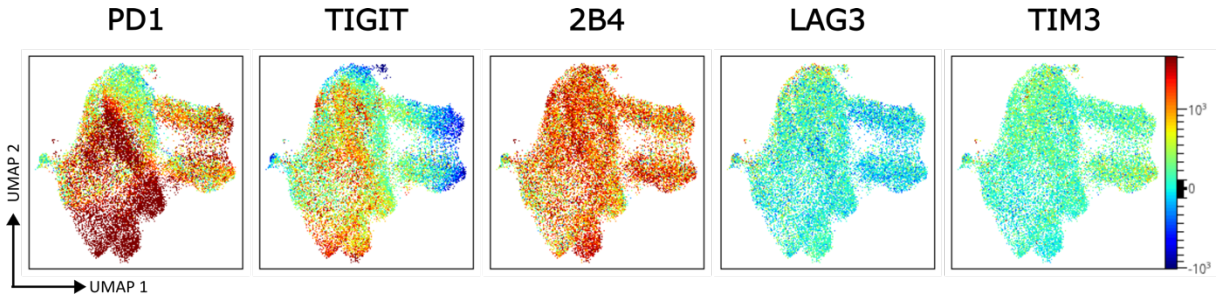

Figure 28: Checkpoints on CMV-specific T-cells

UMAPs showing the expression and distribution of the checkpoints PD1, TIGIT, 2B4, LAG3 and TIM3 on CMV-specific T-cells (n = 90). As per the colour bar, dark red indicates higher expression with blue indicating no expression.

The same analysis was carried out on the EBV-tetramer^{+} cells (Figure 29). In line with the manual gating (Figure 16b), it shows that all EBV tetramer^{+} cells display some level of PD1. It also shows a wide range of TIGIT expression, with populations positive for PD1 and TIGIT, whilst 2B4 expression was modest and not as strong as on the CMV-specific population. Similarly, due to their low expression, it is difficult to accurately assess the expression of TIM3 and LAG3.

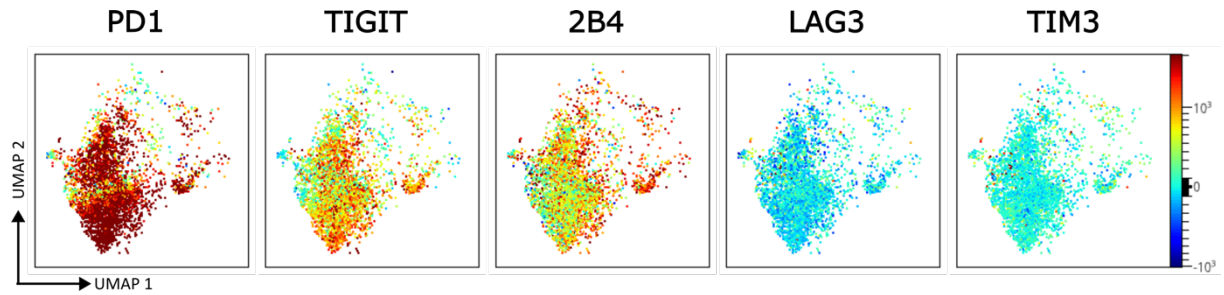

Figure 29: Checkpoints on EBV-specific T-cells

UMAPs showing the expression and distribution of the checkpoints PD1, TIGIT, 2B4, LAG3 and TIM3 in the EBV-specific T-cells (n = 50). As per the colour bar, dark red indicates higher expression with blue indicating no expression.

3.2.6.3 Comparing clusters

When comparing conditions in flow cytometry data, identifying changes in the abundance of cell populations is a key challenge. To address this, statistical analysis can be conducted using the edgeR package, which was originally developed for RNA sequencing data. The algorithm works by modelling the count data- whether it's gene expression levels in RNA-seq or cell counts in flow cytometry- to analyse differences in abundances across conditions (Lun et al., 2017). In this dataset, edgeR was used to compare the CMV to EBV specific populations (Figure 30a).

The data shows that cells in clusters 6 and 4 were significantly upregulated in the EBV-specific T-cells in comparison to the CMV, whereas clusters 8 and 11 were downregulated. Figure 30b shows layout of the various clusters and along with the data in Figure 28 and Figure 29 shows that clusters 4 and 6 were cells which strongly express PD1 and TIGIT, whereas cluster 11 is largely PD1 and TIGIT negative and 2B4 positive. This is in line with the data in Figure 22 which

showed that there was a population of CMV-specific T-cells that solely expressed 2B4. Cluster 8 shows a similar phenotype but with PD1 expression.

a)

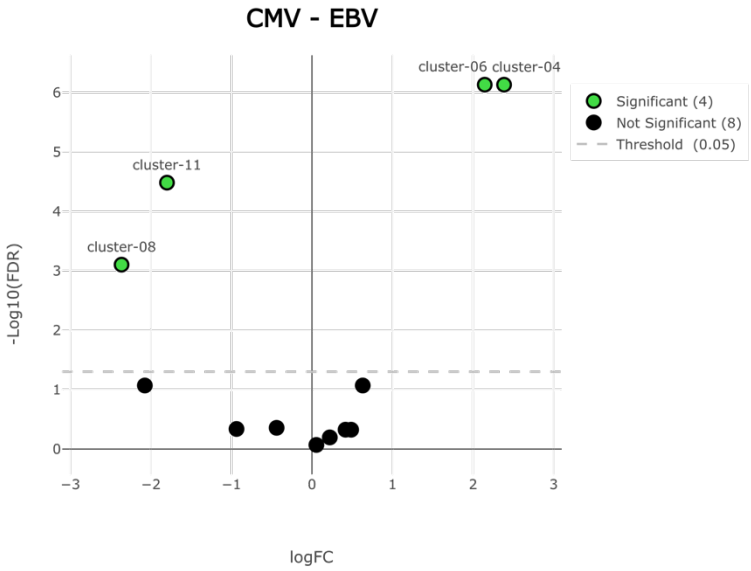

b)

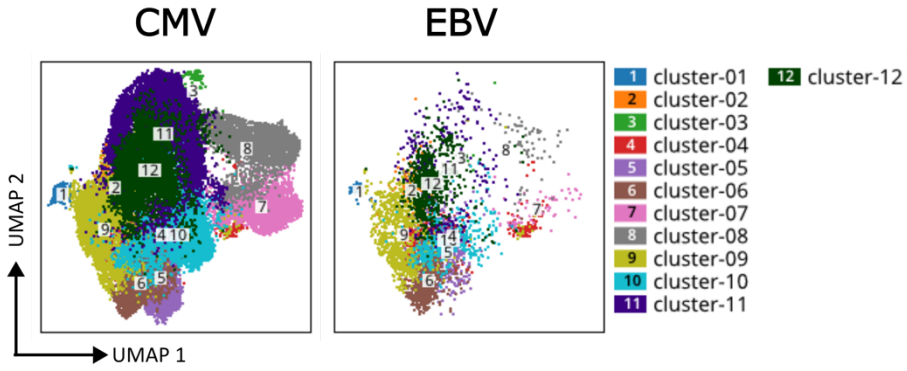

Figure 30: Volcano plot showing the statistical difference in cell clusters between CMV-specific and EBV-specific T-cells

a) edgeR analysis generated volcano plot indicating the statistical differences between the clusters in CMV vs EBV specific T-cells. A statistical p value of <0.05 is indicated by green dots above the threshold line, clusters to the right of 0 indicate the fold change increase in expression whereas the clusters to the left indicate a significant downregulation. Black dots under the threshold line indicate clusters with no significant changes. The data was plotted against false discovery rate (FDR), an adjusted p-value which reduces the chances of false positives.

b) UMAPs of the CMV and EBV specific T-cells by cluster

This is supported by Figure 31 which shows a numerical representation of the distribution of cell percentage distribution within each cluster in order to get an indication of which clusters contain the most cells with the upregulated clusters indicated by asterisks. This method shows an increase in the percentage of cells in clusters 8 and 11 in the CMV-tetramer^{+} population and 4, 6 and 9 in the EBV-tetramer^{+} population.

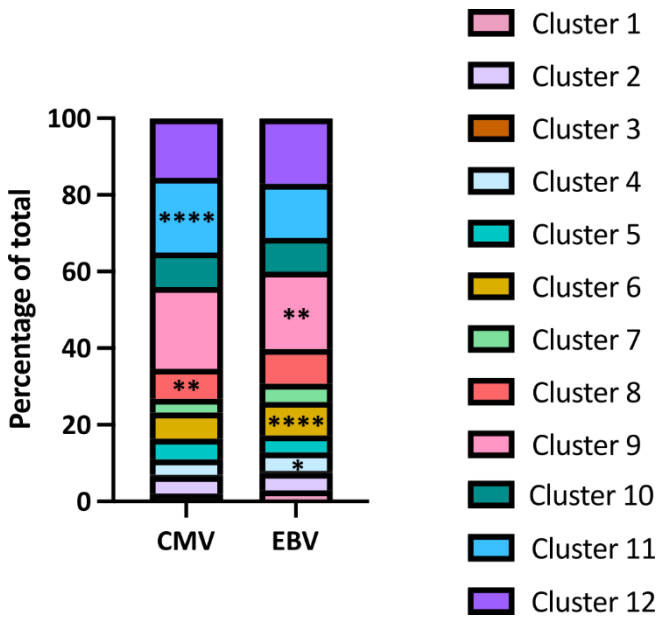

Figure 31: Cluster distribution

Graph showing the average percentage of cells in each cluster for CMV-specific and EBV-specific CD8^{+} T-cells. Statistical analysis performed with Mann-Whitney test on the values in each cluster. The upregulated population is indicated by the *. * $p < 0.05$; ** $p < 0.01$; *** $p < 0.001$; **** $p < 0.0001$

To further phenotype these markers, heatmaps and density plots were used. The density plots are found in Figure 32. The plots reveal that clusters 4 and 6, which are upregulated in the EBV-specific T-cell populations, are largely CCR7^{-} CD45RA^{-} indicating a T_{EM} phenotype. Some

of the cells displayed co-expression of HLA-DR and CD38, indicating activation, and there was a mixture of CD27 and CD28 expression.

Conversely, clusters 8 and 11 display a $CCR7^-$ $CD45RA^+$ phenotype, indicating a T_{EMRA} phenotype; in line with this, they also do not exhibit CD27 or CD28 expression. They are also negative for HLA-DR and CD38 although, interestingly, cluster 8 shows positivity for CD69 expression, indicating recent activation.

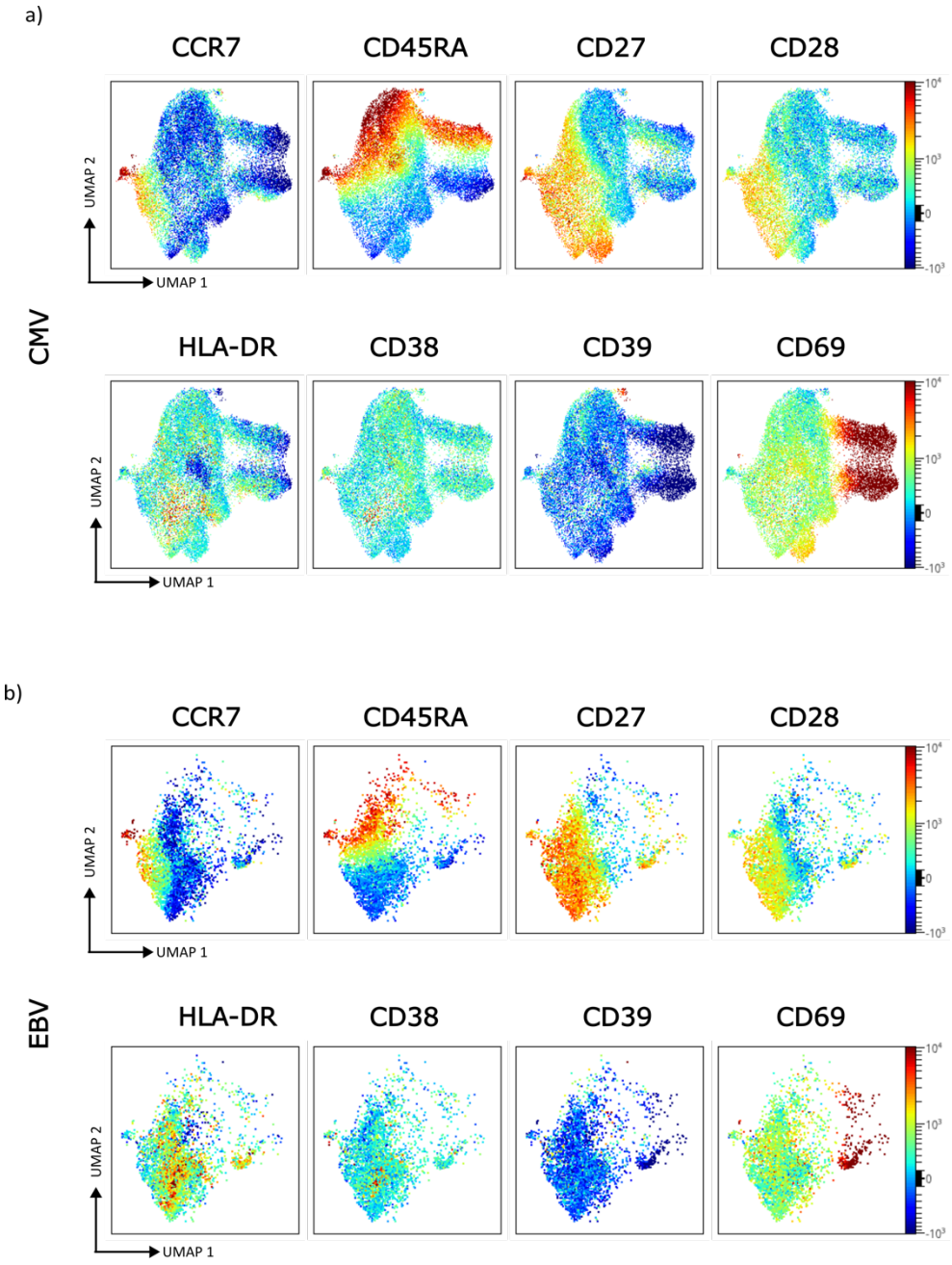

Figure 32: Density plots of phenotype of CMV and EBV specific T-cells

a) UMAPs showing the concatenated CMV-specific T-cells with the expression of various phenotypic markers

b) UMAPs showing the concatenated EBV-specific T-cells with the expression of various phenotypic markers

As per the colour bar, dark red indicates higher expression with dark blue indicating no expression.

Finally, as the UMAPs demonstrated a stark split between the CD27 and CD28 positive and negative populations, these were analysed in more detail using manual gating (Figure 33). CMV-specific T-cells are known to display a downregulation of both markers, and this is supported by the data with EBV displaying a relative upregulation of CD27 and CD28, both individually and in combination, in comparison to the tetramer$^-$ and CMV-tetramer$^+$ populations ($p < 0.0001$ in all cases). CMV-tetramer$^+$ T-cells also displayed a downregulation of the dual-positive cells in comparison to the tetramer$^-$ cells ($p = 0.041$).

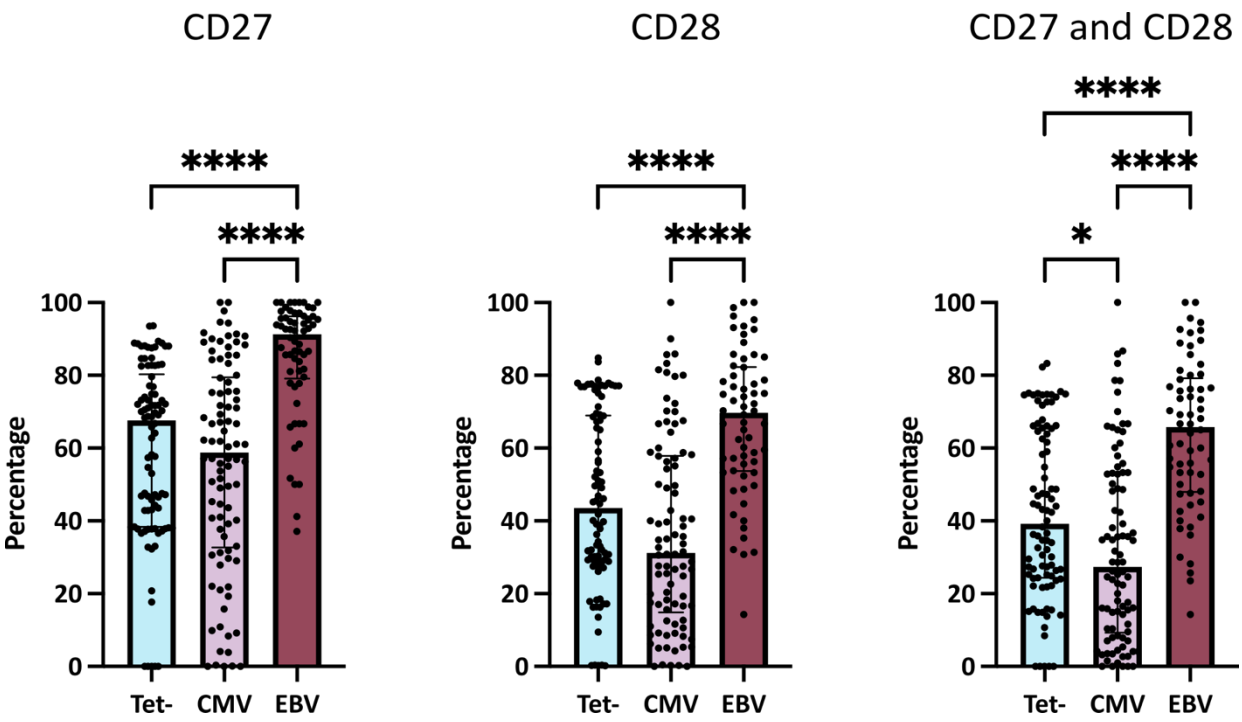

Figure 33: CD27 and CD28 expression on virus-specific T-cells

Summary of expression of CD27, CD28 and dual-positive CD27 and CD28 cells from tetramer$^-$, CMV and EBV-specific CD8$^+$ T-cells. Each dot represents one tetramer response. Bars represent the percentage median of each phenotype (± interquartile range). Statistical analysis performed with Kruskal-Wallis test with Dunn's multiple comparisons test with * $p < 0.05$; ** $p < 0.01$; *** $p < 0.001$; **** $p < 0.0001$

As CD28 plays a role in the PD1 signalling pathway, PD1 expression was analysed on $CD28^+$ and $CD28^-$ cells (Figure 34). Interestingly, whilst showing no differences in the $tetramer^-$ population, in the CMV-specific population, the $CD28^-$ population displayed significantly more PD1 than the $CD28^+$ ($p = 0.0003$). The opposite effect was observed in the EBV-specific population with the $CD28^+$ population expressing significantly more PD1 ($p < 0.0001$).

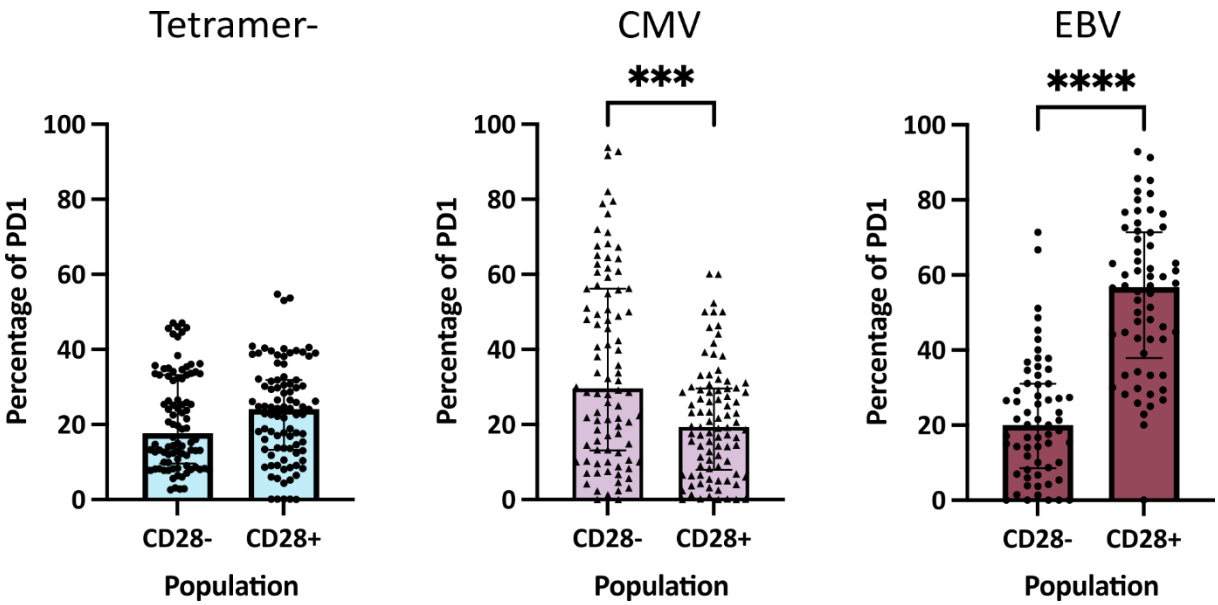

Figure 34: PD1 expression by CD28 population

Summary of PD1 expression on $CD28^-$ and $CD28^+$ cells from $tetramer^-$, CMV and EBV-specific $CD8^+$ T-cells. Each dot represents one tetramer response. Bars represent the percentage median of each phenotype (± interquartile range). Statistical analysis performed with Kruskal-Wallis test with Dunn's multiple comparisons test with * $p < 0.05$; ** $p < 0.01$; *** $p < 0.001$; **** $p < 0.0001$

3.2.6.4 Phenotype of virus-specific T-cells with differential epitope specificity

An important feature of this study was the ability to look at the phenotype of tetramer-specific T-cell responses against different epitopes. As such the UMAPs across the different tetramers were analysed for CMV-specific (Figure 35) and EBV-specific responses (Figure 36). Visually, whilst there were differences in the expression in different clusters, cells responding to the different epitopes were displayed across all the clusters.

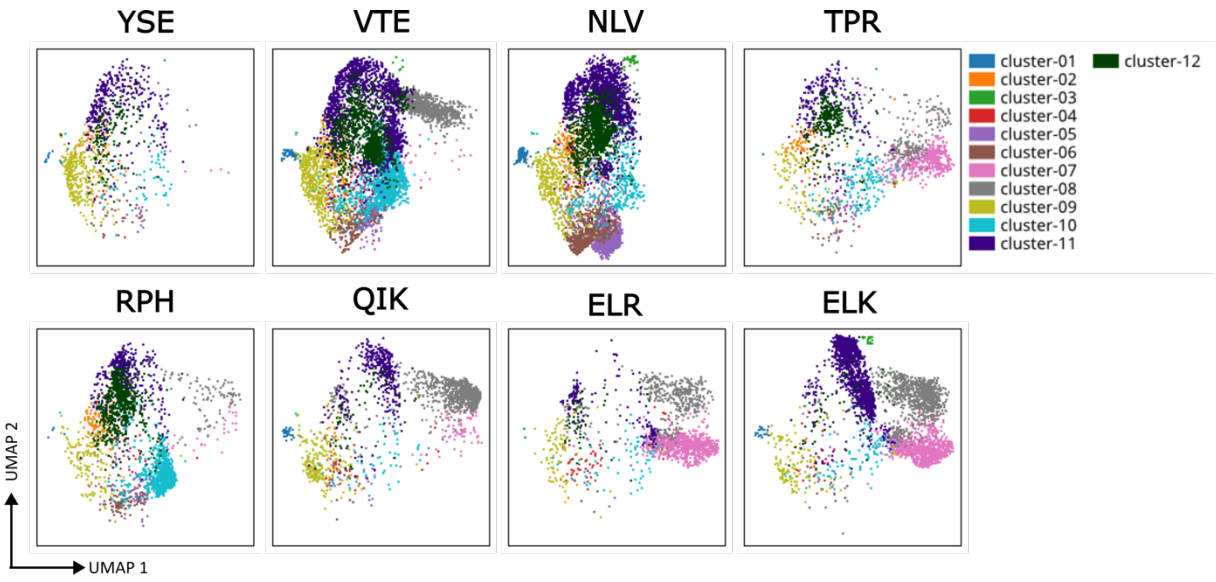

Figure 35: CMV UMAPs by epitope

UMAPs were concatenated based on the CMV epitope specificity with the following number of donors in each plot: YSE – 8, VTE- 14, NLV- 15, TPR- 8, RPH- 8, QIK- 7, ELR- 4, ELK- 7. Plots are coloured by cluster.

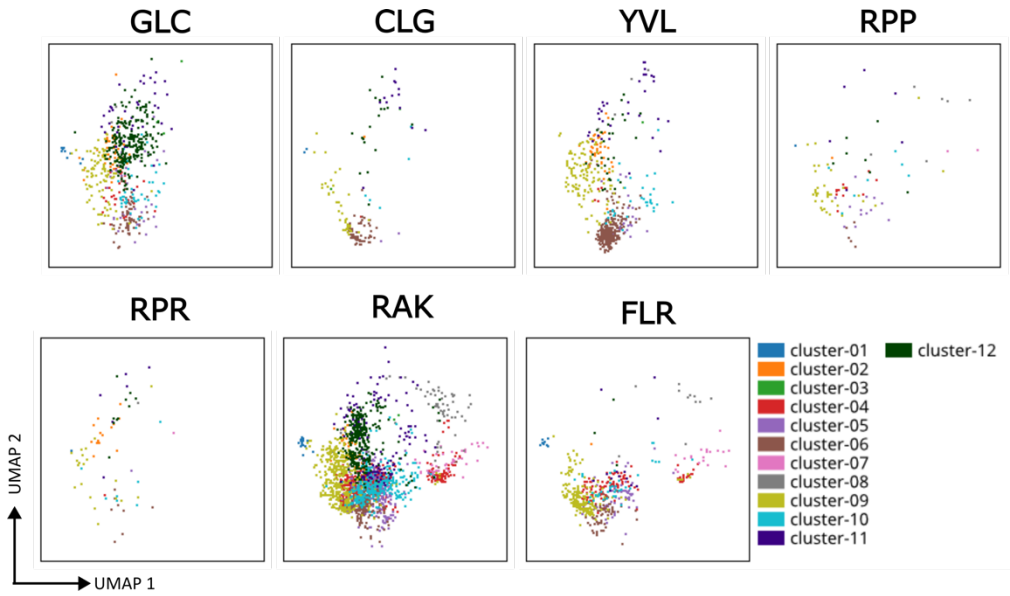

Figure 36: EBV UMAPs by epitope

UMAPs were concatenated based on the EBV epitope specificity with the following number of donors in each plot: GLC- 7, CLG- 5, YVL- 5, RPP-5, RPR- 3, RAK- 3, FLR- 3. Plots are coloured by cluster.

For further analysis, CMV-specific T-cells were analysed based on which protein the target epitope was expressed from: pp65 (YSE, NLV, RPH, TPR) or IE1 (QIK, ELR, ELK). As there was only one epitope (VTE) for the pp50 protein this was excluded from this analysis as it did not facilitate a comprehensive overview of the immune response to epitopes across the protein.

Figure 37 shows the percentage of pp65-specific or IE1-specific T-cell responses that fall within each cluster. A wide range of responses is seen within each cluster, for example in the percentage of IE1-specific T-cell responses within cluster 8 ranging from 0-82%. Interestingly, the percentage of pp65-specific T-cells within clusters 2, 5, 6 and 12 were significantly increased in comparison to IE1-specific T-cells ($p < 0.0001$, $p = 0.0495$, $p = 0.043$ and $p = 0.0007$ respectively). Clusters 2 and 12 are of similar phenotype, with both displaying a T_{EMRA}

phenotype, with a subset of the cells expressing CD27 and co-expression of the checkpoints PD1, TIGIT and 2B4 as well as low levels of TIM3 and LAG3 as per the heatmap in Figure 27 and the expression plots in Figure 28 and Figure 32. Clusters 5 and 6 are T_{EM} populations that also display strong expression of PD1 with co-expression of TIGIT and some 2B4.

On the other hand, the percentage of IE1-specific T-cells was increased in cluster 7 in comparison to the pp65-specific T-cells ($p = 0.0015$). This cluster demonstrates co-expression of a lower level of PD1 with high 2B4 however little to no TIGIT expression. It also exhibits a T_{EM} phenotype however is negative for CD27 and CD28 indicating they are on their way to becoming terminally differentiated. There is low-level HLA-DR/CD38 expression however increased CD69 expression.

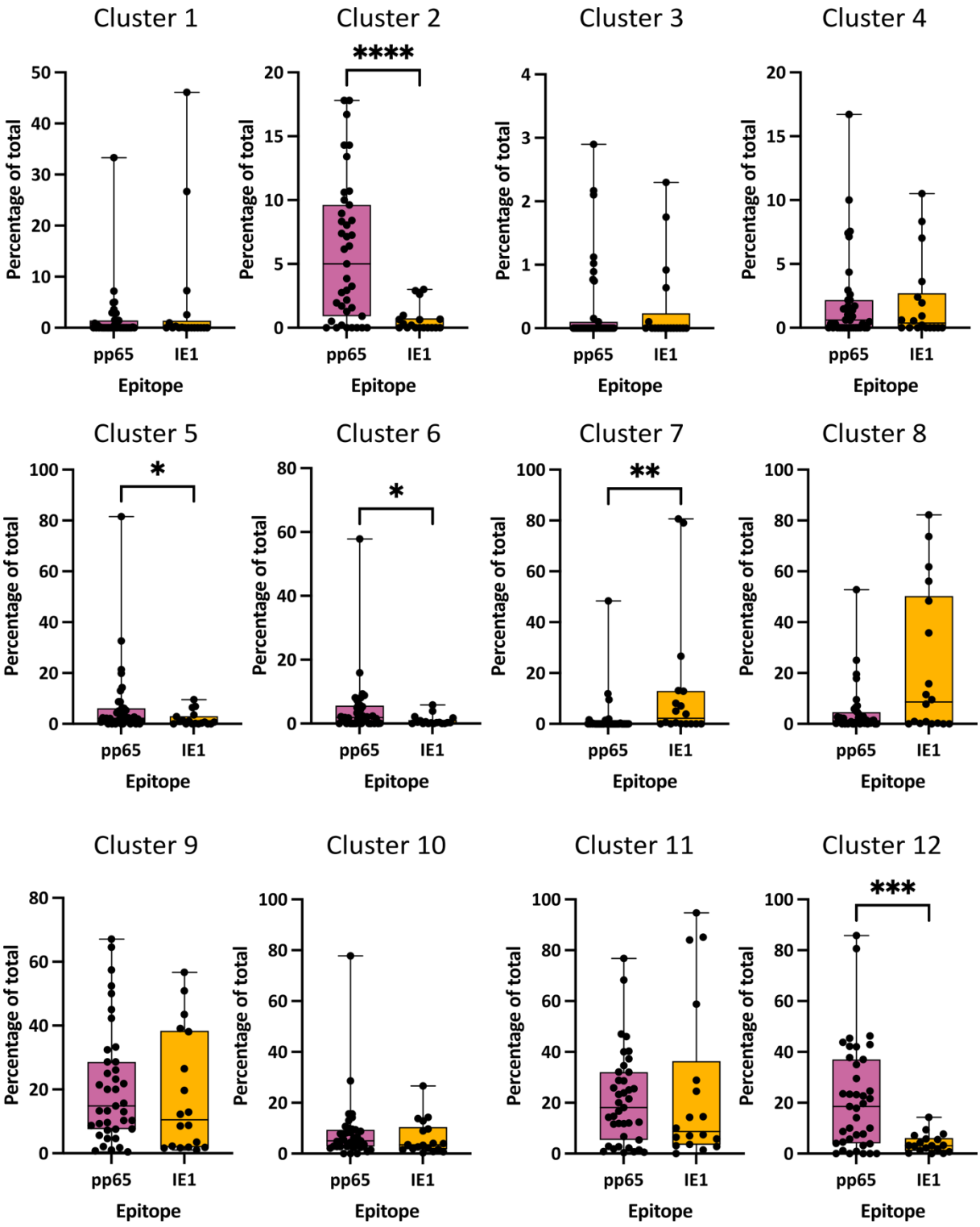

Figure 37: Distribution of CMV-specific T-cell responses by cluster

Summary of the percentages of T-cell responses to the CMV proteins pp65 (n=39) and IE1 (n=18) that were present in each cluster. Statistical analysis performed with Mann-Whitney test. Each dot represents one tetramer response. Bars represent the percentage median of each phenotype (± interquartile range) with * p <0.05; ** p <0.01; *** p <0.001; **** p <0.0001

EBV-specific T-cells were next analysed according to protein specificity (Figure 38). However, as these were targeted against a range of different proteins, they were analysed in relation to whether the target proteins were expressed in the lytic (YVL, GLC, RPR and RAK) or latent (CLG, RPP and FLR) stages of the viral life cycle. The percentage of T-cell responses to lytic epitopes that were present in the cluster 2 and cluster 12 were significantly increased in comparison to the latent epitopes ($p = 0.0007$ and $p = 0.041$ respectively). Conversely, there was a significant increase in cells in cluster 9 that were specific for a latent epitope ($p = 0.0270$). This cluster exhibits a T_{CM} phenotype with high expression of CD27 and CD28 and HLA-DR/CD38, along with mid-high expression of PD1, TIGIT and 2B4.

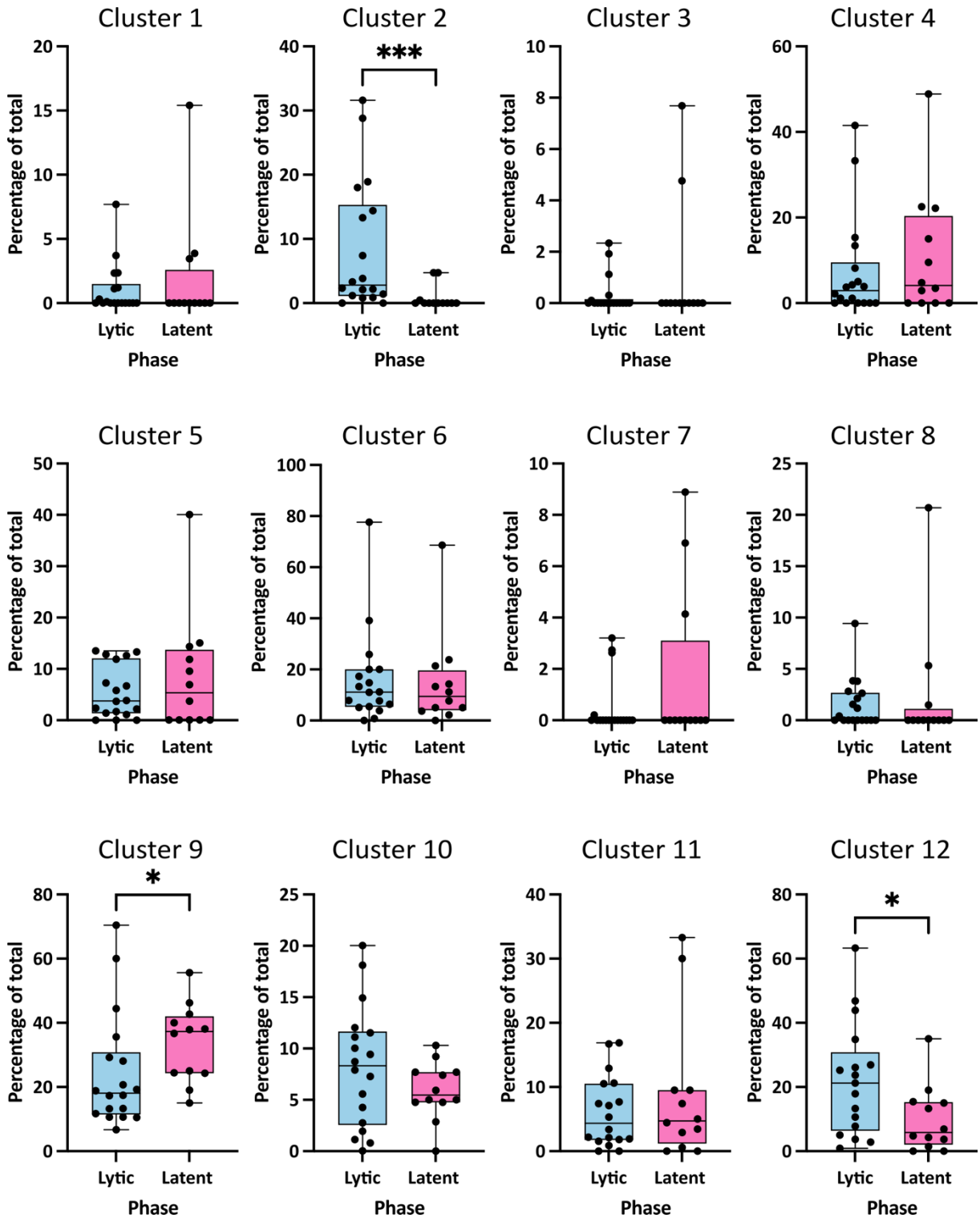

Figure 38: Distribution of EBV-specific T-cell responses by cluster

Summary of the percentages of T-cell responses to EBV, based on what phase of the cycle they were expressed in: lytic (n=18) or latent (n=12), that were present in each cluster. Statistical analysis performed with Mann-Whitney test. Each dot represents one tetramer response. Bars represent the percentage median of each phenotype (± interquartile range) with * p <0.05; ** p <0.01; *** p <0.001; **** p <0.0001

3.2.6.5 Functional analysis of CMV-specific T-cells in relation to PD-1 expression

In order to assess the relative functional properties of the $PD1^+$ and $PD1^-$ subsets, CMV-tetramer$^+$ cells were next sorted based on their PD1 status (Figure 39). Singlet cells and lymphocytes were initially identified by using FFC and SSC height, width and area. Then, the removal of the dump channel cells ($CD14^+$ and $CD19^+$) and dead cells ensured no monocytes or B-cells were present. $CD3^+$ and $CD8^+$ cells were identified together with the PE-conjugated tetramer cells and finally $PD1^+$ subsets. To ensure that $PD1^+$ cells were accurately identified, an FMO control was used which did not contain PD1. Also, to ensure that the cells selected for analysis were definitively of $PD1^+$ or $PD1^-$ phenotype, the cells with intermediate levels of PD1 were not included in the analysis, with a focus on the cells producing a higher amount of PD1.

As cell count was a limiting factor for analysis, and as the percentage of CMV-specific T-cells is much higher than EBV-specific populations, this work was performed solely for CMV-specific T-cell populations. Furthermore, whilst the cells sorted for each donor were specific for one tetramer, a range of tetramers was used across the donors to obtain a suitable number of virus-specific T-cells.

a)

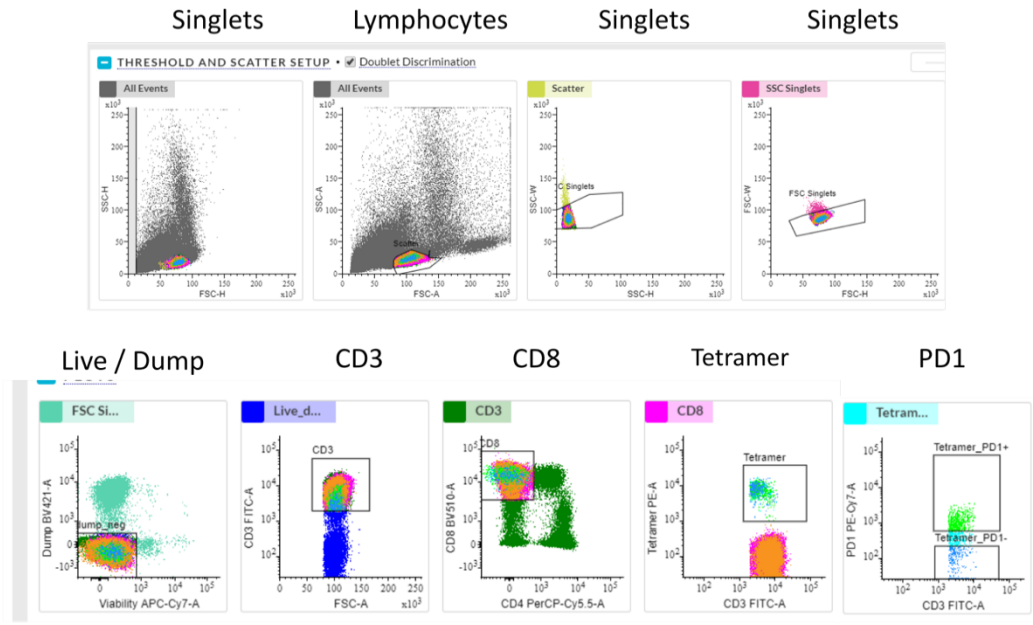

b)

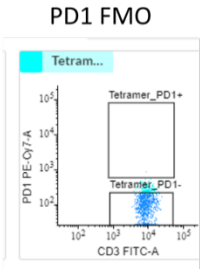

Figure 39: Cell sorting gating strategy to isolate CMV-specific T-cells in relation to PD-1 expression

a) Representative gating strategy to identify $PD1^+$ and $PD1^-$ CMV-$tetramer^+$ T-cells. Samples were stained with the antibody panel (Table 9) before flow cytometric analysis. Row 1 demonstrates singlet and lymphocyte discrimination. Row 2 from left to right: Live/dump, CD3, CD8, Tetramer and $PD1^{+/-}$ gating

b) Matched FMO control for PD1 staining

Sorted cells were incubated overnight with LCLs pulsed with peptide that matched the tetramer that was used for the sorting for that donor. As LCLs are peptide-pulsed, they display the antigen on their surface for recognition by the T-cells. LCLs express PDL1 and PDL2, thus ensuring engagement of PD1 on the sorted T-cells. This was confirmed by antibody staining that showed that over 80% of LCLs were dual-positive for PDL1 and PDL2 in every donor used in this study (n=6; Figure 40).

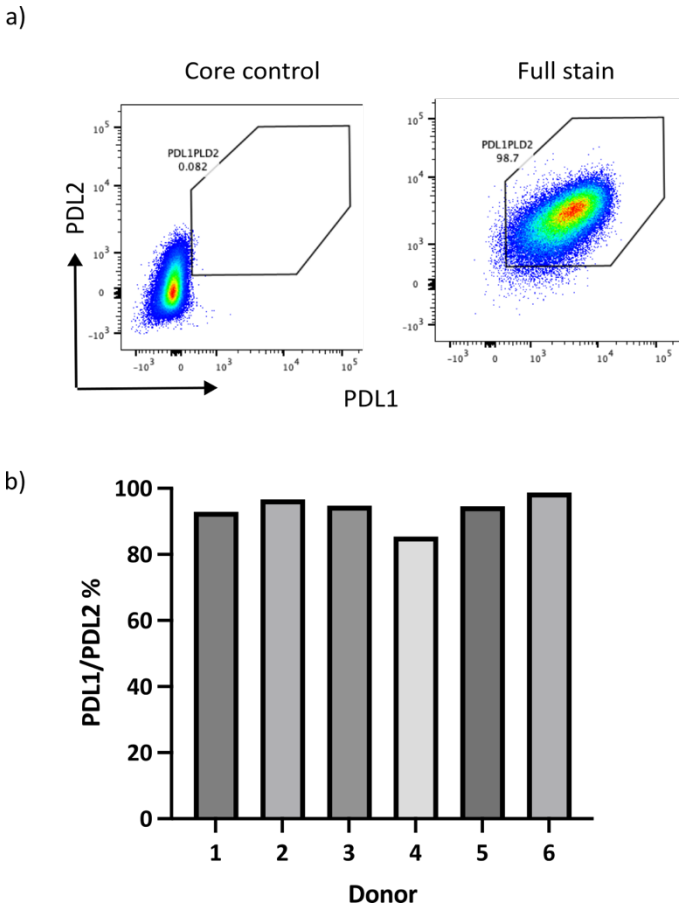

Figure 40: PDL1 and PDL2 is expressed by LCLs

- **a)** Representative gating strategy of PDL1 and PDL2 staining on LCLs in a control sample without the antibodies, and a fully stained sample.
- **b)** Percentage of dual-positive PDL1 and PDL2 staining across LCLs from 6 donors which were used for the co-culture assay

The PD1$^+$ and PD1$^-$ cells were incubated overnight at a ratio of 1:10 with the peptide-pulsed LCLs, along with some wells comprising no peptide-pulsed LCL controls. Supernatant was harvested and cytokines that had been released were analysed with the bead-based Legendplex assay. As TNFα, IFNγ, Granzyme B and Perforin are known to be released by CMV-specific T-cells, these were targeted for the analysis. Figure 41 shows the release of these cytokines from the PD1$^+$ and PD1$^-$ CMV-specific T-cells when cocultured with the peptide-pulsed LCLs. The PD1$^+$ population exhibited a significant increase of IFNγ in comparison to the PD1$^-$ cells ($p = 0.0244$). Whilst not significant, the TNFα, Granzyme B and Perforin release showed a similar trend ($p = 0.3$, $p = 0.1$ and $p = 0.5$ respectively).

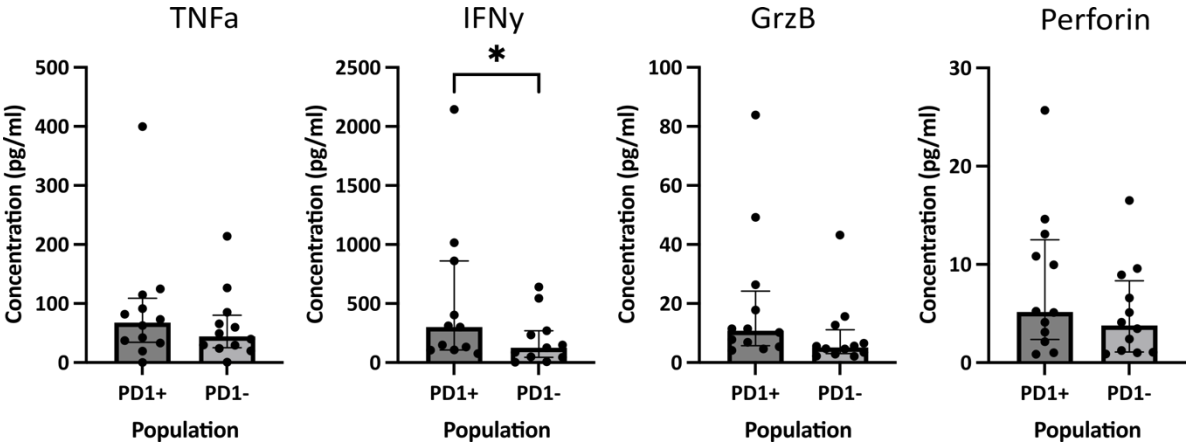

Figure 41: Cytokine release from PD1+/- CMV-specific T-cells following peptide stimulation

TNFα, IFNγ, Granzyme B and Perforin release as detected in the supernatant of PD1$^+$ and PD1$^-$ CMV-tetramer$^+$ T-cells when co-cultured with peptide-pulsed LCLs.

Cytokines were detected by the Legendplex assay. Each dot represents one donor response. Bars represent the percentage median of each phenotype (± interquartile range). Statistical analysis performed with Wilcoxon test with * p <0.05; ** p <0.01; *** p <0.001; **** p <0.0001

To further assess the impact of PD1 and PDL1/2 engagement, the antibody pembrolizumab, which binds to PD1 and blocks receptor interaction, was next added at a final concentration of 1μg/ml and cytokine response re-assessed. The presence of pembrolizumab led to significant increase in production of TNFα and IFNγ from PD-1^+ T-cells (Figure 42a; $p = 0.0210$ and $p = 0.0049$ respectively). Whilst not statistically significant, a similar trend was seen in the production of granzyme B ($p = 0.47$) although no change was seen in perforin production. No observable differences were seen in cytokine response from $PD1^-$ populations in the presence of PD1 blockade.

a)

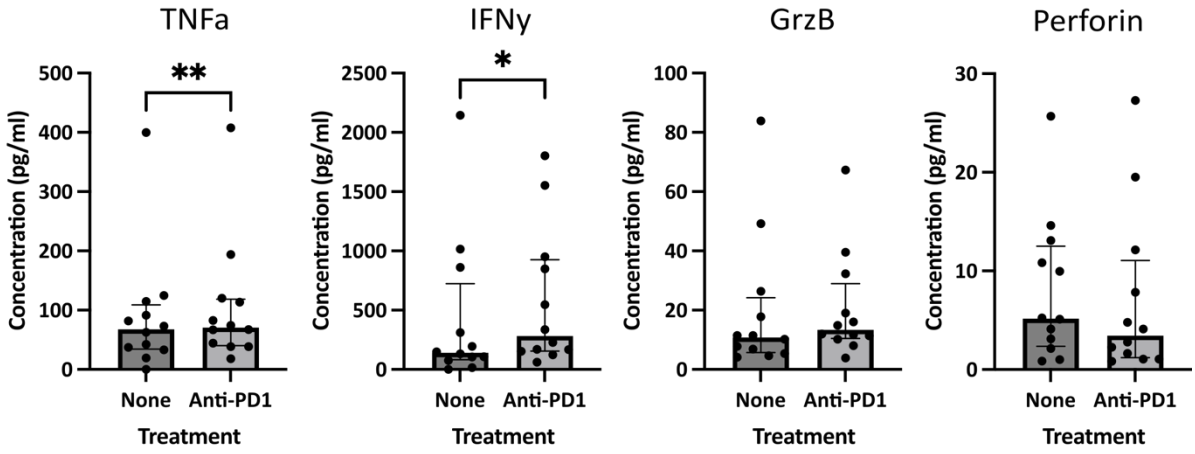

b)

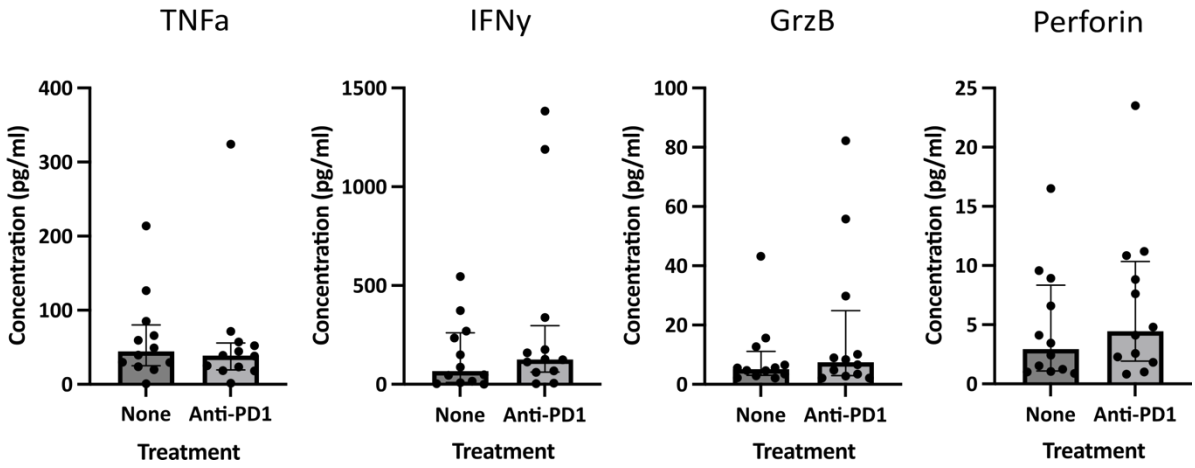

Figure 42: Cytokine release from PD1+/- CMV-specific T-cells following peptide stimulation and incubation with pembrolizumab

a) TNFα, IFNγ, Granzyme B and Perforin release as detected in the supernatant in $PD1^+$ CMV-tetramer$^+$ T-cells when co-cultured with peptide-pulsed LCLs with and without the anti-PD1 drug pembrolizumab.

b) TNFα, IFNγ, Granzyme B and Perforin release as detected in the supernatant in $PD1^-$ CMV-tetramer$^+$ T-cells when co-cultured with peptide-pulsed LCLs with and without the anti-PD1 drug pembrolizumab.

Cytokines were detected by the Legendplex assay. Each dot represents one donor response. Bars represent the percentage median of each phenotype (± interquartile range). Statistical analysis performed with Wilcoxon test with * $p < 0.05$; ** $p < 0.01$; *** $p < 0.001$; **** $p < 0.0001$

3.2.6.6 PD1 expression is dynamic on CMV-specific T-cells over time

Finally, the stability of PD1 expression over time was assessed. Parry *et al.* showed that PD1 expression on $CD4^+$ CMV-$tetramer^+$ T-cells remained stable over time, with the expression level potentially being determined by the viral load at the time of primary infection (Parry et al., 2021). I therefore decided to investigate the stability of PD1 expression in a similar way on CD8 cells. The expression of PD1 was measured on $PD1^+$ and $PD1^-$ sorted CMV-specific T-cells that were cultured overtime.

CMV-specific $CD8^+$ T-cells were sorted in the same was as Figure 39 before being stimulated with irradiated peptide-pulsed LCLs such that the cells would proliferate into polyclonal cell lines. As PD1 expression is affected by stimulation, the cells were not assessed until day 14 to ensure that PD1 would no longer be affected by the stimulation. Interestingly, the data shows that PD1 does not remain stable on either the $PD1^+$ or $PD1^-$ CMV-specific cell populations (Figure 43).

In particular, the percentage of cells expressing PD1 in the $PD1^+$ cohort starts to drop between day 0 and day 14, with a significant decrease seen between day 0 and 28 ($p = 0.038$).

Conversely, in the $PD1^-$ population, there is an immediate increase in the percentage of cells expressing PD1 between day 0 and 14 ($p = 0.0006$) however, the trend decreases after that point.

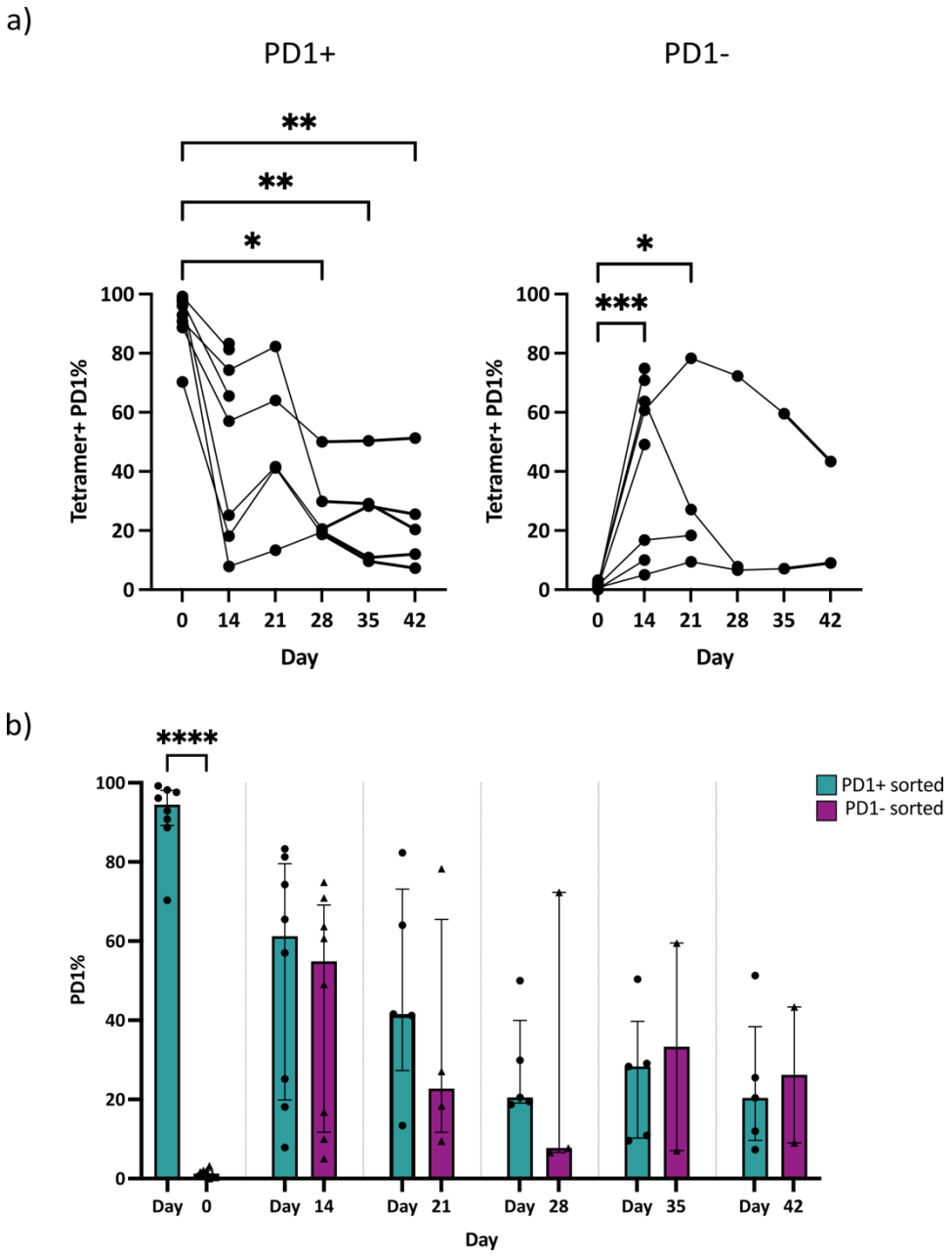

Figure 43: PD1 expression does not remain stable on polyclonal CMV-specific T-cells following peptide stimulation

a) The expression of PD1 on $PD1^{+}$ and $PD1^{-}$ CMV-specific T-cells as measured once every 7 days from day 14. Each dot represents one donor response). Statistical analysis performed with Kruskal-Wallis test with $p < 0.05$.

b) Comparison of the differences in expression between the $PD1^{+/-}$ cells at each timepoint. Each dot represents one donor response. Statistical analysis performed with Kruskal-Wallis test with * $p < 0.05$; ** $p < 0.01$; *** $p < 0.001$; **** $p < 0.0001$

3.3 Discussion

CMV is a highly immunogenic pathogen that elicits strong and sustained immune responses, particularly from $CD8^+$ T-cells. Whilst previous work has analysed the memory phenotype and some checkpoint expression on these viral-specific T-cells, this study builds on this by characterising the responses of $CD8^+$ T-cells to a wide range of CMV peptides from three CMV proteins. Furthermore, as a comparison we analyse in-depth the response to a range of EBV peptides. The findings offer valuable insights into the dynamics of viral-specific immune responses, including differences between the behaviour of CMV and EBV-specific T-cells, as well as variations across individual epitopes.

3.3.1 $CD8^+$ T-cell responses to viral epitopes

The initial analysis quantified the $CD8^+$ T-cell responses to CMV and EBV epitopes, revealing considerable variation in the percentage of cells responding to different epitopes. For CMV-specific T-cells, there was a wide range in response, from 0.01%-24% (Figure 12a), with a particularly high response to the pp50 VTE epitope when compared to the pp65 YSE epitope. This highlights that some epitopes may elicit a much stronger immune response, which could reflect differences in age, antigenic presentation or immunodominance. Interestingly, in HLA-A2 positive donors, Elkington, *et al.* observed pp65 to be the most immunodominant epitope followed by IE1, with pp50 displaying the weakest T-cell responses. However, when expanded to cover a wide range of epitopes, the responses to the HLA-A1 VTE epitope were consistently dominant across the cohort (Elkington et al., 2003). This data is supported by this study which confirm VTE responding T-cells to be one of the most immunodominant responses, with one donor exhibiting 24% of all $CD8^+$ T-cell responses to be specific for this epitope.

In contrast, EBV-specific T-cells exhibited lower overall responses (0.001%-2.29%) (Figure 12b), with significant differences between lytic and latent epitopes. For example, T-cells specific to the RAK epitope showed a stronger response than latent epitopes RPP and CLG. These differences may reflect the distinct immunological environments in which these viral proteins are expressed, as lytic cycle antigens are typically more immunogenic and lead to a stronger and more dominant T-cell response, shaping the hierarchy of T-cell specificity (Sharma et al., 2024, Tierney et al., 2015). Furthermore, the replication of herpesviruses involves the sequential expression of IE, E and L proteins, which play distinct roles in the viral life cycle (Dorothea et al., 2023). The response of $CD8^+$ T-cells has been shown to be biased towards IE proteins followed by E and finally least reactive to L stage proteins indicating a reduction in epitope presentation across the lytic cycle (Pudney et al., 2005, Steven et al., 1997). This is supported by the data in Figure 12b which shows the IE lytic protein BZLF1 and the E lytic protein BMLF1 as having the two highest $CD8^+$ T-cell response rates, with the latent proteins, in particular LMP2 and EBNA3A, demonstrating the smallest response rates,

3.3.2 CMV-specific T-cells display phenotypically distinct memory markers compared to EBV-specific T-cells

Memory phenotyping revealed that the composition of memory subsets differed significantly between CMV and EBV-specific T-cells. CMV-specific T-cells were predominantly of the T_{EM} ($CCR7^-$ $CD45RA^-$) and T_{EMRA} phenotype ($CCR7^-$ $CD45RA^+$), which is consistent with previous studies showing that CMV induces a robust, terminally differentiated effector memory response (Zangger and Oxenius, 2022, Klenerman and Oxenius, 2016, van den Berg et al., 2019, Gordon et al., 2017). The presence of a high number of circulating T_{EM} cells could

indicate increased immune surveillance in order to suppress CMV-reactivation (Torti and Oxenius, 2012). On the other hand, T_{EMRA} cells are associated with immunosenescence, a process characterised by the gradual deterioration of the immune system with age, contributing to reduced immune competence. These cells exhibit several hallmarks of aging, including a decline in proliferative capacity, increased DNA damage and telomere shortening, which can impair their ability to respond effectively to new infections. Despite these senescence-associated changes, T_{EMRA} cells maintain potent cytotoxic functions, such as high expression of perforin and granzyme B. These senescent characteristics can weaken immune surveillance and support viral persistence (Weltevrede et al., 2016, Guo et al., 2023). However, a study by Pereira *et al.* demonstrated that CMV-specific $CD8^+$ T-cells exhibit increased expression of NK receptors and reduced antigen responsiveness, suggesting that their functional decline may result from altered signalling rather than intrinsic senescence (Pereira et al., 2020). These atypical T-cell responses of a high percentage of CMV-specific T-cells, and a primarily T_{EMRA} phenotype, are attributed to low-level antigen persistence caused by sporadic viral reactivation events despite the virus achieving latency (Seckert et al., 2012, Torti and Oxenius, 2012, Snyder, 2011).

Conversely, EBV-specific T-cells were more likely to exhibit the T_{CM} and T_{EM} phenotypes. This difference in memory profile allows for an increased sensitivity to antigen stimulation and rapid recall response while still retaining the ability to proliferate and differentiate (Weltevrede et al., 2016). Notably, latent epitopes in EBV were associated with an increased proportion of T_{CM} cells compared to lytic epitopes, indicating a potential need for long-term surveillance during the latent phase of EBV infection. Previous work has shown that both EBV- and HIV-specific T-cells express relatively little CD45RA (van den Berg et al., 2019). Supporting

a less-differentiated status for the EBV-specific T-cells, they also exhibited a significant increase in CD27 and CD28 expression in comparison to CMV-specific T-cells. Previous studies have also shown that EBV-specific T-cell express low levels of the differentiation marker CD57 yet higher levels of CD62L, a marker that distinguishes central memory from effector memory cells (Yang et al., 2011, Khan et al., 2004).

3.3.3 Potential determinants of the phenotypic differences between CMV and EBV-specific profiles

CMV establishes latency primarily in myeloid lineage cells such as monocytes and macrophages and exhibits minimal viral gene expression during this phase. However, reactivation causes the virus to replicate and produce new viral progeny. Reactivation can occur due to immunosuppression (e.g. iatrogenic transplantation-associated immune suppression), stress, inflammation or other environmental factors (Bego and St. Jeor, 2006, Collins-McMillen et al., 2018). Whilst there is considerable research into the effects of CMV reactivation in immunocompromised individuals, there is little research done into the frequency of reactivation of CMV and EBV in healthy donors. This is likely due to the sporadic and infrequent nature of the reactivation and difficulty detecting the virus, with CMV DNA being difficult to detect in the PBMC.

Interestingly, previous studies have shown that the percentage of circulating antigen-specific T_{CM} cells increase with time after infection. This has particularly been studied in cells in response to LCMV infection (Wherry et al., 2003, Jabbari and Harty, 2006, Masopust et al., 2006). This may reflect a transition to a long-lived memory state which suggests a role in long-term immune surveillance and recall responses (Wherry et al., 2003, Jabbari and Harty, 2006).

Masopust *et al.* expanded on this, finding that these cells also maintain robust proliferative capacity and cytokine production, enabling rapid responses upon antigen re-encounter (Masopust et al., 2006).

EBV undergoes latency in B-cells and exhibits distinct latency programs (Latency 0, I, II and III) which vary depending on the environment (i.e. germinal centres or memory B-cells) (Murata et al., 2021). The virus can then be reactivated by stimulation from immunological signals or differentiation to the plasma cell state (Care et al., 2023).

The differences in the checkpoint and activation profiles expressed by the virus reactive T-cells could further indicate that the T_{CM} EBV-specific T-cells are more functionally activated and able to suppress EBV reactivation quicker, supporting Wherry *et al.* who showed that T_{CM} cells mediated considerably more rapid control of a viral infection in comparison to the T_{EM} subset (Wherry et al., 2003). Conversely, as CMV reactivation occurs and more virions are shed, this could lead to a) the differentiation T_{EMRA} phenotype and b) the expanded populations of CMV-specific T-cells observed in elderly individuals as more T-cells react to the virus.

3.3.4 Differential expression of checkpoint protein expression on viral-specific T-cells

The main aim of my work in this chapter was to assess the expression of the immune checkpoint molecules PD1, TIGIT, 2B4, TIM3 and LAG3 which are critical regulators of T-cell function and exhaustion. PD1 is a critical immune checkpoint that negatively regulates T-cell activation and function and has long been known to play an important role during chronic viral infection such as LCMV, HIV and HCV , where it is upregulated and associated with exhaustion

(Barber et al., 2006, Day et al., 2006, Wherry et al., 2007, Petrovas et al., 2006, Urbani et al., 2006). Despite its established role in immune exhaustion, the precise physiological function of PD1 on virus-specific T-cells remains uncertain.

Interestingly, prior studies have shown that $CD4^+$ CMV-specific T-cells display consistent expression of PD-1 over time, irrespective of activation status, and that the PD-1 expression pattern was related to viral load at the time of primary infection. This study aimed to explore this further in the CD8-specific cohort by deep immunophenotyping of CMV-specific cells and comparison of the associated phenotype with that of EBV-specific populations.

In line with published literature, the percentage of $CD8^+$ cells expressing PD1 is increased on CMV-specific T-cells in comparison to the tetramer-negative population, and this pattern was even more marked on the EBV-specific subset. However, the intensity of PD1 expression, as measured by median fluorescence intensity, was somewhat lower on the CMV-specific T-cells in comparison to both the tetramer-negative and EBV-specific cells.

It is widely known that upregulation of checkpoint expression can indicate a state of exhaustion for T-cells, with this phenotype present notably on tumour infiltrating lymphocytes (TIL) and on viral-specific T-cells in some chronic infections such as HIV or HCV (van den Berg et al., 2019) (Thommen and Schumacher, 2018, Wherry, 2011). However, it is known that CMV-specific T-cells retain functional ability and can produce cytotoxic granules including granzyme B and perforin (Harari et al., 2009). Indeed, prior studies have also shown CMV-specific T-cells to exhibit less PD1 and TIM3 than EBV-specific T-cells (Hertoghs et al., 2010, Sauce et al., 2007) and less PD1, 2B4 and TIM3 than HIV-specific T-cells (He et al., 2008, Sauce

et al., 2007). My work sought to comprehensively analyse the co-expression of multiple checkpoints and to relate this to activation status.

In addition to PD1, I showed that TIGIT and TIM3 were expressed by a higher percentage of EBV-specific T-cells compared to CMV, with CMV-specific T-cells expressing increased 2B4 (Figure 17). 2B4, also known as CD244, is a member of the SLAM facility of receptors, and is known to contribute to the killing of viral-infected cells by viral-specific T-cells and is also overexpressed on exhausted viral-specific T-cells in cases such as HCV, HIV and HBV (Aldy et al., 2011, Bengsch et al., 2010, Raziorrouh et al., 2010). Its importance in viral clearance is shown by the observation that HTLV-I-specific $CD8^+$ T-cells show impaired degranulation and IFNγ production in response to 2B4 blockade. The mechanisms behind the differential expression of 2B4 on CMV-specific T-cells compared to EBV is unclear but could potentially relate to differential frequency or strength of stimulation.

A broad diversity in co-expression of 2B4, TIGIT, TIM3 and LAG3 was seen on virus-specific cells but PD-1 was a common shared determinant. In general, checkpoint expression on CMV-specific T-cells was somewhat lower in comparison to the EBV-specific pool. This profile may relate to my work in Chapter 4 where the $PD1_{HIGH}$ subset of CMV-specific T-cells expressed higher level of checkpoint proteins, that may reflect exhaustion, in comparison to the $PD1_{MID}$. Circulating CMV-specific T-cells are largely $PD1_{MID}$ in phenotype and this is in keeping with their established profile of strong functional cytotoxicity.

As EBV-specific T-cells exhibited high amounts of PD1, it was important to elucidate whether these cells expressed features of activation or additional markers of potential exhaustion. The data showed strong co-expression of PD1 with the inhibitory receptors TIGIT and 2B4. TIGIT

can also be a marker of T-cell exhaustion, particularly when co-expressed with other checkpoints such as TIM3 and LAG3 (Chauvin and Zarour, 2020). However, in this study, PD1 expressing T-cells showed very little to no expression of TIM3 and LAG3 indicating that in this case, the marker may not be indicative of an exhausted population.

Furthermore, the PD1$^+$ EBV-specific T-cells also showed increased expression of HLA-DR and CD38 co-expression in comparison to CMV-specific populations. The co-expression of HLA-DR and CD38 can indicate proliferation and activation of cells (Ndhlovu et al., 2015, Agrati et al., 2016) and high dimensional data further reveal that this subset also express high levels of PD1, TIGIT and 2B4. The increase in HLA-DR and CD38 suggests that, at least on a subset of EBV-specific CD8 T-cells, the PD1 expression may be a marker of activation, as further supported by the lack of TIM3 and LAG3 expression. Whilst it was not possible to carry out functional studies on the EBV-specific T-cells, due to the nature of their low expression, if PD1 is indeed a marker of activation on these cells, the higher PD1 expression on the EBV cells further supports them being more activated than the CMV-specific cohort.

3.3.5 Differences in protein checkpoint expression between virus-specific T-cells targeting IE and E proteins

One additional observation in my analysis was the difference in the phenotype of CD8$^+$ T-cells responding to the pp65 and IE1 proteins. Whilst representing only a small subset of cells, cells in cluster 2 that responded to pp65 were increased in comparison to IE1. These T_{EMRA} phenotype cells did not display markers of terminal differentiation and retained CD27 and some CD28 expression. This indicates that they are pre-effector type 1 (pE1) (T_{EMRA} CD27$^+$ CD28$^+$), the most immature T_{EMRA} subset (Kudryavtsev et al., 2022). These are less cytotoxic

than the T_{EMRA} cells that have lost expression of CD27 and CD28, with only a small portion of them expressing granzyme B and perforin (Rufer et al., 2003). Indeed, cluster 12, which represented T_{EMRA} cells with downregulated of CD27 and CD28, is more substantial. This is line with previous studies which identified this as the primary T_{EMRA} population followed by a small population of pE2 phenotype $CD27^+$ $CD28^-$ cells and then less than 5% displaying a pE1 phenotype (Rufer et al., 2003, Wills et al., 2002). These cells also displayed co-expression of the activation markers HLA-DR and CD38.

Conversely the phenotype of cells that primarily were responding to IE1 proteins were $CD27^-$ $CD28^-$ T_{EM} cells, termed EM3 cells. This effector subset displayed an upregulation of the activation markers CD69, HLA-DR and CD38, indicating recent and ongoing activation. As IE1 proteins are expressed early in the viral replication life cycle, these could be responding to recent reactivation of the virus.

3.3.6 CMV-specific $PD1^+$ $CD8^+$ T-cells are more functional than $PD1^-$ cells

In addition to extensive phenotypic profiling of checkpoint expression on virus-specific T-cells it was essential to undertake functional studies. Interestingly, and somewhat counter to what I was expecting, my data revealed that $PD1^+$ CMV-specific T-cells expressed a strong cytokine response to antigen stimulation that the $PD1^-$ subset did not. This was most notable for IFNγ expression, with a similar trend for increased expression of TNFα, granzyme B and perforin.

An important factor here may relate to the relative level of PD1 expression on the T-cell. A recent paper by Weiss *et al.* generated a mouse model using CRISPR-Cas9 to delete an open chromatin region that appeared to be specific to T-cell exhaustion. This deletion produced mice with intermediate levels of PD1 expression, rather than the $PD1_{HIGH}$ phenotype typically

seen in exhausted cells. By comparing this to mice lacking the PD1 gene locus, *Pdcd1* ($PD1^-$) and wild-type mice which included a $PD1_{HIGH}$ population, they were able to assess the effect of varying levels of PD1 expression on cell activity. They determined that cells with intermediate expression of PD1 displayed effector phenotypes with gene expression of *Klrg1* and *Gzmb* and an ability to control viral infection better than both mice with wild-type PD1 and $PD1^-$ cells. An important determinant in relation to this was the observation that *Pdcd1*-knockout mice demonstrate an increase in other negative regulatory mechanisms (Weiss et al., 2024). Additional murine studies have also shown the importance of the PD1/PD-L1 pathway in determining a functional CD8 memory T-cell pool (Pauken et al., 2020, Kalia et al., 2021). Despite these findings, it was notable that Weiss *et al.* did find that *Pdcd1*-knockout mice did elicit T-cell responses with increased levels of IFNγ and TNF production which contrasts with my study and may indicate species-specific differences in functional correlates (Weiss et al., 2024).

Given that $PD1^+$ T-cells showed higher levels of Th1 cytokine production than $PD1^-$ cells following antigen recognition, despite concurrent engagement of the inhibitory PD1:PDL1 interaction, it is important to consider why this apparent paradoxical response may occur.

The inhibitory cellular response that is triggered through PD1 engagement is thought to be mediated through downregulation of signalling via the T-cell receptor and the co-stimulatory molecule CD28 (Liu et al., 2024). In this regard a potential observation that may be of interest is that many CMV-specific T-cells express a CD28-negative phenotype and the relative impact of PD1 engagement for this cell population may therefore be attenuated. Of note, many CD28-negative CMV-specific T-cells express CD137, also known as 4-1BB, a membrane protein that

belongs to the TNF-receptor superfamily (Waller et al., 2007). 4-1BB is expressed primarily on the surface of activated cytotoxic $CD8^+$ T-cells and helper $CD4^+$ T-cells, but can also be induced upon activation on other immune cells, including B-cells, NK-cells and monocytes (Singh et al., 2024). CD137 is an important co-signal for antigen-experienced CD8 T-cells which not only generates effector functions but also promotes the increase of IFNγ expression (Bukczynski et al., 2004, Zhang et al., 2007, Reithofer et al., 2021). CMV-specific $CD8^+$ T-cells have been shown to upregulate CD137 shortly after stimulation and its ligand CD137L has been shown to be provide key stimulation for proliferation of $CD28^-$ cells (Waller et al., 2007). CD137L is expressed on antigen presenting cells such as dendritic cells and B-cells (Kwon, 2015) and it is therefore likely that CD137L was also expressed on the LCLs presenting cells that I used in the functional assays. In this case, the PD1 status of the cell may merely be reflecting its activated status but not be acting as a major negative regulator of cellular function. However, my work did show that PD1-blockade did act to further enhance cytokine production from $PD1^+$ CMV-specific T-cells. Further work to assess the potential importance of $CD28^+$ and $CD137^+$ T-cell subsets in this regard will be of interest.

3.3.7 Conclusions

This study provides a comprehensive analysis of checkpoint protein expression on $CD8^+$ T-cell responses to CMV and EBV epitopes and uncovered significant differences in immune dynamics between these two chronic viral infections.

CMV-specific $CD8^+$ T-cells exhibited strong and diverse responses across a range of epitopes, while EBV-specific responses were generally lower in magnitude, albeit with notable differences between responses against lytic and latent epitopes. Memory phenotyping

revealed a predominance of the T_{EM} and T_{EMRA} phenotypes in CMV-specific -cells whereas EBV-specific T-cells showed a more balanced distribution of T_{CM} and T_{EM} phenotypes, indicative of a more controlled viral latency. The determinants of the differential phenotype, most likely related to the frequency and magnitude of viral reactivation, remain uncertain and need further investigation.

The main focus of this chapter was on checkpoint protein expression where, again, significant differences were seen between the two virus-specific populations. An essential correlate of this phenotype is the functional capacity of differential T-cell subsets and an unexpected observation was heightened cytokine production from $PD1^+$ CMV-specific T-cells in response to antigen recognition. Further work will be needed to extend these studies further in relation to combinatorial checkpoint expression and viral protein specificity.

3.3.8 Limitations and future work

Whilst difficult due to the sensitivity of the detection and the infrequent nature of the reactivation, it would be interesting to carry out a longitudinal study assessing the phenotype and expansion of the CMV and EBV-specific T-cell response over time and in response to reactivation. This would allow further understanding of how our immune system controls these viruses and the difference adaptations involved.

A limitation of this study was the limited number of virus-specific T-cells available as these constitute such a small percentage of the total PBMC. Generation of $CD8^+$ T-cell CMV-specific clones could be helpful here, but these do not recapitulate function in the stable physiological state as they require many weeks of antigen stimulation. Similarly, functional studies in this way should be carried out on EBV-specific T-cells. Extended intracellular and intranuclear

staining could allow for further analysis of cytokines such as TNFα and IFNγ, proliferation markers such as Ki67, and transcription factors such as TCF-1 which would provide further information on cellular function, proliferation and 'stemness'. Additional assays to determine cytotoxicity, such as the LDH cytotoxicity assay, could also be carried out to determine T-cell response following antigen engagement. It would also be interesting to carry out functional analysis in the presence or blockade of additional checkpoint proteins such as 2B4 to see how these affect the T-cell response.

Finally, it would be interesting to analyse the expression of CD28, the primary co-stimulatory marker, and other markers such as CD137 on the sorted CMV-specific T-cells and to relate this to their response to PD1 inhibition. The presence of CD137 on the LCL antigen presenting cells also needs to be defined. Furthermore, if experiments could be repeated with a larger number of cells I would also like to harvest and assess virus-specific cells for analysis following antigen-stimulation and relate their transcriptional and functional response to the pattern of checkpoint profile.

CHAPTER 4: THE CMV-SPECIFIC $CD8^+$ T-CELL PHENOTYPE WITHIN OVARIAN CANCER TISSUE AND ITS RELATIONSHIP TO PD1 EXPRESSION

4.1 Introduction

Tumour infiltrating lymphocytes (TILs) are diverse populations of immune cells that infiltrate tumours and play crucial roles in anti-tumour immunity. Their presence, antigen-specificity and functional characteristics can significantly influence the success of therapies such as immunotherapy and chemotherapy (Li et al., 2021, Qian et al., 2023). For instance, TILs that recognise specific tumour antigens and possess robust effector functions are more likely to contribute to effective tumour clearance. However, they are often exhausted or dysfunctional due to chronic stimulation in the tumour microenvironment (TME). One mechanism by which this occurs is through expression of high levels of inhibitory receptors that suppress effector responses (Topalian et al., 2012, Ribas and Wolchok, 2018). Although checkpoint blockade treatment has led to remarkable therapeutic responses in some cancer subtypes, perhaps most notably melanoma, its efficacy is limited to a minority of cancer patients (Nowicki et al., 2018). Understanding the detailed features of TIL, including their phenotype and antigen specificity, is essential for improving and predicting the efficacy of checkpoint blockade therapies.

Simoni, Y. *et al.* conducted a comprehensive investigation into the antigen specificity of TILs within colorectal and lung cancer patients, aiming to understand the role of TILs within the TME. Despite screening for over 1,000 potential neoantigen epitopes, they identified only two within tumour tissues, which is surprisingly low given the high mutation burden often seen with these cancers. However, the team discovered a significant presence of TILs that were specific for unrelated viral epitopes, such as CMV, EBV and influenza. Specifically 16 cancer-unrelated epitope specific T-cells were identified, confirming that these virus-specific T-cells

are not only capable of infiltrating tumours, but may also play a functional role within the TME (Simoni et al., 2018). A large study using single-cell RNA sequencing technology also identified 'bystander' non-tumour specific TILs in omental lesions in patients with ovarian cancer which were identified through presence of a $CD39^{-}$ $CD69^{-}$ signature (Yang et al., 2022).

These findings underscore the complex nature of TIL populations and suggest that if there are functional cells that are not dysregulated by chronic stimulation, these could potentially influence the immune response within cancerous tissues. Furthermore, they could also offer insights into new therapeutic strategies, such as through 'redirection' towards cancer cells. Moreover, as it is difficult to identify and assess tumour neoantigen-specific T-cells due to their low frequency, studying viral-specific T-cells that are specific for a known epitope provides a model to analyse the phenotype of antigen-specific T-cells within the TME.

High-grade serous ovarian cancer (HGSOC) is the most common and deadliest form of ovarian cancer, often diagnosed at an advanced stage, resulting in a dismal five-year survival rate of less than 30%. Whilst being termed 'ovarian cancer', this also encompasses cancers that may have originated in the fallopian tube, as research has established that up to 80% of ovarian carcinomas may have originated in the fimbrial end of the fallopian tube (Crum et al., 2007, Carlson et al., 2008, Kurman and Shih Ie, 2008). For this reason, tissue from both the fallopian tube and the ovary were classed as primary tumour as these are the locations where the tumours originate. The most common metastatic sites are the peritoneum and omentum which form when clusters of cells detach from the primary tumour and are carried by the peritoneal fluid throughout the peritoneal cavity (Berek et al., 2021, Lengyel, 2010). For the purposes of my study these are classed as the secondary tumour sites.

One of the key challenges in understanding the importance of the immune response against HGSOC is the phenotypic and functional complexity of the TME (Labidi-Galy et al., 2017, Cox et al., 2021). TILs have been suggested to play an important role in mediating disease control with one study of 186 patients demonstrating that 55% of patients with detectable $CD3^+$ TILs exhibited a 5-year survival of 38%, compared to 4.5% in patients with no detectable TILs (Zhang et al., 2003). It has been further shown that $CD8^+$ TILs are particularly correlated with this increased survival benefit (Sato et al., 2005).

Ovarian cancers usually respond initially to chemotherapy, but these responses are typically short term. Clinical responses to immunotherapy are also suboptimal and understanding of the TME and the specific actions of TILs is therefore crucial for developing effective therapeutic strategies (Hudry et al., 2022, Lengyel, 2010).

This study focuses on the analysis of $CD8^+$ T-cell responses against the immunodominant herpesviruses cytomegalovirus (CMV) and Epstein-Barr Virus (EBV) in ovarian cancer. Whilst there is no direct evidence that CMV infection or reactivation is associated with the development or progression of ovarian cancer, some studies suggest that the virus may reactivate within tumours. In particular, it has been shown that patients whose tumours exhibit high expression of the CMV immediate-early (IE) and phosphoprotein-65 (pp65) proteins tend to have a more advanced stage of disease and shorter survival outcomes (Carlson et al., 2018, Rådestad et al., 2018). This implies that CMV could either be playing a role in promoting cancer progression or that the immunosuppressive metabolic conditions within the tumour microenvironment may lead to reactivation of the virus. However, another large-scale study showed that CMV DNA was present in only 0.5% of cases with 5.2% of cases

being positive for EBV DNA (Ingerslev et al., 2019). This finding for EBV is supported by another study finding EBV DNA present in 10% of malignant ovarian cancer cases (Shokouh et al., 2020). EBV, which is also a herpesvirus, was the first identified oncogenic virus in humans and is associated with the development of a variety of malignancies including nasopharyngeal carcinoma and non-Hodgkin lymphoma (Yu and Robertson, 2023).

Virus-specific T-cells, such as those reactive to CMV and EBV, can act as bystander TILs, serving as a comparison point between PBMC and tumour tissue. Studying these bystander TILs offers insights into how the TME influences the phenotype and functionality of the immune cells, impairing their anti-tumour activity.

My work in this chapter aimed to investigate the presence of CMV-specific and EBV-specific $CD8^+$ T-cells within the peripheral blood and the TME of ovarian cancer patients. Specifically, I assessed the phenotype of the T-cells to understand i) the effect the TME has on the phenotype of CMV-specific and EBV-specific TILs and ii) to provide a model to understand the characteristics of antigen-specific TILs in the TME. Firstly, the presence of CMV-specific and EBV-specific T-cells in ovarian tumours was assessed using MHC-I tetramer technology to confirm they were infiltrating the tissue. Secondly, the phenotype of these cells was analysed using classical flow cytometry gating methods and high dimensional analysis to assess TIL heterogeneity. Finally, subsets of interest were further interrogated using classical biaxial gating strategies.

4.2 Results

4.2.1 Determining CMV status and HLA type

Patients undergoing debulking surgery were recruited with fully informed consent for this study. Peripheral blood and tissue sections were received in MACS Tissue Storage Solution (Miltenyi) for preparation and digestion before long term storage in liquid nitrogen.

As there was no serum available, the presence of a T-cell response to CMV peptide stimulation was used as a measure of CMV infection status. Here I used the TAPI-0 assay whereby, upon stimulation with JPT Pan-CMV Select Pepmix^{TM} , cells were assessed for activation using the dual positivity of TNF-α secretion and the activation marker CD69 (Figure 44). TNF-α exists in two forms, a transmembrane form and a soluble form, and the transmembrane form is cleaved by the TNF-α converting enzyme (TACE), a membrane-bound disintegrin metalloproteinase, to release the soluble form of TNF-α (Jang et al., 2021). Preventing this cleavage using the TNF-α Processing Inhibitor 0 (TAPI-0) keeps TNF-α anchored to the cell surface, allowing for identification of antigen-specific T-cells through assessment of cytokine production by flow cytometry rather than intracellular staining (Haney et al., 2011).

The gating strategy in Figure 44a demonstrates identification of singlet samples by using FSC-H and FSC-A in order to remove large doublet cells and small pieces of debris. Lymphocytes are then selected based on their size using SSC-A and FSC-A before the live cells by removing the dump channel (CD14 to identify monocytes and CD19 to identify B-cells) and the viability dye which discriminates by staining dying dead and dying cells. The CD3 population is

identified by gating against FSC-A and the CD8 and CD4 populations gated against each other in order to confirm that the selected CD8 cells are also CD4 negative.

This gating strategy was used to identify $CD8^+$ cells throughout the chapter.

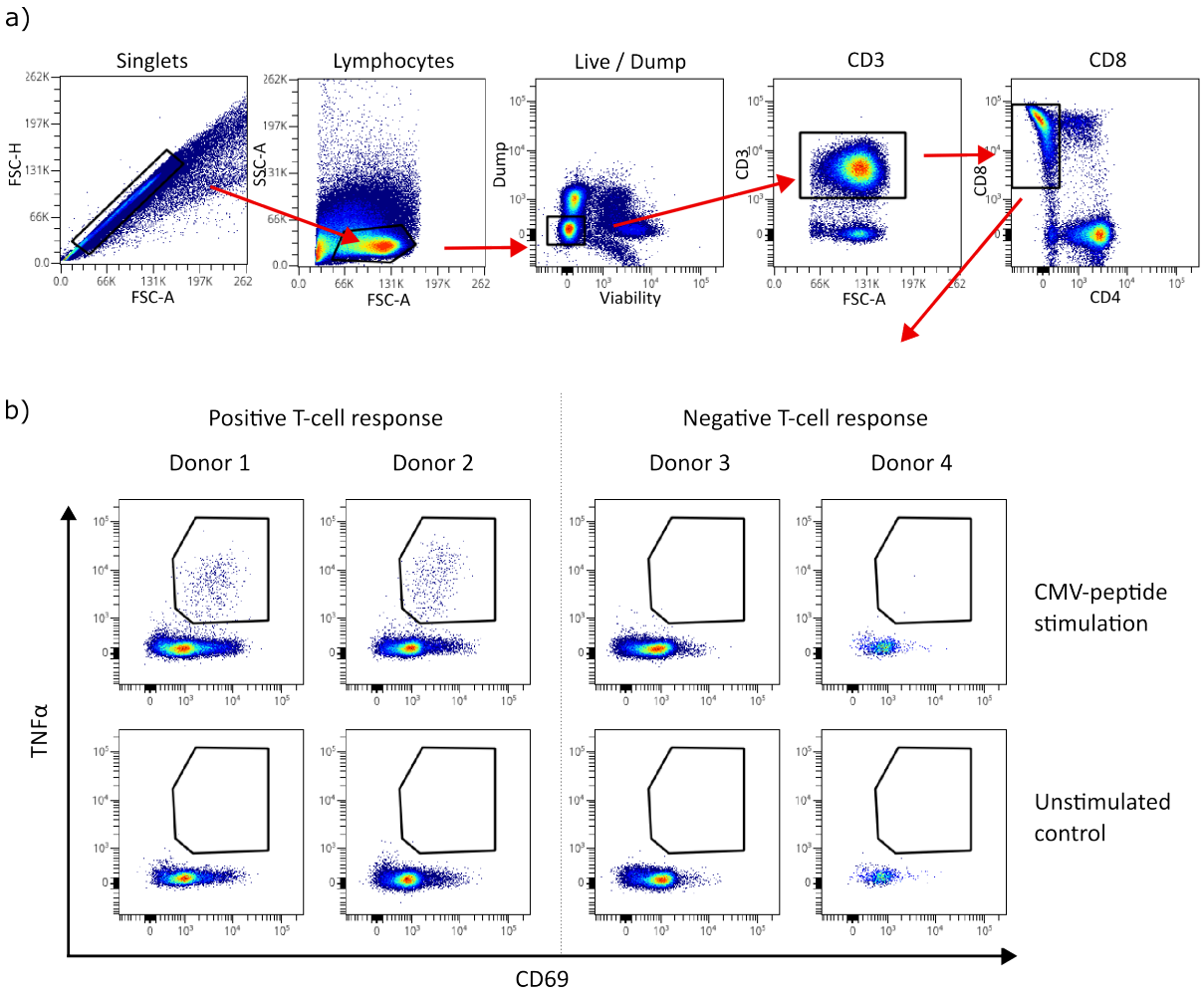

Figure 44: TAPI-0 assay to assess CMV status.

- **a)** Gating strategy to identify $CD8^+$ T-cells. Samples were thawed, stimulated with CMV Pepmix™ and stained with the antibody panel (Table 13) before flow cytometric analysis. From left to right: singlets discrimination, lymphocytes, Live/ dump negative cells, T-cells and $CD8^+$ cells. This gating strategy was used throughout all $CD8^+$ T-cell analysis.
- **b)** Representative gating example of dual positive TNF-α^+ *and CD69*$^+$ *cells.* Two examples of CMV positive donors (left panel) with the CMV stimulated cells (top panel) and the unstimulated control (bottom panel). Two examples of CMV negative donors (right panel).

A total of n=29 donors were assessed using this assay, with 10 being identified as having a positive dual TNFα and CD69 response to CMV peptide in comparison to the unstimulated control and were therefore deemed to be CMV-positive.

Due to very low cell counts, and the need for sufficient number of cells for the TAPI-0 assay, it was not possible to guarantee enough DNA from a small pellet for full PCR HLA-typing. Therefore, in the same experiment, anti-HLA antibodies were used in order to identify the HLA type of the donors. Representative examples of HLA-A2, HLA-B7 and HLA-B8 staining can be seen in Figure 45a alongside a known negative control to confirm there was no non-specific binding of the antibodies. As there were no commercially available antibodies to stain for HLA-A1, a small PBMC pellet was taken in order to extract DNA using the DNeasy Blood & Tissue Kit (Qiagen). For CMV^+ donors, DNA was extracted and positivity for HLA-A*0101 (A1) assessed using primer set 1 in Table 9 and PCR as per the conditions in Table 10. Figure 45b shows an example of patient samples with the control primers present in every lane, and bands indicating positivity for HLA-A1 in lanes 3, 4, 5, 7 and 8. Of these donors, n=5 HLA-A1 donors were identified; HLA-A2 n=5, HLA-B7 n=8 and HLA-B8 n=5.

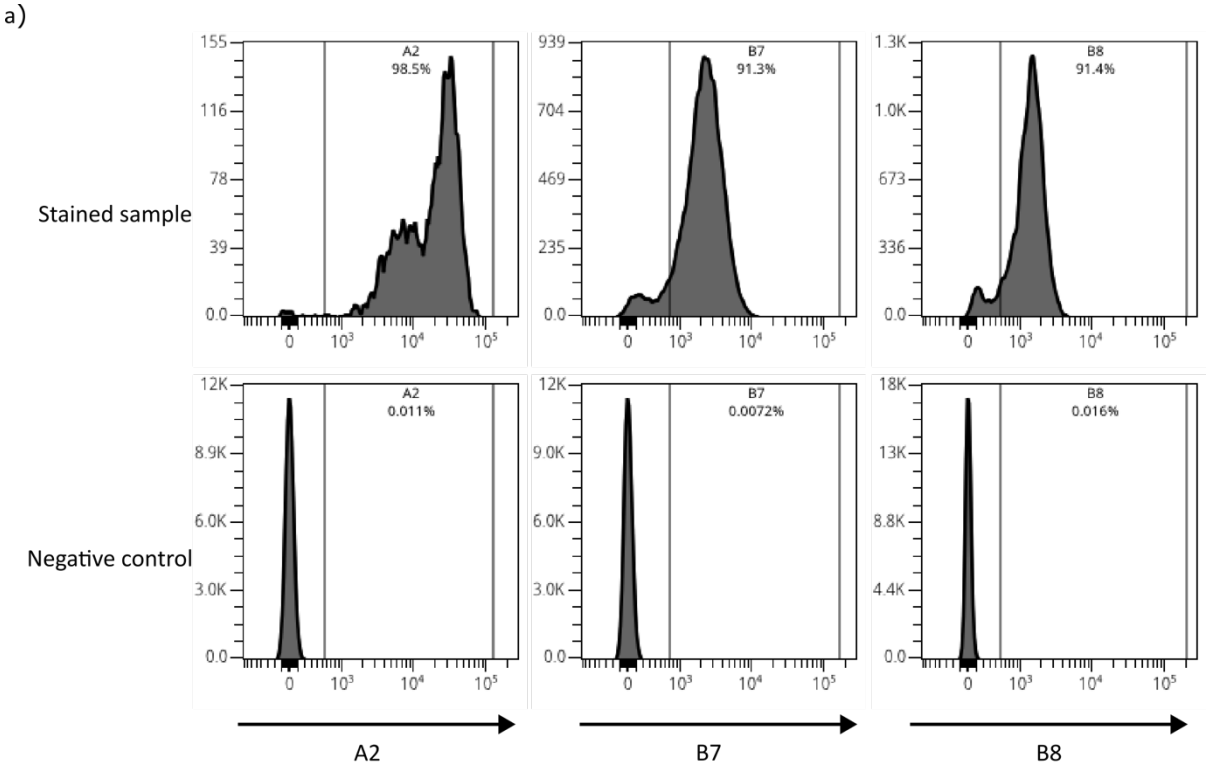

Figure 45: HLA typing of ovarian cancer patients

a) Histograms showing HLA-A2, HLA-B7 and HLA- B8 antibody staining with the top panel showing the stained samples and the bottom showing known negative control samples. Patients with a peak in the positive gate were identified as being that HLA type.

b) 1% agarose gel to test for HLA A1. Lane 1: Bioline HyperLadder™ 100bp; Lanes 2-12: CMV+ donors with primer set 1 (Table 9). The control primer bands are present in all lanes at 796 base pairs (bp). Boxes indicate the presence of bands of the product size of interest (629bp). In this example donors in lanes 3, 4, 5, 7 and 8 exhibit a band indicating they are HLA-*A*0101*.

4.2.2 Patient Cohort

After CMV infection status and HLA type had been identified, the final cohort that was selected for detailed immune phenotyping is shown in Table 18. It was not possible to obtain matched PBMC, primary and secondary tissue for each patient. This initial cohort consisted of 16 PBMC samples, 14 primary samples with samples from the fallopian tube, ovary and adnexa, and 19 secondary samples from the omentum, peritoneum and lymph node.

Table 18: Summary of number of CMV-positive donors with an HLA type suitable for tetramer staining and the location of the sample i.e. PBMC, primary or secondary tumour samples.

		Location					
Category	**Donors**	Fallopian Tube	Ovary	Adnexa	Omentum	Peritoneum	Lymph Node
PBMC	**16**						
Primary	**14**	4	7	3			
Secondary	**19**				13	5	1

4.2.3 Tetramer staining

Due to the low cell number, I stained samples with master mixes of tetramers (CMV tetramers- Table 11 and EBV tetramers- Table 12) that were specific for the HLA types of the donor. Samples were stained with CMV-tetramers (PE) and EBV-tetramers (APC) if matching tetramers were available. $CD8^+$ T-cells were selected as shown in Figure 44a, before tetramer gating was performed (Figure 46). Positive CMV-tetramer and EBV-tetramer staining was seen across PBMC, primary and secondary tumour samples.

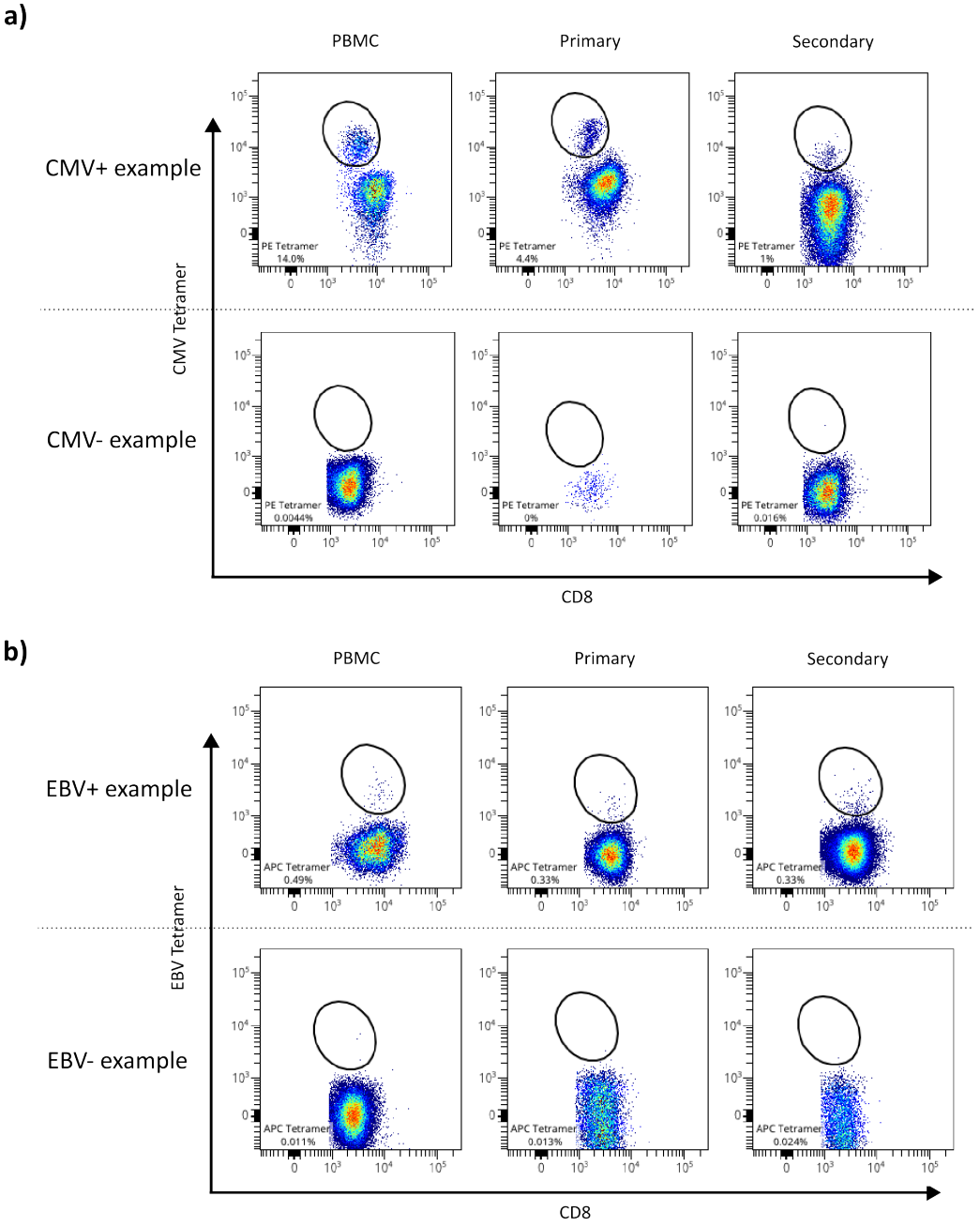

Figure 46: Representative examples of tetramer gating on CMV and EBV positive donors.

a) Representative gating strategy showing the identification of CMV-tetramer specific T-cells on PE on the $CD8^+$ T-cell population. A CMV negative donor (no detectable T-cell response on the TAPI assay) was included as a negative control to ensure there was no non-specific tetramer binding.

b) Representative gating strategy showing the identification of EBV-tetramer specific T-cells on PE on the $CD8^+$ T-cell population. A donor with no detectable tetramer response is also shown.

4.2.4 Definition of a cohort of patients with identifiable CMV- or EBV Tetramer-specific T-cell response

As not every donor displayed a distinct tetramer response, the final cohort of patients that underwent tetramer analysis is shown in Table 19. A positive tetramer response was determined as representing >0.05% of total CD8+ T-cells. In total the final cohort consisted of 10 PBMC samples, 8 Primary samples and 14 Secondary tumour samples.

Table 19: Summary of number of CMV+ donors with a CMV-tetramer$^+$ response and the location of the sample i.e. PBMC, primary or secondary tumour samples.

		Location					
Category	**Donors**	Fallopian Tube	Ovary	Adnexa	Omentum	Peritoneum	Lymph Node
PBMC	**11**						
Primary	**8**	2	5	1			
Secondary	**14**				9	4	1

Similarly, EBV-tetramer staining was next undertaken and samples with a sufficient tetramer$^+$ response were used for the final analysis, shown in Table 20. The EBV-tetramer$^+$ cohort consisted of 6 PBMC samples, 3 Primary samples and 7 Secondary tumour samples.

Table 20: Summary of number of EBV+ donors with an EBV-tetramer^{+} response and the location of the sample i.e. PBMC, primary or secondary tumour samples.

		Location					
Category	**Donors**	Fallopian Tube	Ovary	Adnexa	Omentum	Peritoneum	Lymph Node
PBMC	**6**						
Primary	**3**	1	1	1			
Secondary	**7**				4	2	1

Clinical characteristics of the patients used can be found in Table 21.

Table 21: Summary of the patient clinical characteristics of women enrolled within the research study

CMV T-cell response	**n/total n**
Positive	17/21
Negative	4/21
Diagnosis	
High-grade serous ovarian cancer	5/21 (24%)
Low-grade serous ovarian cancer	2/21 (10%)
Serous fallopian tube	5/21 (24%)
Carcinosarcoma	1/21 (5%)
Clear cell carcinoma	1/21 (5%)
Endometrioid	1/21 (5%)
Granulosa cell tumour	1/21 (5%)
Hepatobiliary tumour	1/21 (5%)
Unknown	4/21 (5%)
Surgery	
None	1/21 (5%)
Primary Debulking Surgery	9/21 (43%)
Secondary Debulking Surgery	1/21 (5%)
Delayed Debulking Surgery	3/21 (14%)
Staging laparoscopy	1/21 (5%)
Biopsy	1/21 (5%)
Unknown	5/21 (24%)
Number of chemotherapy cycles	
3	1/3 (33%)
4	2/3 (66%)

An outline of the samples used in the remainder of the study and their locations based on donor can be seen in Figure 47.

	CMV			EBV		
Donor	PBMC	Primary	Secondary	PBMC	Primary	Secondary
1	■		■			
2	■					
3	■		■	■		■
4	■			■		
5	■	x2	x2			
6	■		x2	■	■	x2
7	■	x2		■	■	
8	■	■	■			
9	■		■	■		■
10	■		■			
11	■	■	■	■		■
12		■			■	
13			x2			
14			■			■
15			■			■

Figure 47: Samples used for analysis

Diagram showing the samples used in the analysis for this chapter indicating the location of the sample and their donor. A green square indicates a sample. Donors with multiple locations are indicated ‘x2’ for example if one donor had secondary samples from both the omentum and peritoneum.

4.2.5 Memory phenotype of viral specific T-cells in ovarian cancer

A high parameter flow cytometry panel was utilised initially to comprehensively phenotype the cells ('OvCa- surface' panel, Table 13) This was done alongside tetramer staining, thereby allowing in-depth characterisation of tetramer$^+$ CD8$^+$ cells.

4.2.5.1 The tumour tissue displays an effector memory phenotype

To assess the memory phenotype of the T-cells I used the surface markers CD45RA and CCR7. This allowed discrimination of T-cells that are Naïve (CCR7$^+$ CD45RA$^+$), central memory (T_{CM}) (CCR7$^+$ CD45RA$^-$), effector memory (T_{EM}) (CCR7$^-$ CD45RA$^-$) and effector memory with CD45RA expression (T_{EMRA}) (CCR7$^-$ CD45RA$^+$) (Figure 48a).

Figure 48b shows a summary of the memory phenotypes displayed by the CD8$^+$ T-cell population. In the PBMC population, the most common phenotype was T_{EMRA} with a median expression of 39%. However, this is significantly decreased in the primary (14%) and secondary (7%) TIL populations where the dominant population is T_{EM} (median = 28%, 67% and 54% respectively; $p < 0.0001$ and $p < 0.0001$ for primary and secondary against PBMC).

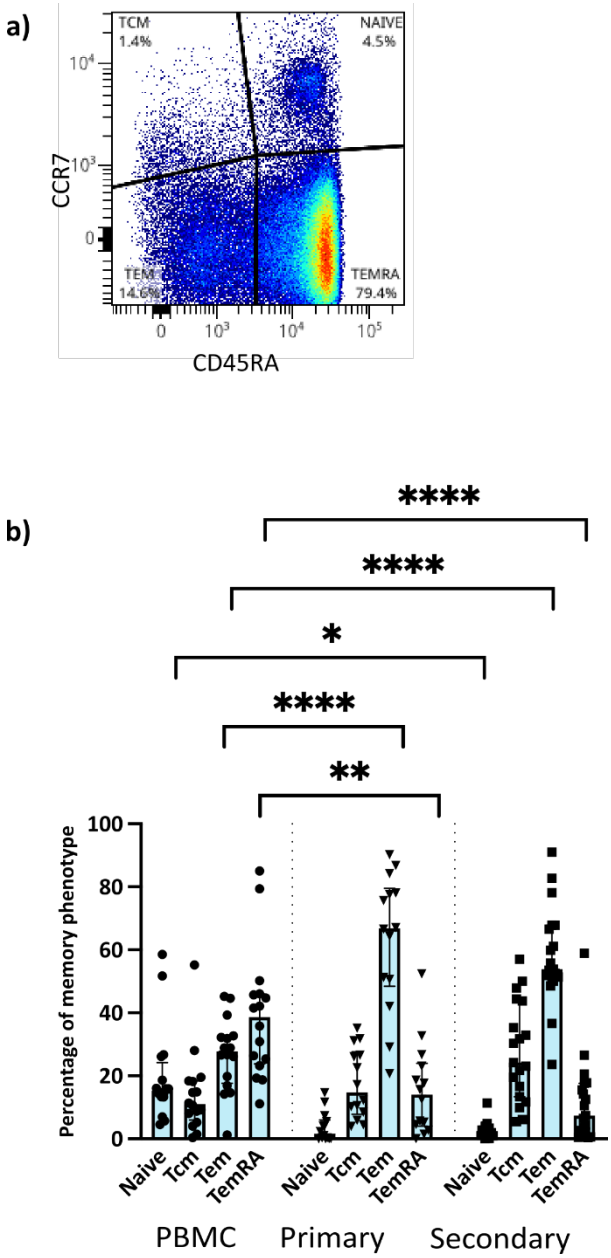

Figure 48: Memory phenotype of PBMC and TILs in OvCa patients

a) Representative gating strategy showing the four memory phenotypes on a tumour sample. Naïve T-cells (T_N), ($CCR7^+$ $CD45RA^+$), central memory (T_{CM}) ($CCR7^+$ $CD45RA^-$), effector memory (T_{EM}) ($CCR7^-$ $CD45RA^-$) and effector memory with CD45RA expression (T_{EMRA}) ($CCR7^-$ $CD45RA^+$).

b) Summary of the percentage of T-cell memory phenotypes on $CD8^+$ T-cells across the PBMC, Primary and Secondary TIL populations. Each dot indicates data from one donor. Bars represent the percentage median of each checkpoint (± interquartile range). Statistical analysis performed with two-way ANOVA with main effects only with Tukey's multiple comparisons test with * p <0.05; ** p <0.01; *** p <0.001; **** p <0.0001.

Memory phenotypes were next analysed on the viral-specific populations by applying the memory gate to the CMV-tetramer$^+$ and EBV-tetramer$^+$ cells (Figure 49). Similarly to the CD8$^+$ population, both CMV-tetramer$^+$ and EBV-tetramer$^+$ cells showed a decrease in the T_{EMRA} phenotype between the PBMC and the primary and secondary TILs (CMV median = 55%, 14% and 9.9% respectively; EBV median = 34%, 0% and 1.6% respectively). In the CMV-tetramer$^+$ population this decrease was statistically significant between the PBMC and the primary T|IL ($p = 0.03$) and the PBMC and the secondary TIL ($p < 0.0001$). The dominant memory population within the tumour was the T_{EM} cells which displayed a median expression of 67% in the primary TILs, and 46% in the secondary TILs. The T_{EM} population also significantly increases from the PBMC to the EBV-tetramer$^+$ primary population ($p = 0.0008$).

Interestingly, the CMV-tetramer$^+$ population also shows a significant increase in T_{CM} cells between the PBMC where there is very little expression (median = 3.44%) and the secondary TILs (median = 32%; $p = 0.03$). Whilst also trending upwards in the primary samples (median = 17.5%) it is not significant. This indicates there are less terminally differentiated cells in the tissue populations in comparison to the PBMC. The same effect is seen in the EBV-tetramer$^+$ populations with an increase between the PBMC (median = 19.2%) and secondary TILs (median = 47.4%; $p = 0.0244$).

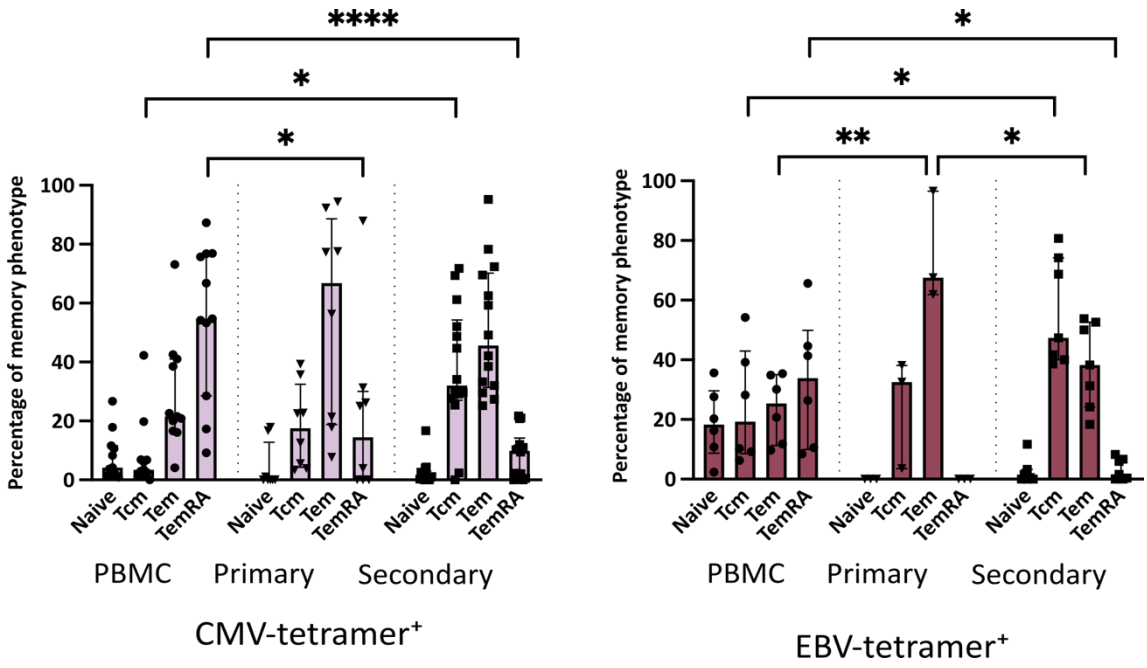

Figure 49: Memory phenotyping viral specific T-cells in the PBMC and TILs

Summary of the percentage of T-cell memory phenotypes on CMV-tetramer$^+$ and EBV y=tetramer$^+$ T-cells across the PBMC, Primary and Secondary TIL populations. Each dot indicates data from one donor. Bars represent the percentage median of each checkpoint (± interquartile range). Statistical analysis performed with two-way ANOVA with main effects only with Tukey's multiple comparisons test with * p <0.05; ** p <0.01; *** p <0.001; **** p <0.0001.

4.2.6 Higher checkpoint expression is present in the tumour tissue

Following the gating of tetramer-specific T-cells, I next analysed the surface expression of the key checkpoint protein PD1 (Figure 50). Significant increases in relative PD1 expression were seen when comparing PBMC to both the primary and secondary cohorts in the CMV-tetramer$^+$ population (median for PBMC = 45%, primary = 77%, secondary = 70%; p = 0.014 and p = 0.0007 respectively). Analysis of the EBV-tetramer$^+$ cohort showed a similar effect (median PBMC 22%, primary 81%, secondary 76%; p = 0.006 and p < 0.0001 respectively). This profile was also seen in the tetramer-negative CD8+ cells (median PBMC 32%, primary 64%,

secondary 62%; $p < 0.0001$ and $p < 0.0001$ respectively,). Together showing that a much higher percentage of CD8$^+$ cells from all three study groups express PD1 within tissue.

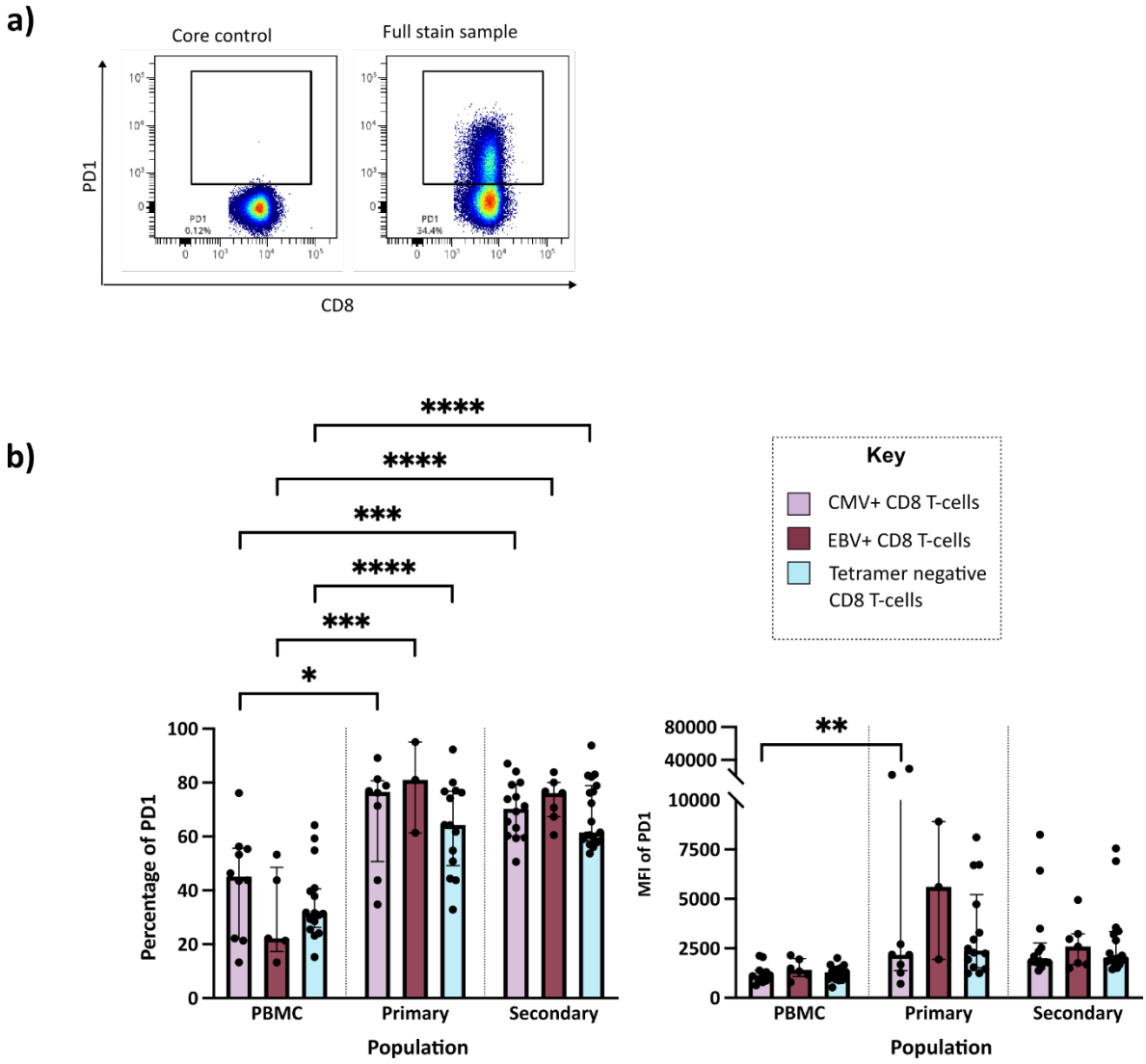

Figure 50: PD1 expression on viral specific T-cells

a) Representative dot plots of PD1 staining with the negative core control

b) Summary of the percentage of PD1 expression and MFI of PD1$^+$ population on CMV-tetramer$^+$ T-cells, EBV-tetramer$^+$ T-cells and tetramer negative T-cells. Each dot indicates data from one donor. Bars represent the percentage median of each checkpoint (± interquartile range). Statistical analysis performed with two-way ANOVA with main effects only with Tukey's multiple comparisons test with * $p < 0.05$; ** $p < 0.01$; *** $p < 0.001$; **** $p < 0.0001$.

The median-fluorescence intensity (MFI) of the $PD1^+$ population were also analysed to compare potential differences in the relative number of PD1 molecule at the cell surface. Of note, the CMV-$tetramer^+$ population exhibits a higher intensity of PD1 expression within the primary TIL population (median = 2179) in comparison to the PBMC (median = 1146, p = 0.0087). A similar trend was seen for cells within secondary tissue. EBV-specific T-cells showed a similar profile, indeed with dramatic MFI expression within primary tissue, but the number of samples limited statistical power.

Antibodies against three other checkpoint proteins, TIGIT, LAG3 and TIM3, were also included in the flow cytometry panel and the percentage expression of these on the CMV-$tetramer^+$ and EBV-$tetramer^+$ $populations^-$ is shown in Figure 51.

The expression levels of the different checkpoints were highly variable as represented by the range of percentage expression and the fluorescent intensity. Whilst there was variability between donors, TIGIT was the most expressed checkpoint in the PBMC compartment, with a median of 28% of CMV-$tetramer^+$ T-cells expressing TIGIT. This was mirrored in the EBV-$tetramer^+$ compartment with 41% expressing TIGIT, and the numbers remained high in the tetramer negative compartment with 30% expressing TIGIT.

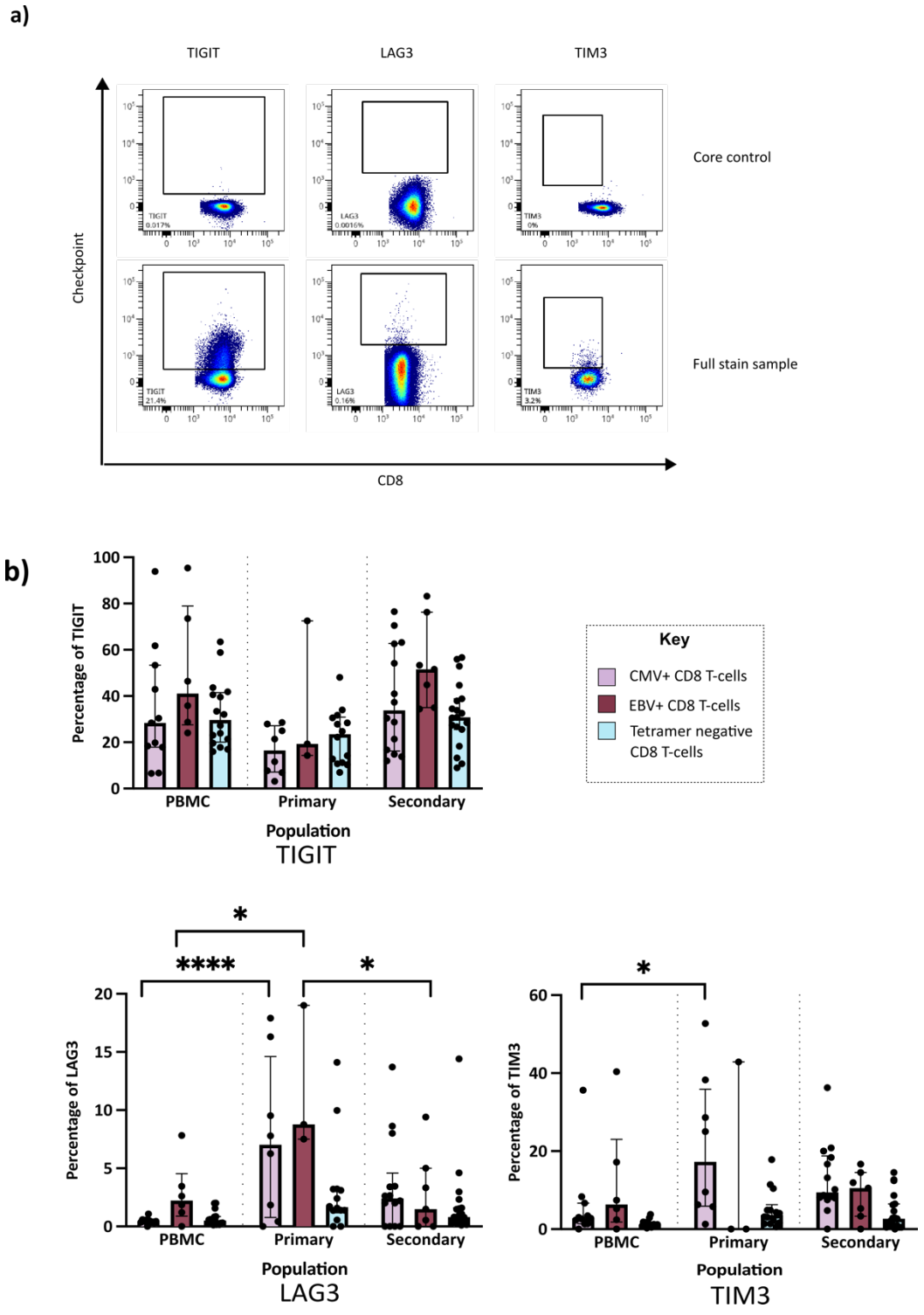

Figure 51: Checkpoint expression on PBMC and TILs

a) Representative dot plots of TIGIT, LAG3 and TIM3 staining with the negative core control

b) Summary of the percentage of checkpoint expression of TIGIT, LAG3 and TIM3 on CMV-tetramer^{+} T-cells, EBV-tetramer^{+} T-cells and tetramer negative T-cells. Each dot indicates data from one donor. Bars represent the percentage median of each checkpoint (± interquartile range). Statistical analysis performed with two-way ANOVA with main effects only with Tukey's multiple comparisons test with * p <0.05; ** p <0.01; *** p <0.001; **** p <0.0001.

Whilst expression of LAG3 and TIM3 were much lower, interestingly, there was a significant increase in expression of both markers on CMV-tetramer^{+} cells in primary TIL populations. LAG3 on CMV-specific T-cells increased from 0.44% in blood to 7.0% ($p < 0.0001$) in TIL with TIM3 increasing from 2.75% to 17% ($p = 0.017$). In the EBV-specific T-cell population there was also an increase of LAG3 expression from the PBMC (median = 2.2%) to the primary TIL population (median = 8.8%; $p = 0.0272$). However, of note, LAG3 expression trended lower in the secondary TIL population with there being a significant decrease from the primary to secondary EBV specific population (median = 1.5%; $p = 0.0325$). A summary of the median checkpoint values can be found in Table 22.

Table 22: Summary of median checkpoint expression percentage from CMV-specific, EBV-specific and tetramer- cells in the PBMC, primary and secondary tissue

		Checkpoint median expression (%)			
Category	**Population**	**PD1**	**TIGIT**	**TIM3**	**LAG3**
PBMC	CMV^{+}	45.1	28.4	2.8	0.44
	EBV^{+}	22.2	41.1	6.3	2.2
	Tetramer^{-}	31.5	26.7	1.1	0.5
Primary	CMV^{+}	76.6	16.5	17.3	7
	EBV^{+}	81	19.3	0	8.8
	Tetramer	64.3	23.45	3.6	1.7
Secondary	CMV^{+}	70.3	33.85	3.6	2.4
	EBV^{+}	76.1	51.6	9.5	1.5
	Tetramer	61.5	30.8	10.5	0.8

Next, I assessed the MFI of the checkpoint positive populations for these checkpoints (Figure 52). The checkpoints LAG3, TIM3 and TIGIT retained consistent levels of fluorescence intensity between the PBMC and tumour populations. However, the MFI for TIGIT for the EBV-tetramer$^+$ population on the PBMC (median = 587) and primary (median = 766) populations displayed a higher intensity of TIGIT than the tetramer$^-$ populations (PBMC median = 531 and primary median = 545; p = 0.023 and 0.023 respectively).

Table 23: Summary of median checkpoint expression (MFI) of the positive checkpoint gate from CMV-specific, EBV-specific and tetramer- cells in the PBMC, primary and secondary tissue

		Checkpoint median expression (MFI)			
Category	**Population**	**PD1**	**TIGIT**	**TIM3**	**LAG3**
PBMC	CMV$^+$	1146	508	774	1563
	EBV$^+$	1419	587	636	1625
	Tetramer$^-$	1291	531	775	1618
Primary	CMV$^+$	2179	538	876	2121
	EBV$^+$	5609	766	1574	2204
	Tetramer	2390	545	788	1360
Secondary	CMV$^+$	1845	702	723	1558
	EBV$^+$	2596	683	671	1685
	Tetramer	2043	570	725	1544

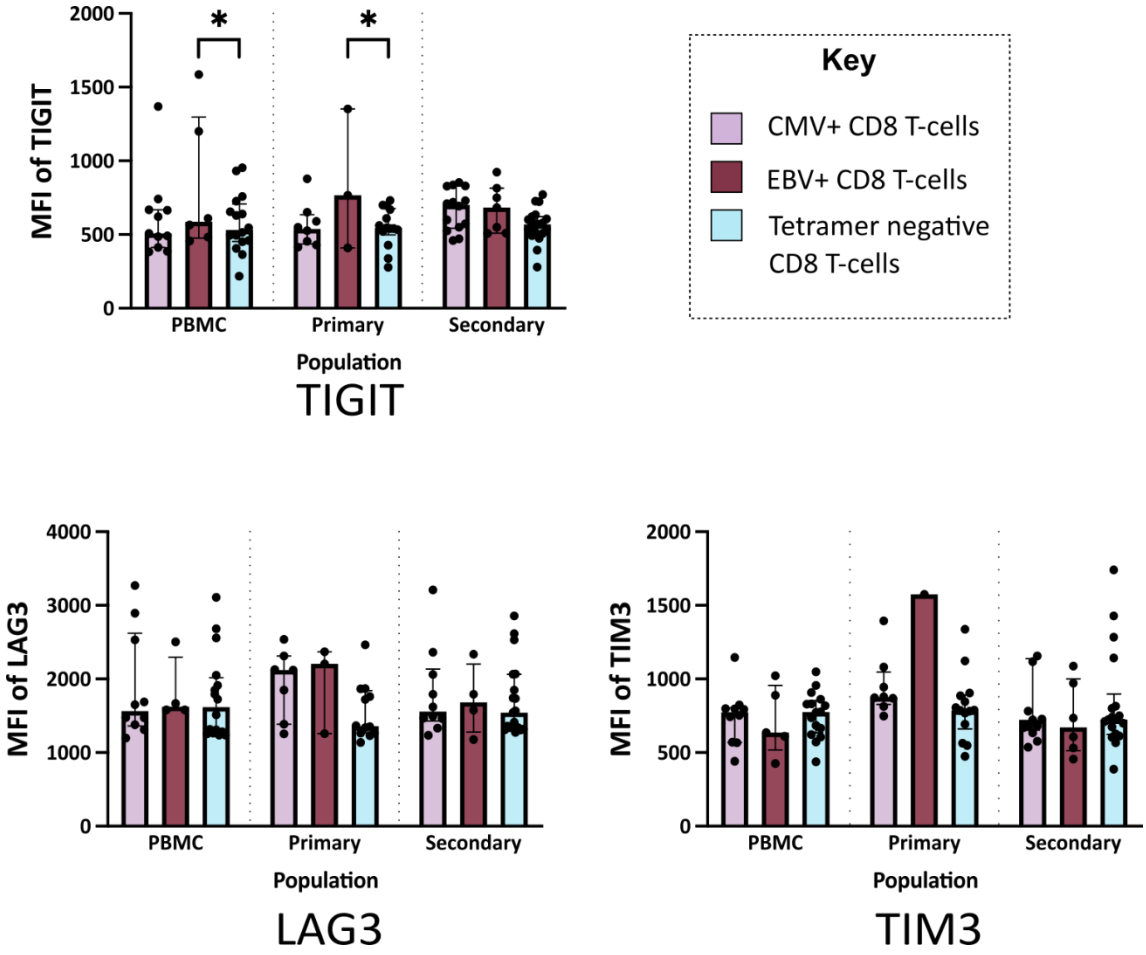

Figure 52: Checkpoint MFI for PBMC vs primary vs secondary TILs

Median fluorescence intensity (MFI) for the checkpoint positive populations for the checkpoints TIGIT, LAG3 and TIM3 for CMV-tetramer$^+$ cells, EBV-tetramer$^+$ cells and tetramer$^-$ cells in the PBMC, primary and secondary TIL populations. Bars represent the percentage median MFI of each checkpoint (±interquartile range). Statistical analysis performed with two-way ANOVA with main effects only with Tukey's multiple comparisons test with * p <0.05; ** p <0.01; *** p <0.001; **** p <0.0001.

4.2.7 High dimensional analysis of checkpoint co-expression on $CD8^+$ T-cells

I next utilised high-dimensional analysis to obtain a better overview of the phenotypes of the cell populations and easily identify the combinations of other markers they were expressing. FlowSOM was used to cluster the cells and the dimensionality reduction algorithm UMAP was selected to visualise the data. All files were uploaded to OMIQ with compensation and scaling applied. Following the gating strategy in Figure 46, 5000 $CD8^+$ T-cells from each donor were subsampled out. The FlowSOM algorithm using elbow metaclustering was used to cluster the cells on all markers with the exception of markers already utilised or gated out in the pre-gating: CD3, viability dye, CD4, CD8 and the dump channel. To visualise the data, UMAP was selected as the dimensionality reduction algorithm. This was run with the following settings: Neighbours: 15, Minimum Distance: 0.4, Components: 2, Metric: Euclidean, Learning Rate: 1, Epochs: 200, Random Seed: 8049, Embedding Initialisation: spectral.

Clusters were analysed using a combination of a heatmap and histograms to determine the expression of markers within each cluster, alongside visually inspecting where the clusters sat on the UMAP plot. This way several clusters were merged leaving a total of 12 distinct clusters as shown in UMAP plots in Figure 53a.

Key differences were clear from these initial plots, for example clusters 3, 4, 8 and 7 are present in the TIL samples but minimal in the PBMC. Primary analysis using the heatmap in Figure 53b confirms these to have high expression of CD103 and CD69 which are markers typically associated with tissue resident memory (T_{RM}) populations. It should be noted that the colours in the heatmap are scaled by columns rather than row, which is not possible using the OMIQ software. Therefore, whilst some markers may look equally positive within one

cluster due to the colour scaling, the cell values indicate otherwise. This is particularly prevalent with the APC-tetramer staining which as shown by the UMAPs in Figure 53c has very low-level expression throughout. Therefore, this marker was not analysed further by high-dimensional.

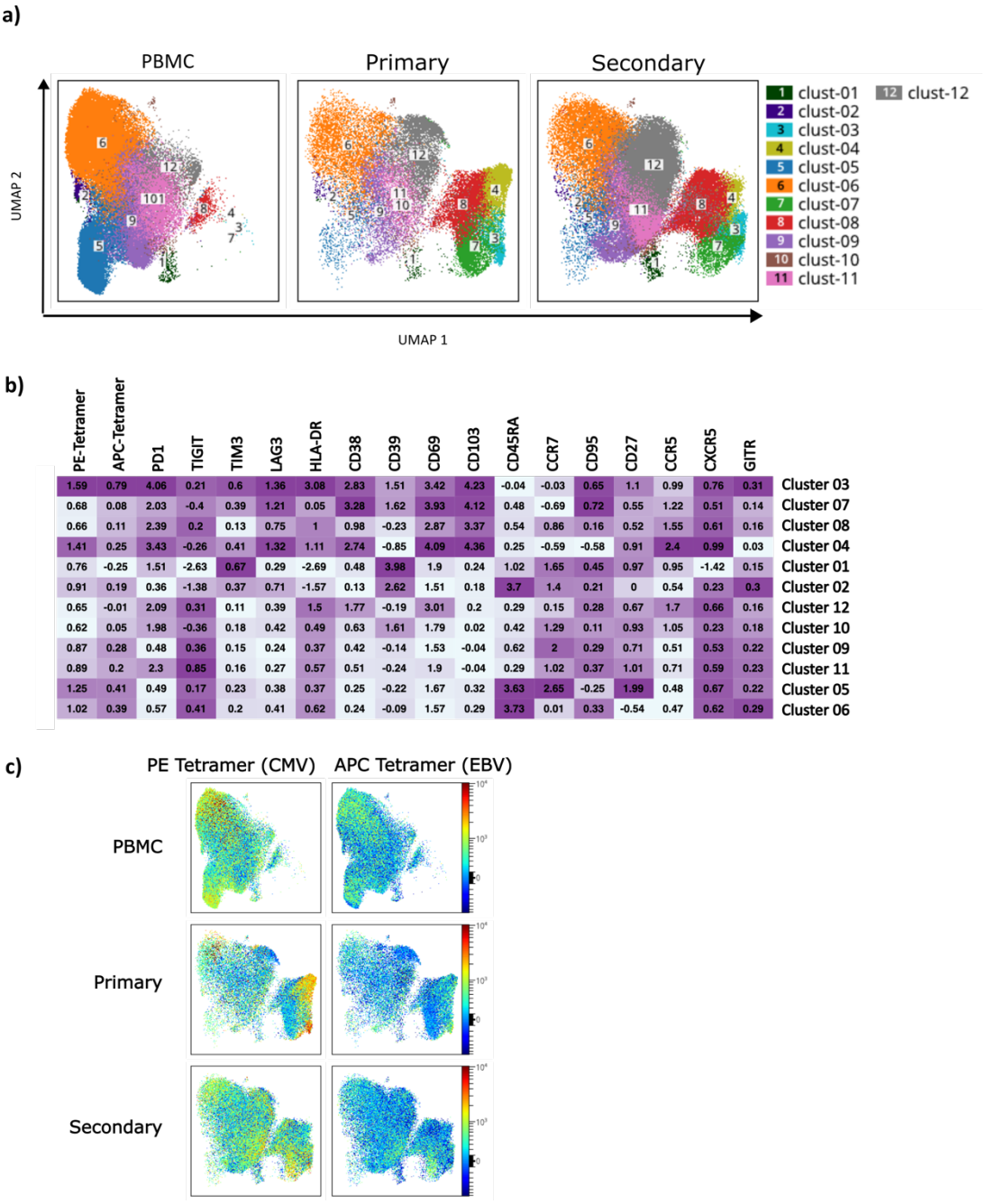

Figure 53: Twelve distinct clusters were identified through multidimensional analysis of cell populations following multi-parametric flow cytometry

- **a)** UMAPs showing the concatenated PBMC (n=16), primary (n=14) and secondary (n=19) samples with the 12 identified clusters overlaid.
- **b)** Heatmap showing the expression of the markers across the 12 different clusters. The shade of colour corresponds to the cell value with a darker shade indicating higher expression. The cell values for each marker are median ArcSinH values and are scaled individually to allow relative comparison between each cluster.
- **c)** UMAPs showing the density of PE-tetramer (CMV) and APC-tetramer (EBV)expression across the concatenated PBMC (n=16), primary (n=14) and secondary (n=19) samples. As per the colour bar, dark red indicates higher expression with dark blue indicating no expression.

4.2.8 Considerable heterogeneity of CD8+ T-cell phenotype within tumour tissue is observed between different patients

As the range of checkpoint expression showed significant variation, the UMAPs were next visualised on a sample-by-sample basis to see the different distributions of cells.

A comparison of 9 samples shown in Figure 54 reveals that, whilst PBMC samples are broadly placed within a similar UMAP pattern between donors, albeit with variation in the density of cells, the primary and secondary TILs show considerable spatial variation between the donors, indicating increased levels of cellular heterogeneity within tissue.

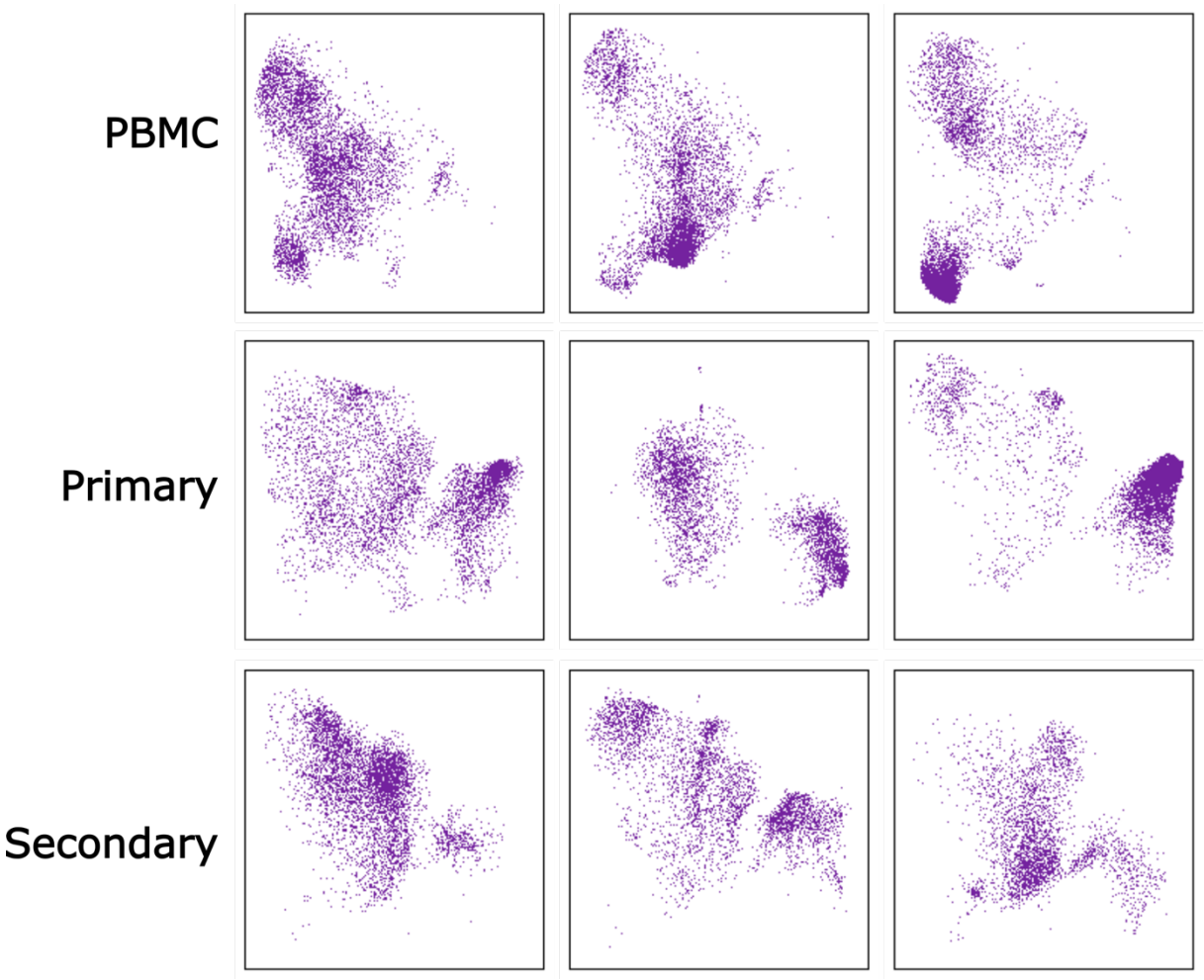

Figure 54: Representation of UMAPs of relative checkpoint expression patient

Representative example of UMAPs of 3 PBMC samples, 3 primary samples and 3 secondary samples from different donors showing the distribution of 5000 $CD8^+$ T-cells per donor. Each dot represents one cells and the location on the map represents the cluster it is in and its relationship with the nearest neighbours.

In light of this pattern, I next went on to assess the relative contribution of individual patients to the cluster profile. As such, a heatmap was used to show the percentage distribution of cells from each patient into the individual clusters. This showed that some clusters, such as cluster 6, were dominant across many patients whilst some patients had large proportions of

cells fell into other clusters. Examples here were cluster 3 for donors 5 and 6, and cluster 7 for donors 19 and 20.

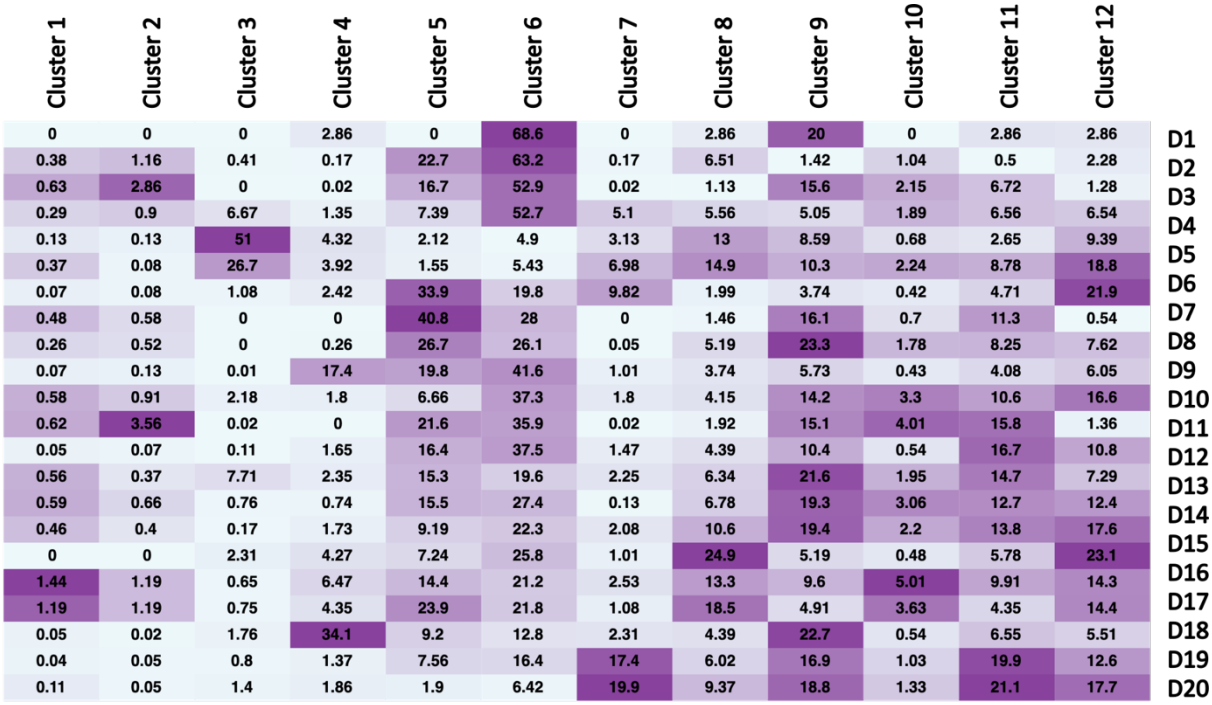

Figure 55: Heatmap showing distribution of clusters making up one donor

Heatmap showing the percentage of cells in each cluster per donor. The values in each cell indicate the percentage. The shade of colour corresponds to the cell value with a darker shade indicating higher expression. The cell values for each marker are median ArcSinH values and are scaled individually to allow relative comparison between each donor.

In order to further analyse the expression of markers across the UMAPs I next used coloured-continuous scatterplots. Initial analysis was based on tissue residency profile as defined by CD69 and CD103 expression (Figure 56).

This confirmed that clusters 3, 4, 7 and 8, which make up the right-hand island, are strongly expressing these proteins and exhibiting a T_{RM} phenotype. Interestingly, these UMAPs also

identify a population, largely defined as cluster 12, that exhibits high CD69 expression but low CD103 expression and is present primarily within the TILs.

a)

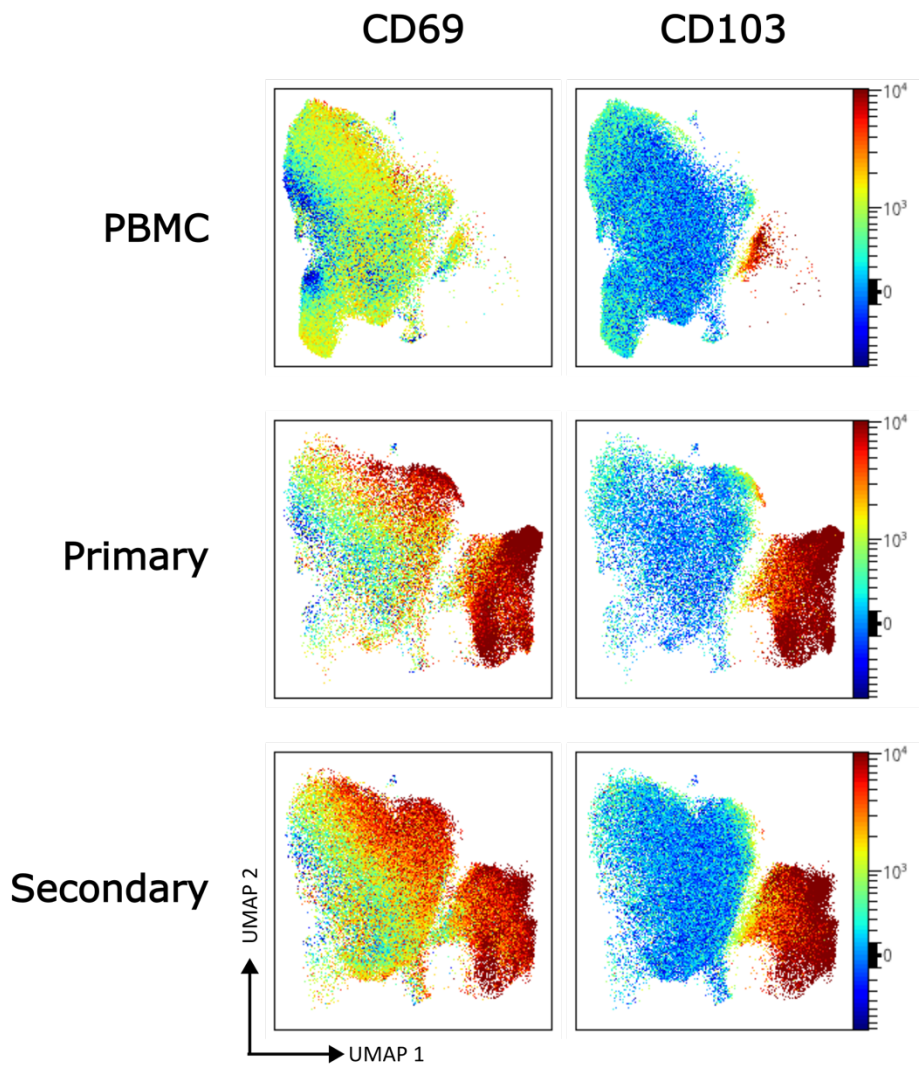
CD69
CD103
PBMC
Primary
Secondary
10^4
10^3
0
UMAP 2
UMAP 1

b)

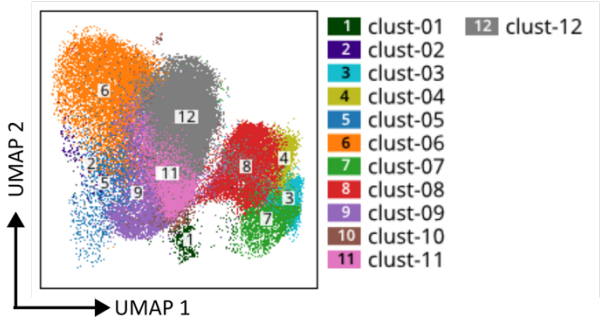
1 clust-01
2 clust-02
3 clust-03
4 clust-04
5 clust-05
6 clust-06
7 clust-07
8 clust-08
9 clust-09
10 clust-10
11 clust-11
12 clust-12
UMAP 2
UMAP 1

Figure 56: Distribution of CD69 and CD103 expression across the UMAP

a) UMAPs showing the density of CD69 and CD103 expression across the concatenated PBMC (n=16), primary (n=14) and secondary (n=19) samples. As shown in the colour bar, dark red indicates higher expression with dark blue indicating no expression.
b) UMAPs showing the concatenated secondary (n=19) samples with the 12 identified clusters overlaid.

To next identify the relative distribution of checkpoint protein expression across these clusters the intensity of checkpoint expression was also analysed using coloured-continuous scatterplots (Figure 57a).

PD1 in particular, shows much higher expression in the primary and secondary samples in comparison to the PBMC, with a lot of expression coming from the T_{RM} populations. It also, of interest, shows a bigger range in intensity than the PBMC populations with intermediate expression in cluster 12 which showed high CD69 expression but low $CD103^{-}$. This is in line with the manual-gating data which showed increases of PD1 in the TILs in comparison to PBMC.

The UMAPs also show that the T_{RM} clusters exhibit very low-level expression of LAG3 which is not present in the PBMC, and small portions of cells expressing TIM3 whereas interestingly, TIGIT is showing low-mid expression levels across a wider range of clusters.

As this study is particularly interested in the viral specific T-cells, the CMV-$tetramer^{+}$ cells were also investigated with their expression highlighted in Figure 57b. Interestingly, they were not phenotypically distinct enough to form their own cluster, but exhibit a range of phenotypes across the clusters. CMV-$tetramer^{+}$ T-cells are expressed in the clusters that expressing T_{RM} markers and are co-expressing a particularly high level of PD1, however they are also

expressed in clusters which express intermediate or low levels of PD1. As the CMV-tetramer^{+} T-cells that strongly express PD1 are only present in the tissues, this makes them interesting for further analysis.

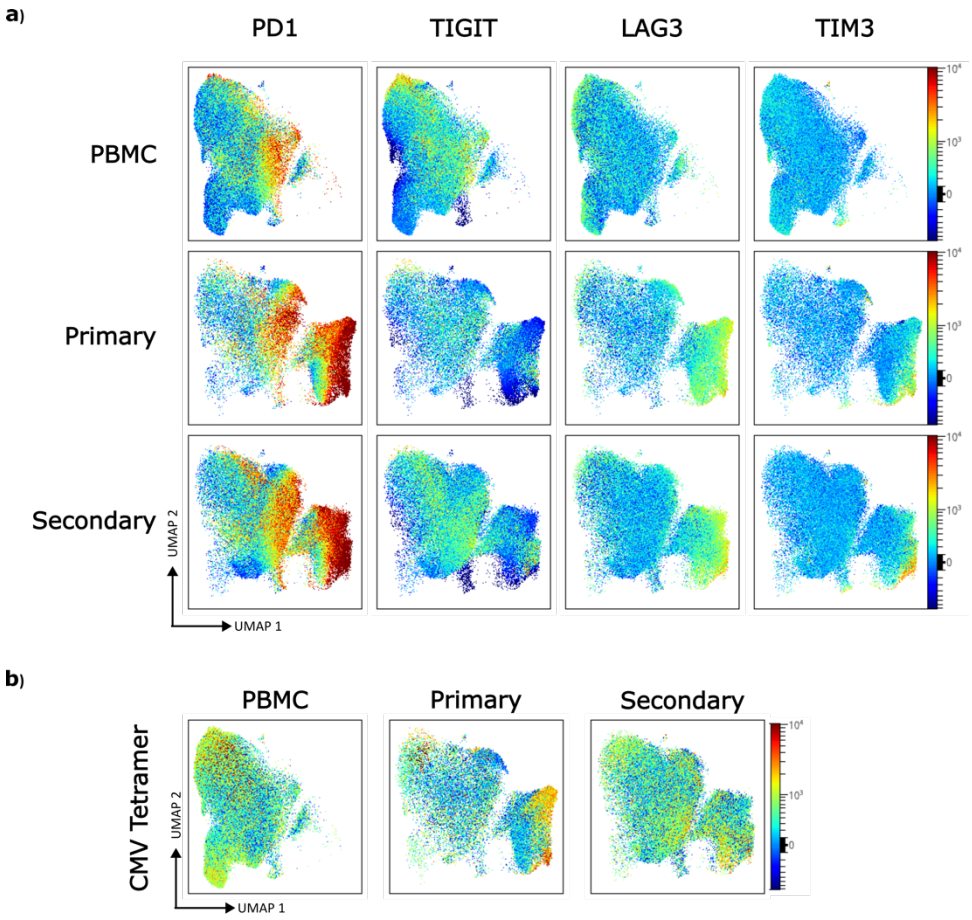

Figure 57: UMAPs showing checkpoint and tetramer intensity

a) UMAPs showing the expression and distribution of the checkpoints PD1, TIGIT, LAG3 and TIM3 across the concatenated PBMC (n=16), primary (n=14) and secondary (n=19) samples. As per the colour bar, dark red indicates higher expression with dark blue indicating no expression.

b) UMAPs showing the expression and distribution of CMV-tetramer^{+} cells across the concatenated PBMC (n=16), primary (n=14) and secondary (n=19) samples. As per the colour bar, dark red indicates higher expression with dark blue indicating no expression.

4.2.8.1 Comparing clusters

I next used the edgeR algorithm to compare T-cell cluster distribution between the PBMC and tissues (Figure 58).

A significant increase of clusters 3, 4, 7 and 8 was seen in both the primary and secondary TIL populations in comparison to the PBMC. As previously identified, these are the clusters expressing T_{RM} markers (CD103 and CD69) whilst also strongly expressing PD1.

A decrease in cluster 2, 5 and 6 was apparent within the secondary TILs whilst clusters 5 and 6 were also reduced in the primary TILs in comparison to the PBMC populations. An interesting characteristic of these clusters is they display low expression of PD1 in comparison to the other clusters (Figure 53b). Of note, no significant changes were seen between the two TIL populations,

Given these observations, T_{RM} subgroups and populations expressing different levels of the PD1 checkpoint were targeted for further analysis.

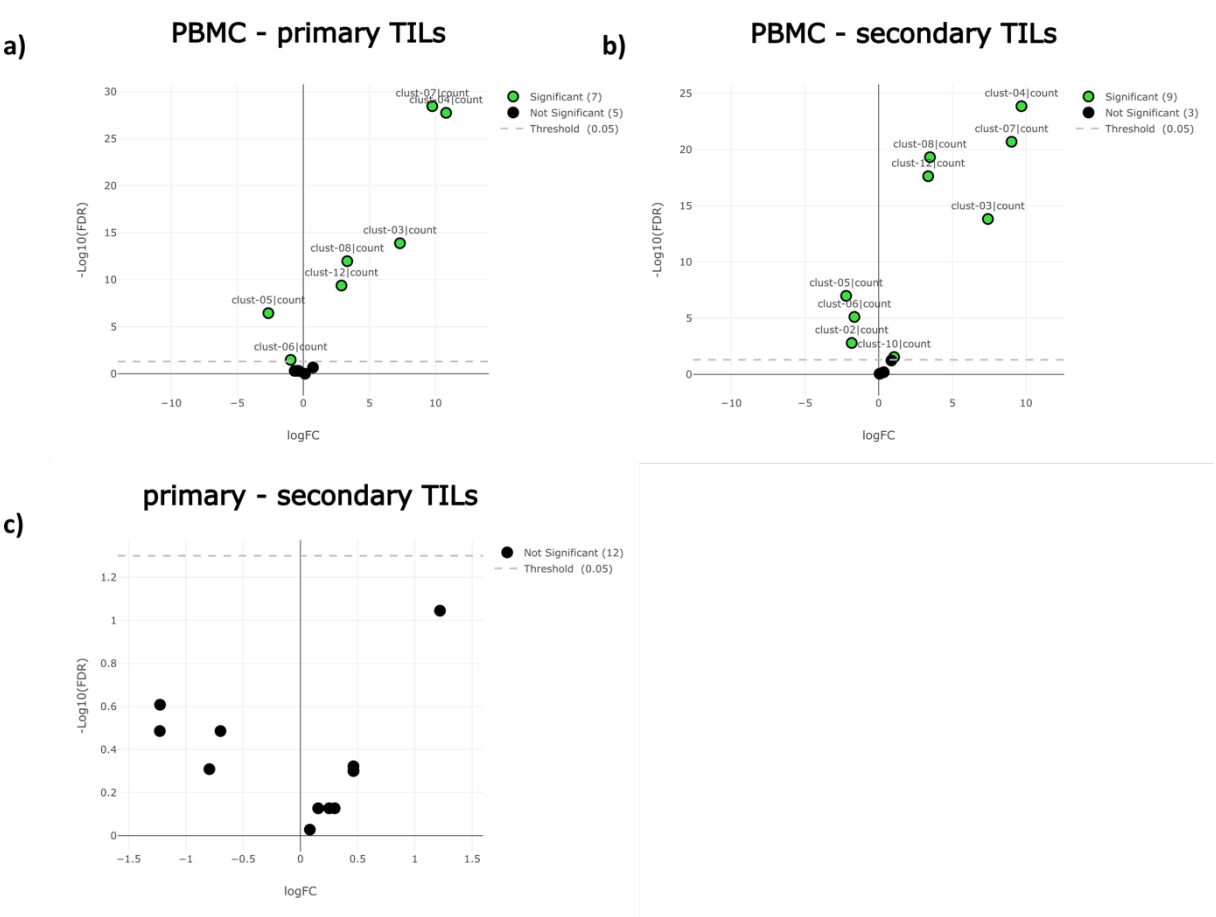

Figure 58: Volcano plots showing the statistical differences between the populations

EdgeR analysis generated volcano plots indicating any statistical differences between the clusters in:

- **a)** PBMC vs primary TILs
- **b)** PBMC vs secondary TILs
- **c)** Primary vs secondary TILs

A statistical p-value of <0.05 is indicated by green dots above the threshold line, clusters to the right of 0 indicate the fold change increase in expression whereas the clusters to the left indicate a significant downregulation. Black dots under the threshold line indicate clusters with no significant changes. The data was plotted against false discovery rate (FDR), an adjusted p-value which reduces the chances of false positives.

4.2.9 Tissue resident memory T-cells

As the high dimensional analysis had shown that a proportion of CMV-tetramer$^+$ CD8$^+$ T-cells displayed a T_{RM} phenotype I undertook further biaxial gating analysis to identify what other surface markers are expressed on these cells. Gating on the T_{RM} markers CD103 and CD69 was used to identify the relevant population (Figure 59a), with this gating then applied to the tetramer$^+$ populations.

Figure 59c confirms that T_{RM} cells were present in all the CMV-tetramer$^+$ and EBV-tetramer$^+$ populations, as well as the tetramer$^-$ populations, (primary: median 28%, 62% and 39% respectively; secondary: median 15%, 23% and 17% respectively). These differences were highly significant between PBMC and the primary TILs for all three populations ($p = 0.0004$, 0.0258 and <0.0001 respectively) and between PBMC and secondary TILs for CMV-tetramer$^+$ and tetramer$^-$ populations ($p=0.0029$ and <0.0001 respectively). No double positive CD103$^+$ CD69$^+$ cells were seen in PBMC in any population.

There was considerable variation in the proportion of tetramer$^+$ cells that expressed T_{RM} markers in primary TILs. For CMV-tetramer$^+$ and EBV-tetramer$^+$ CD8$^+$ cells the proportion of T_{RM} expression ranged from 4-78% and 62-72% respectively, whilst in secondary TIL these values were 9-53% and 5-61% respectively. It should be noted that the sample size of the EBV-tetramer$^+$ primary pool is only 3 which may contribute to the smaller range in expression.

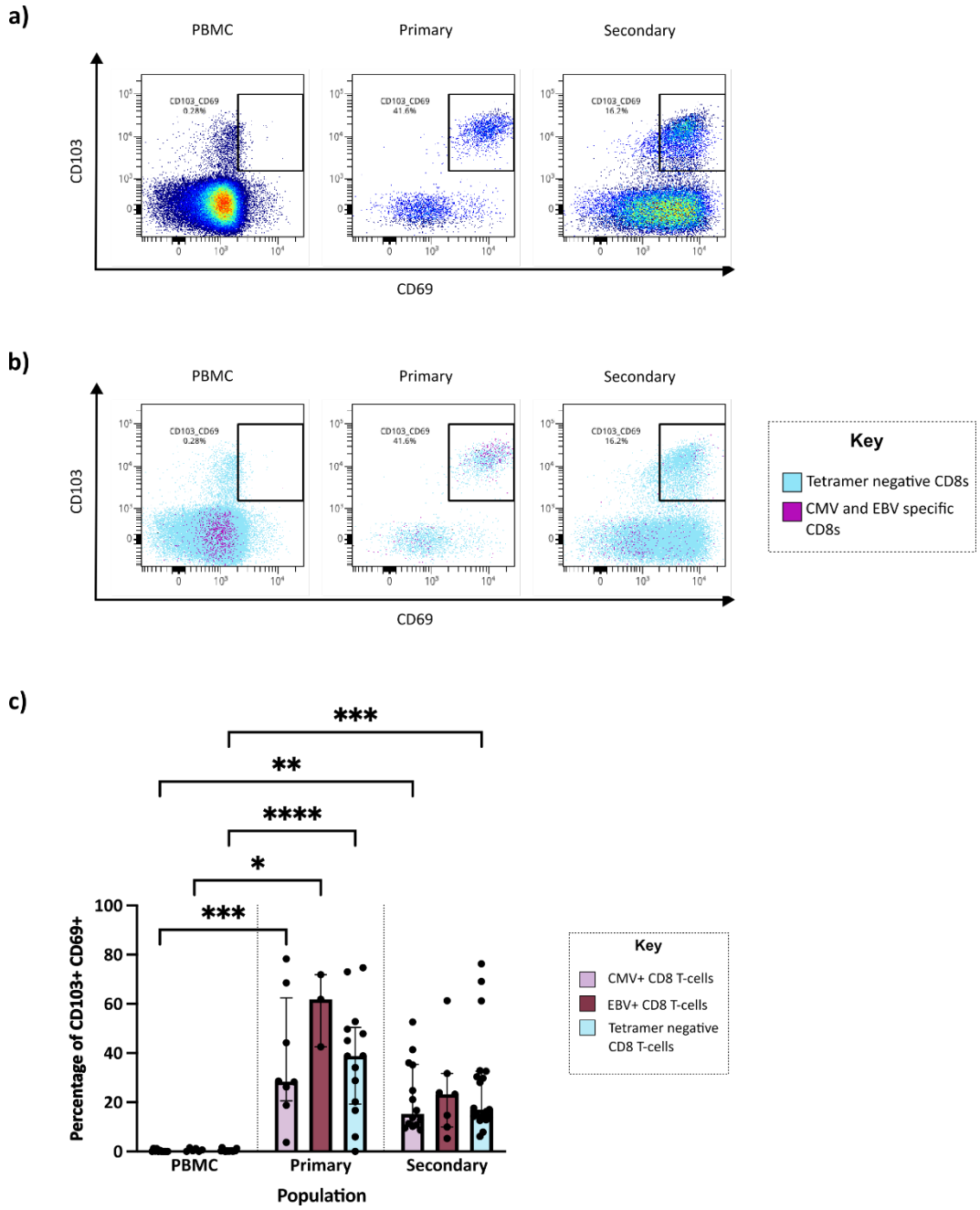

Figure 59: Tetramer specific T_{RM} cells are present in the TILs

a) Representative gating example of the $CD103^+$ $CD69^+$ T_{RM} CD8 T-cells on PBMC, primary and secondary TIL populations

b) Representative example of the CMV-tetramer$^+$ and EBV-tetramer$^+$ populations overlaid on the tetramer$^-$ populations

c) Summary of the percentage of T_{RM} expression on CMV-tetramer$^+$ T-cells, EBV-tetramer$^+$ T-cells and tetramer negative T-cells. Each dot indicates data from one donor. Bars represent the percentage median of each checkpoint (± interquartile range). Statistical analysis performed with two-way ANOVA with main effects only with Tukey's multiple comparisons test with * p <0.05; ** p <0.01; *** p <0.001; **** p <0.0001.

In order to assess the percentage of T_{RM}^{+} tetramer-specific $CD8^{+}$ cells, the percentage of tetramer-specific cells which fell in the T_{RM}^{+} or T_{RM}^{-} gates were analysed (Figure 60).

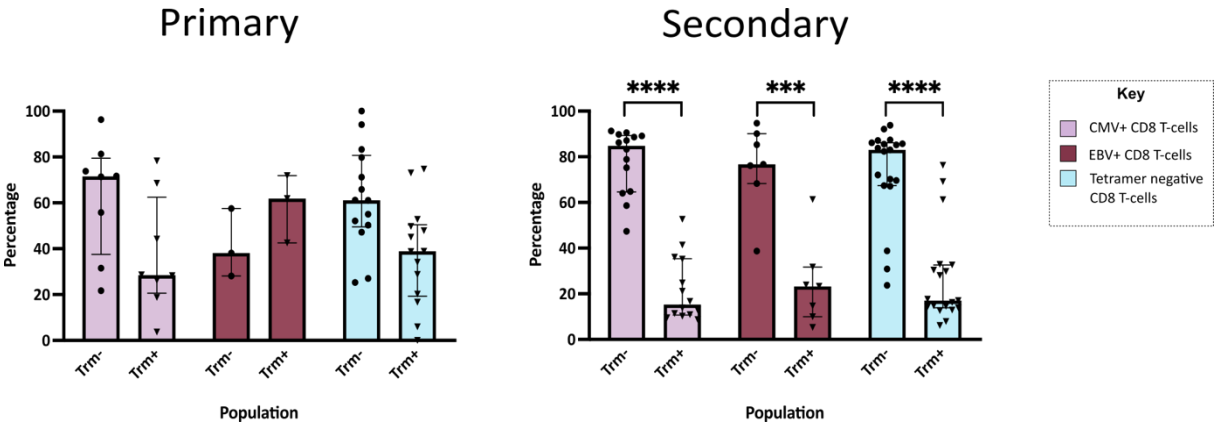

Figure 60: T_{RM}^{+} and T_{RM}^{-} expression by tetramer specific CD8s

Summary of the percentage of T_{RM}^{+} and T_{RM}^{-} expression on CMV^{+} T-cells, EBV^{+} T-cells and tetramer negative T-cells. Each dot indicates data from one donor. Bars represent the percentage median of each checkpoint (± interquartile range). Statistical analysis performed with two-way ANOVA with main effects only with Tukey's multiple comparisons test with * p <0.05; ** p <0.01; *** p <0.001; **** p <0.0001.

The proportion of virus-specific cells that expressed a TRM phenotype was higher in the primary TIL subset such that there was no significant difference in the size of the T_{RM}^{-} and T_{RM}^{+} populations. However, TRM subsets were reduced in secondary TIL such that T_{RM}^{-} cells were dominant in all 3 cellular subgroups. However, this data does highlight that there are CMV-tetramer^{+} and EBV-tetramer^{+} T_{RM}^{+} cells in the primary TILS (median = 28% and 62% respectively) and in the secondary TILs (median = 15% and 23% respectively).

As indicated by the high dimensional analysis, the $CD103^{+}CD69^{+}$ populations were also positive for several checkpoint markers. In order to analyse this in more depth, I applied the checkpoint gates for PD1, TIGIT, LAG3 and TIM3 to the T_{RM}^{+} and T_{RM}^{-} populations (Figure 61).

The CMV-$tetramer^{+}$ CD8s and the $tetramer^{-}$ cells have an increase of the checkpoint PD1 in the T_{RM}^{+} population in both the primary TILs (median = 100% and 90% respectively) and in the secondary TILs (median = 98% and 85% respectively). This is in comparison to the T_{RM}^{-} populations (primary TILs median = 57% and 51% respectively; secondary TILs median = 66% and 84% respectively; $p < 0.0001$ for all conditions). This is also seen in the EBV-$tetramer^{+}$ population in the secondary population ($p = 0.0026$) and whilst not significant, also trends in a similar direction with the EBV-$tetramer^{+}$ in the primary compartment ($p = 0.14$).

The median values for PD1 expression on EBV-$tetramer^{+}$ cells in the T_{RM}^{+} population are 100% in primary TILs and 96% in secondary TILs, whilst comparable values for the T_{RM}^{-} compartment were 50% and 69% respectively. The EBV-$tetramer^{+}$ population in the secondary TILs also exhibited higher expression of TIGIT in both the T_{RM}^{-} (median = 53%) and T_{RM}^{+} (median = 42%) populations compared to the $tetramer^{-}$ compartments (median = 31% and 25% respectively; $p = 0.045$ and $p = 0.045$ respectively). CMV-$tetramer^{+}$ populations showed a wide range of TIGIT expression in the T_{RM}^{-} (12 - 81%) and T_{RM}^{+} populations (0 – 75%).

Interestingly, both LAG3 and TIM3 displayed a significant increase on the CMV-$tetramer^{+}$ T-cells in the T_{RM}^{+} compartment (median = 8% and 27% respectively) in comparison to the T_{RM}^{-} compartment (median = 0.5% and 5% respectively) in the secondary TILs ($p = 0.0061$ and $p = 0.0001$ respectively). They also displayed an upregulation of both markers in comparison to the $tetramer^{-}$ population (LAG3 $p = 0.0061$ and TIM3 $p = 0.0004$).

Together these data show that expression of several checkpoint proteins is upregulated on virus-specific T_{RM}^{+} populations. This may indicate development of a potential 'exhausted' phenotype in this setting, but confirmation of this status would require functional assessment.

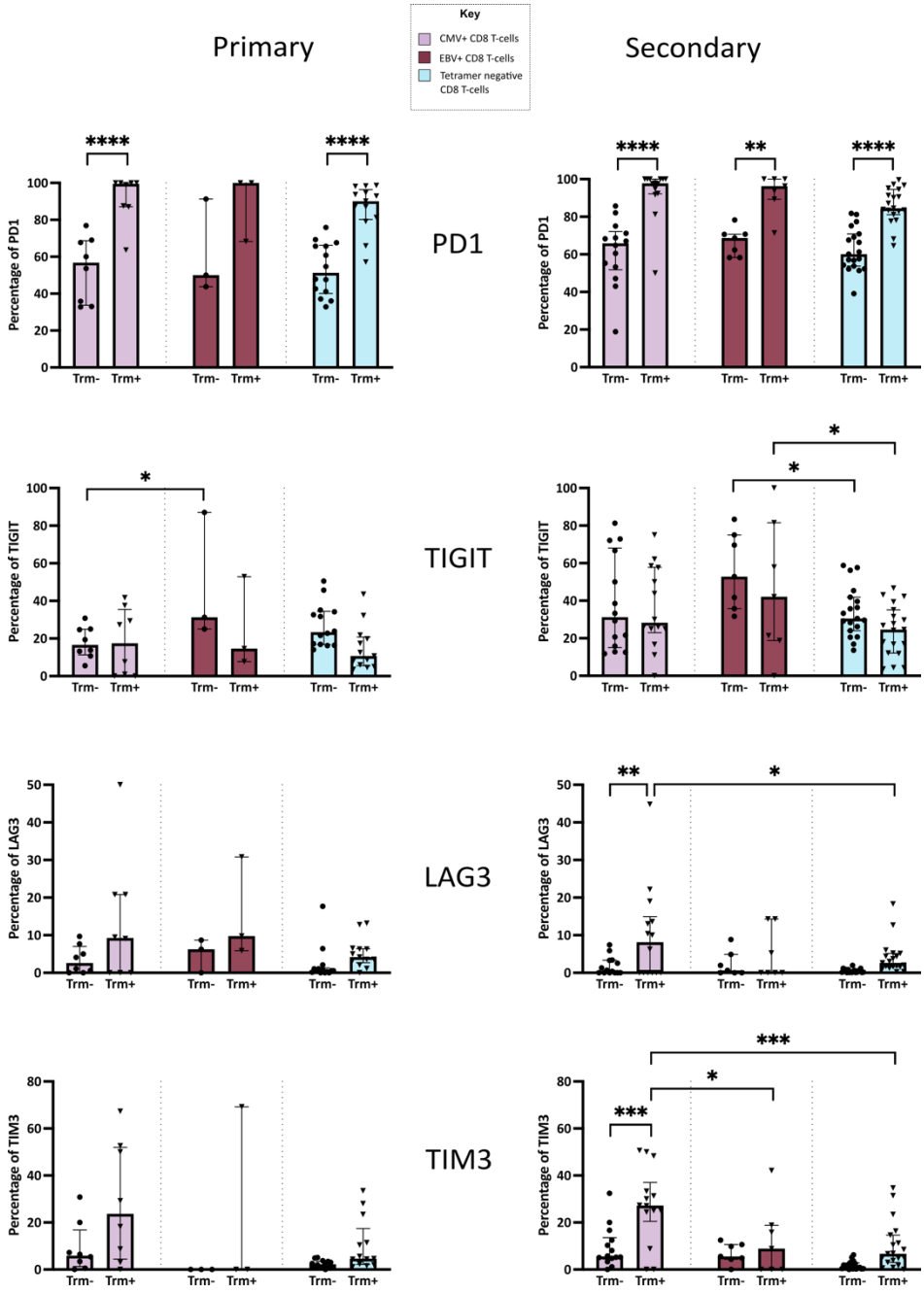

Figure 61: Checkpoint expression on the T_{RM}^{+} and T_{RM}^{-} populations.

Summary of the percentage of PD1, TIGIT, LAG3 and TIM3 on the CMV-tetramer^{+}, EBV-tetramer^{+} and tetramer^{-} T_{RM}^{+} and T_{RM}^{-} populations in the primary and secondary TILs. Each dot indicates data from one donor. Bars represent the percentage median of each checkpoint (± interquartile range). Statistical analysis performed with two-way ANOVA with main effects only with Tukey's multiple comparisons test with * p <0.05; ** p <0.01; *** p <0.001; **** p <0.0001.

4.2.10 $PD1_{HIGH}$ T-cells

Given that the high-dimensional data had revealed differences in PD1 distribution between PBMC and TIL, and density plots had shown particularly strong PD1 expression in TILs, I next decided to analyse expression of PD1 in greater detail. In particular, I was interested to assess co-expression of additional surface proteins in combination with PD1.

Interestingly, analysis of dot plot representation of PD1 expression revealed a $PD1_{HIGH}$ population present in TIL that is not present in PBMC (Figure 62a). On the basis of this, I next categorised cells into $PD1_{MID,}$ $PD1_{HIGH}$ or $PD1_{NEG}$ subgroups. Virus-specific tetramer^{+} cells were overlaid on to this analysis (Figure 62b).

$PD1_{MID}$ and $PD1_{HIGH}$ cells were overrepresented in tissue and as such the $PD1_{NEG}$ proportion was somewhat increased within PBMC (Figure 62c). $PD1_{MID}$ population distributions were broadly equivalent but $PD1_{HIGH}$ populations were seen almost exclusively within TIL populations. Indeed, $PD1_{HIGH}$ CMV-tetramer^{+} CD8 cells increase between the PBMC and primary TIL populations ($p = 0.0092$). Whilst not significant the median also increases from the PBMC (0.09%) to the secondary TILs (12%) ($p = 0.22$).

a)

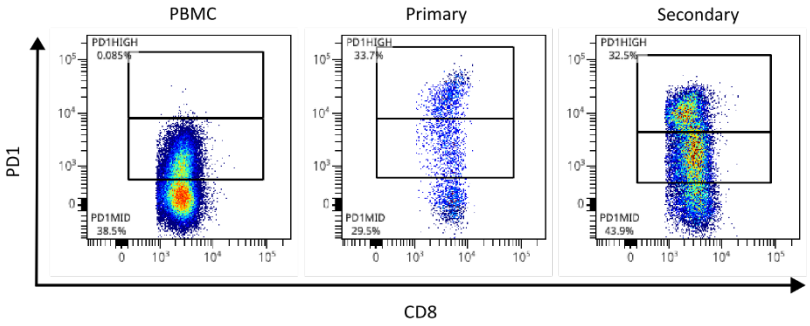
PBMC
Primary
Secondary
PD1HIGH
0.085%
33.7%
32.5%
PD1MID
38.5%
29.5%
43.9%
PD1
CD8

b)

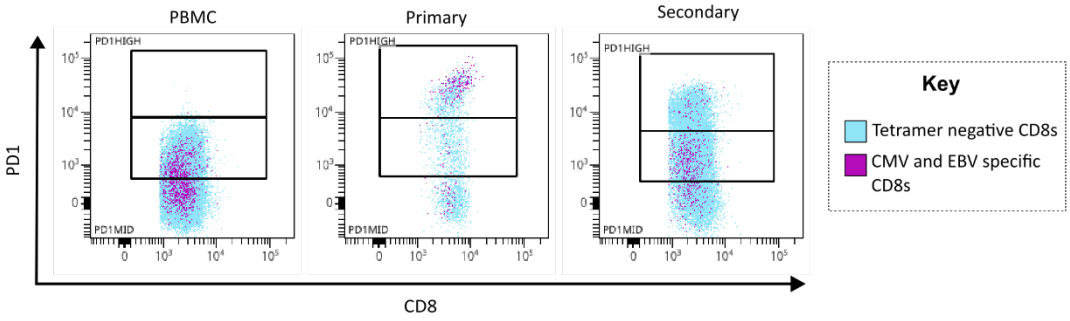
PBMC
Primary
Secondary
PD1HIGH
PD1MID
PD1
CD8
Key
Tetramer negative CD8s
CMV and EBV specific CD8s

c)

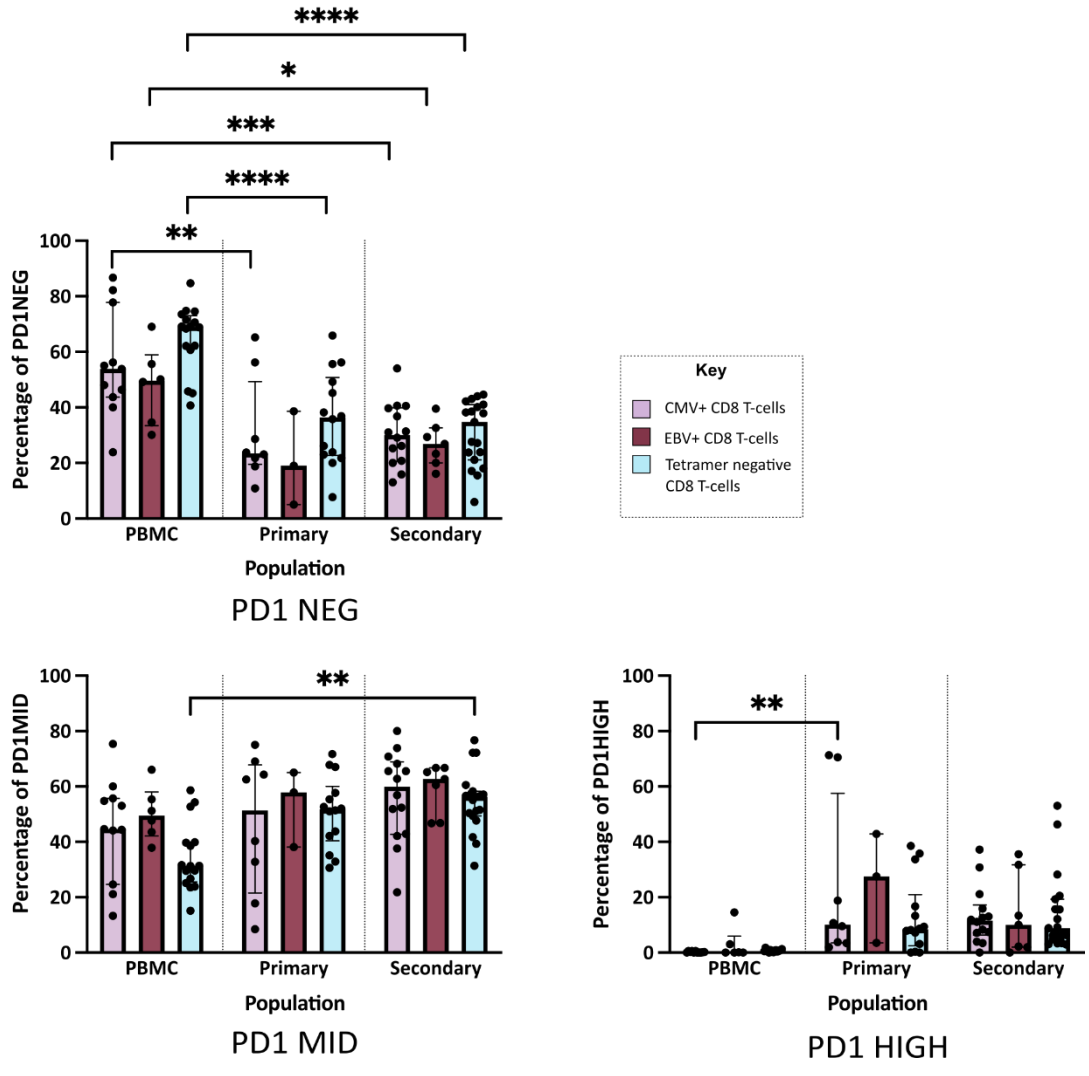
****
*
***
****
**
Percentage of PD1NEG
PBMC
Primary
Secondary
Population
Key
CMV+ CD8 T-cells
EBV+ CD8 T-cells
Tetramer negative CD8 T-cells
PD1 NEG
Percentage of PD1MID
PD1 MID
Percentage of PD1HIGH
PD1 HIGH

Figure 62: PD1high CD8$^+$ T-cell populations are present in TIL but not PBMC

a) Representative dot plots showing the gating of the $PD1_{MID}$ and $PD1_{HIGH}$ populations across the PBMC, primary and secondary TILs. A NOT gate was used to identify remaining cells and classify them as $PD1_{NEG}$. The $PD1_{HIGH}$ population only present in the TIL samples.

b) Summary of the percentage of $PD1_{NEG}$, $PD1_{MID}$ and $PD1_{HIGH}$ populations on the CMV-tetramer$^+$, EBV-tetramer$^+$ and tetramer$^-$ populations within the PBMC, primary and secondary TILs. Each dot indicates data from one donor. Bars represent the percentage median of each checkpoint (± interquartile range). Statistical analysis performed with two-way ANOVA with main effects only with Tukey's multiple comparisons test with * p <0.05; ** p <0.01; *** p <0.001; **** p <0.0001.

To further analyse these cells, the expression of other checkpoints on the $PD1_{NEG}$, $PD1_{MID}$ and $PD1_{HIGH}$ cells was investigated. In particular, the aim here was to assess how PD1 expression correlated with markers of T-cell activation or exhaustion (Figure 63).

Interestingly, TIGIT showed no significant changes between the $PD1_{MID}$ and $PD1_{HIGH}$ populations in either the primary or secondary tissue. It did show that there was significantly more TIGIT expressed on the EBV-tetramer$^+$ cells than the tetramer$^-$ cells in both the $PD1_{MID}$ ($p = 0.0009$) and $PD1_{HIGH}$ ($p = 0.0145$) populations in the secondary tissue.

On the other hand, both LAG3 and TIM3 exhibited significant increases on the CMV-tetramer$^+$ populations in the secondary tissue between the $PD1_{MID}$ (median = 0.1% and 10% respectively) and $PD1_{HIGH}$ populations (median = 8% and 29% respectively; $p = 0.0013$ and $p = 0.0002$ respectively). Both checkpoints also increased significantly from the $PD1_{NEG}$ to $PD1_{HIGH}$ TILs in both the primary and secondary tissue but not between the $PD1_{NEG}$ and $PD1_{MID}$ TILs, indicating increased expression in the $PD1_{HIGH}$ TILs in all populations. Furthermore, the CMV-tetramer$^+$ cells in the $PD1_{HIGH}$ compartment exhibited significantly more LAG3 and TIM3 compared to the tetramer$^-$ cells in the primary ($p = 0.0132$ and $p = 0.0287$ respectively) and secondary ($p =$

0.0006 and p = 0.0109 respectively) tissue. This data indicated a more exhausted phenotype for the CMV-tetramer^{+} cells in particular which were displaying upregulation of various checkpoints alongside high expression of PD1. A summary of the checkpoint medians can be found in Table 24.

Table 24: Summary of median checkpoint expression percentage from the $PD1_{MID}$ and $PD1_{HIGH}$ populations

Summary of the median checkpoint expression percentage from the different PD1 populations in the CMV-specific, EBV-specific and tetramer- cells in the primary and secondary tissue. Comparisons that were significantly increased from the $PD1_{NEG}$ population (not shown) have been indicated with * p <0.05; ** p <0.01; *** p <0.001; **** p <0.0001

Category	Population	Population	TIGIT	TIM3	LAG3
Primary	CMV^{+}	$PD1_{MID}$	16.7	12.7	0.2
		$PD1_{HIGH}$	30.4	34.8***	16.6***
	EBV^{+}	$PD1_{MID}$	37.5	0	10
		$PD1_{HIGH}$	0.0	0	20*
	$Tetramer^{-}$	$PD1_{MID}$	21.9	3.2	2
		$PD1_{HIGH}$	12.7	17.5	4.6
Secondary	CMV^{+}	$PD1_{MID}$	38.5*	9.7	0.1
		$PD1_{HIGH}$	40.8*	29.1****	17.9****
	EBV^{+}	$PD1_{MID}$	58.6	9.1	2.4
		$PD1_{HIGH}$	63.6	14.3	0
	$Tetramer^{-}$	$PD1_{MID}$	30.9	1.4	0.4
		$PD1_{HIGH}$	37.2	6.4**	2.3

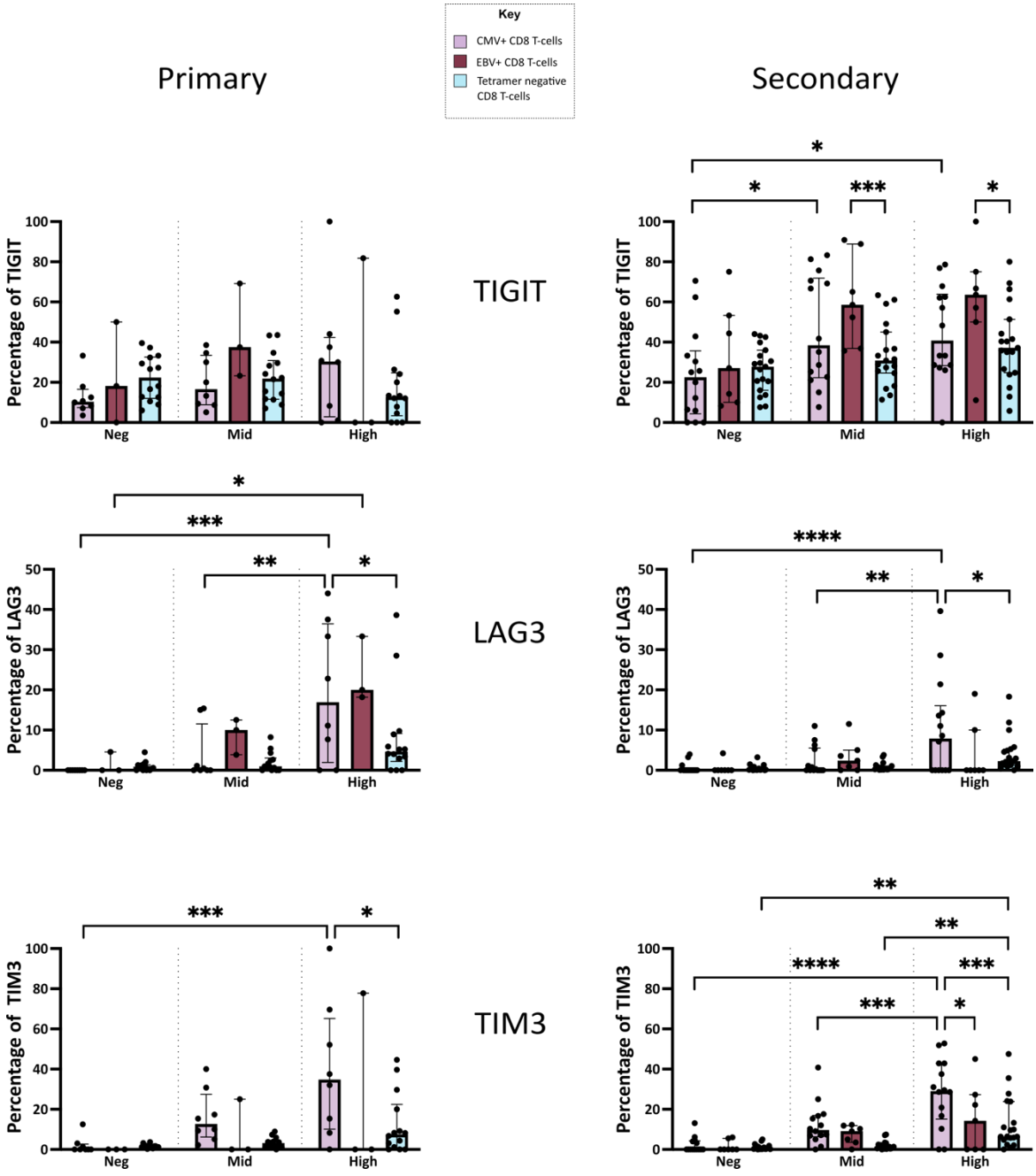

Figure 63: Summary of checkpoint expression on $PD1_{NEG}$, $PD1_{MID}$ and $PD1_{HIGH}$ cells

Summary of the percentage of checkpoints on $PD1_{NEG,}$ $PD1_{MID}$ and $PD1_{HIGH}$ populations on the CMV-tetramer^{+}, EBV-tetramer^{+} and tetramer^{-} populations in the primary and secondary TILs. Each dot indicates data from one donor. Bars represent the percentage median of each checkpoint (± interquartile range). Statistical analysis performed with two-way ANOVA with main effects only with Tukey's multiple comparisons test with * p <0.05; ** p <0.01; *** p <0.001; **** p <0.0001.

In order to identify potential determinants of the increased expression of checkpoint proteins on the $PD1_{HIGH}$ population I next assessed the relative expression of markers of activation or potential exhaustion. In particular, I determined the pattern of co-expression of CD38 and HLA-DR in order to assess activation status, whilst expression of the ectoenzyme CD39 was used to indicate potential exhaustion. The relative expression of these markers was analysed on the $PD1_{NEG,}$ $PD1_{MID}$ and $PD1_{HIGH}$ populations in the TIL samples (Figure 64).

Interestingly, CMV-tetramer$^+$ $CD8^+$ T-cells exhibited an increase in both HLA-DR/CD38 co-expression and CD39 expression in the $PD1_{HIGH}$ compartment (HLA-DR/CD38 primary TIL median 30%, secondary TIL 29%; CD39 primary TIL 79%, secondary TIL 85%) (Figure 64b).

There is no difference in HLA-DR^+CD38^+ expression in the tetramer$^-$ subset, however in the primary tissue there is an increase in the CMV-tetramer$^+$ population between the $PD1_{NEG}$ (median = 1.1%) and $PD1_{HIGH}$ (median = 29.6%) p = 0.0008) and also between the $PD1_{MID}$ (median = 3.1%) and $PD1_{HIGH}$ populations (median = 29.6%; p = 0.0012). There is also an increase in the EBV-tetramer$^+$ population between $PD1_{NEG}$ and $PD1_{HIGH}$ (p = 0.0259) confirming that $CD8^+$ T-cells specific for both viruses were increased in the $PD1_{HIGH}$ population. The same trends were seen with CMV-tetramer$^+$ T-cells in the secondary tissue. Both the CMV-tetramer$^+$ and EBV-tetramer$^+$ cells displayed an upregulation of HLA-DR / CD38 in the $PD1_{HIGH}$ population (median = 29.6% and 45.5% respectively) compared to the tetramer$^-$ cells (median = 10.1%; p = 0.0295 and p = 0.0205 respectively). This data indicates that high levels of PD1 expression on virus specific T-cells associate with recent activation.

In the secondary tissue, there was also a very substantial increase in CD39 expression on the CMV-tetramer$^+$ $PD1_{HIGH}$ cells (median = 85%) in comparison to the $PD1_{NEG}$ (median = 62%; p =

0.0055) and the $PD1_{MID}$ populations (median = 62%; p = 0.0368). Again, both the CMV-tetramer^{+} and EBV-tetramer^{+} cells displayed an upregulation of CD39 in the $PD1_{HIGH}$ population compared to the tetramer^{-} cells (p = 0.0012 and p = 0.0187 respectively). As CD39 is often associated with decreased function of T-cells this could potentially indicate some degree of immune exhaustion of cells within tissue.

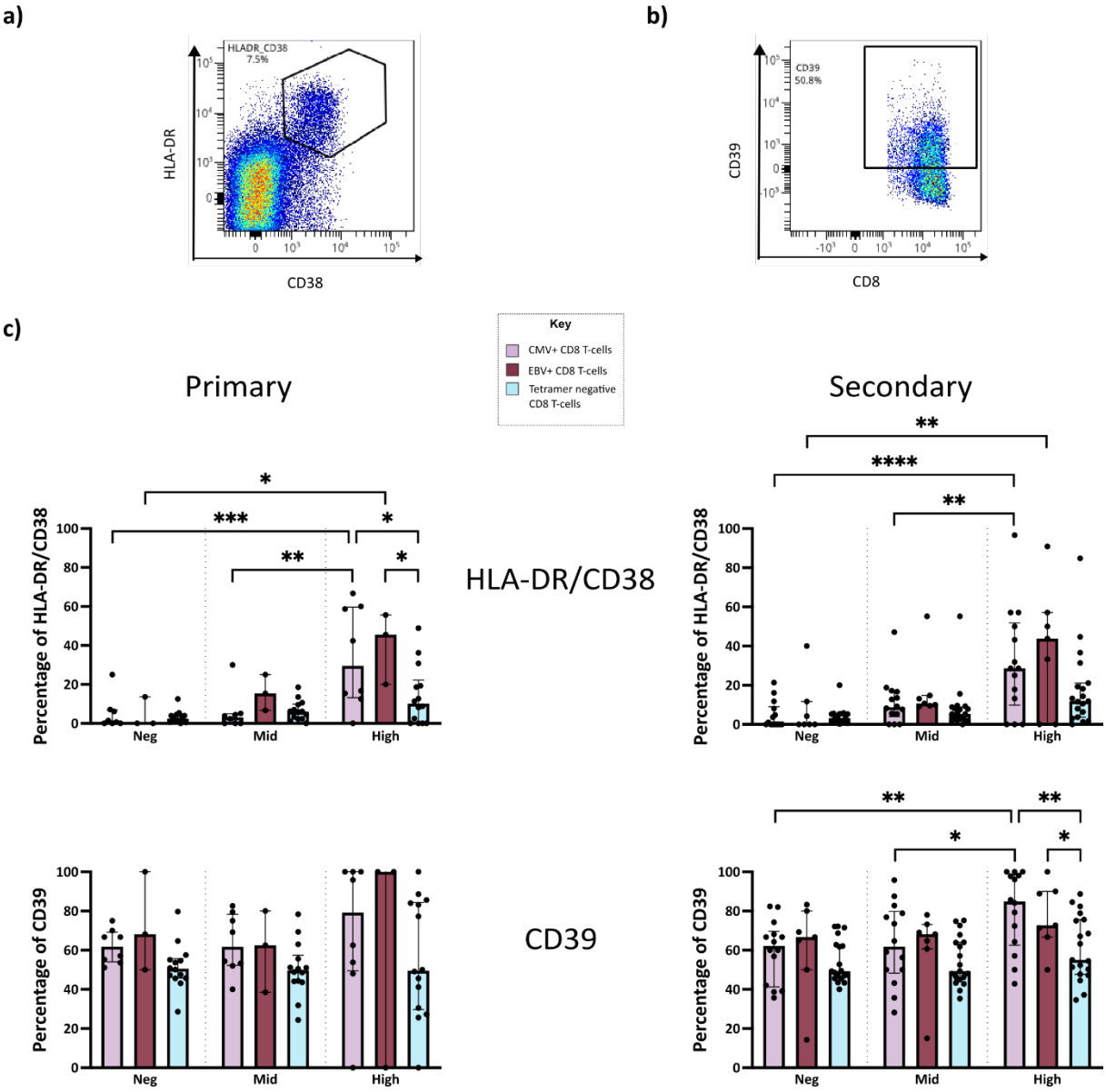

Figure 64: HLA-DR/CD38 co-expression and CD39 expression

- **a)** Representative gating example of dual positive HLA-DR and CD38 cells on the $CD8^+$ population indicating activated cells
- **b)** Representative gating example of $CD39^+$ cells on the $CD8^+$ population
- **c)** Summary of the percentage of HLA-DR/CD38 and CD39 expression on $PD1_{NEG}$, $PD1_{MID}$ and $PD1_{HIGH}$ populations on the CMV-tetramer$^+$, EBV-tetramer$^+$ and tetramer$^-$ populations in the primary and secondary TILs. Each dot indicates data from one donor. Bars represent the percentage median of each checkpoint (± interquartile range). Statistical analysis performed with two-way ANOVA with main effects only with Tukey's multiple comparisons test with * p <0.05; ** p <0.01; *** p <0.001; **** p <0.0001.

As CD39 has also been shown to be a marker of activated T_{RM} cells (Talhouni et al., 2023), further analysis was undertaken on the level of PD1 expression on the T_{RM} populations. As previous data had shown that almost all T_{RM} cells expressed some degree of PD1 (Figure 61) only the $PD1_{MID}$ and $PD1_{HIGH}$ populations were included in the analysis (Figure 65). Boolean gating was used to discriminate the $T_{RM}^{+/-}$ populations before application of the $PD1_{MID}$ and $PD1_{HIGH}$ gates.

Interestingly, whilst no difference was seen in the percentage of cells expressing medium levels of PD1 between the T_{RM}^{-} and T_{RM}^{+} populations, a substantial difference was seen in relation to the distribution of $PD1_{HIGH}$ cells.

Indeed, very few CMV-tetramer^{+} and EBV-tetramer^{+} T_{RM}^{-} cells expressed a $PD1_{HIGH}$ phenotype (median of CMV-tetramer^{+}, EBV-tetramer^{+} and tetramer^{-} in the primary TILs: 3.3% 0% and 3.1% respectively; and in the secondary TILs 3.3%, 3.9% and 4.6% respectively), indicating that the $PD1^{HIGH}$ population was being driven almost exclusively by T_{RM}^{+} cells. There was a wide range in the percentage of T_{RM}^{+} cells expressing $PD1_{HIGH}$ in the primary (0 – 96.7%) and the secondary (0 – 84.4%) tissues. Both the primary and secondary tissues exhibited significant increases in the percentage of cells exhibiting a $PD1_{HIGH}$ phenotype ($p = 0.0081$ and $p < 0.0001$ respectively). In the tetramer^{-} compartment of the secondary tissue there was also a significant increase between the T_{RM}^{-} and T_{RM}^{+} populations ($p = 0.001$), whilst this was trending in the primary tissue it was not statistically significant ($p = 0.2246$).

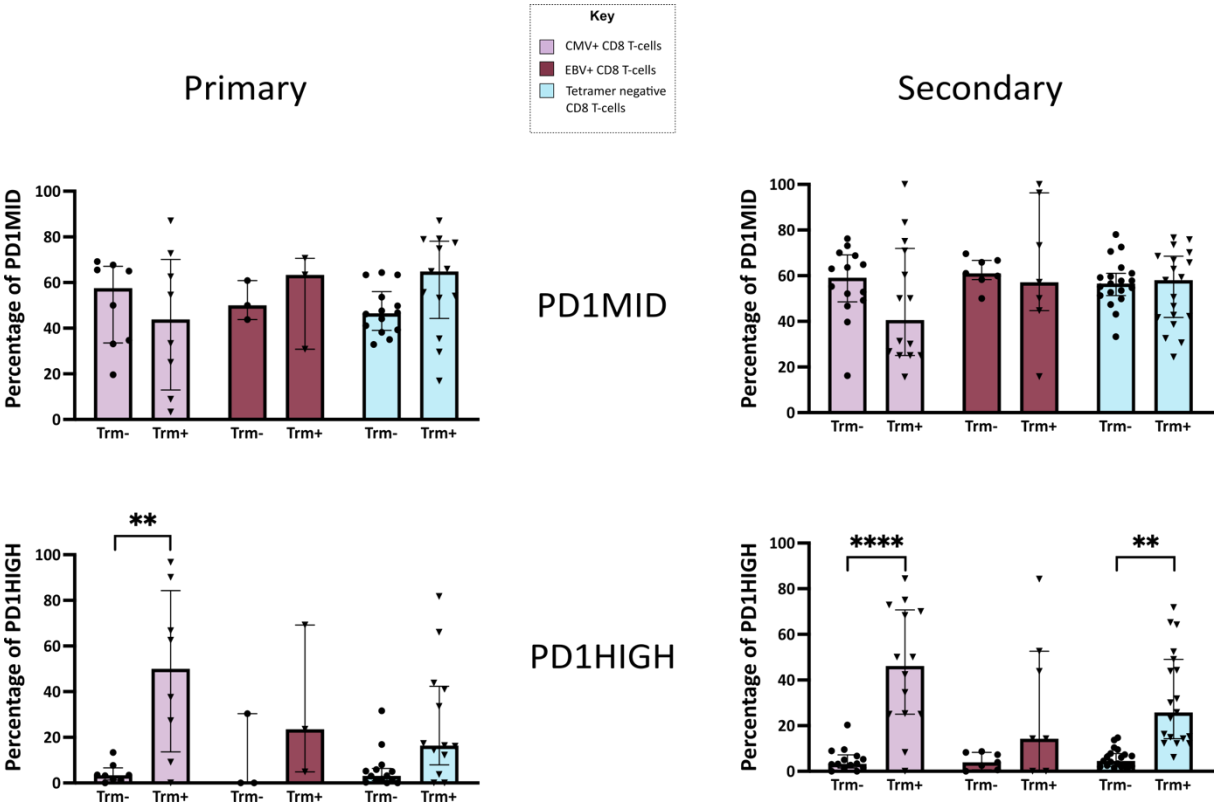

Figure 65: The expression levels of PD1 on T_{RM} cells

Summary of the percentage of T_{RM}^{+} and T_{RM}^{-} cells expressing medium (PD1MID) and high (PD1HIGH) levels of PD1 on the CMV-tetramer^{+}, EBV-tetramer^{+} and tetramer^{-} populations in the primary and secondary TILs. Boolean gating was used to discriminate the $T_{RM}^{+/-}$ populations before application of the $PD1_{MID}$ and $PD1_{HIGH}$ gates. Each dot indicates data from one donor. Bars represent the percentage median of each checkpoint (± interquartile range). Statistical analysis performed with two-way ANOVA with main effects only with Tukey's multiple comparisons test with * p <0.05; ** p <0.01; *** p <0.001; **** p <0.0001.

Given this data, further analysis was undertaken into the features of the T_{RM}^{+} clusters 3, 4, 7 and 8 in order to evaluate a more detailed phenotype.

Clusters 3, 4, 7, and 8 were isolated from the heatmap shown in Figure 53a which had shown the expression levels of the different cell surface proteins in the different clusters (Figure 66a). This showed that all populations show high expression of PD1 ($PD1_{HIGH}$ phenotype). Furthermore, all show a predominant T_{EM} phenotype. The heatmap and UMAPs were next explored to further phenotype these cells.

Clusters 4 and 3 were of particular interest as these had the most intense expression of PD1. Interestingly, CMV-tetramer^{+} T-cells are focussed within these two clusters. Cluster 3 also co-expresses TIGIT, LAG3, TIM3, HLA-DR, CD38 and CD39. Together this data indicates that these cells may be more activated rather than exhausted. Cluster 4 is similar except that TIGIT expression is much lower, comparable with Figure 63 which show that the percentage of cells expressing TIGIT varies widely amongst donors and is not particularly increased in $PD1_{HIGH\ cells}$. Another very marked feature was that expression of HLA-DR and CCR5 was differential between clusters 3 and 4. In particular, HLA-DR staining was very intense on cluster 3 whilst CCR5 was found at high levels on cluster 4.

a)

CD103	CD69	PD1	PE-Tetramer	APC-Tetramer	TIGIT	LAG3	TIM3	HLA-DR	CD38	CD39	CCR7	CD45RA	CD95	CD27	CCR5	CXCR5	GITR	
4.23	3.42	4.06	1.59	0.79	0.21	1.36	0.6	3.08	2.83	1.51	-0.03	-0.04	0.65	1.1	0.99	0.76	0.31	Cluster 03
4.12	3.93	2.03	0.68	0.08	-0.4	1.21	0.39	0.05	3.28	1.62	-0.69	0.48	0.72	0.55	1.22	0.51	0.14	Cluster 07
3.37	2.87	2.39	0.66	0.11	0.2	0.75	0.13	1	0.98	-0.23	0.86	0.54	0.16	0.52	1.55	0.61	0.16	Cluster 08
4.36	4.09	3.43	1.41	0.25	-0.26	1.32	0.41	1.11	2.74	-0.85	-0.59	0.25	-0.58	0.91	2.4	0.99	0.03	Cluster 04

b)

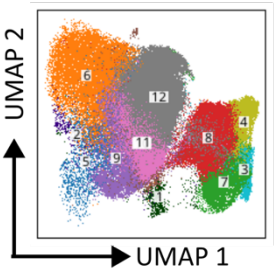

c) CMV Tetramer

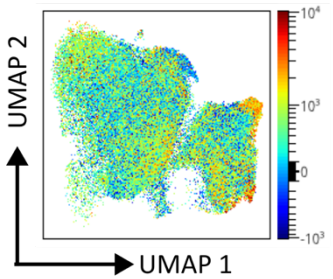

d)

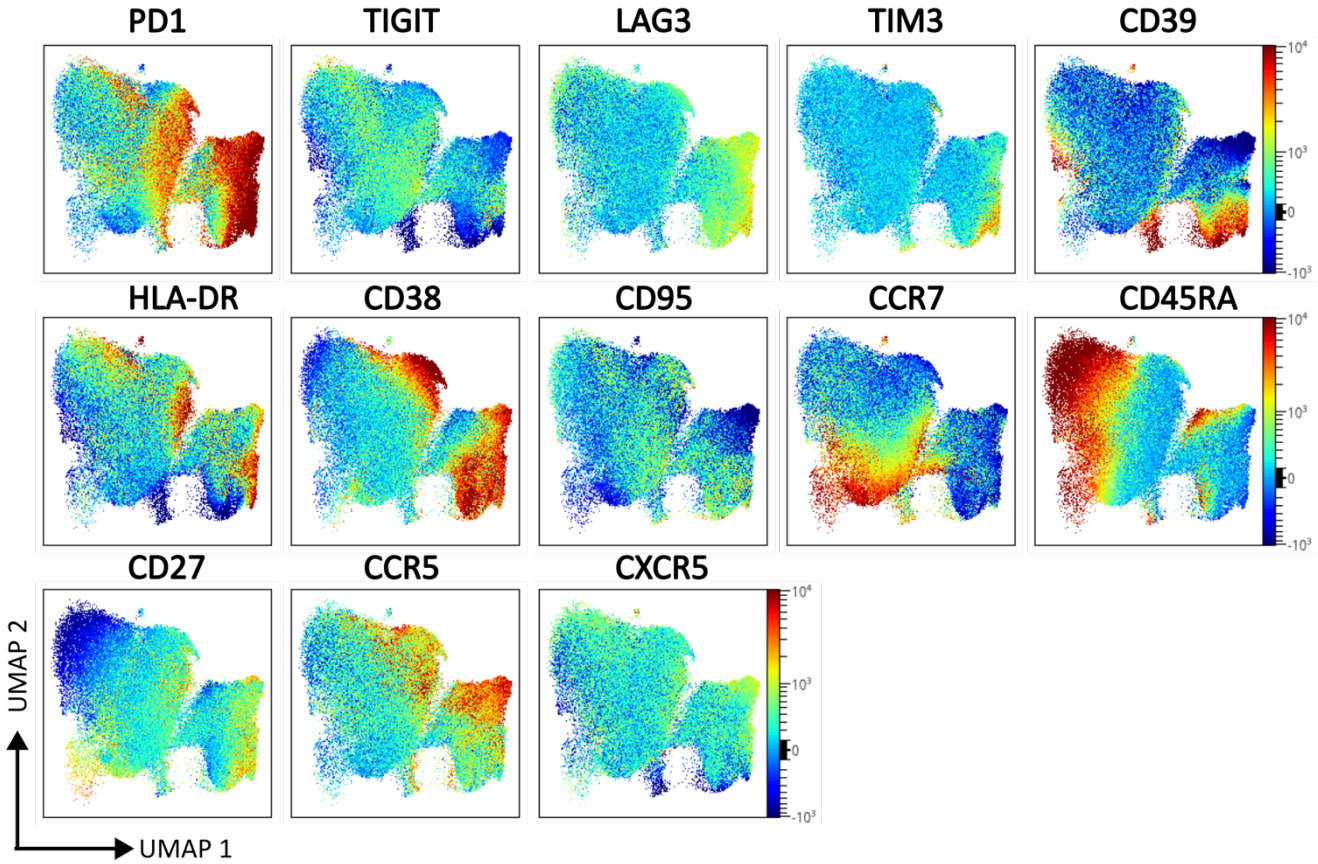

Figure 66: In depth evaluation of other phenotypic characteristics of the T_{RM}^+ populations

a) Heatmap extract taken from the heatmap in Figure 53 showing the expression of markers on the T_{RM}^+ clusters 3, 4, 7 and 8. The shade of colour corresponds to the cell value with a darker shade indicating higher expression. The cell values for each marker are median ArcSinH values and are scaled individually to allow relative comparison between each cluster.

b) UMAPs showing the concatenated TIL samples (n=33) with the 12 identified clusters overlaid.

c) UMAP plots showing the location of the CMV-tetramer$^+$ cells within the clusters (n=33). As per the colour bar, dark red indicates higher expression with dark blue indicating no expression.

d) UMAP plots showing the expression of markers across the concatenated TIL samples (n=33). As per the colour bar, dark red indicates higher expression with dark blue indicating no expression.

Some degree of PD1 expression was also seen in cluster 12 and this is likely to represent the previously identified $PD1_{MID}$ population. This is supported by the UMAPs in Figure 66d that show that these cells do not display co-expression of the other checkpoints and show little to no expression of CD39. HLA-DR and CCL5 are expressed on many cells within the subset and, somewhat unlike the $PD1_{HIGH}$ population, these are often co-expressed. CD38. Some of these cells also express CCR7 suggesting a potential T_{CM} phenotype, supported by the mid-range expression of CD95.

4.3 Discussion

Infiltrating $CD8^+$ T-cells are central to the immune response within tumours. Indeed, the presence of TIL within epithelial ovarian cancer (EOC) has linked to improved patient outcome in several studies. In a pivotal study from 2003 Zhang *et al.* analysed 186 EOC tissue samples and found that patients with $CD3^+$ TILs had a survival rate of 38% compared to just 4.5% in those with no detectable TILs (Zhang et al., 2003) whilst $CD4^+$ and $CD8^+$ TILs have also been shown as a positive correlate (Colombo et al., 2023).

However, a key question in relation to these data relates to the antigenic specificity of this T-cell infiltrate. In cancers, $CD8^+$ T-cells can recognise tumour-associated antigens (TAAs) and neoantigens. However, virus-specific T-cells, such as those targeting CMV, EBV and influenza, have also been identified within the TME of certain malignancies (Simoni et al., 2018). It is currently uncertain if these cells are simply transiting from the blood and play no functional role within tissue or if they play an active role in suppressing local viral replication. As such, a comprehensive analysis of the phenotype and function of viral-specific TILs is crucial for advancing our understanding of the immune landscape of cancers. If these T-cells are functional then there remains a potential for their activity to be 're-directed' against tumour targets whilst a 'bystander' effect in suppressing tumour growth is also possible. As such, this information could be of value in the design of novel therapeutic strategies.

4.3.1 CMV and EBV-tetramer positive T-cells are present in ovarian tumour tissue

The use of MHC tetramers has revolutionised the study of antigen-specific T-cells by enabling the direct detection and detailed phenotypic analysis of T-cell populations. Using these reagents I identified CMV-specific and EBV-specific T-cells within primary or secondary sections of tumour in patients with a variety of subtypes of ovarian cancer. This allowed me to assess their relative prevalence and phenotype at these sites.

The presence of virus-specific T-cells in tumours raises important questions regarding their role. In particular they could be merely circulating through the tumour or be actively attracted and retained within the TME, possibly responding to bystander inflammation or viral antigen presentation from cells within the TME, potentially even including tumour cells.

Whilst several studies have assessed the potential presence of CMV within tumour tissue, specifically aiming to identify viral nucleic acid or proteins, (Mitchell et al., 2008, Batich et al., 2017) little such research has been carried out in ovarian tumours. Furthermore, reports to date have been contradictory in relation to interpretation. Shanmughapriya *et al.* reported that the CMV gene glycoprotein B could be detected in 50% of epithelial ovarian cancer patients (Carlson et al., 2018, Shanmughapriya et al., 2012). This is supported by Carlson *et al.* who detected the CMV proteins IE1 and pp65 in 8/10 and 4/10 ovarian carcinoma patients respectively by immunohistochemistry and *in situ* hybridization (Carlson et al., 2018). This group also observed the presence of CMV DNA in 100% of patients although the sample size was only 3 (Carlson et al., 2018). Conversely, a large 2019 study using RT-PCR detected CMV DNA in only 1/191 (0.5%) of patients with epithelial ovarian carcinoma. In contrast, EBV DNA was detected in 10/191 (5.2%) of patients (Ingerslev et al., 2019). A further study using nested

PCR, a method which increases sensitivity and specificity, detected CMV in 19/27 (70.4%) of ovarian cancer samples, however when assessed with RT-PCR, this fell to 2/27 (7.4%) (Paradowska et al., 2019). If CMV infection is low-grade, and therefore only detectable by employing sensitive techniques, this might suggest why studies utilising standard PCR and RT-PCR observe a low prevalence of CMV-infection.

4.3.2 Virus-specific $CD8^+$ T-cells display an activated phenotype within ovarian cancer tissue

To provide further insight into why virus-specific T-cells may be present within the TME I undertook a detailed study of the activation status and phenotype of these populations.

Firstly, the memory phenotype of $CD8^+$ T-cells was defined by distribution within the naïve, central memory, effector memory and EMRA subsets. Viral-specific T-cells in the tumours exhibited an enriched T_{EM} phenotype with 67% and 46% of CMV-specific T-cells in the primary and secondary tissues respectively exhibiting this phenotype, with corresponding values of 68% and 67% for EBV-specific T-cells. This profile was in marked contrast to a T_{EMRA} biased phenotype in the PBMC (Figure 48). This T_{EM} phenotype could represent local activation by viral antigen, although the inflammatory microenvironment and local release of cytokines may also lead to antigen-independent immune cell activation. Substantial proportions of CMV-specific T_{EM} cells have previously been observed in non-malignant tissue (Pardieck et al., 2018).

An additional notable feature was that CMV-tetramer$^+$ T-cells demonstrated considerable expression of checkpoint proteins PD1 (Figure 50), LAG3 and TIM3 (Figure 51) and that this profile varied between the cells in PBMC and those in the primary tissue.

PD1 expression was increased on all of the three sub-populations of CD8+ T-cells that I studied within TILs: CMV-tetramer$^+$, EBV-tetramer$^+$ and tetramer-negative populations. As previously discussed, PD1 is a marker of recent T-cell activation but in the setting of chronic antigen expression, and in association with co-expression of other checkpoint proteins, it can be a hallmark of T-cell exhaustion (He and Xu, 2020).

The activated phenotype of CMV-tetramer$^+$ and EBV-tetramer$^+$ T-cells within the TME could be attributed to several factors. One possibility is that tumour cells present viral epitopes through MHC molecules, leading to direct activation of virus-specific T-cells via TCR recognition. Alternatively, the inflammatory TME might induce T-cell activation independently of TCR stimulation. Indeed, factors such as pro-inflammatory cytokines, hypoxia, or stress signals in the TME might drive this 'bystander activation' without direct antigen engagement. Membrane markers that distinguish between antigen-specific and bystander activation are this of considerable interest and CD39 is of interest in this regard (Whiteside et al., 2018).

4.3.3 A population of viral-specific T-cells display a Tissue Resident Memory phenotype

Virus-specific cells could potentially be found within tumour biopsies due either to transient flow through the vascular system or presence within the tissue resident lymphoid population. CD8$^+$ T_{RM} T-cells are vital for pathogen control, including viral infections, and persist in peripheral tissues over long periods of time (Topham and Reilly, 2018). Co-expression of the CD103 and CD69 proteins is used to define T_{RM} cells and as such I was able to use this to determine the presence of virus-specific cells within this compartment. CD69, an early activation marker, is upregulated in T_{RM} precursors as they migrate into peripheral tissue,

where it engages with sphingosine-1-phosphate receptor-1, inhibiting T-cell egress and ensuring tissue retention (Mackay et al., 2013, Mackay et al., 2015). CD103, an integrin, plays a role in tethering T-cells to epithelial cells, further promoting their retention in the tissue environment (Szabo et al., 2019).

The majority of virus-specific T-cells were seen to display a T_{RM}^- phenotype but substantial populations of T_{RM}^+ cells were also observed. T_{RM} cells are known to play an important role in viral immunity and are poised to support the control of localised infections. For instance, a murine model of cutaneous infection with herpes simplex virus (HSV) showed that virus-specific T_{RM} cells were elicited at the site of infection where their persistence supported protection against local HSV challenge (Gebhardt et al., 2009). Furthermore, a study into murine CMV (MCMV) found that T_{RM} cells in the salivary gland contribute to local control (Thom et al., 2015).

Interestingly, whilst local antigen stimulation has been shown to be necessary for the formation of $CD4^+$ T_{RM} cells, it is postulated that $CD8^+$ T_{RM} cells can migrate to tissue and upregulate markers of residency. This pool of T_{RM} cells is then replenished by circulating T_{EM} cells (Thom et al., 2015, Zheng and Wakim, 2022).

4.3.4 $PD1_{HIGH}$ cells display an exhausted phenotype

My findings further demonstrated that T_{RM} cells exhibit increased PD1 expression. As an inhibitory receptor, this upregulation of PD1 might be expected to lead to functional impairment following engagement with PDL1 and PDL2 within the TME. It was also noteworthy that these $PD1_{HIGH}$ populations, which are almost exclusively a T_{RM} phenotype, express high levels of additional checkpoint proteins such as TIGIT, LAG3 and TIM3. The co-

expression of these proteins on TILs has been associated with poor clinical outcome in cancer patients and is ascribed to T-cell exhaustion (Saleh et al., 2020, Chen and Li, 2023). To further support this potential phenotype, the data in Figure 64 demonstrates that several $PD1_{HIGH}$ populations, in particular the CMV-tetramer^{+} population, display upregulation of the exhaustion marker CD39. CD39 is an ectoenzyme which leads to the production of an immunosuppressive form of adenosine and prior literature indicates that CD39^{+} TILs exhibit features of functional exhaustion, such as impaired cytokine production and proliferation (Gupta et al., 2015, Canale et al., 2018, Timperi and Barnaba, 2021). This is supported by findings from this study, which reveal that a $PD1_{HIGH}$ TIL population in ovarian tumour tissue displays upregulation of CD39, alongside other inhibitory checkpoints indicating an exhausted phenotype. Whilst CD39 has been well-documented as marker of exhaustion in circulating HCV and HIV-specific T-cells, CMV and EBV-specific T-cells have generally been observed to remain CD39 negative (Gupta et al., 2015). CD39 has been shown to act as a marker of tumour reactivity in patients with lung and colorectal cancer and variation in expression between patients has been related to factors such as tumour mutational status (Simoni et al., 2018). However, in murine models, CMV-specific T-cells have been shown to upregulate CD39 even in the absence of antigen stimulation. This suggests that CD39 expression may be more closely associated with tissue localisation rather than being strictly a marker of functional exhaustion due to chronic antigen exposure (Smith and Snyder, 2021).

$PD1_{MID}$ populations exhibited lower expression of additional inhibitory checkpoints compared to the $PD1_{HIGH}$ population, as well as reduced CD39 expression. This observation suggests that the $PD1_{MID}$ cells may reflect a more activated and less exhausted phenotype relative to their $PD1_{HIGH}$ counterparts. This differential expression supports the notion that PD1 levels on T-

cells may distinguish between exhaustion and activation states and is further supported by the high dimensional data in Figure 66 which highlights that the population of cells expressing a lower amount of PD1, are not as terminally differentiated as the $PD1_{HIGH}$ clusters. Indeed, these $PD1_{MID}$ cells display more of a T_{EM} and T_{CM} phenotype in comparison to the T_{EM} and T_{EMRA} phenotype of the $PD1_{HIGH}$ cells.

This data is important as it identifies two distinct populations of cells based on their PD1 expression and shows that viral-specific T-cells are also capable of expressing this varied phenotype.

The success of PD1 blockade in cancer treatment is thought to act primarily through re-engagement of functional activity in PD1-expressing TILs. However, even in tumours with a high frequency of PD1-positive T-cells, the patient responses to PD1 blockade can vary (Sharpe and Pauken, 2018, Wu et al., 2019). T-cells expressing a $PD1_{HIGH}$ phenotype could be considered deeply exhausted, and it may be that these cells have reduced ability to be reactivated.

In contrast, $PD1_{MID}$ cells may represent a less exhausted, more activated phenotype, retaining some capacity for effector functions. These cells could potentially be more responsive to PD1 blockade, and it could be these cells that papers show to regain cytotoxic activity and produce higher levels of key immune mediators such as IFN-γ and granzyme B after treatment (Kamphorst et al., 2017). If this is the case, it could be postulated that $PD1_{MID}$ cells, rather than $PD1_{HIGH}$ cells, could serve as a biomarker for a favourable response to PD1 therapy.

This is supported by Weiss *et al.* (2024), who observed that in mouse models, the level of PD1 expression can affect T-cell function and viral control. In samples that did not have a

population of high PD1 expression, they observed a significant reduction in the TOX marker, which is associated with exhaustion, along with a decrease in apoptosis and an increase in KLRG1, an effector marker. They also found that mice without the $PD1_{HIGH}$ population were able to control LCMV infection more effectively than wild-type mice, whereas PD1 knockout mice led to an increase in exhaustion via other mechanisms, such as an increase in CTLA4 (Weiss et al., 2024).

This detailed analysis can reveal insights into the immune landscape, particularly the activation or exhaustion status and potential responsiveness of these T-cells to immunotherapies. Understanding these phenotypic differences is crucial for developing targeted therapeutic strategies that could reinvigorate the immune response in cancer. An important step would be to analyse the response of viral-specific T-cells to checkpoint blockade in the tumour to see if the level of PD1 does affect the reinvigoration of the cells. Furthermore, as supported by Weiss *et al.,* epigenetic editing of the PD1 gene to exclude the $PD1_{HIGH}$ population could provide a promising strategy to inducing cells which are able to respond to PD1-blockade.

4.3.5 Harnessing viral specific T-cells for treatment

As this data showed, the most common phenotype of the virus-specific T-cells in the primary and secondary tissue were $PD1_{MID}$ and did not display markers of tissue retention. A study by Rosato *et al.* also demonstrated that CMV-specific and EBV-specific T-cells were able to infiltrate various solid tumours and retain the ability to recognise viral antigens. Importantly, they elucidated that the cells could be repurposed to target tumour antigen, offering a potential strategy to enhance tumour-specific immunotherapy. In support of this approach,

virus-specific T-cells were found within the tumour in all patients who had detectable virus-specific T-cells within PBMC (Rosato et al., 2019). Given that the percentage of CMV-specific T-cells in the blood can reach up to 10% for one tetramer alone, this presents an intriguing therapeutic avenue. Furthermore, as CMV-specific T-cell responses can increase with age, and ovarian cancer frequently affects older women, this may represent an approach to harness large populations of functional T-cells for effector response (Rosato et al., 2019, Nobuoka et al., 2013). Additionally, targeting virus-specific T-cells might synergize with checkpoint blockade by reducing exhaustion and restoring their cytotoxic activity, potentially increasing the efficacy of immunotherapies in ovarian cancer, a disease where traditional immunotherapy approaches like PD1 blockade have shown limited success.

4.3.6 Limitations

Tetramer staining can be affected by the digestion methods used to tissue preparation and a limitation is that the resolution of the tetramer^{+} populations by flow cytometry was not as optimal as in PBMC. One method is to use the protein kinase inhibitor dasatinib which inhibits TCR downregulation, thereby stabilising tetramer binding. This strategy maximises recovery of antigen specific T-cells, although it has been shown to primarily benefit MHC-II tetramer binding rather than MHC-I (Rius et al., 2018). Additionally, to improve the detection of rare T-cells, the use of MHC-dextramers or dodecamers can be used, which has been shown to enhance staining efficiency compared to conventional tetramers (Huang et al., 2016). Furthermore, the tetramer-specific response in this study is limited to available tetramers. Whilst the use of MHC-I tetramers presenting epitopes from three immunogenic proteins for CMV and five for EBV provides a broad analysis of the virus-specific T-cells however, this

approach could be expanded by including additional tetramers to cover a wider range of viral epitopes and proteins. By increasing the diversity of epitopes presented by the tetramers, the recovery of virus-specific T-cells would likely improve. It should also be highlighted that for this reason, there will be virus-specific T-cells within the tetramer$^-$ population of different specificities that have not been stained by the tetramers. Additionally, due to low cell numbers, this study did not distinguish which viral epitopes were recognised, limiting the specificity of the findings. A more detailed approach, such as staining with individual tetramers, or using a barcoded tetramer strategy based on the patients HLA-type, would allow for better identification of the specific T-cell responses to different viral proteins. This could enable deeper insights into how particular viral antigens drive immune responses in the context of complex immune environments such as the TME.

Another aspect that could improve the tetramer response observed would be to use fresh samples instead of frozen however, this was outside the scope of this study within the timeframe. This would potentially allow an increased number of tetramer-specific cells to be detected and might allow for further work in order to elucidate the function of these cells, for example to analyse cytokine release by intracellular cytokine staining or ELISPOT assay. This could help to determine if the $PD1_{HIGH}$ T-cells are capable of producing cytokines in response to stimulation or are functionally exhausted.

Another limitation was that tumour tissue slides were unable to be obtained to carry out staining to determine the presence and location of virus-specific proteins and analyse if they were being expressed by the tumour. This could help further answer the question as to whether the cells are circulating T_{EM} cells that have upregulated T_{RM} markers and retained

within the tumour, or whether they are cells that are virus-specific due to reacting to antigen stimulation within the tumour.

Critically, an essential future aim must be to assess the functional activity of virus-specific T-cells in relation to their relative expression of PD1. In particular, building on from my findings in previous chapters, it will be fascinating to assess the relative cytotoxicity, cytokine and proliferation profile of these distinct virus-specific T-cell populations.

4.3.7 Conclusions

Investigating immune infiltrates and identifying biomarkers in ovarian cancer is essential for personalised treatment strategies. Analysing the phenotype of TILs helps to understand the TME, where the immune cells often face immunosuppressive conditions. The study indicates that most virus-specific T-cells do not transition into a $PD1_{HIGH}$ T_{RM} phenotype. Instead, they exhibit $PD1_{MID}$ characteristics, with only a subset becoming T_{RM} cells. The fact that these T-cells can both circulate through, and remain in tumour, suggests their potential as targets in therapeutic interventions.

The key implications of this study are $PD1_{MID}$ T-cells represent a unique population with distinct characteristics compared to $PD1_{HIGH}$ cells. The identification of significant populations of tissue resident cells, potentially reinforced and sustained from the large population of circulating populations suggests indicates a dual behaviour that makes virus-specific T-cells a promising target for therapies that aim to modulate immune responses.

CHAPTER 5: PROSPECTIVE ANALYSIS OF THE CMV-SPECIFIC T-CELL PHENOTYPE DURING PD1 INHIBITION THERAPY IN PATIENTS WITH LUNG CANCER

5.1 Introduction

The immune checkpoint protein PD1 has an inhibitory action on immune cell function upon binding to its ligands PDL1 or PDL2. In the setting of cancer, the expression of these ligands is found on many tumour subtypes and is thought to play an important role in allowing the cancer to escape recognition from tumour-specific T-cells (Han et al., 2020). Antibodies against PD1 have been used clinically in an approach called 'checkpoint blockade'. Checkpoint blockade has become a cornerstone in treating many cancers such as melanoma and lung-cancer (McLane et al., 2019).

The most commonly used PD1 blocking antibodies, pembrolizumab and nivolumab, have shown significant clinical success by reactivating exhausted T-cells, improving patient outcomes and, in some cases, leading to durable responses. Retrospective analyses have shown no significant difference in the clinical efficacy of these two different antibodies (Moser et al., 2020, Peng et al., 2017). PD1 blockade is particularly effective in tumours with high mutational burden, as this leads to an increased generation of somatic neoantigens to which T-cells can target (Lee et al., 2018).

PD1-blockade has also been shown to influence the 'host-pathogen immune setpoint' in the setting of viral infection. Ahn *et. al* demonstrated that, in mice with acute infection, LCMV-specific T-cells increased expression of granzyme B and accelerated virus elimination in response to anti-PD1 or anti-PDL1 antibodies (Ahn et al., 2018). Klein *et al.* showed similar results with LCMV-infected mice exhibiting significant reductions in viral load along with increases in LCMV-specific $CD8^+$ T-cell responses when treated with anti-PDL1 (Klein et al., 2020). This was supported by another study which demonstrated increased immune effector

functions in LCMV-specific T-cells in mice that received PD1 blockade (Barber et al., 2006). Similarly, mice with inactivation of the genes that encode PD1 or PDL1 displayed increased proliferation and reduced apoptosis in response to acute retroviral infection (David et al., 2019). It has also been demonstrated that in mice with LCMV infection, virus-specific T-cells showed increased contraction in PD1-deficient mice. The authors further showed that PD1 played a critical role in the survival of bystander memory T-cells with PD1-deficient mice exhibiting increased mortality in comparison to their PD1-sufficient counterparts, possibly due to a lack of protective immunity to prior infections (Kalia et al., 2021). However, to date there is little information on how PD1 blockade can impact on the functional properties of CMV-specific T-cells.

Pembrolizumab is a humanised monoclonal anti-PD1 antibody that has been widely investigated in several cancers, showing notable efficacy in both melanoma and non-small cell lung carcinoma (NSCLC). In melanoma, pembrolizumab demonstrated overall response rates between 21-31%, whilst in NSCLC response rates ranged from 19-25%. These results have led to its approval for these, and other, malignancies (Kwok et al., 2016, Garon et al., 2015).

Lung cancer remains the leading cause of cancer-related mortality in the USA, with NSCLC accounting for 80-85% of all cases. NSCLC is comprised of three main histological subtypes: adenocarcinoma, squamous-cell carcinoma and large-cell carcinoma. Adenocarcinoma is the most common subtype, often seen in non-smokers, while squamous-cell carcinoma is more prevalent among smokers. Large-cell carcinoma, though less frequent, tends to be more aggressive (Zappa and Mousa, 2016, Simeone et al., 2019).

The PEPS2 trial was a phase II clinical study which investigated the efficacy and safety of pembrolizumab in patients with NSCLC. In NSCLC the performance status (PS) is an independent prognostic factor for patient survival and, notably, previous studies have focussed predominantly on patients with a PS of 0-1. In contrast, the unique aspect of the PEPS2 clinical trial was the focus on patients with a PS of 2.

The performance status of a patient focuses on three aspects: symptoms, severity and mobility. Performance status 2 indicates individuals that are active for more than half of the day yet exhibit symptoms which reflects a moderate level of functional impairment (Dajczman et al., 2008). These patients had also all undergone previous treatment, primarily chemotherapy or radiotherapy and surgery.

By including this population of patients the trial aimed to address an important gap in the literature and evaluate treatment options across a broader spectrum of patients in order to optimise therapy for all individuals affected by NSCLC (Middleton et al., 2020).

In this study I assess how systemic treatment with anti-PD1 therapy may affect the phenotype and function of CMV-specific and EBV-specific T-cells. I address this by carrying out in-depth characterisation of these populations within PBMC following pembrolizumab therapy.

5.2 Results

5.2.1 Patient Cohort

Assessment of CMV serostatus and HLA typing was carried out by Jusnara Begum prior to this study. Assessment of CMV serostatus was carried out by in-house CMV IgG ELISA, and assessment of donor HLA by PCR and gel electrophoreses, as described in Chapter 2.

In this chapter, I carried out tetramer staining using a master-mix of all available tetramers (CMV tetramers as in Table 11 and EBV tetramers as in Table 12) with epitopes that were specific for the HLA of the donor to capture as many virus-specific cells as possible within the low cell counts. This allowed me to capture multiple tetramer$^+$ responses to immunodominant epitopes at the same time to maximise the number of CMV-specific or EBV-specific T-cells analysed.

A summary of the donors used in the study can be found in Table 25.

Blood was taken from patients prior to treatment with 200mg pembrolizumab and treatment was given every 3 weeks. The drug has a half-life of 26 days with a clearance rate of 0.22L/day which is unaffected by age or gender (Dang et al., 2016).

Table 25: Summary of the patient characteristics of donors enrolled within the research study

Total donors (n)	**58**	
CMV status (n/total)		
Positive	18/58 (31%)	
Negative	40/58 (69%)	
Age bracket	**Total donors (n/total)**	**CMV+ donors (n/CMV^{+} total)**
41-50	1/58 (2%)	0/1 (0%)
51-60	8/58 (14%)	1/7 (14%)
61-70	17/58 (29%)	6/17 (35%)
71-80	28/58 (48%)	10/28 (36%)
81-90	4 (7%)	1/4 (25%)
Sex		
Male	32/58 (55%)	9/18 (50%)
Female	26/58 (45%)	9/18 (50%)
Death Cause		
Total	46/58 (79%)	14/18 (78%)
Lung cancer related	42/46 (91%)	14/14 (100%)
Other Cancer	1 (2%)	0/14 (0%)
Other non-cancer	1 (2%)	0/14 (0%)
Other treatment related	1 (2%)	0/14 (0%)
Not known	1 (2%)	0/14 (0%)

5.2.2 IgG4 optimisation

All analysis in this chapter was focused on the $CD8^+$ T-cell population and the gating strategy in Figure 67 was used. $CD8^+$ T-cells were selected by gating on singlet cells according to width and height; lymphocytes according to forward and side scatter; live cells; cells negative for the dump channel markers CD14 and CD19 which would indicate monocytes and B-cells; $CD3^+$ cells, and finally $CD8^+$ $CD4^-$ cells to establish the $CD8^+$ population (Figure 11a). This gating strategy was used for all future analysis throughout the chapter to identify $CD8^+$ cells.

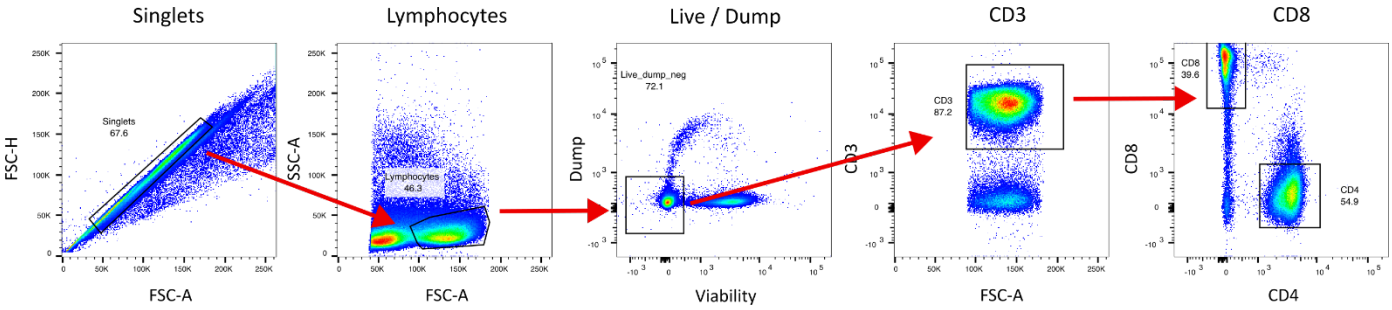

Figure 67: CD8 gating strategy

Gating strategy to identify $CD8^+$ T-cells. Samples were thawed and stained with the antibody panel 'PEPS2- surface' (Table 13) before flow cytometric analysis. From left to right: singlets discrimination, lymphocytes, Live/ dump negative cells, T-cells and $CD8^+$ cells. This gating strategy was used throughout all $CD8^+$ T-cell analysis.

An important aim of my study was to assess the phenotype of $PD1^+$ T-cells following pembrolizumab therapy. However, pembrolizumab is itself an antibody against PD1 and thus has the potential for stearic inhibition of binding of additional antibodies against PD1.

For this reason, another method was needed to assess the cells responding to the drug.

Pembrolizumab is a humanised IgG4 antibody (Scapin et al., 2015) and therefore an anti-IgG4 antibody was conjugated to PE-Cy5 and used in an attempt to identify and phenotype cells that had bound pembrolizumab.

To optimise the IgG4 staining and get the best resolution, I incubated cells from healthy laboratory donors with pembrolizumab and stained them with antibodies in the presence of various buffers. Brilliant Stain Buffer (BSB) (BD), FCR block (BioLegend) and human serum (Sigma-Aldrich) were tested (Figure 68).

Results showed little difference in the resolution between the different buffers with the percentage of IgG4 detection on the $CD8^+$ T-cells remaining similar (BSB- 11.2%, FCR block- 11.3%, Human Serum- 10.1%), BSB was selected for future staining as this also ensures good resolution between the other BD Brilliant™ antibodies in the panel.

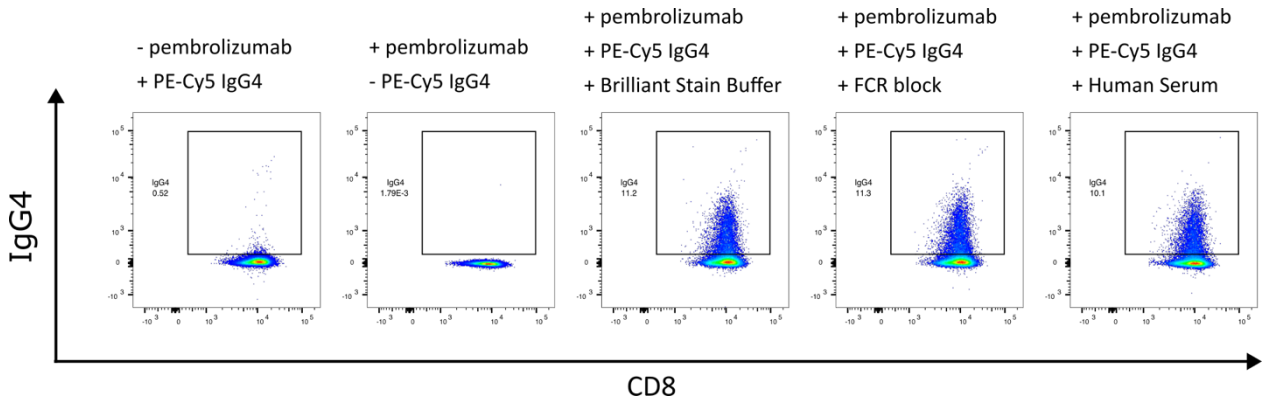

Figure 68: Optimisation of identification of pembrolizumab binding to T-cells

Dot plots showing IgG4 staining on $CD8^+$ T-cells. Cells were incubated with antibody in the presence of pembrolizumab, with the exception of the '- pembrolizumab' FMO control. Staining was carried out in different buffers to optimise resolution of IgG4 staining. All samples contained the PE-Cy5 conjugated IgG4 with the exception of the -PE-Cy5 IgG4' control which was included to confirm there was no spillover fluorescence. The buffers used were Brilliant Stain Buffer (BD), FCR block (BioLegend) and Human Serum (Sigma).

5.2.3 Overall phenotype of viral-specific T-cells in patients with NSCLC

In initial work I undertook flow cytometric phenotyping on samples that had been taken prior to pembrolizumab treatment (cycle 0) to define the profile of circulating virus-specific T-cells in patients with NSCLC.

A representative example of the CMV-tetramer and EBV-tetramer staining can be seen in Figure 69.

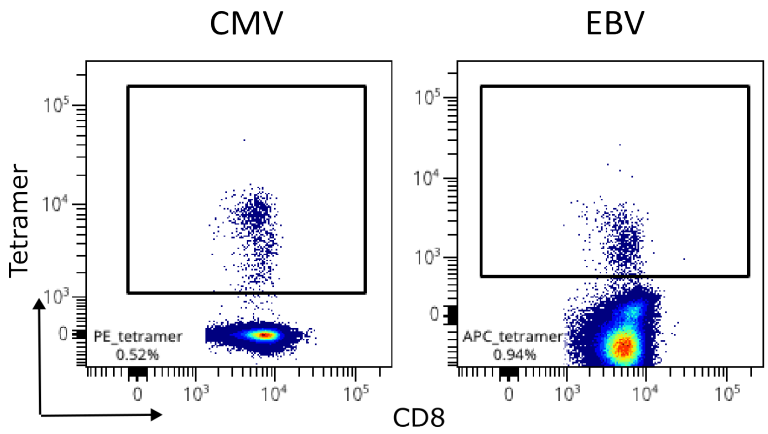

Figure 69: Tetramer staining of virus-specific T-cells in patients with NSCLC

Representative dot plots showing CMV-tetramer (PE) staining and EBV-tetramer (APC) staining on $CD8^+$ T-cells

All donors that tested positive for CMV-specific IgG antibodies were stained together with some CMV-negative donors. CMV-positive donors were stained with available tetramers for the epitopes specific for their HLA-genotype and patients with a clear tetramer-specific T-cell population were included in the analyses. A positive tetramer stain was defined by >0.05% of cells in the $tetramer^+$ gate and with good resolution from the negative population. A healthy donor control with a tetramer stain and a no-tetramer control was included with every run to ensure no non-specific tetramer binding. The final number of samples analysed at every stage can be found in in Table 26.

Table 26: Summary of the number of donors with an HLA genotype suitable for tetramer staining within the PEPS2 cohort. Samples from every donor were not available at every timepoint. Cycle 0 is the baseline sample, prior to any treatment. EOT denotes End of Treatment.

	Cycle										
	0	**1**	**2**	**3**	**4**	**5**	**6**	**7**	**8**	**9**	**EOT**
Tetramer-negative donors (n)	21	20	18	15	3	0	8	0	0	6	3
CMV$^+$ donors (n)	13	13	13	13	1	0	6	0	0	6	2
EBV$^+$ donors (n)	9	8	7	4	1	0	4	0	0	2	1

The memory phenotypes of the cells were assessed using the surface markers CCR7 and CD45RA to identify naïve (CCR7$^+$ CD45RA$^+$), central memory (T_{CM}; CCR7$^+$ CD45RA$^-$), effector memory (T_{EM}; CCR7$^-$ CD45RA$^-$) and effector memory cells with re-expression of CD45RA (T_{EMRA}; CCR7$^-$ CD45RA$^+$).

The memory phenotypes were established in Figure 70. The CMV-tetramer$^+$ T-cell response was comprised primarily of T_{EM} and T_{EMRA} cells (median = 50% and 32% respectively), with very few Naïve (median = 2.6%) and T_{CM} (median = 5%) cells. The T_{CM} compartment had significantly more EBV-tetramer$^+$ (median = 20%; p = 0.0019) and tetramer$^-$ cells (median = 15%; p = 0.0081) in comparison to CMV-tetramer$^+$ pool. The EBV-tetramer$^+$ cells also displayed a primarily T_{EM} phenotype, with a median of 58%, with a significant increase in this population in comparison to the tetramer$^-$ (median = 38%; p = 0.0427). Whilst not significant, the CMV-tetramer$^+$ population was also showing a trend of increasing in comparison to the tetramer$^-$ cells (p = 0.62) however these CMV-tetramer$^+$ T-cells displayed a wide range of T_{EM} expression (10 - 89%).

There were very few EBV- tetramer$^+$ T-cells with a T_{EMRA} phenotype (median = 6.5%), with the CMV- tetramer$^+$ and tetramer$^-$ T_{EMRA} populations significantly increased (p = 0.0057 and p = 0.024 respectively).

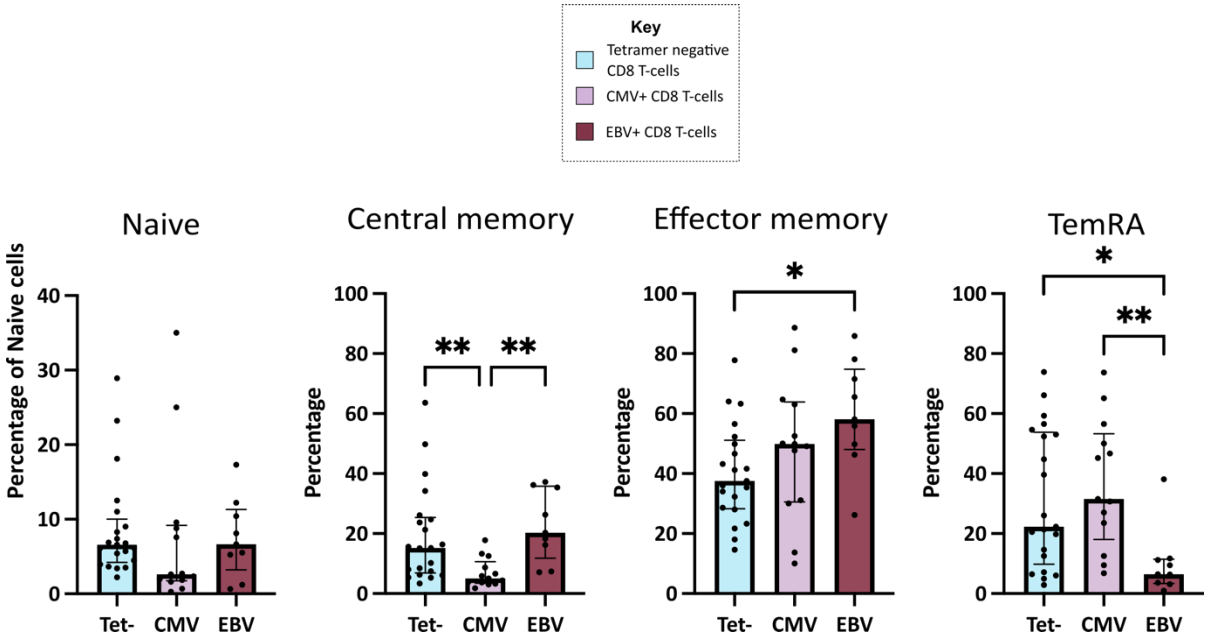

Figure 70: Memory phenotype of virus-specific T-cells in NSCLC patients pre-treatment with pembrolizumab

Summary of the percentage of T-cell memory phenotypes: naïve (CCR7$^+$ CD45RA$^+$), central memory (T_{CM}; CCR7$^+$ CD45RA$^-$), effector memory (T_{EM}; CCR7$^-$ CD45RA$^-$) and effector memory cells with re-expression of CD45RA (T_{EMRA}; CCR7$^-$ CD45RA$^+$). on tetramer$^-$, CMV- tetramer$^+$, and EBV- tetramer$^+$ CD8$^+$ T-cells in patients with NSCLC. Each dot represents one tetramer response. Bars represent the percentage median of each phenotype (± interquartile range). Statistical analysis performed with Kruskal-Wallis test with Dunn's multiple comparisons test with * p <0.05; ** p <0.01; *** p <0.001; **** p <0.0001.

Next, I analysed checkpoint expression on these T-cell populations (Figure 71). As these samples had been taken prior to any treatment with pembrolizumab the expression of PD1 could also be assessed. In line with data in my previous chapters the checkpoints PD1, TIGIT and 2B4 were the most commonly expressed proteins (median expression on CMV-tetramer$^+$ T-cells = 22%, 25% and 79% respectively), with less expression of TIM3 and LAG3 (median expression on CMV-tetramer$^+$ cells = 6.7% and 1.9% respectively). PD1 and TIGIT were highly expressed on the EBV- tetramer$^+$ CD8$^+$ T-cells (median = 76% and 78% respectively), with a significant increase in these markers from the CMV- tetramer$^+$ ($p = 0.01$ and $p = 0.0005$ respectively) and tetramer$^-$ ($p = 0.0055$ and $p = 0.0142$ respectively) populations. There was no change in the percentage of cells expressing PD1 between the tetramer$^-$ (median = 24.1%) and the CMV- tetramer$^+$ (median = 21.7%) compartments.

There was also a significant increase in the percentage of CMV-tetramer$^+$ CD8$^+$ T-cells expressing 2B4 in comparison to the tetramer$^-$ ($p = 0.0280$) although there was an extremely wide range of 2B4 expression on the tetramer$^-$ population (5.02% - 89%). There was also a trend towards an increase in 2B4 expression on the EBV- tetramer$^+$ population in comparison to the tetramer$^-$ ($p = 0.3703$).

Whilst there were no changes between the populations expressing TIM3 and LAG3, the median of cells expressing LAG3 was increased in the CMV- tetramer$^+$ (median = 1.9%) and EBV-specific populations (median = 1.4%) in comparison to the tetramer$^-$ (median = 0.54%).

Together this data shows a marked difference in the range of checkpoint expression between the viral-specific cells and the general CD8$^+$ population in patients with NSCLC (Table 16).

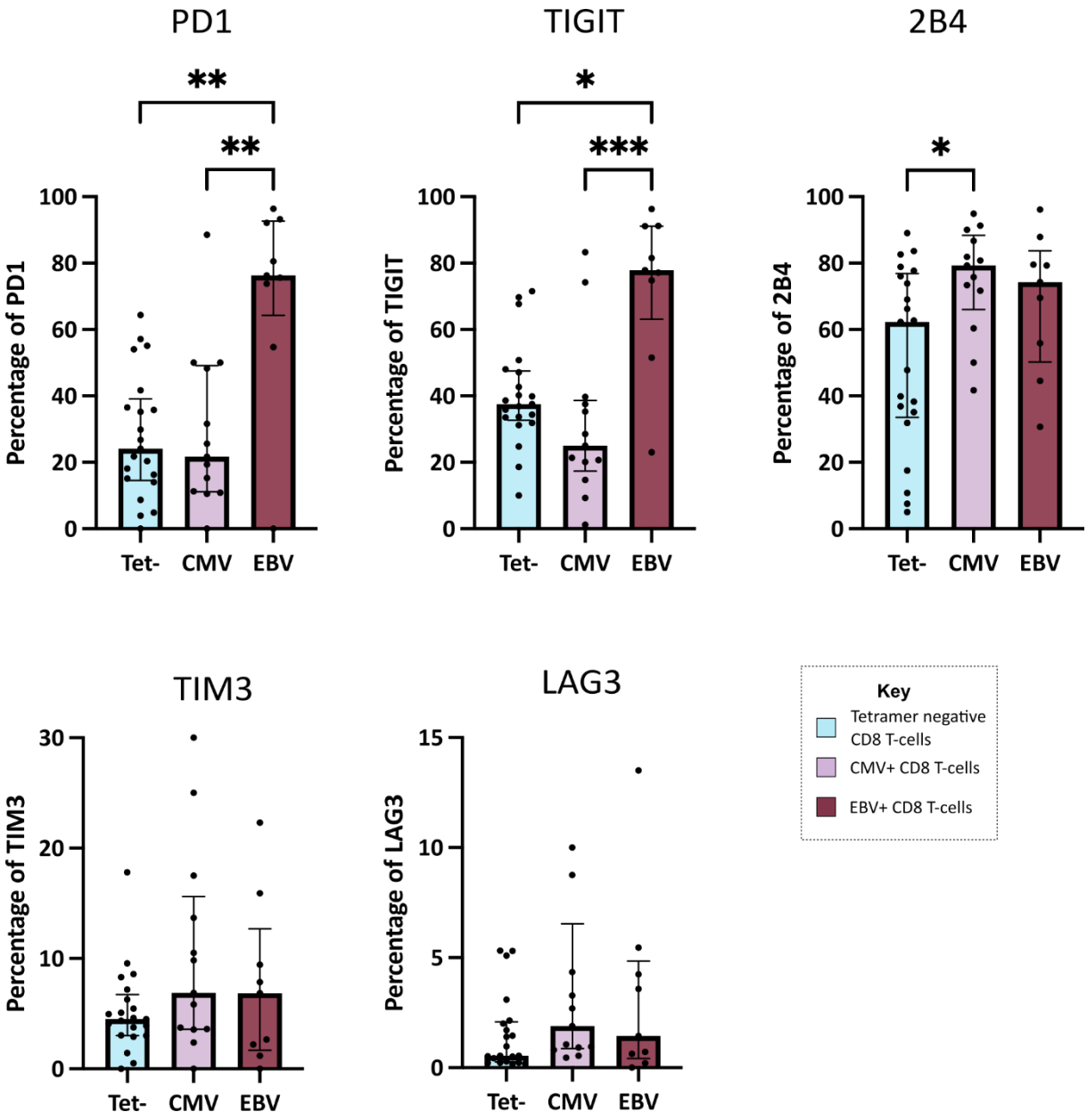

Figure 71: Checkpoint expression on virus-specific T-cells in NSCLC patients pre-treatment with pembrolizumab

Summary of the percentage of checkpoints PD1, TIGIT, 2B4, TIM3 and LAG3 in patients with NSCLC. on tetramer^{-}, CMV- tetramer^{+}, and EBV- tetramer^{+} CD8^{+} T-cells in patients with NSCLC. Each dot represents one tetramer response. Bars represent the percentage median of each phenotype (± interquartile range). Statistical analysis performed with Kruskal-Wallis test with Dunn's multiple comparisons test with * p <0.05; ** p <0.01; *** p <0.001; **** p <0.0001.

Table 27: Summary of median checkpoint expression percentage from CMV-tetramer$^+$, EBV-tetramer$^+$ and tetramer$^-$ cells in the PBMC pre-treatment in NSCLC patients

	Checkpoint median expression (%)				
Population	**PD1**	**TIGIT**	**2B4**	**TIM3**	**LAG3**
CMV-tetramer+	22	25	79	6.9	1.9
EBV-tetramer$^+$	76	78	74	6.9	1.4
Tetramer$^-$	24	38	62	4.5	0.5

To further assess the phenotype of the cells, I utilised the activation markers HLA-DR and CD38 (Figure 72). Expression of these proteins was increased on the EBV-tetramer$^+$ population compared to the CMV-tetramer$^+$ and tetramer$^-$ populations (medians = 5.6%, 2.8% and 2.8% respectively; p = 0.039 and 0.0065 respectively), indicating that the EBV- tetramer$^+$ T-cells were likely more activated than the other two populations.

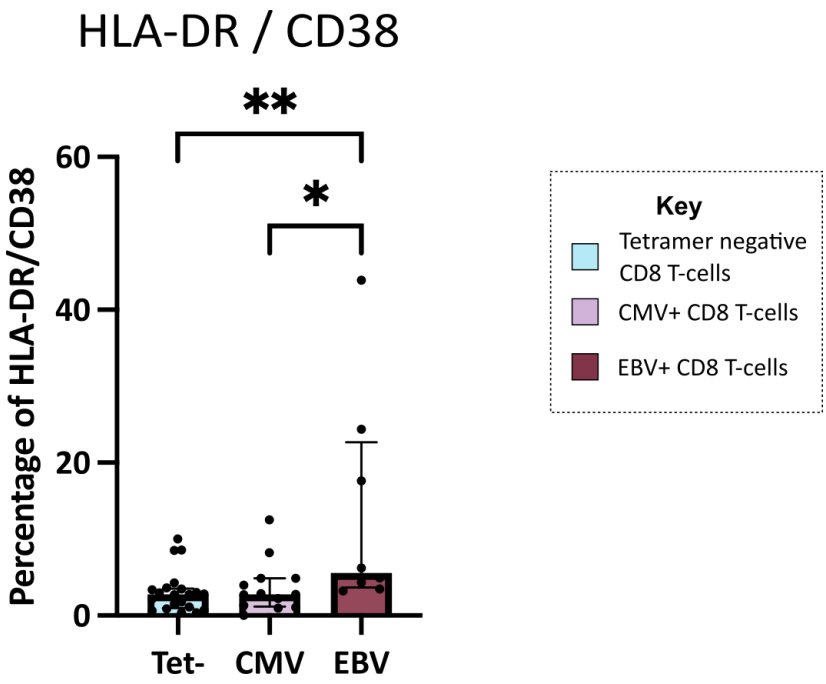

Figure 72: HLA-DR and CD38 expression on virus-specific T-cells in NSCLC patients pre-treatment with pembrolizumab

Summary of the percentage of tetramer$^-$, CMV-tetramer$^+$ and EBV- tetramer$^+$ T-cells expressing the activation markers HLA-DR and CD38 in patients with NSCLC. Each dot represents one tetramer response. Bars represent the percentage median of each phenotype (± interquartile range). Statistical analysis performed with Kruskal-Wallis test with Dunn's multiple comparisons test with * p <0.05; ** p <0.01; *** p <0.001; **** p <0.0001.

Using cytokine and intranuclear staining, I was able to further phenotype the cells to assess granzyme B production, expression of the transcription factors T-bet and TCF, and expression of the nuclear protein and proliferation marker Ki67. As permeabilization can affect cell surface staining, I confirmed that the tetramer staining was still successful despite this approach (Figure 73a). Representative examples of granzyme B, Ki67, TCF1 and T-bet staining are also shown.

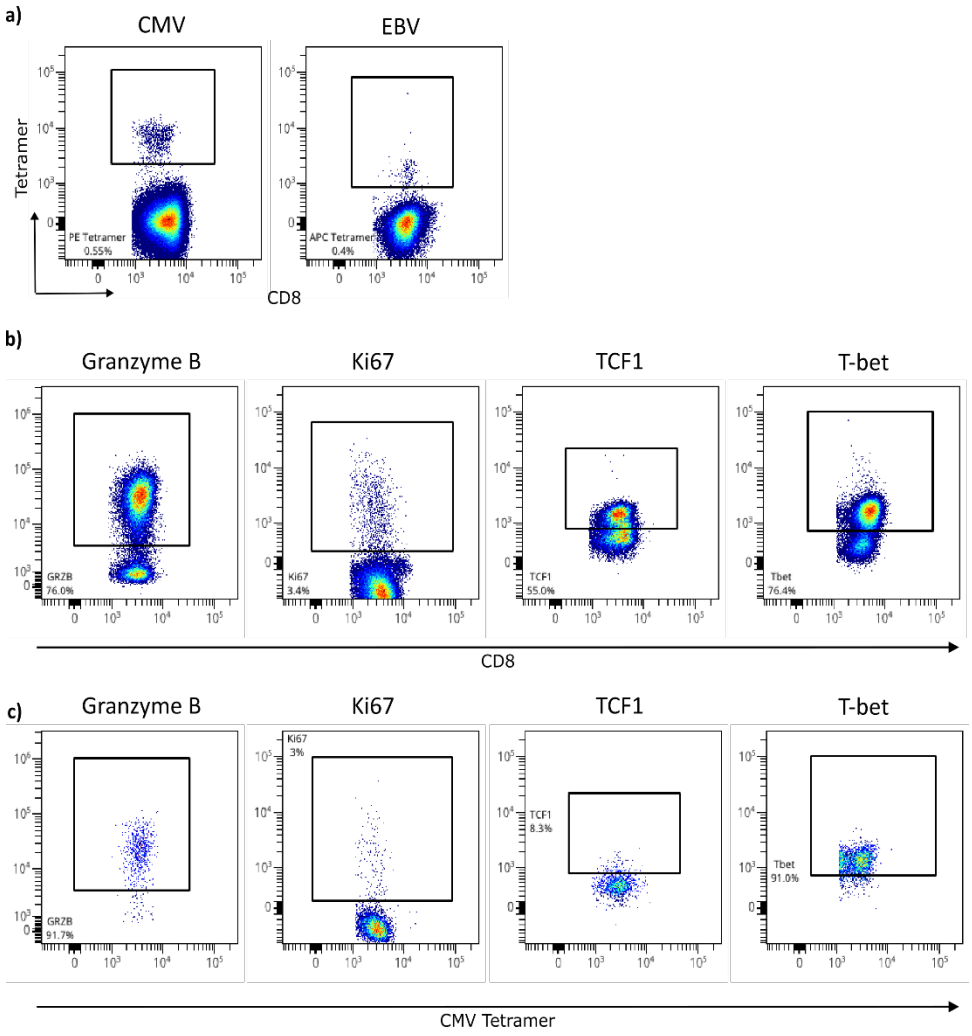

Figure 73: Intracellular and intranuclear staining of virus-specific T-cells

- **a)** Representative dot plots showing staining for CMV and EBV-specific tetramer response on the intranuclear stained samples
- **b)** Representative dot plots showing intranuclear staining for Granzyme B, Ki67, TCF1 and T-bet on CD8 T-cells
- **c)** Representative dot plots showing intranuclear staining for Granzyme B, Ki67, TCF1 and T-bet on CMV-tetramer specific T-cells

Of note, Figure 74 shows the CMV- tetramer^{+} T-cells expressed significantly more granzyme B (median = 95%) in comparison to the tetramer^{-} (median = 72%; $p < 0.0001$) and EBV-specific (median = 73%; $p = 0.019$) populations, with at least 79% of CMV-specific CD8^{+} T-cells in each donor expressing granzyme B. Furthermore, 10/11 donors displayed over 90% of CMV-

tetramer^{+} T-cells positive for granzyme B expression. A much wider range was seen with the tetramer^{-} compartment with as little as 4% of CD8^{+} T-cells in one donor expressing granzyme B.

However, the tetramer^{-} compartment did display an increase in the transcription factor TCF1 (median = 12%) in comparison to the CMV- tetramer^{+} cells (median = 5.2%; p = 0.05). There were no changes observed in the nuclear protein Ki67 or the transcription factor T-bet expression between the populations.

A summary of this data can be found in Table 28.

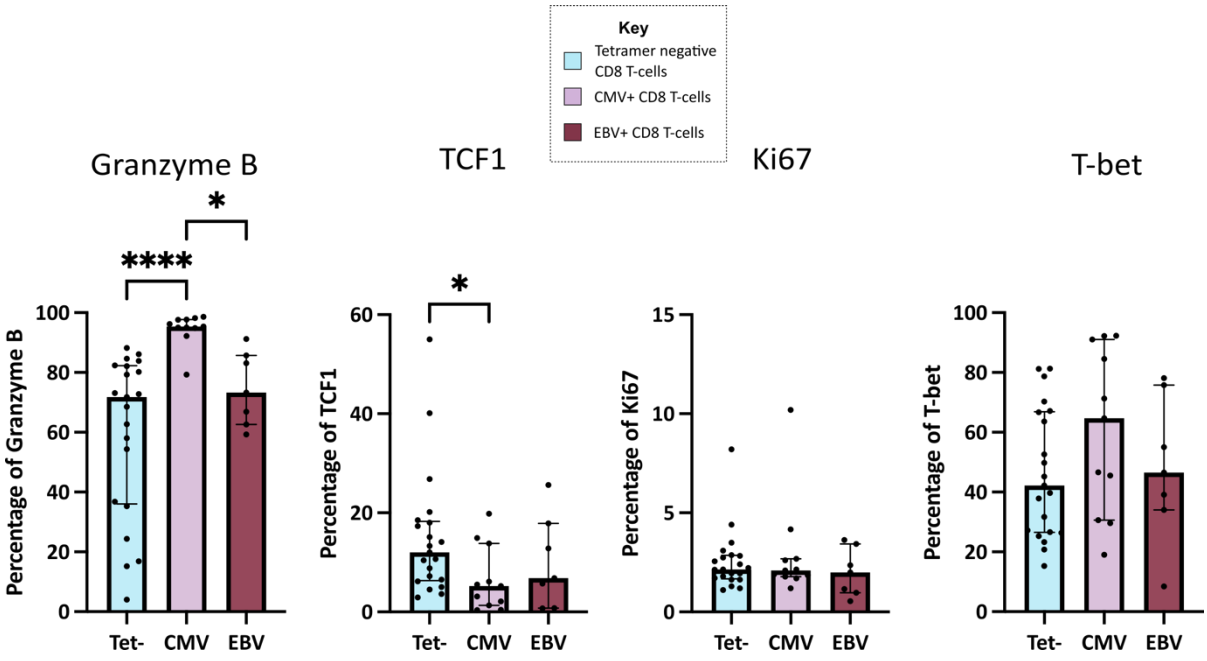

Figure 74: Cytokine and transcription factor expression in virus-specific T-cells in NSCLC patients pre-treatment with pembrolizumab

Summary of the percentage of tetramer^{-}, CMV-tetramer^{+} and EBV- tetramer^{+} T-cells expressing granzyme B, TCF1, Ki67 and T-bet in patients with NSCLC. Each dot represents one tetramer response. Bars represent the percentage median of each phenotype (± interquartile range). Statistical analysis performed with Kruskal-Wallis test with Dunn's multiple comparisons test with * p <0.05; ** p <0.01; *** p <0.001; **** p <0.0001.

Table 28: Summary of median Granzyme B (GrzB), TCF1, Ki67 and T-bet expression percentage from CMV-tetramer$^+$, EBV-tetramer$^+$ and tetramer$^-$ cells in the PBMC pre-treatment in NSCLC patients

	Checkpoint median expression (%)			
Population	**GrzB**	**TCF1**	**Ki67**	**T-bet**
CMV-tetramer+	95	5.2	2.1	65
EBV-tetramer$^+$	73	6.8	2	47
Tetramer$^-$	72	12	2.1	42

5.2.4 The T-cell phenotypes of NSCLC patient's vs healthy donors

As there appeared to be differences between the NSCLC baseline samples and the data from the healthy donors in Chapter 3, I took age matched sample sets to compare to determine key changes to the T-cell populations. Details of the donors used in this portion of the study can be found in Table 29.

Table 29: Summary of the characteristics of the donors used when comparing NSCLC patients to healthy donors.

Age bracket		NSCLC patients (n)	Healthy donors (n)
50-59	*Tetramer*$^-$		11 (32 responses)
	CMV-tetramer$^+$		11 (32 responses)
	EBV-tetramer$^+$		5 (10 donors)
60-69	*Tetramer*$^-$	10	
	CMV-tetramer$^+$	4	
	EBV-tetramer$^+$	4	
Sex			
Male	*Tetramer*$^-$	4/10 (40%)	3/11 (27%)
	CMV-tetramer$^+$	0/4 (0%)	3/11 (27%)
	EBV-tetramer$^+$	2/4 (50%)	2/5 (40%)
Female	*Tetramer*$^-$	6/10 (60%)	8/11 (73%)
	CMV-tetramer$^+$	4/4 (100%)	8/11 (73%)
	EBV-tetramer$^+$	2/4 (50%)	3/5 (60%)
HLA-type and epitope			
Mastermix	*CMV-tetramer*$^+$	4/4 (100%)	
	EBV-tetramer$^+$	4/4 (100%)	
HLA-type and CMV tetramers			
HLA-A*0101 YSE			6/32 (19%)
HLA-A*0101 VTE			8/32 (25%)
HLA-A*0201 NLV			2/32 (6%)
HLA-B*0702 TPR			4/32 (13%)
HLA-B*0702 RPH			4/32 (13%)
HLA-B*0801 QIK			3/32 (9%)
HLA-B*0801 ELR			2/32 (6%)
HLA-B*0801 ELK			3/32 (9%)
HLA-type and EBV tetramers			
HLA-A*0201 YVL			2/10 (20%)
HLA-A*0201 CLG			1/10 (10%)
HLA-A*0201 GLC			1/10 (10%)
HLA-B*0702 RPP			1/10 (10%)
HLA-B*0702 RPR			1/10 (10%)
HLA-B*0801 RAK			2/10 (20%)
HLA-B*0801 FLR			2/10 (20%)

Figure 75 shows the expression of PD1 on virus-specific T-cells in the healthy donors (tetramer$^-$ and CMV-positive donors comprised of 32 tetramer responses across 11 donors and EBV-positive donors comprised of 10 tetramer responses from 5 donors) in comparison to the baseline NSCLC patients (tetramer$^-$ n = 10, CMV- tetramer$^+$ n = 4, EBV- tetramer$^+$ n = 4). It should be noted that these NSCLC patients have all undergone previous therapy: chemotherapy and/or radiotherapy and surgery.

Interestingly, whilst there was a large decrease between the percentage of PD1$^+$ cells in the CMV-tetramer$^+$ compartment between the healthy donors and NSCLC patients (p = 0.029) and a decreasing trend in the tetramer$^-$ compartment (p = 0.051), there was a slight increase in the expression on EBV-tetramer$^+$ T-cells (p = 0.43). The median expression in the tetramer$^-$ population fell from 50- 33% between healthy donors and NSCLC patients, and 53– 24% in the CMV-tetramer$^+$ population. In comparison, the median of the EBV-tetramer$^+$ population was 78% in the healthy donors and 86% in the NSCLC patients. These findings indicate potential differences in how the functional activity of virus-specific T-cells can be modulated by the diagnosis of lung cancer and its associated treatment.

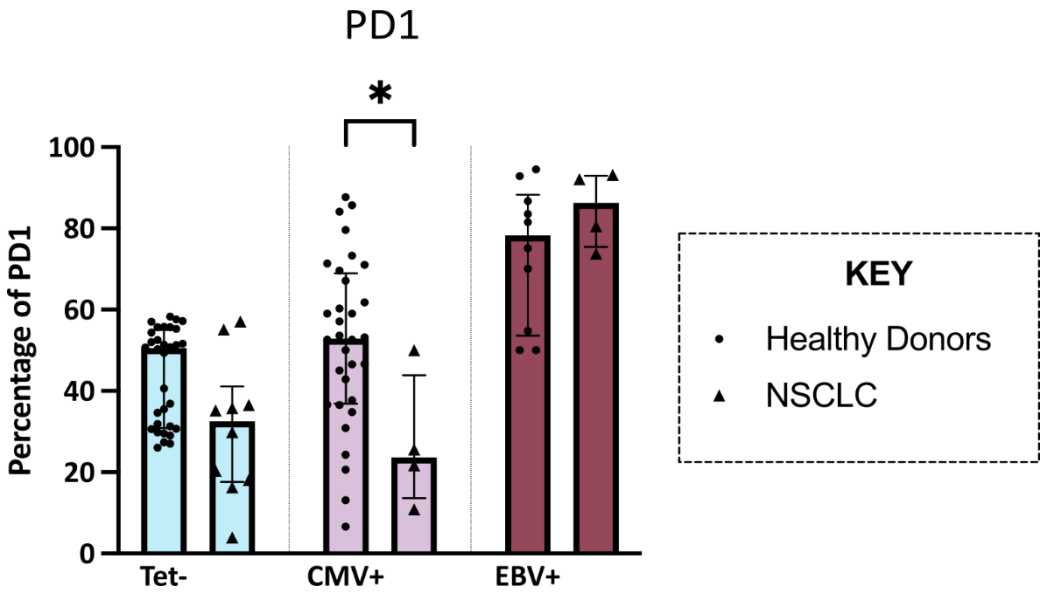

Figure 75: PD1 expression on virus-specific T-cells in healthy donors vs baseline NSCLC patients

Summary of the percentage of tetramer$^-$ (NCSLC n = 10), CMV-tetramer$^+$ (NSCLC n = 4), and EBV-tetramer$^+$ (NSCLC n = 4) T-cells expressing PD1 in healthy donors (CMV-specific and tetramer$^-$ n = 32 tetramer responses from 11 donors, EBV-specific responses n = 10 tetramer responses from 5 donors) vs patients with NSCLC before treatment with pembrolizumab. Each point represents one tetramer response. Bars represent the percentage median of each phenotype (± interquartile range). Statistical analysis performed with Mann-Whitney test between the healthy donor and NSCLC patients within each compartment with * p <0.05; ** p <0.01; *** p <0.001; **** p <0.0001.

To further investigate this, expression of the other checkpoints: 2B4, TIGIT, LAG3 and TIM3 were analysed (Figure 76). Of note, in the CMV-tetramer$^+$ population there was an increase in both 2B4 and LAG3 between the healthy donor and NSCLC cohorts (p = 0.039 and p = 0.0021 respectively). The median of CMV-tetramer$^+$ cells expressing 2B4 rose from 54% in healthy donors to 77% in NSCLC patients and LAG3 from 0.3-3.1%. There was also a trend towards an increase in the tetramer$^-$ population in the NSCLC patients expressing TIM3 and LAG3 (p =

0.051 and p = 0.16 respectively) however, this was not mirrored in the viral- tetramer^{+} compartments.

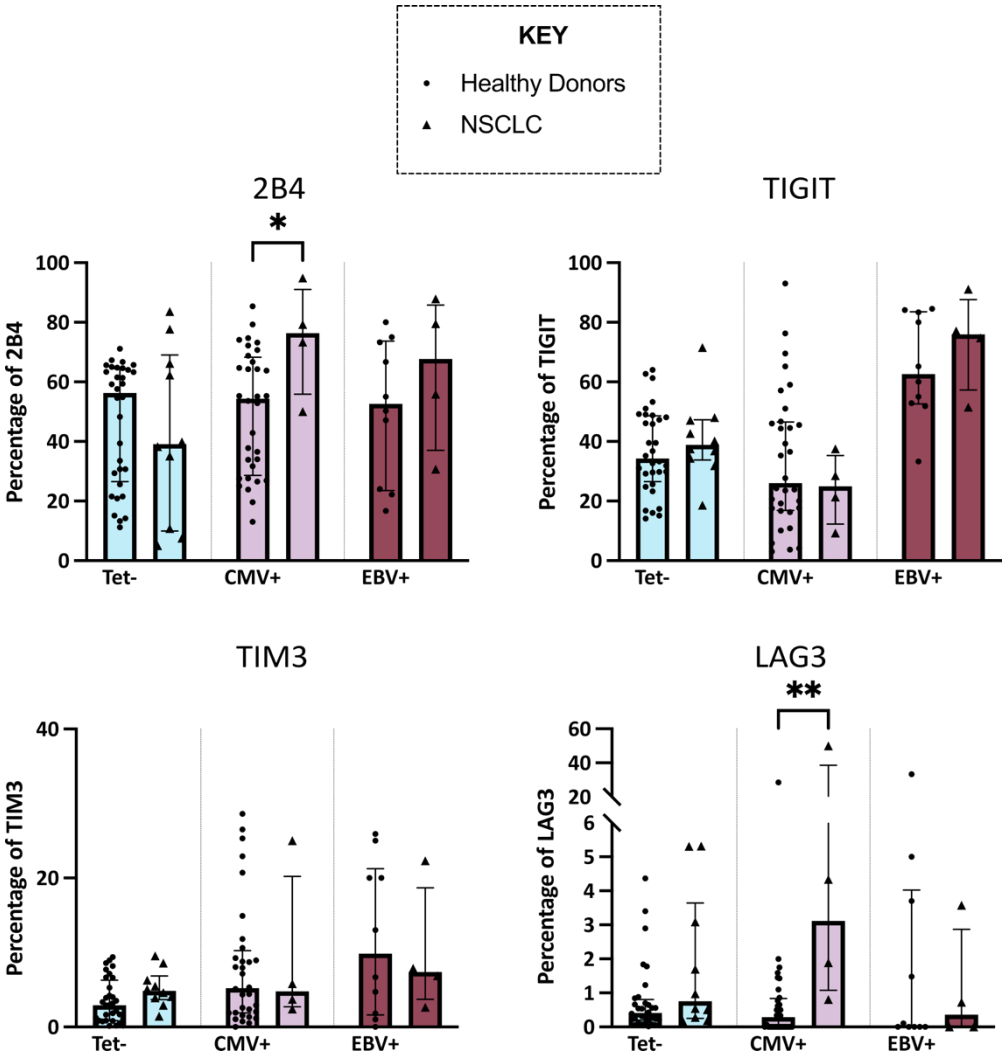

Figure 76: Checkpoint expression on viral-specific T-cells in healthy donors vs NSCLC patients

Summary of the percentage of tetramer$^-$ (NCSLC n = 10), CMV-tetramer$^+$ (NSCLC n = 4), and EBV-tetramer$^+$ (NSCLC n = 4) T-cells expressing 2B4, TIGIT, TIM3 and LAG3 in healthy donors (CMV-specific and tetramer$^-$ n = 32 tetramer responses from 11 donors, EBV-specific responses n = 10 tetramer responses from 5 donors) vs patients with NSCLC before treatment with pembrolizumab. Each point represents one tetramer response. Bars represent the percentage median of each phenotype (± interquartile range). Statistical analysis performed with Mann-Whitney test between the healthy donor and NSCLC patients within each compartment with * p <0.05; ** p <0.01; *** p <0.001; **** p <0.0001.

5.2.5 Phenotypic analysis of T-cell subpopulations following pembrolizumab therapy

Next, I undertook assessment of the phenotypes of the T-cells at various timepoints in response to ongoing cycles of pembrolizumab therapy.

Initially the T-cell response was assessed by analysing $CD8^+$ and $CD4^+$ T-cell responses over time as a percentage of the total CD3 response (Figure 77). Interestingly, there were no significant changes in the populations across the cycles indicating that PD1 blockade has no major differential activity at regulating factors that determine the CD4:CD8 T-cell ratio within blood. Next, the phenotype of the tetramer-specific response was assessed (Figure 78). Importantly, no change was seen in the percentage of CMV-$tetramer^+$ or EBV-$tetramer^+$ cells at any of the cycles after treatment with pembrolizumab.

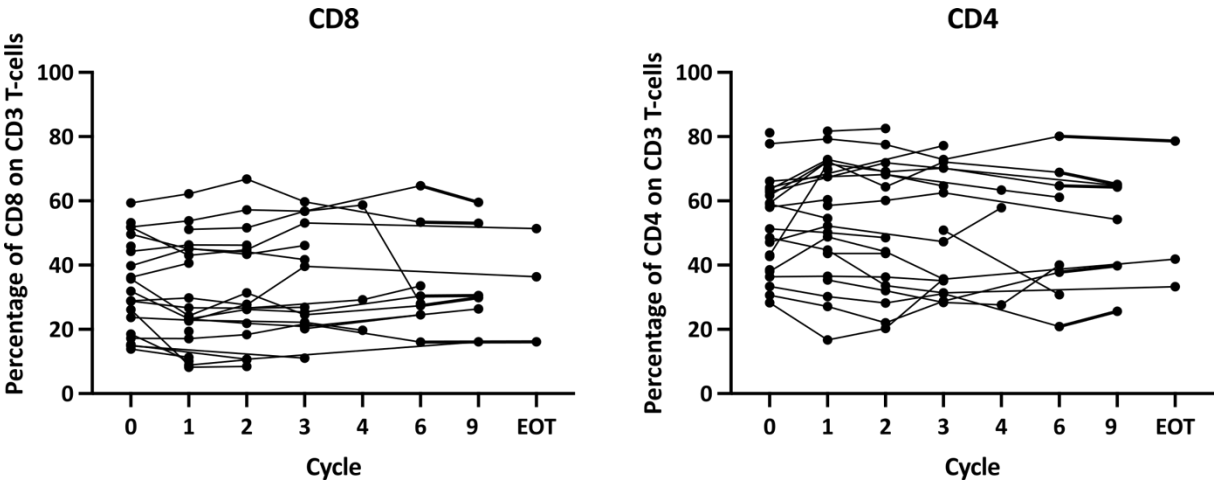

Figure 77: CD8 and CD4 expression on T-cells in patients undergoing pembrolizumab treatment

Summary of the percentage of CD8 and CD4 T-cell responses out of the total CD3 response after treatment with pembrolizumab. There were no significant changes across the cycles. Statistical analysis performed with Kruskal-Wallis test with Dunn's multiple comparisons test with $p < 0.05$.

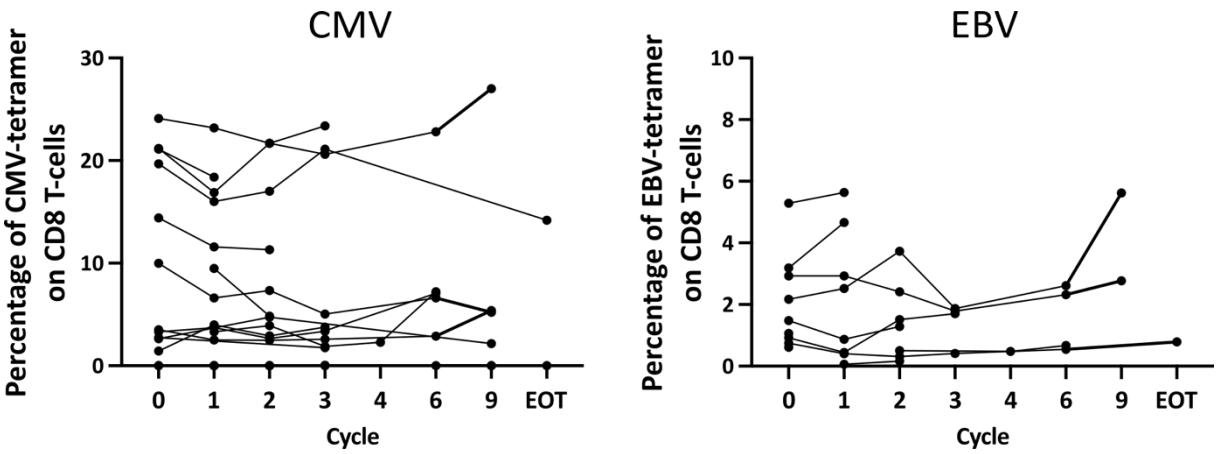

Figure 78: Percentage of virus-specific T-cells in blood of patients following PD1 blockade

Summary of the percentage of CMV and EBV specific CD8 T-cell responses out of the total CD3 response after treatment with pembrolizumab. There were no significant changes across the cycles. Statistical analysis performed with Kruskal-Wallis test with Dunn's multiple comparisons test with $p < 0.05$.

Closer inspection did suggest that some alteration in tetramer-percentage may be observed between cycles 0 and 1. As such, I next undertook paired analysis to determine any changes in the tetramer-specific compartments between cycles 0 and 1 (Figure 79). Cycle 0 is a pre-treatment baseline so the change between cycle 0 and 1 is due to one cycle of treatment. As paired analysis was undertaken, this reduced the sample size to a cohort of CMV n = 11 and EBV n = 7. Whilst there was no change in the EBV- tetramer$^+$ T-cells with some samples increasing and some decreasing between the cycles, the percentage of CMV- tetramer$^+$ T-cells did decrease between cycles 0 and 1 ($p = 0.032$).

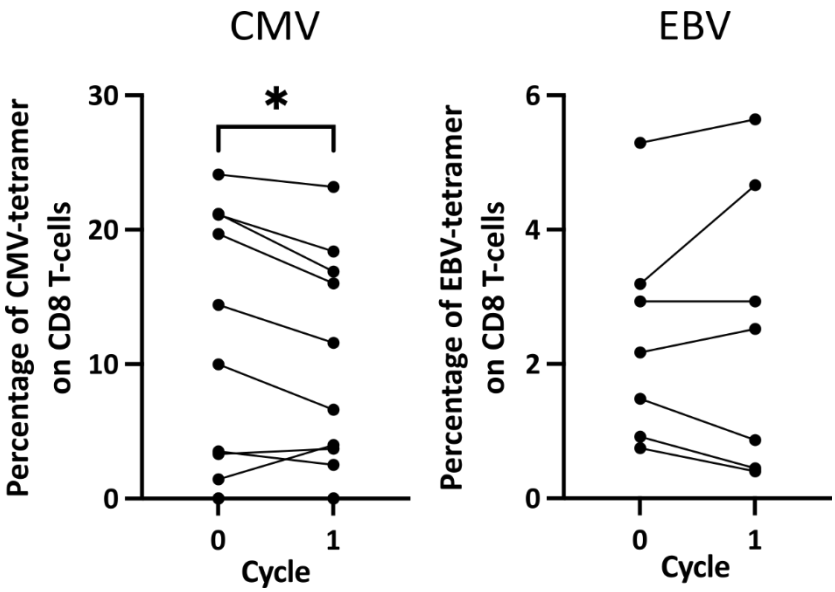

Figure 79: Virus-specific T-cell populations between cycle 0 and 1 of pembrolizumab

Summary of the percentages of CMV and EBV- tetramer^{+} CD8^{+} T-cells at cycle 0 (pre-treatment) and 1 (3 weeks after one dose) (CMV n= 11, EBV n= 7). Statistical analysis performed with Wilcoxon matched-pairs signed rank test with $p < 0.05$.

5.2.6 Phenotyping the T-cell response to pembrolizumab

I next went on to use IgG4-specific staining to identify pembrolizumab-bound T-cells (Figure 80). Unexpectedly, despite the samples being taken before administration of pembrolizumab, a high percentage of cells were seen to express IgG4 (1.3-34%).

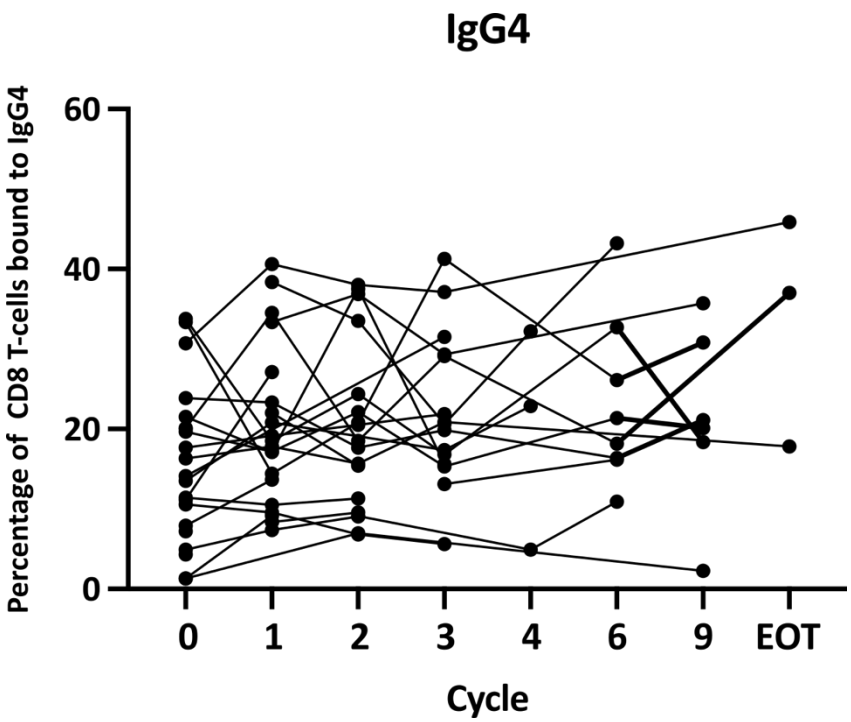

Figure 80: Detection of pembrolizumab using an anti-IgG4 antibody bound to T-cells during pembrolizumab therapy

Summary of percentage of $CD8^+$ T-cells bound to anti-IgG4 after treatment with pembrolizumab. There were no significant changes across the cycles. Statistical analysis performed with Kruskal-Wallis test with Dunn's multiple comparisons test with $p < 0.05$. There was no statistical differences observed across the cycles.

The optimisation experiments had shown that I would not expect high background staining of IgG4 and I would not expect IgG4 to be bound to T-cells at this high percentage without the presence of pembrolizumab. The basis for this experimental observation could not be delineated. As such, I was unable to identify PD-1 specific T-cells during my analysis of the PEPS cohort. This was unfortunate but I was still able to focus on analysis of the overall T-cell, CMV-specific, and EBV-specific $CD8^+$ T-cell responses.

To further phenotype the $CD8^+$ T-cells, the expression of the checkpoints 2B4, TIGIT, LAG3 and TIM3 were assessed, as shown in Figure 81. As observed in the previous chapters, the most

expressed checkpoints apart from PD1, were 2B4 and TIGIT, with a median of 62% and 38% respectively at cycle 1. LAG3 and TIM3 were expressed by a smaller percentage of T-cells, with medians of 0.5% and 4.5% respectively at cycle 1.

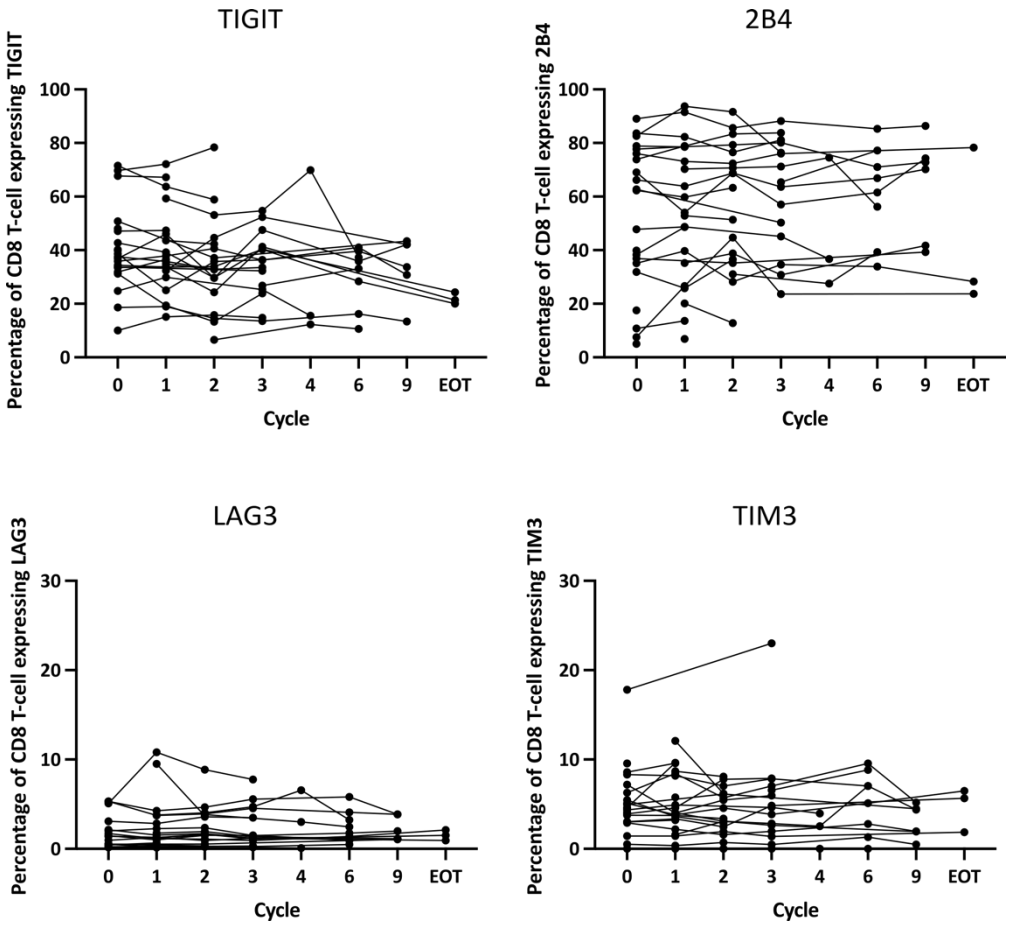

Figure 81: Checkpoint expression on CD8 T-cells after treatment

Summary of percentage of $CD8^+$ T-cells expressing the checkpoints TIGIT, 2B4, LAG3 and TIM3 after treatment with pembrolizumab. There were no significant changes across the cycles. Statistical analysis performed with Kruskal-Wallis test with Dunn's multiple comparisons test with $p < 0.05$. There was no statistical differences observed across the cycles.

As with the previous data, matched samples from cycles 0 and 1 were focussed on to give an indication of immediate effects the treatment was having on the T-cell response (Figure 82). Whilst there were no changes after one dose of treatment in the tetramer$^-$ or EBV-specific CD8$^+$ responses, interestingly there was a significant increase of TIGIT ($p = 0.0078$) and 2B4 ($p = 0.032$) in the CMV- tetramer$^+$ compartment. Whilst not significant, there was also trends of an increase in the percentage of CMV- tetramer$^+$ CD8$^+$ T-cells expressing TIM3 ($p = 0.38$) and a weak decrease in LAG3 ($p = 0.92$) with the trend in decreasing LAG3 being mirrored in both the tetramer$^-$ ($p = 0.25$) and EBV- tetramer$^+$ ($p = 0.22$) compartments.

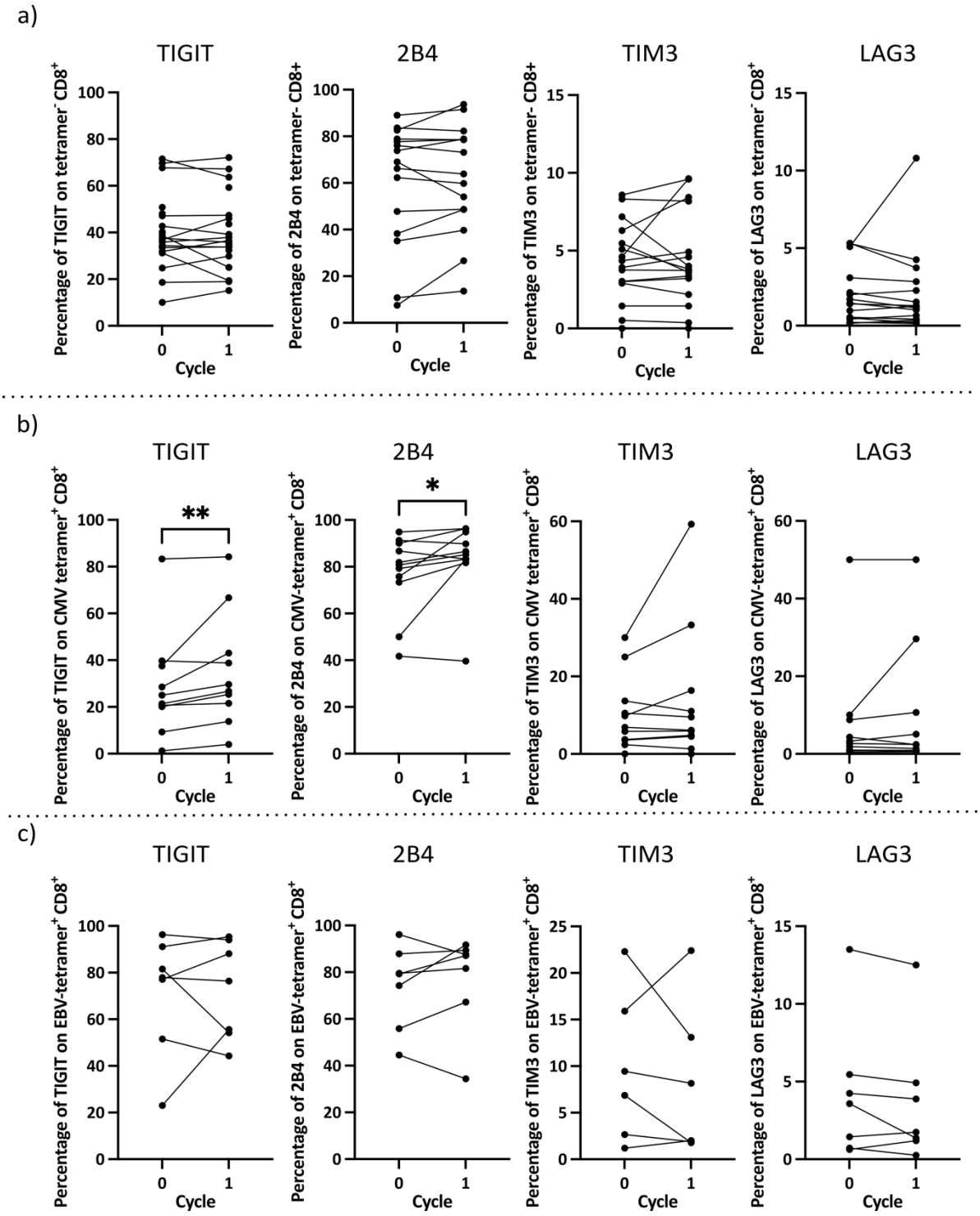

Figure 82: Checkpoint expression on virus-specific T-cells after one cycle of pembrolizumab

Summary of the percentage of 2B4, TIGIT, TIM3 and LAG3 expression on a) tetramer$^-$ (n = 15), b) CMV- tetramer$^+$ (n = 11) and c) EBV- tetramer$^+$ (n = 7) CD8$^+$ T-cells at cycle 0 (pre-treatment) and 1 (3 weeks after one dose of pembrolizumab). Statistical analysis performed with Wilcoxon matched-pairs signed rank test with * $p < 0.05$; ** $p < 0.01$

To identify activation, I assessed the co-expression of the markers HLA-DR and CD38 on all three compartments (Figure 83). Whilst not significant, there was a trend of an increase in HLA-DR/CD38 co-expression in the tetramer$^-$ compartment after one cycle of treatment (median at cycle 1 = 2.9%; median at cycle 2 = 3.2%; p = 0.0833).

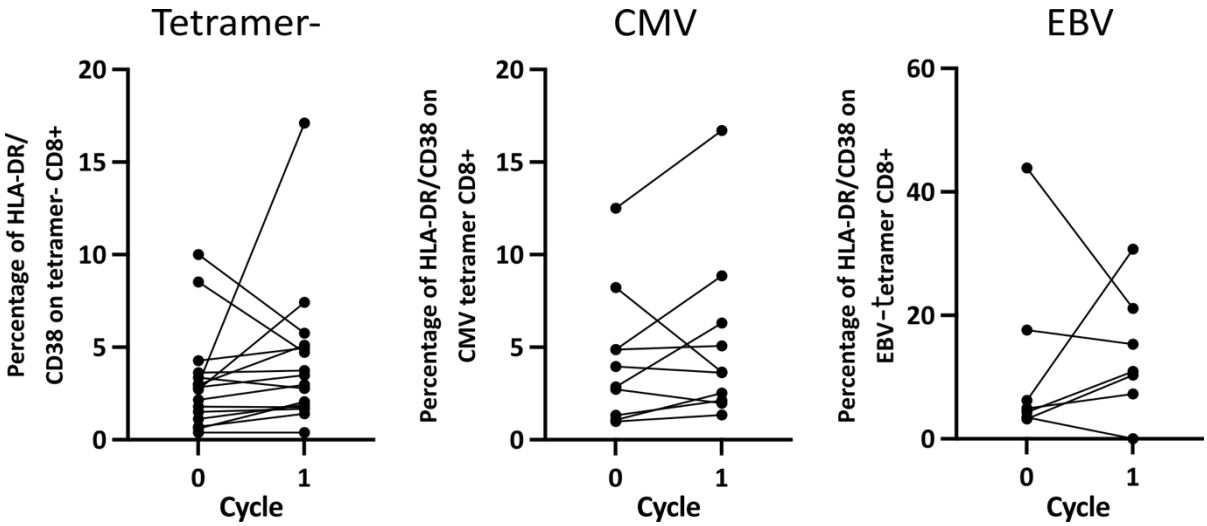

Figure 83: Expression of activation markers on T-cells following pembrolizumab

Summary of the percentage of cells co-expressing HLA-DR and CD38 on tetramer$^-$ (n = 15), CMV- tetramer$^+$ (n = 11) and EBV- tetramer$^+$ (n = 7) CD8$^+$ T-cells at cycle 0 (pre-treatment) and 1 (3 weeks after one dose of pembrolizumab). Statistical analysis performed with Wilcoxon matched-pairs signed rank test with $p < 0.05$. There was no statistical difference between populations.

To further assess how the T-cell populations were changing in response to pembrolizumab, the memory phenotypes were analysed using the markers CD45RA and CCR7. These allowed the establishment of naïve ($CD45RA^{+}CCR7^{+}$), central memory ($CD45RA^{-}CCR7^{+}$), effector memory ($CD45RA^{-}CCR7^{-}$) and T_{EMRA} ($CD45RA^{+}CCR7^{-}$) phenotypes.

Whilst no significant changes were seen there was a trend towards an increase in the CMV-tetramer^{+} populations of T_{CM} cells after one dose of pembrolizumab ($p = 0.083$) and a decrease in T_{EMRA} ($p = 0.067$) cells.

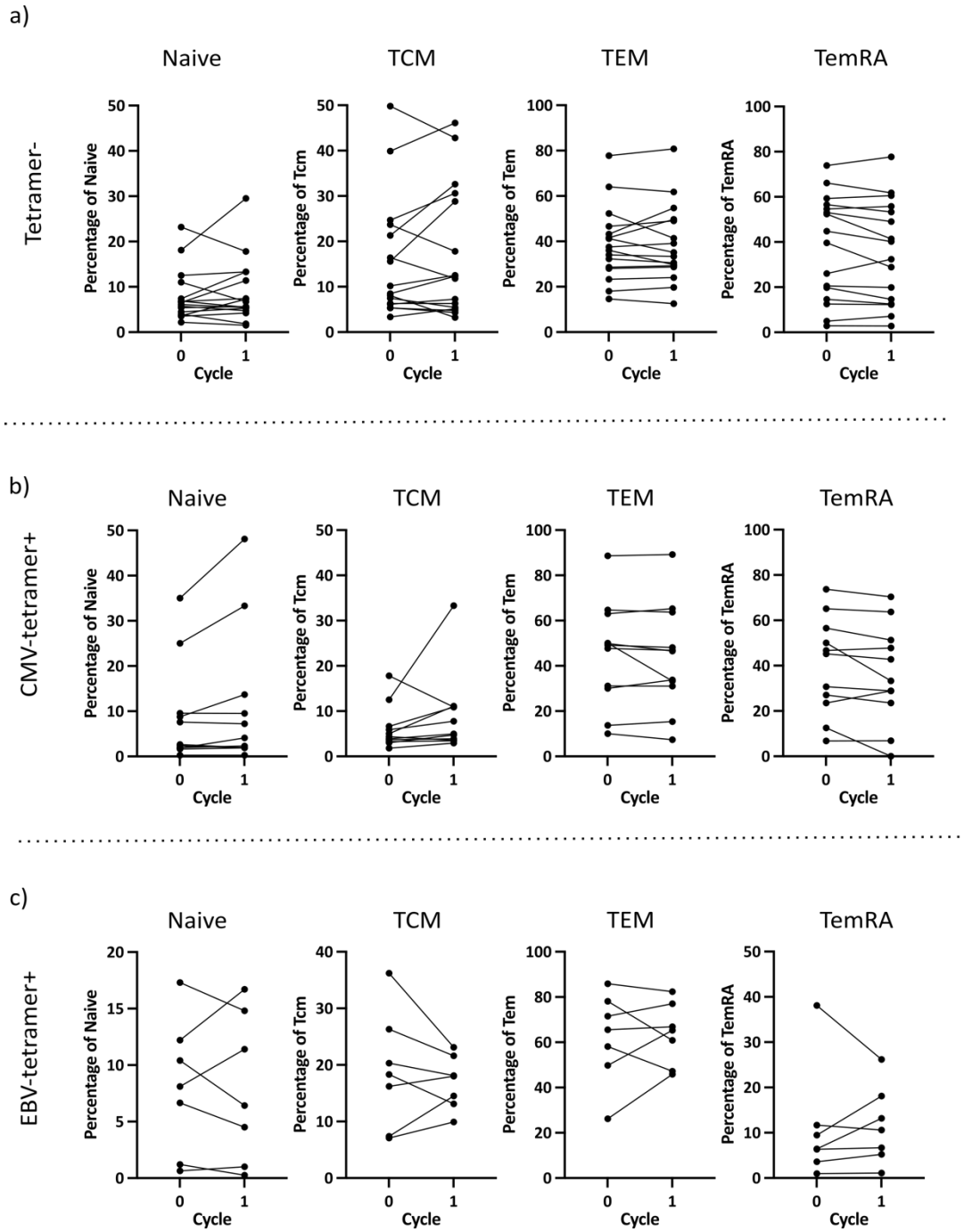

Figure 84: Memory phenotypes of virus-specific T-cells after one cycle of pembrolizumab

Summary of the percentage of naïve, central memory, effector memory and T_{EMRA} phenotypes on a) tetramer^{-} (n = 15), b) CMV- tetramer^{+} (n = 11) and c) EBV- tetramer^{+} (n = 7) CD8^{+} T-cells at cycle 0 (pre-treatment) and 1 (3 weeks after one dose of pembrolizumab). Statistical analysis performed with Wilcoxon matched-pairs signed rank test with $p < 0.05$. There was no statistical difference between populations.

5.2.7 The intracellular response to pembrolizumab

Next, I carried out analysis of the cytotoxicity marker granzyme B, the proliferation marker Ki67 and the transcription factors TCF-1 and T-bet.

As the cell count required for intranuclear staining is higher, there were less samples available for this analysis with a cohort of n = 15 tetramer$^-$ samples, n = 8 CMV-tetramer$^+$ samples and n = 5 EBV-tetramer$^+$ samples (Figure 85).

Whilst there were no significant changes, interestingly expression of the marker granzyme B, a mediator of cytotoxicity, showed a decreasing trend after one cycle of treatment in the CMV-tetramer$^+$ T-cell response (p = 0.48) and the EBV- tetramer$^+$ T-cell response (p = 0.63), but no change was seen in the tetramer$^-$ T-cell compartment. The median percentage of cells expressing granzyme was higher in the viral-specific cells (CMV median = 97%, EBV median = 83%) in comparison to the tetramer$^-$ compartment (median = 73%).

The transcription factor TCF1 is an effector transcription factor that plays a role in the proliferation of stem-like antigen-specific CD8$^+$ T-cells, and has been shown to predict an increased survival after checkpoint inhibitor therapy (Koh et al., 2022). Whilst pembrolizumab had no effect on the percentage of cells expressing TCF1, a lower median was observed in the CMV-tetramer$^+$ and EBV-tetramer$^+$ T-cells expressing TCF1 (median = 2.6% and 6.8% respectively) in comparison to the tetramer$^-$ compartment (median = 11%).

The marker Ki67 is a useful marker to highlight T-cell proliferation. Whilst this data showed a trend towards an increasing percentage of tetramer$^-$ cells expressing the intranuclear marker (p = 0.14), there was very little change in the CMV (p = 0.74) and EBV (p = 0.81) compartments.

There was no change in the expression of the transcription factor T-bet.

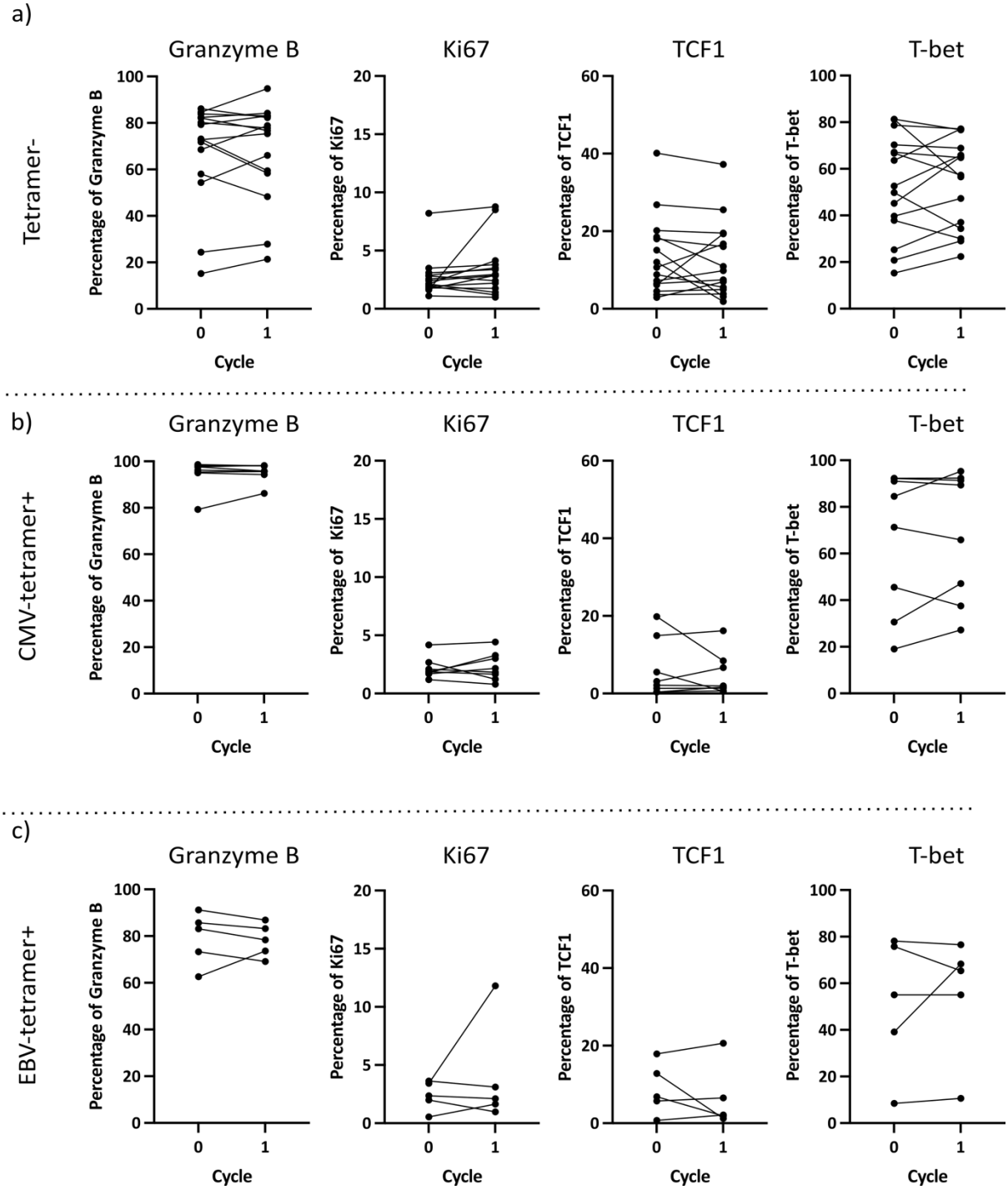

Figure 85: Cytokine and transcription factor expression in T-cells in relation to pembrolizumab treatment

Summary of the percentage of granzyme B, Ki67, TCF1 and T-bet expression on a) tetramer$^-$ (n = 15), b) CMV- tetramer$^+$ (n = 8) and c) EBV- tetramer$^+$ (n = 5) CD8$^+$ T-cells at cycle 0 (pre-treatment) and 1 (3 weeks after one dose of pembrolizumab). Statistical analysis performed with Wilcoxon matched-pairs signed rank test with $p < 0.05$. There was no statistical difference between populations.

The wider literature indicates TCF1 to be an important marker of $PD1^+$ T-cells which respond to checkpoint blockade (Koh et al., 2022). Therefore, markers of activation and proliferation (HLA-DR/CD38, Ki67 and TIGIT) were assessed on the $TCF1^+$ populations (Figure 86).

Whilst there were no significant changes in the $TCF1^+$ populations, some cell compartments did show trends. Primarily, the percentage of EBV- $tetramer^+$ $TCF1^+$ cells expressing HLA-DR and CD38 showed an increasing trend with 4/5 of the samples increasing after treatment with pembrolizumab (median cycle 1 = 2.8% and median cycle 2 = 11.3%; p = 0.13). Interestingly the opposite effect was seen in the CMV- $tetramer^+$ compartment with 5/8 of the samples showing a decrease in HLA-DR and CD38 co-expression on the $TCF1^+$ cells (median cycle 1 = 4.2% and median cycle 2 = 1.9%; p = 0.38). There was no trend observed in the $tetramer^-$ compartment.

Similarly, with Ki67 expression on $TCF1^+$ cells, the EBV compartment showed 4/5 donors with increased expression after one cycle of treatment (median cycle 1 = 4% and median cycle 2 = 9.4%; p = 0.38). This was mirrored in the $tetramer^-$ compartment with 10/15 samples showing an increase in expression (median at cycle 1 = 2.3% and median at cycle 2 = 2.5%; p = 0.14), however no trend was observed in the CMV- $tetramer^+$ compartment.

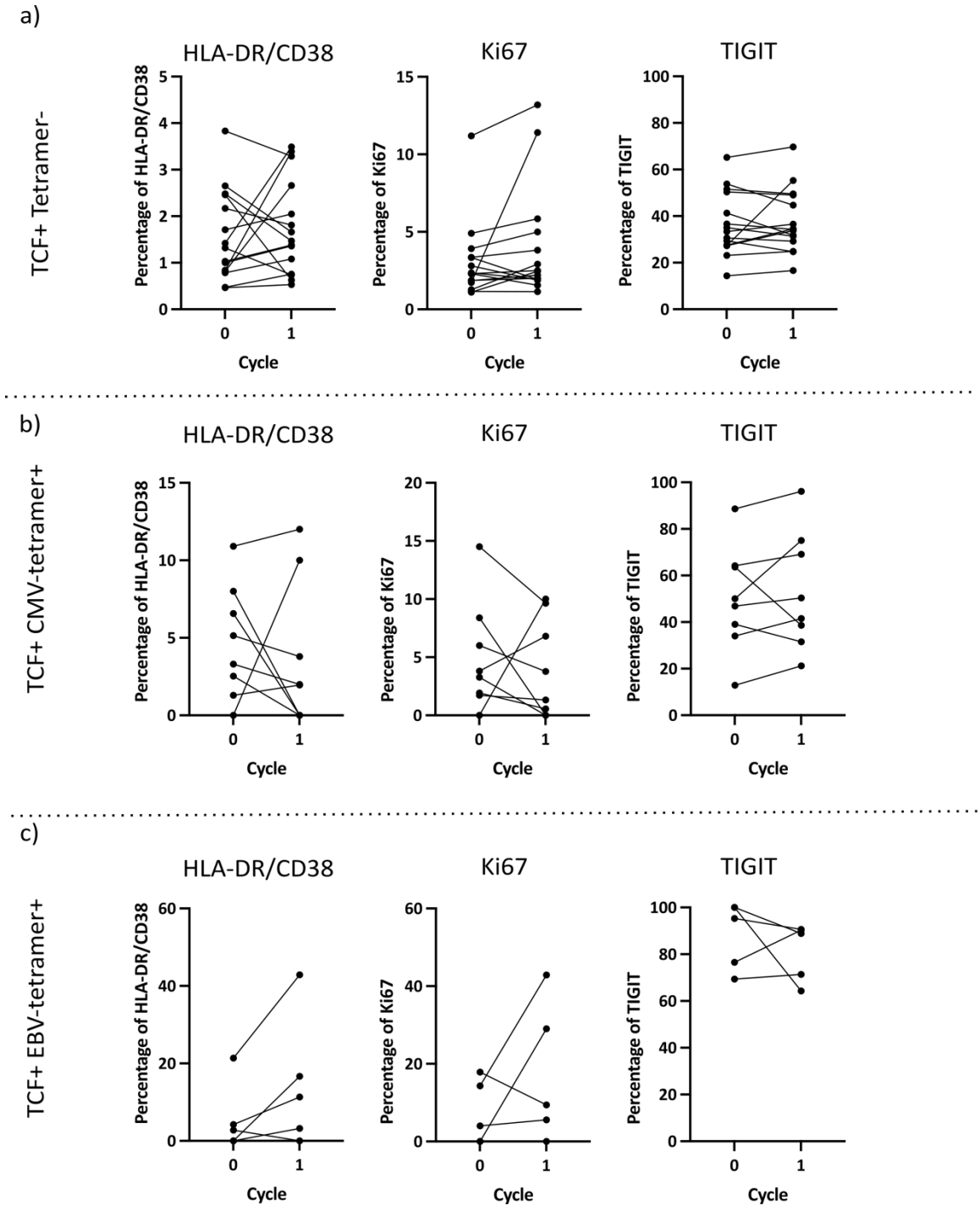

Figure 86: Activation and proliferation markers on TCF1$^+$ virus-specific cells

Summary of the percentage of TCF1$^+$ cells expressing HLA-DR/CD38, Ki67 and TIGIT on a) tetramer$^-$ (n = 15), b) CMV- tetramer$^+$ (n = 8) and c) EBV- tetramer$^+$ (n = 5) CD8$^+$ T-cells at cycle 0 (pre-treatment) and 1 (3 weeks after one dose of pembrolizumab). Statistical analysis performed with Wilcoxon matched-pairs signed rank test with $p < 0.05$. There was no statistical difference between populations.

5.2.8 CMV and EBV antibody titres in response to pembrolizumab

Finally, to assess for any changes in the IgG antibody levels of CMV and EBV after treatment with pembrolizumab, ELISAs were carried out. An in-house CMV-IgG ELISA, as described in Chapter 2, was used to assess the CMV-specific IgG levels in the CMV-seropositive donors (Figure 87). This was carried out prior to this study by Ms Jusnara Begum. The CMV-IgG titres remained stable over time following pembrolizumab treatment.

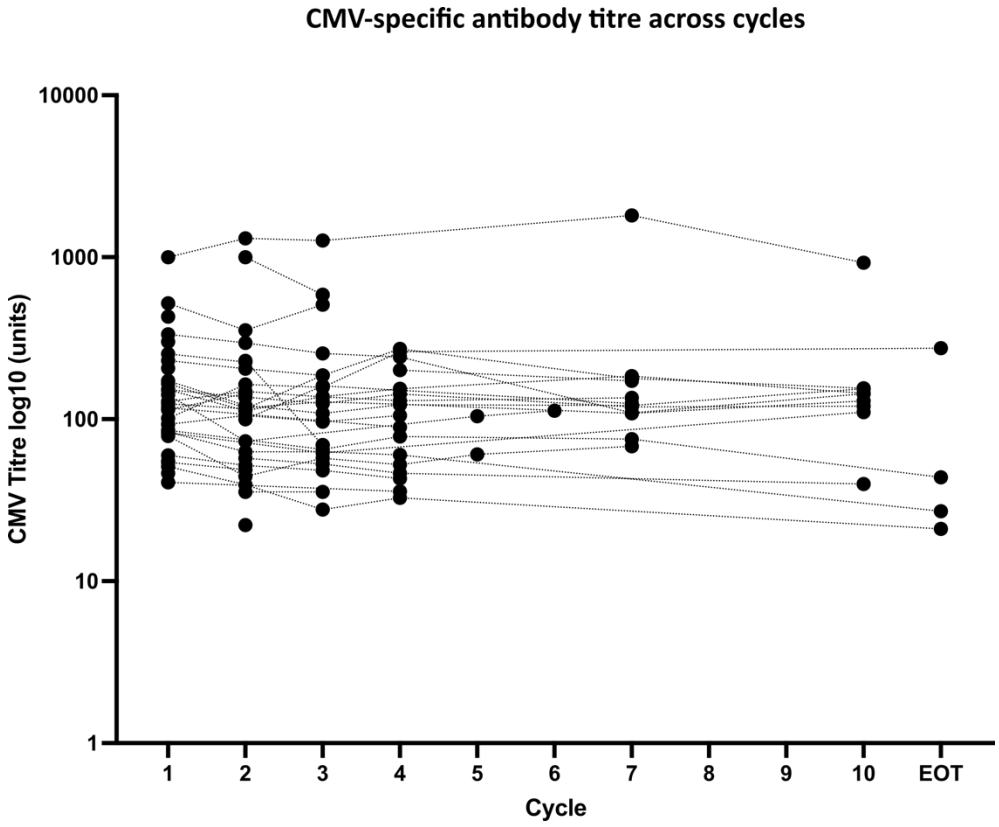

Figure 87: CMV IgG titre after treatment with pembrolizumab

Summary of CMV IgG titre for CMV-positive donors after cycles of treatment with pembrolizumab. There were no significant changes across the cycles. Statistical analysis performed with Kruskal-Wallis test with Dunn's multiple comparisons test with $p < 0.05$. There was no statistical differences observed across the cycles.

I also carried out an ELISA to detect EBV-specific antibodies using an EBV EBNA-1 IgG kit (alpha diagnostic) to assess EBV EBNA-1 IgG levels after treatment with ongoing cycles of pembrolizumab in the EBV-positive donors (Figure 88). The EBV IgG titres remained stable over time and there was no change in the EBNA3-IgG detected after treatment with pembrolizumab.

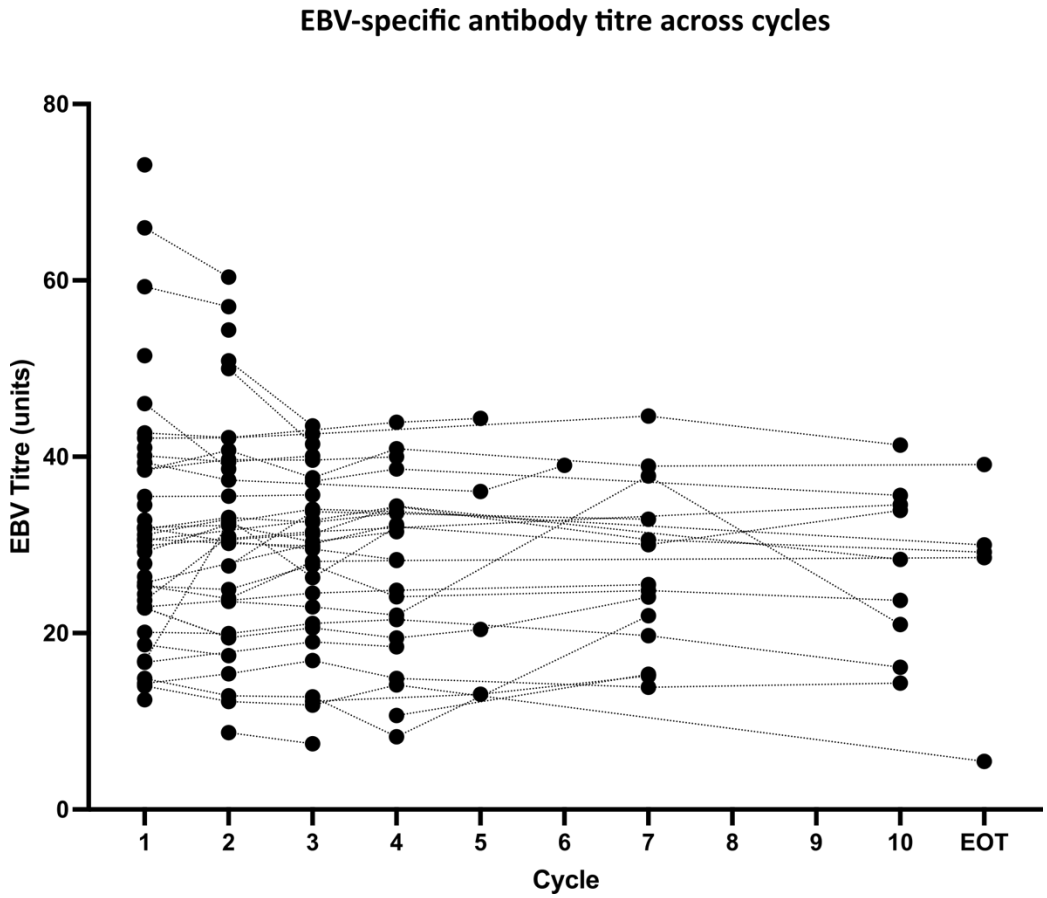

Figure 88: EBV IgG titre after treatment with pembrolizumab

Summary of EBV IgG titre for EBV-positive donors after cycles of treatment with pembrolizumab. There were no significant changes across the cycles. Statistical analysis performed with Kruskal-Wallis test with Dunn's multiple comparisons test with $p < 0.05$. There was no statistical differences observed across the cycles.

5.3 Discussion

PD1 blockade has revolutionised cancer treatment. However, little literature to date has focused on the response of viral-specific T-cells to this therapy, particularly in relation to the stage of treatment cycle. As T-cell responses against herpesviruses form such a significant compartment of the T-cell repertoire, and also tend to express high level of PD1, it is important to understand how therapies such as PD1 blockade can affect them. Furthermore, as research is being developed in relation to harnessing the viral-specific T-cell response to help treatment (Rosato et al., 2019, Millar et al., 2020), it is valuable to understand how PD1-blockade may have an impact on determinants of T-cell function. The findings in this study offer insights into the dynamics of the general T-cell, CMV-specific and EBV-specific populations in response to pembrolizumab , one of the most widely used PD1-blocking antibodies in clinical practice.

5.3.1 Differences in the baseline characteristics of viral-specific T-cells in patients with NSCLC

My initial analysis focussed on the baseline characteristics of the T-cells in patients with NSCLC. Whilst the overall immune composition of patients undergoing therapies has been widely studied, the inclusion of phenotyping viral-specific T-cells is a novel feature of this study.

T_{EM} and T_{EMRA} phenotypes dominate the CMV- tetramer^{+} compartment in comparison to EBV which is primarily composed of T_{CM} and T_{EM} cells. Whilst most reports on $CD8^{+}$ T_{EMRA} cells indicate a terminally differentiated subset with a short telemeter length and low proliferative capacity (Lee et al., 2021), this is challenged by data in viral-specific T-cells. Studies have found that upon antigenic stimulation with cytokine support, CMV-specific $CCR7^{-}CD27^{-}$ $CD45RA^{+}$

T_{EMRA} cells undergo clonal expansion, reverting to a $CD45RA^-$ phenotype with the cells re-expressing CCR7 (van Leeuwen et al., 2002, Wills et al., 2002). The high number of CMV-specific T_{EMRA} cells at baseline could therefore indicate cells that have not recently seen antigen.

One of the reasons EBV cells may have more recently seen antigen is that EBV has been implicated in forms of lung cancer. One subtype of NSCLC, pulmonary lymphoepithelioma-like carcinoma (LELC), shows a strong association with EBV infection. In a study conducted in China, 93.8% (30/32) of LELC cases tested positive for EBV-encoded small RNA (EBER) via in-situ hybridisation (ISH)) (Han et al., 2000). For this reason, the EBV-specific T-cells could be seeing viral antigen more frequently and by staying in this more activated state, might be less likely to enter the T_{EMRA} phase, and instead continue to respond to persistent viral antigen in the tumour environment. I was not able to study potential expression of EBV within tumour samples from this patient cohort in my study.

The data in this chapter also shows that CMV-specific T-cells expressed increased amounts of granzyme B in comparison to EBV. Granzyme B is a key marker of cytotoxic T-cell activity, responsible for initiating apoptosis in target cells. It activates the caspase cascade by cleaving caspase-3, ultimately leading to cell death. It plays a crucial role in immune responses, particularly for eliminating virus-infected or malignant cells (Hay and Slansky, 2022). As the EBV-specific T-cells express significantly less granzyme B, it suggests these cells are less functional, which along with the increased PD1 and TIGIT, could indicate dysregulation of the cells due to repeated antigen stimulation.

There is no substantial evidence supporting the presence of CMV infection within lung tumours, or the expression of CMV proteins or DNA in such contexts. Therefore, it is less likely that CMV-specific T-cells in these tumours are encountering antigen, which may explain their relatively less dysfunctional phenotype. These cells are therefore more likely to enter a "resting" T_{EMRA} state while maintaining their ability to produce granzyme B, indicating preserved cytotoxic functionality.

5.3.2 CMV-specific T-cells display less PD1, but more 2B4 and LAG3, in NSCLC patients compared to healthy donors

As expected, there are differences in the checkpoint profiles of patients with performance status 2 NSCLC who have undergone previous treatment and healthy donors.

Interestingly, the expression of PD1 is lower on the circulating T-cells in the NSCLC patients than in the healthy donors. As the data in Chapter 3 shows the $PD1^+$ CMV-specific T-cells are indeed the more functional cells, with an increase in IFNγ production in the $PD1^+$ cells, and an increasing trend in TNFα, granzyme B and perforin production, it may be that downregulation of PD1 in fact indicates dysregulation of these cells. This is in line with a study which found CMV and Flu-specific $CD8^+$ T-cells to be predominantly of a $PD1^-$ $TIGIT^-$ phenotype in patients with melanoma (Chauvin et al., 2015b).

Conversely, there was an increase in 2B4 and LAG3 expression on CMV-$tetramer^+$ T-cells in particular. Chronic expression of these markers typically represent a dysregulated cell state and are upregulated in response to chronic antigenic stimulation (Mariuzza et al., 2024, Utzschneider et al., 2020). A study by Li, *et al.* (2019) demonstrated similar findings with a reduction in PD1 yet an increase in 2B4 on circulating $CD8^+$ T-cells in comparison to T-cells in

tumour tissues (Li et al., 2019). This has implications as LAG3 blockade in particular is starting to be implemented in combination with PD1 blockade to treat cancers such as melanoma, with positive outcomes such as improved overall survival being observed (Kreidieh and Tawbi, 2023). However, given the expression of LAG3 on peripheral CMV-tetramer^{+} CD8^{+} cells in NSCLC patients, it could lead to an increase in immune-related adverse effects, particularly given what a large compartment of the T-cell response is dedicated to CMV-specific responses in older individuals. Treatment via a local injection may be able to counteract this by targeting more localised T-cells rather in comparison to a systemic infusion.

Previous studies have highlighted that, whilst only a small subset, patients undergoing checkpoint blockade can present with CMV-related adverse events such as CMV-related gastritis or colitis due to T-cells targeting sites of CMV infection such as the gastrointestinal tract (Tay et al., 2022, Anastasopoulou et al., 2023). Therefore, it is important to consider how emerging checkpoint blockade treatments may affect these circulating T-cells if they are displaying upregulation of LAG3 and 2B4.

5.3.3 CMV-specific T-cells express checkpoint proteins in response to pembrolizumab therapy

Whilst pembrolizumab works by blocking PD1, the analysis of other checkpoint molecules (2B4, TIGIT, LAG3 and TIM3) allowed for the detection of any other interesting patterns in the T-cell populations. After one cycle of pembrolizumab, CMV-specific CD8^{+} T-cells showed a significant increase in TIGIT and 2B4. This increase may indicate that the CMV-specific T-cells are becoming more activated after treatment, although a potential for short term functional exhaustion should also be considered. This additional checkpoint expression could reflect a

compensatory mechanism whereby alternative inhibitory pathways are upregulated during antigen engagement when the PD1-PDL1 interaction is blocked. TIGIT, in particular, has been shown to be linked with PD1 expression, with an upregulation of TIGIT being observed on $CD8^+$ T-cells specific for the tumour antigen NY-ESO-1 in response to PD1 blockade in melanoma patients (Chauvin et al., 2015b). TIGIT competes with the marker CD226 (DNAM-1) for ligands as they both bind to poliovirus receptor (PVR) and nectin-2 (CD112) which are both expressed on APCs, tumours and virus-infected cells (Shibuya and Shibuya, 2021). A study showed a deficiency in CD226 led to reduced efficacy in PD1 blockade and furthermore, revealed with RNA-seq that expression of *CD226* was closely correlated with *PDCD1* and *TIGIT* (Banta et al., 2022). These highlight that the PD1 and TIGIT pathways may be closely linked and could provide an explanation for why TIGIT increases in response to checkpoint blockade. Furthermore, the dual blockade of both TIGIT and PD1 has been shown to enhance antitumour immunity in multiple mouse studies (Johnston et al., 2014, Hung et al., 2018, Ge et al., 2021).

As Chauvin *et al.* showed a 1.5 fold increase in the MFI of TIGIT expression on NY-ESO-1 specific T-cells in response to PD1-blockade, and the increase in TIGIT in this study was only observed on the CMV-specific T-cells, it could indicate an antigen-specific phenomenon (Chauvin et al., 2015b).

Interestingly, the co-expression of HLA-DR and CD38 was shown to have the biggest increase in the $tetramer^-$ compartment after one cycle of pembrolizumab. This indicates that the PD1 blockade is increasing the activation of a substantial population of T-cells, albeit of unknown antigenic specificity. It could be possible that these represent some of the tumour-specific T-cells that are believed to mediate the therapeutic activity of pembrolizumab treatment. This

effect was not seen on the CMV-specific population indicating these cells are not becoming more activated.

If PD-1 blockade were to impact negatively on the activity of CMV-specific T-cells then this could indeed lead to a decrease in effective viral control, potentially resulting in increased viremia. I did not undertake any functional studies of the CMV-specific T-cell pool in my thesis and so cannot interpret this directly. I did observe a shift in the T-cell phenotype of this population over time, with a reduction in T_{EMRA} and an increase in T_{CM} cells as they revert to a $CCR7^{+}$ $CD45RA^{-}$ phenotype.

While few significant changes were observed in the CMV-specific and EBV-specific T-cells in response to pembrolizumab, this observation is important given recent studies exploring the potential of harnessing viral-specific T-cells to treat malignancies. Indeed, several studies are exploring how viral-specific T-cells could be redirected or enhanced to target tumours. EBV-specific T-cells, for example, have been historically investigated in EBV-associated cancers, with the infusion of EBV-specific T-cells displaying antitumour activity in EBV-positive nasopharyngeal carcinoma patients (Straathof et al., 2005, Huang et al., 2017). More recent studies are also beginning to investigate this in conjugation with other treatments such as chemotherapy with the patients receiving both therapies displaying a progression free survival of 7.6 months vs 3.7 months for the patients receiving the EBV-specific T-cell infusion alone (Chia et al., 2014). This highlights the importance of virus-specific T-cells as a form of therapy, and it is important to understand how they may react to immunotherapy if it was to be given in combination to ensure optimal results.

Furthermore, other studies are investigating the use of viral-specific T-cells in other ways. For example reactivating viral-specific T-cells to arrest tumour growth (Rosato et al., 2019) or by using antibody-peptide epitope conjugates to deliver CMV-derived epitopes for presentation on the tumour surface to encourage targeting by CMV-specific T-cells (Millar et al., 2020). These approaches could offer a viable alternative or complement to cancers that are resistant to checkpoint inhibitors alone. Understanding how other immunotherapies may impact viral-specific T-cells is crucial for optimising combination treatments.

5.3.4 PD1 blockade does not affect CMV and EBV antibody levels

Finally, the work showed that the antibody titres for CMV and EBV IgG did not change in response to treatment. This is not entirely surprising as a study by Tay, *et al.* (2021) found that out of 11485 cancer patients undergoing some form of checkpoint blockade, only 62 had detectable CMV DNA throughout treatment and CMV disease was only detected in 10 of these (16%) (Tay et al., 2022). Conversely, in immunosuppressed patients, CMV reactivation can occur due to immune-related adverse events. Treatments such as checkpoint blockade compromise immune function, enabling local viral reactivation, which becomes difficult to control due to the ongoing immunosuppression (Franklin et al., 2017, Anastasopoulou et al., 2023). CMV reactivation has been shown to be associated with increased CMV-specific IgG titre (Kawamura et al., 2021, Arcuri et al., 2020). As the data in this study showed little changes in the overall T-cell response, and no significant changes in the antibody titres, it suggests that PD1 blockade in this case does not lead to significant changes in the balance of the herpesvirus-specific immune response and viral load.

5.3.5 Limitations and future work

One of the limitations of this study was the ability to effectively discriminate the cells that are responding directly to pembrolizumab. Future work should involve further optimisation of IgG4 staining to allow for direct detection of the cells bound to pembrolizumab as it is important to determine the direct effect the drug has on the viral-specific T-cells.

Another major limitation was the difficulty in linking the data with the clinical outcomes. Due to the patients having all received significant previous treatment, and being at a more advanced stage of cancer, a significant proportion died early on in treatment. Furthermore, almost all patients exhibited multiple side effects. It would be interesting to assess side effects that may be directly related to CMV or EBV, such as CMV-related colitis or gastritis, although it has been reported that cases of CMV reactivation and therefore related side effects in patients who had not received immunosuppressants, is rare (Anastasopoulou et al., 2023).

Additionally, it was not always possible to receive samples at every cycle, therefore, it would be interesting to have matched samples for the first four cycles of treatment for a more comprehensive analysis of the effect of the drug on T-cells.

A further limitation of this study was the small amount of cells available, meaning tetramers had to be combined to ensure the highest amount possible of viral-specific T-cells were detected, due to them comprising such a small percentage of total PBMC. It would be interesting to assess the responses individually, and also to expand the tetramers used to cover a wider variety of epitopes.

Another limitation in regards to the tetramers, is that it is not possible to collect all the viral-specific T-cells due to availability of tetramer, therefore despite using tetramers for known

immunodominant epitopes, it is likely the tetramer$^-$ compartment will contain some cells specific for other tetramers. One way to diminish the amount of cells not being analysed would be to identify cells using stimulation by a peptide pool spanning a wide range of peptides. However, this presents its own challenges as the stimulation will affect the phenotype of the T-cells.

The small number of cells also meant it was not possible to extract DNA for PCR to quantify viral DNA. Importantly, this could give an indication of whether the checkpoint blockade is indeed leading to increased viremia of CMV and how the levels of EBV change. This could also be achieved if urine samples were able to be collected.

Finally, it would be interesting to assess the viral-specific T-cells present in the tumour, as the data in Chapter 5 showed that there was an increase in the MFI of PD1 within the tumour, it would be interesting to evaluate if the effect of PD1-blockade on viral-specific T-cells within the tumour to understand if they did indeed become more activated.

5.3.6 Conclusions

This study offers valuable insights into the response of virus-specific T-cells in NSCLC patients undergoing treatment with pembrolizumab. While the role of PD1 inhibitors in cancer therapy is well established, the effect of such treatments on virus-specific T-cells, in particular CMV and EBV-specific, remains less understood, despite the significant proportion of these cells within the T-cell compartment.

This study highlights the unique behaviours of CMV-specific and EBV-specific T-cells, identifying notable differences in phenotypes, checkpoint expression and activation markers. CMV-specific T-cells were primarily T_{EMRA} cells, which may indicate a “resting” state,

contributing to long-term viral control while maintaining cytotoxic potential. Conversely, EBV-specific T-cells displayed more activation markers (HLA-DR/CD38), suggesting frequent antigen encounters within the tumour environment, possibly due to latent viral reactivation.

Importantly, the study also suggests the impact of pembrolizumab on viral-specific T-cells differs depending on the virus, with the CMV-specific T-cells showing an increase in some inhibitory markers such as TIGIT, but this effect not mirrored in the EBV-specific T-cells. With ongoing research investigating the potential for viral-specific T-cells to enhance tumour-targeting capabilities, understanding how PD1 blockade affects these T-cells is crucial for optimising combination therapies.

Overall, this research underscores the complexity of viral-specific T-cell dynamics in the context of immunotherapy and highlights the need for further exploration into how they can be effectively integrated into therapies.

CHAPTER 6: FINAL DISCUSSION

Cytomegalovirus is a member of the β-herpesvirus family and has evolved with mammalian hosts to establish lifelong persistent infection. The virus generally persists asymptomatically in healthy individuals and is controlled by sustained immune surveillance. The $CD8^+$ T-cell response plays a key immune role in suppression of viral reactivation and this cell formed the focus of my study (Riddell et al., 1992, Elkington et al., 2003, Sylwester et al., 2005). CMV-specific T-cell populations constitute a large portion of the overall $CD8^+$ T-cell repertoire in CMV seropositive people and this can increase further with age (Klenerman and Oxenius, 2016, Kim et al., 2015).

The focus of my thesis was on the expression of the checkpoint protein PD1 on CMV-specific $CD8^+$ T-cells. My findings were often compared to the immune response to EBV which allowed me to highlight distinctions in immune dynamics between these chronic infections. In initial work I assessed the relative scale of the $CD8^+$ T-cell response against CMV and EBV as this could impact on the potential relevance of checkpoint protein function. The magnitude of the CMV-specific $CD8^+$ T-cell response was typically larger than that of the EBV-specific pool, and this was particularly notable in the immune response against EBV proteins from the latent phase of viral replication. CMV-specific T-cells were mostly of the T_{EM} and T_{EMRA} phenotypes, whilst EBV-specific responses often included a sizable T_{CM} pool.

Of interest, the expression of checkpoint proteins was typically somewhat lower on CMV-specific T-cells in comparison to the EBV-specific response. In addition, there were clear differences in relative expression of individual proteins with 2B4 being observed preferentially on CMV-specific cells whilst TIGIT was more represented on the EBV-specific T-cell pool. Somewhat unexpectedly, despite PD1 expression being typically associated with functional

exhaustion, I observed that CMV-specific $PD1^+$ $CD8^+$ T-cells were enhanced in relative production of TNFα and IFNγ.

I next went on to characterise viral-specific $CD8^+$ T-cells in ovarian cancer, confirming the presence of these T-cells in the tissue and identifying a subset of $PD1_{HIGH}$ T_{RM} cells with upregulation of checkpoint markers PD1, LAG3 and TIM3. This $PD1_{HIGH}$ pool was found only in tissue and the checkpoint profile was markedly different to that seen on the $PD1_{MID}$ population that is dominant in blood. Further functional analysis of these subsets is now required in order to delineate their relative role and function.

Finally, I examined virus-specific T-cell phenotype and function in patients with lung cancer who were undergoing treatment with PD-1 inhibitors. This patient group have undergone chemotherapy regimens prior to consideration for PD1 inhibition and this may relate to the observation that PD1 expression was somewhat reduced on the CMV-specific T-cell pool whilst increased on the EBV-specific response. It will be of interest to assess viral load measurement of the two viruses in this population group to assess if this is a determinant of this differential profile. Pembrolizumab treatment was seen to lead to relatively small changes in checkpoint molecule expression on virus-specific T-cells, with TIGIT being the most notable in this regard.

Together this data highlights the multiple roles PD1 may play in immune regulation.

PD1 is expressed on a variety of haematopoietic cells and, upon engagement of its ligands PD-L1 or PD-L2, exerts a inhibitory effect on cellular activation (Keir et al., 2008). PD1 expression is a marker of recent activation of T-cells and can also act as a marker of exhaustion during chronic stimulation of T-cells as seen within tumour microenvironments (Wu et al., 2014, Ahn

et al., 2018) or chronic viral infections such as HIV (Trautmann et al., 2006), HBV (Boni et al., 2007) and HCV (Radziewicz et al., 2007).

The potential importance of PD1 expression on CMV-specific T-cells remains unclear. Previous research has established that CMV-specific $CD8^+$ T-cells are functional and can produce Th1 cytokines such as TNFα and IFNγ, illustrating a likely key role in immune defence against infection (Hosie et al., 2017). A notable finding from my study was that $PD1^+$ CMV-specific T-cells release more Th1 cytokines compared to the $PD1^-$ population. As such, in the setting of CMV infection, PD1 expression may indicate activation and enhanced cellular function, rather than exhaustion, and thus contrasting with its role in T-cell exhaustion observed in states of poorly controlled chronic infections (Day et al., 2006, Sandu et al., 2020).

Interestingly, the regulation and functional correlates of PD1 expression on $CD4^+$ viral-specific T-cells appears different from its role on $CD8^+$ T-cells. While $CD8^+$ T-cell responses are critical in controlling viral infections by directly targeting infected cells, the $CD4^+$ compartment also plays a crucial role in the immune response. Specifically, $CD4^+$ T-helper cells assist in the generation and maintenance of virus-specific $CD8^+$ T-cells, enhancing the overall immune response (van Leeuwen et al., 2006, Widmann et al., 2008, Boeckh et al., 2003).

Prior work has shown that the expression of PD1 on $CD4^+$ cells is not linked to activation or exhaustion, but instead appears to be influenced by a 'set point', which correlates with the viral load present during primary infection (Parry et al., 2021). This contrasts with the typical role of PD1 on $CD8^+$ T-cells, where it marks activation or exhaustion depending on the context of the infection or malignancy. Furthermore, the study by Parry *et al.* showed that PD1 expression remains stable on antigen-specific $CD4^+$ T-cell populations despite recent antigen

stimulation. This PD1 expression 'set point' concept suggests that PD1 on $CD4^+$ T-cells may be less about dynamic change in response to recent activation and more reflective of long-term viral control dynamics, which may also influence the quality and scope of the $CD8^+$ T-cell response.

My work further shows that CMV-specific and EBV-specific T-cells are able to enter ovarian tissue. The infiltration of viral-specific T-cells has been previously demonstrated in various tumours (Simoni et al., 2018, Wei and Ishizuka, 2021, Crough et al., 2012). However, to the best of my knowledge, my work is the first in-depth phenotype of CMV-specific and EBV-specific $CD8^+$ T-cells in primary and metastatic ovarian cancer tissues. Chapter 4 demonstrates the presence of $PD1_{MID}$ and $PD1_{HIGH}$ viral-specific T-cells in the tissue, whilst PBMC only displayed the $PD1_{MID}$ population, at levels of PD1 comparable to that seen in the healthy donors in Chapter 3. The data in Chapter 3 suggests that this $PD1_{MID}$ population is functional, indeed with increased cytokine production, and suggests that this capacity may be functional within tissue. In contrast, cells with $PD1_{HIGH}$ phenotype might be expected to have somewhat reduced capacity. This is supported by a study by Kansy, B. *et al.* showing that an increased number of $PD1_{HIGH}$ TIL was associated with worse disease-free survival, with the dysfunctional T-cell demonstrating impaired IFNγ production (Kansy et al., 2017). Interestingly, the opposite effect was seen on $CD4^+$ T-cells in patients with follicular lymphoma whereby $PD1_{HIGH}$ cells displayed less exhaustion in comparison to a $PD1_{LOW}$ subset which displayed an upregulation of TIM3 and were unable to produce IFNγ in response to stimulation (Yang et al., 2015). This once again highlights the substantial differences in the dynamics and role of PD1 amongst different T-cell subsets and across different cancers.

Novel therapies involving harnessing viral-specific T-cells are providing promising strategies for treatment in certain tumours. The detection of CMV antigens in glioblastoma has allowed for new therapies such as adoptive transfer of CMV-specific T-cells, or vaccination with pp65-specific dendritic cells, which when administered in combination with other treatment, are displaying improved results such as increased overall survival and progression free survival (Crough et al., 2012, Batich et al., 2017). This may be feasible for glioblastoma as several studies have shown that CMV infection may act to drive tumour progression. However, this is not confirmed for other malignancies. Therefore, further studies are investigating immunotherapies that may act to repurpose T-cells to target the tumour (Sefrin et al., 2019, van der Wulp et al., 2024). This is particularly useful as CMV-specific T-cells take up such a significant portion of the T-cell repertoire, and my data indicates that the $PD1_{MID}$ cells are functional and therefore may be able to effectively target tumour cells in this setting.

In conclusion, the collective insights from this study highlight key distinctions between the immune responses of CMV-specific and EBV-specific $CD8^+$ T-cells, emphasising the diverse reactivity of CMV-specific T-cells. These exhibit activation despite chronic stimulation, suggesting they remain functional for ongoing immune surveillance. This study also sheds light on the nuanced role of PD1, revealing it as a potential marker for more activated cells on CMV-specific T-cells. Further exploration into repurposing viral-specific T-cells could offer significant therapeutic advantages, particularly in combination with other treatment. However, overall, the insights from this study provide a strong foundation for developing novel immunotherapeutic approaches, with implications for treating tumours that may not be showing optimal response rates due to the difficulty in harnessing exhausted T-cells that are specific for tumour-specific antigens.

CHAPTER 7: BIBLIOGRAPHY

ADAMS, E. J., GU, S. & LUOMA, A. M. 2015. Human gamma delta T cells: Evolution and ligand recognition. *Cell Immunol,* 296**,** 31-40.
ADAMSON, C. S. & NEVELS, M. M. 2020. Bright and Early: Inhibiting Human Cytomegalovirus by Targeting Major Immediate-Early Gene Expression or Protein Function. *Viruses,* 12**,** 110.
AGRATI, C., CASTILLETTI, C., CASETTI, R., SACCHI, A., FALASCA, L., TURCHI, F., TUMINO, N., BORDONI, V., CIMINI, E., VIOLA, D., LALLE, E., BORDI, L., LANINI, S., MARTINI, F., NICASTRI, E., PETROSILLO, N., PURO, V., PIACENTINI, M., DI CARO, A., KOBINGER, G. P., ZUMLA, A., IPPOLITO, G. & CAPOBIANCHI, M. R. 2016. Longitudinal characterization of dysfunctional T cell-activation during human acute Ebola infection. *Cell Death Dis,* 7**,** e2164.
AGRAWAL, S., KHOKHAR, A. & GUPTA, S. 2019. Cytomegalovirus Colitis in Primary Hypogammaglobulinemia With Normal CD4+ T Cells: Deficiency of CMV-Specific CD8+ T Cells. *Front Immunol,* 10**,** 399.
AHMAD, F., SHANKAR, E. M., YONG, Y. K., TAN, H. Y., AHRENSTORF, G., JACOBS, R., LARSSON, M., SCHMIDT, R. E., KAMARULZAMAN, A. & ANSARI, A. W. 2017. Negative Checkpoint Regulatory Molecule 2B4 (CD244) Upregulation Is Associated with Invariant Natural Killer T Cell Alterations and Human Immunodeficiency Virus Disease Progression. *Front Immunol,* 8**,** 338.
AHMADZADEH, M., JOHNSON, L. A., HEEMSKERK, B., WUNDERLICH, J. R., DUDLEY, M. E., WHITE, D. E. & ROSENBERG, S. A. 2009. Tumor antigen-specific CD8 T cells infiltrating the tumor express high levels of PD-1 and are functionally impaired. *Blood,* 114**,** 1537-44.
AHN, E., ARAKI, K., HASHIMOTO, M., LI, W., RILEY, J. L., CHEUNG, J., SHARPE, A. H., FREEMAN, G. J., IRVING, B. A. & AHMED, R. 2018. Role of PD-1 during effector CD8 T cell differentiation. *Proceedings of the National Academy of Sciences,* 115**,** 4749-4754.
AI, L., CHEN, J., YAN, H., HE, Q., LUO, P., XU, Z. & YANG, X. 2020. Research Status and Outlook of PD-1/PD-L1 Inhibitors for Cancer Therapy. *Drug Des Devel Ther,* 14**,** 3625-3649.
ALDY, K. N., HORTON, N. C., MATHEW, P. A. & MATHEW, S. O. 2011. 2B4+ CD8+ T cells play an inhibitory role against constrained HIV epitopes. *Biochemical and Biophysical Research Communications,* 405**,** 503-507.
ALP, N. J., ALLPORT, T. D., VAN ZANTEN, J., RODGERS, B., SISSONS, J. G. & BORYSIEWICZ, L. K. 1991. Fine specificity of cellular immune responses in humans to human cytomegalovirus immediate-early 1 protein. *J Virol,* 65**,** 4812-20.
ALTMAN, J. D., MOSS, P. A., GOULDER, P. J., BAROUCH, D. H., MCHEYZER-WILLIAMS, M. G., BELL, J. I., MCMICHAEL, A. J. & DAVIS, M. M. 1996. Phenotypic analysis of antigen-specific T lymphocytes. *Science,* 274**,** 94-6.
AMIR EL, A. D., DAVIS, K. L., TADMOR, M. D., SIMONDS, E. F., LEVINE, J. H., BENDALL, S. C., SHENFELD, D. K., KRISHNASWAMY, S., NOLAN, G. P. & PE'ER, D. 2013. viSNE enables visualization of high dimensional single-cell data and reveals phenotypic heterogeneity of leukemia. *Nat Biotechnol,* 31**,** 545-52.

ANASTASOPOULOU, A., SAMARKOS, M., DIAMANTOPOULOS, P., VOURLAKOU, C., ZIOGAS, D. C., AVRAMOPOULOS, P., KOUZIS, P., HAANEN, J. & GOGAS, H. 2023. Cytomegalovirus Infections in Patients Treated With Immune Checkpoint Inhibitors for Solid Malignancies. *Open Forum Infect Dis,* 10**,** ofad164.

ANDERSON, ANA C., JOLLER, N. & KUCHROO, VIJAY K. 2016. Lag-3, Tim-3, and TIGIT: Co-inhibitory Receptors with Specialized Functions in Immune Regulation. *Immunity,* 44**,** 989-1004.

APPAY, V., DUNBAR, P. R., CALLAN, M., KLENERMAN, P., GILLESPIE, G. M. A., PAPAGNO, L., OGG, G. S., KING, A., LECHNER, F., SPINA, C. A., LITTLE, S., HAVLIR, D. V., RICHMAN, D. D., GRUENER, N., PAPE, G., WATERS, A., EASTERBROOK, P., SALIO, M., CERUNDOLO, V., MCMICHAEL, A. J. & ROWLAND-JONES, S. L. 2002. Memory CD8+ T cells vary in differentiation phenotype in different persistent virus infections. *Nature Medicine,* 8**,** 379-385.

ARCURI, L. J., SCHIRMER, M., COLARES, M., MARADEI, S., TAVARES, R., MOREIRA, M. C. R., ARAUJO, R. C., LERNER, D. & PACHECO, A. G. F. 2020. Impact of Anti-CMV IgG Titers and CD34 Count Prior to Hematopoietic Stem Cell Transplantation from Alternative Donors on CMV reactivation. *Biol Blood Marrow Transplant,* 26**,** e275-e279.

ARIZTIA, E. V., LEE, C. J., GOGOI, R. & FISHMAN, D. A. 2006. The tumor microenvironment: key to early detection. *Crit Rev Clin Lab Sci,* 43**,** 393-425.

ARMSTRONG, D. K., ALVAREZ, R. D., BAKKUM-GAMEZ, J. N., BARROILHET, L., BEHBAKHT, K., BERCHUCK, A., CHEN, L. M., CRISTEA, M., DEROSA, M., EISENHAUER, E. L., GERSHENSON, D. M., GRAY, H. J., GRISHAM, R., HAKAM, A., JAIN, A., KARAM, A., KONECNY, G. E., LEATH, C. A., LIU, J., MAHDI, H., MARTIN, L., MATEI, D., MCHALE, M., MCLEAN, K., MILLER, D. S., O'MALLEY, D. M., PERCAC-LIMA, S., RATNER, E., REMMENGA, S. W., VARGAS, R., WERNER, T. L., ZSIROS, E., BURNS, J. L. & ENGH, A. M. 2021. Ovarian Cancer, Version 2.2020, NCCN Clinical Practice Guidelines in Oncology. *J Natl Compr Canc Netw,* 19**,** 191-226.

BANTA, K. L., XU, X., CHITRE, A. S., AU-YEUNG, A., TAKAHASHI, C., O'GORMAN, W. E., WU, T. D., MITTMAN, S., CUBAS, R., COMPS-AGRAR, L., FULZELE, A., BENNETT, E. J., GROGAN, J. L., HUI, E., CHIANG, E. Y. & MELLMAN, I. 2022. Mechanistic convergence of the TIGIT and PD-1 inhibitory pathways necessitates co-blockade to optimize anti-tumor CD8+ T cell responses. *Immunity,* 55**,** 512-526.e9.

BARBER, D. L., WHERRY, E. J., MASOPUST, D., ZHU, B., ALLISON, J. P., SHARPE, A. H., FREEMAN, G. J. & AHMED, R. 2006. Restoring function in exhausted CD8 T cells during chronic viral infection. *Nature,* 439**,** 682-687.

BARYAWNO, N., RAHBAR, A., WOLMER-SOLBERG, N., TAHER, C., ODEBERG, J., DARABI, A., KHAN, Z., SVEINBJÖRNSSON, B., FUSKEVÅG, O. M., SEGERSTRÖM, L., NORDENSKJÖLD, M., SIESJÖ, P., KOGNER, P., JOHNSEN, J. I. & SÖDERBERG-NAUCLÉR, C. 2011. Detection of human cytomegalovirus in medulloblastomas reveals a potential therapeutic target. *J Clin Invest,* 121**,** 4043-55.

BATICH, K. A., REAP, E. A., ARCHER, G. E., SANCHEZ-PEREZ, L., NAIR, S. K., SCHMITTLING, R. J., NORBERG, P., XIE, W., HERNDON, J. E., 2ND, HEALY, P., MCLENDON, R. E., FRIEDMAN, A. H., FRIEDMAN, H. S.,

BIGNER, D., VLAHOVIC, G., MITCHELL, D. A. & SAMPSON, J. H. 2017. Long-term Survival in Glioblastoma with Cytomegalovirus pp65-Targeted Vaccination. *Clin Cancer Res,* 23**,** 1898-1909.
BECHT, E., MCINNES, L., HEALY, J., DUTERTRE, C.-A., KWOK, I. W. H., NG, L. G., GINHOUX, F. & NEWELL, E. W. 2019. Dimensionality reduction for visualizing single-cell data using UMAP. *Nature Biotechnology,* 37**,** 38-44.
BEGO, M. G. & ST. JEOR, S. 2006. Human cytomegalovirus infection of cells of hematopoietic origin: HCMV-induced immunosuppression, immune evasion, and latency. *Experimental Hematology,* 34**,** 555-570.
BELL, D., BERCHUCK, A., BIRRER, M., CHIEN, J., CRAMER, D. W., DAO, F., DHIR, R., DISAIA, P., GABRA, H., GLENN, P., GODWIN, A. K., GROSS, J., HARTMANN, L., HUANG, M., HUNTSMAN, D. G., IACOCCA, M., IMIELINSKI, M., KALLOGER, S., KARLAN, B. Y., LEVINE, D. A., MILLS, G. B., MORRISON, C., MUTCH, D., OLVERA, N., ORSULIC, S., PARK, K., PETRELLI, N., RABENO, B., RADER, J. S., SIKIC, B. I., SMITH-MCCUNE, K., SOOD, A. K., BOWTELL, D., PENNY, R., TESTA, J. R., CHANG, K., CREIGHTON, C. J., DINH, H. H., DRUMMOND, J. A., FOWLER, G., GUNARATNE, P., HAWES, A. C., KOVAR, C. L., LEWIS, L. R., MORGAN, M. B., NEWSHAM, I. F., SANTIBANEZ, J., REID, J. G., TREVINO, L. R., WU, Y. Q., WANG, M., MUZNY, D. M., WHEELER, D. A., GIBBS, R. A., GETZ, G., LAWRENCE, M. S., CIBULSKIS, K., SIVACHENKO, A. Y., SOUGNEZ, C., VOET, D., WILKINSON, J., BLOOM, T., ARDLIE, K., FENNELL, T., BALDWIN, J., NICHOL, R., FISHER, S., GABRIEL, S., LANDER, E. S., DING, L., FULTON, R. S., KOBOLDT, D. C., MCLELLAN, M. D., WYLIE, T., WALKER, J., O'LAUGHLIN, M., DOOLING, D. J., FULTON, L., ABBOTT, R., DEES, N. D., ZHANG, Q., KANDOTH, C., WENDL, M., SCHIERDING, W., SHEN, D., HARRIS, C. C., SCHMIDT, H., KALICKI, J., DELEHAUNTY, K. D., FRONICK, C. C., DEMETER, R., COOK, L., WALLIS, J. W., LIN, L., MAGRINI, V. J., HODGES, J. S., ELDRED, J. M., SMITH, S. M., POHL, C. S., VANDIN, F., et al. 2011. Integrated genomic analyses of ovarian carcinoma. *Nature,* 474**,** 609-615.
BENGSCH, B., SEIGEL, B., RUHL, M., TIMM, J., KUNTZ, M., BLUM, H. E., PIRCHER, H. & THIMME, R. 2010. Coexpression of PD-1, 2B4, CD160 and KLRG1 on Exhausted HCV-Specific CD8+ T Cells Is Linked to Antigen Recognition and T Cell Differentiation. *PLOS Pathogens,* 6**,** e1000947.
BEREK, J. S., RENZ, M., KEHOE, S., KUMAR, L. & FRIEDLANDER, M. 2021. Cancer of the ovary, fallopian tube, and peritoneum: 2021 update. *Int J Gynaecol Obstet,* 155 Suppl 1**,** 61-85.
BIOLATTI, M., DELL'OSTE, V., PAUTASSO, S., GUGLIESI, F., VON EINEM, J., KRAPP, C., JAKOBSEN, M. R., BORGOGNA, C., GARIGLIO, M., DE ANDREA, M. & LANDOLFO, S. 2018. Human Cytomegalovirus Tegument Protein pp65 (pUL83) Dampens Type I Interferon Production by Inactivating the DNA Sensor cGAS without Affecting STING. *J Virol,* 92.
BLUM, J. S., WEARSCH, P. A. & CRESSWELL, P. 2013. Pathways of Antigen Processing. *Annual Review of Immunology,* 31**,** 443-473.
BOECKH, M., LEISENRING, W., RIDDELL, S. R., BOWDEN, R. A., HUANG, M.-L., MYERSON, D., STEVENS-AYERS, T., FLOWERS, M. E. D., CUNNINGHAM, T. & COREY, L. 2003. Late cytomegalovirus disease and mortality in

recipients of allogeneic hematopoietic stem cell transplants: importance of viral load and T-cell immunity. *Blood,* 101**,** 407-414.
BONI, C., FISICARO, P., VALDATTA, C., AMADEI, B., DI VINCENZO, P., GIUBERTI, T., LACCABUE, D., ZERBINI, A., CAVALLI, A., MISSALE, G., BERTOLETTI, A. & FERRARI, C. 2007. Characterization of hepatitis B virus (HBV)-specific T-cell dysfunction in chronic HBV infection. *J Virol,* 81**,** 4215-25.
BONILLA, F. A. & OETTGEN, H. C. 2010. Adaptive immunity. *Journal of Allergy and Clinical Immunology,* 125**,** S33-S40.
BORLEY, J., WILHELM-BENARTZI, C., BROWN, R. & GHAEM-MAGHAMI, S. 2012. Does tumour biology determine surgical success in the treatment of epithelial ovarian cancer? A systematic literature review. *British Journal of Cancer,* 107**,** 1069-1074.
BRAHMER, J. R., ABU-SBEIH, H., ASCIERTO, P. A., BRUFSKY, J., CAPPELLI, L. C., CORTAZAR, F. B., GERBER, D. E., HAMAD, L., HANSEN, E., JOHNSON, D. B., LACOUTURE, M. E., MASTERS, G. A., NAIDOO, J., NANNI, M., PERALES, M.-A., PUZANOV, I., SANTOMASSO, B. D., SHANBHAG, S. P., SHARMA, R., SKONDRA, D., SOSMAN, J. A., TURNER, M. & ERNSTOFF, M. S. 2021. Society for Immunotherapy of Cancer (SITC) clinical practice guideline on immune checkpoint inhibitor-related adverse events. *Journal for ImmunoTherapy of Cancer,* 9**,** e002435.
BRUBAKER, S. W., BONHAM, K. S., ZANONI, I. & KAGAN, J. C. 2015. Innate immune pattern recognition: a cell biological perspective. *Annu Rev Immunol,* 33**,** 257-90.
BUGGERT, M., TAURIAINEN, J., YAMAMOTO, T., FREDERIKSEN, J., IVARSSON, M. A., MICHAËLSSON, J., LUND, O., HEJDEMAN, B., JANSSON, M., SÖNNERBORG, A., KOUP, R. A., BETTS, M. R. & KARLSSON, A. C. 2014. T-bet and Eomes are differentially linked to the exhausted phenotype of CD8+ T cells in HIV infection. *PLoS Pathog,* 10**,** e1004251.
BUKCZYNSKI, J., WEN, T., ELLEFSEN, K., GAULDIE, J. & WATTS, T. H. 2004. Costimulatory ligand 4-1BBL (CD137L) as an efficient adjuvant for human antiviral cytotoxic T cell responses. *Proc Natl Acad Sci U S A,* 101**,** 1291-6.
BUNCE, M., O'NEILL, C. M., BARNARDO, M. C., KRAUSA, P., BROWNING, M. J., MORRIS, P. J. & WELSH, K. I. 1995. Phototyping: comprehensive DNA typing for HLA-A, B, C, DRB1, DRB3, DRB4, DRB5 & DQB1 by PCR with 144 primer mixes utilizing sequence-specific primers (PCR-SSP). *Tissue Antigens,* 46**,** 355-67.
BURNELL, S. E. A., CAPITANI, L., MACLACHLAN, B. J., MASON, G. H., GALLIMORE, A. M. & GODKIN, A. 2021. Seven mysteries of LAG-3: a multi-faceted immune receptor of increasing complexity. *Immunotherapy Advances,* 2.
CANALE, F. P., RAMELLO, M. C., NÚÑEZ, N., FURLAN, C. L. A., BOSSIO, S. N., SERRÁN, M. G., BOARI, J. T., DEL CASTILLO, A., LEDESMA, M., SEDLIK, C., PIAGGIO, E., GRUPPI, A., RODRÍGUEZ, E. V. A. & MONTES, C. L. 2018. CD39 Expression Defines Cell Exhaustion in Tumor-Infiltrating CD8+ T Cells. *Cancer Research,* 78**,** 115-128.
CAO, Y., WANG, X., JIN, T., TIAN, Y., DAI, C., WIDARMA, C., SONG, R. & XU, F. 2020. Immune checkpoint molecules in natural killer cells as potential targets

for cancer immunotherapy. *Signal Transduction and Targeted Therapy,* 5**,** 250.
CARE, M. A., STEPHENSON, S., OWEN, R., DOODY, G. M. & TOOZE, R. M. 2023. Spontaneous EBV-Reactivation during B Cell Differentiation as a Model for Polymorphic EBV-Driven Lymphoproliferation. *Cancers (Basel),* 15.
CARLSON, J. W., MIRON, A., JARBOE, E. A., PARAST, M. M., HIRSCH, M. S., LEE, Y., MUTO, M. G., KINDELBERGER, D. & CRUM, C. P. 2008. Serous tubal intraepithelial carcinoma: its potential role in primary peritoneal serous carcinoma and serous cancer prevention. *J Clin Oncol,* 26**,** 4160-5.
CARLSON, J. W., RÅDESTAD, A. F., SÖDERBERG-NAUCLER, C. & RAHBAR, A. 2018. Human cytomegalovirus in high grade serous ovarian cancer possible implications for patients survival. *Medicine (Baltimore),* 97**,** e9685.
CHAPLIN, D. D. 2010. Overview of the immune response. *Journal of Allergy and Clinical Immunology,* 125**,** S3-S23.
CHAUVIN, J.-M., PAGLIANO, O., FOURCADE, J., SUN, Z., WANG, H., SANDER, C., KIRKWOOD, J. M., CHEN, T.-H. T., MAURER, M., KORMAN, A. J. & ZAROUR, H. M. 2015a. TIGIT and PD-1 impair tumor antigen-specific $CD8^+$ T cells in melanoma patients. *The Journal of clinical investigation,* 125**,** 2046-2058.
CHAUVIN, J.-M. & ZAROUR, H. M. 2020. TIGIT in cancer immunotherapy. *Journal for ImmunoTherapy of Cancer,* 8**,** e000957.
CHAUVIN, J. M., PAGLIANO, O., FOURCADE, J., SUN, Z., WANG, H., SANDER, C., KIRKWOOD, J. M., CHEN, T. H., MAURER, M., KORMAN, A. J. & ZAROUR, H. M. 2015b. TIGIT and PD-1 impair tumor antigen-specific $CD8^+$ T cells in melanoma patients. *J Clin Invest,* 125**,** 2046-58.
CHEN, C. & LI, Y. 2023. Predictive value of co-expression patterns of immune checkpoint molecules for clinical outcomes of hematological malignancies. *Chin J Cancer Res,* 35**,** 245-251.
CHEN, L. & FLIES, D. B. 2013. Molecular mechanisms of T cell co-stimulation and co-inhibition. *Nature Reviews Immunology,* 13**,** 227-242.
CHIA, W. K., TEO, M., WANG, W. W., LEE, B., ANG, S. F., TAI, W. M., CHEE, C. L., NG, J., KAN, R., LIM, W. T., TAN, S. H., ONG, W. S., CHEUNG, Y. B., TAN, E. H., CONNOLLY, J. E., GOTTSCHALK, S. & TOH, H. C. 2014. Adoptive T-cell transfer and chemotherapy in the first-line treatment of metastatic and/or locally recurrent nasopharyngeal carcinoma. *Mol Ther,* 22**,** 132-9.
COBBS, C. S., HARKINS, L., SAMANTA, M., GILLESPIE, G. Y., BHARARA, S., KING, P. H., NABORS, L. B., COBBS, C. G. & BRITT, W. J. 2002. Human Cytomegalovirus Infection and Expression in Human Malignant Glioma1. *Cancer Research,* 62**,** 3347-3350.
COBURN, S. B., BRAY, F., SHERMAN, M. E. & TRABERT, B. 2017. International patterns and trends in ovarian cancer incidence, overall and by histologic subtype. *International Journal of Cancer,* 140**,** 2451-2460.
COHEN, J. I. 2020. Herpesvirus latency. *J Clin Invest,* 130**,** 3361-3369.
COLLINS-MCMILLEN, D., BUEHLER, J., PEPPENELLI, M. & GOODRUM, F. 2018. Molecular Determinants and the Regulation of Human Cytomegalovirus Latency and Reactivation. *Viruses,* 10.

COLOMBO, I., KARAKASIS, K., SUKU, S. & OZA, A. M. 2023. Chasing Immune Checkpoint Inhibitors in Ovarian Cancer: Novel Combinations and Biomarker Discovery. *Cancers (Basel),* 15.

COX, M., KARTIKASARI, A. E. R., GORRY, P. R., FLANAGAN, K. L. & PLEBANSKI, M. 2021. Potential Impact of Human Cytomegalovirus Infection on Immunity to Ovarian Tumours and Cancer Progression. *Biomedicines,* 9.

CRISTIANI, C. M., GAROFALO, C., PASSACATINI, L. C. & CARBONE, E. 2020. New avenues for melanoma immunotherapy: Natural Killer cells? *Scandinavian Journal of Immunology,* 91**,** e12861.

CROUGH, T., BEAGLEY, L., SMITH, C., JONES, L., WALKER, D. G. & KHANNA, R. 2012. Ex vivo functional analysis, expansion and adoptive transfer of cytomegalovirus-specific T-cells in patients with glioblastoma multiforme. *Immunology & Cell Biology,* 90**,** 872-880.

CRUM, C. P., DRAPKIN, R., MIRON, A., INCE, T. A., MUTO, M., KINDELBERGER, D. W. & LEE, Y. 2007. The distal fallopian tube: a new model for pelvic serous carcinogenesis. *Current Opinion in Obstetrics and Gynecology,* 19**,** 3-9.

DAJCZMAN, E., KASYMJANOVA, G., KREISMAN, H., SWINTON, N., PEPE, C. & SMALL, D. 2008. Should Patient-Rated Performance Status Affect Treatment Decisions in Advanced Lung Cancer? *Journal of Thoracic Oncology,* 3**,** 1133-1136.

DAMANIA, B., KENNEY, S. C. & RAAB-TRAUB, N. 2022. Epstein-Barr virus: Biology and clinical disease. *Cell,* 185**,** 3652-3670.

DANG, T. O., OGUNNIYI, A., BARBEE, M. S. & DRILON, A. 2016. Pembrolizumab for the treatment of PD-L1 positive advanced or metastatic non-small cell lung cancer. *Expert Rev Anticancer Ther,* 16**,** 13-20.

DAVID, P., MEGGER, D. A., KAISER, T., WERNER, T., LIU, J., CHEN, L., SITEK, B., DITTMER, U. & ZELINSKYY, G. 2019. The PD-1/PD-L1 Pathway Affects the Expansion and Function of Cytotoxic CD8+ T Cells During an Acute Retroviral Infection. *Frontiers in Immunology,* 10.

DAY, C. L., KAUFMANN, D. E., KIEPIELA, P., BROWN, J. A., MOODLEY, E. S., REDDY, S., MACKEY, E. W., MILLER, J. D., LESLIE, A. J., DEPIERRES, C., MNCUBE, Z., DURAISWAMY, J., ZHU, B., EICHBAUM, Q., ALTFELD, M., WHERRY, E. J., COOVADIA, H. M., GOULDER, P. J. R., KLENERMAN, P., AHMED, R., FREEMAN, G. J. & WALKER, B. D. 2006. PD-1 expression on HIV-specific T cells is associated with T-cell exhaustion and disease progression. *Nature,* 443**,** 350-354.

DEN BRAANKER, H., BONGENAAR, M. & LUBBERTS, E. 2021. How to Prepare Spectral Flow Cytometry Datasets for High Dimensional Data Analysis: A Practical Workflow. *Frontiers in Immunology,* 12.

DIAMOND, M. S., KINDER, M., MATSUSHITA, H., MASHAYEKHI, M., DUNN, G. P., ARCHAMBAULT, J. M., LEE, H., ARTHUR, C. D., WHITE, J. M., KALINKE, U., MURPHY, K. M. & SCHREIBER, R. D. 2011. Type I interferon is selectively required by dendritic cells for immune rejection of tumors. *J Exp Med,* 208**,** 1989-2003.

DIRKS, J., EGLI, A., SESTER, U., SESTER, M. & HIRSCH, H. H. 2013. Blockade of programmed death receptor-1 signaling restores expression of mostly proinflammatory cytokines in anergic cytomegalovirus-specific T cells. *Transplant Infectious Disease,* 15**,** 79-89.

DJENIDI, F., ADAM, J., GOUBAR, A., DURGEAU, A., MEURICE, G., DE MONTPRÉVILLE, V., VALIDIRE, P., BESSE, B. & MAMI-CHOUAIB, F. 2015. CD8+CD103+ tumor-infiltrating lymphocytes are tumor-specific tissue-resident memory T cells and a prognostic factor for survival in lung cancer patients. *J Immunol,* 194**,** 3475-86.

DOLAN, A., CUNNINGHAM, C., HECTOR, R. D., HASSAN-WALKER, A. F., LEE, L., ADDISON, C., DARGAN, D. J., MCGEOCH, D. J., GATHERER, D., EMERY, V. C., GRIFFITHS, P. D., SINZGER, C., MCSHARRY, B. P., WILKINSON, G. W. G. & DAVISON, A. J. 2004. Genetic content of wild-type human cytomegalovirus. *J Gen Virol,* 85**,** 1301-1312.

DOROTHEA, M., XIE, J., YIU, S. P. T. & CHIANG, A. K. S. 2023. Contribution of Epstein-Barr Virus Lytic Proteins to Cancer Hallmarks and Implications from Other Oncoviruses. *Cancers (Basel),* 15.

DOUBENI, C. A., DOUBENI, A. R. & MYERS, A. E. 2016. Diagnosis and Management of Ovarian Cancer. *Am Fam Physician,* 93**,** 937-44.

DUNKELBERGER, J. R. & SONG, W.-C. 2010. Complement and its role in innate and adaptive immune responses. *Cell Research,* 20**,** 34-50.

DUPONT, L. & REEVES, M. B. 2016. Cytomegalovirus latency and reactivation: recent insights into an age old problem. *Rev Med Virol,* 26**,** 75-89.

DUTSCH-WICHEREK, M. M., SZUBERT, S., DZIOBEK, K., WISNIEWSKI, M., LUKASZEWSKA, E., WICHEREK, L., JOZWICKI, W., ROKITA, W. & KOPER, K. 2019. Analysis of the treg cell population in the peripheral blood of ovarian cancer patients in relation to the long-term outcomes. *Ginekol Pol,* 90**,** 179-184.

DYCK, L. & MILLS, K. H. G. 2017. Immune checkpoints and their inhibition in cancer and infectious diseases. *European Journal of Immunology,* 47**,** 765-779.

DZIURZYNSKI, K., CHANG, S. M., HEIMBERGER, A. B., KALEJTA, R. F., MCGREGOR DALLAS, S. R., SMIT, M., SOROCEANU, L. & COBBS, C. S. 2012. Consensus on the role of human cytomegalovirus in glioblastoma. *Neuro Oncol,* 14**,** 246-55.

ELKINGTON, R., WALKER, S., CROUGH, T., MENZIES, M., TELLAM, J., BHARADWAJ, M. & KHANNA, R. 2003. Ex vivo profiling of CD8+-T-cell responses to human cytomegalovirus reveals broad and multispecific reactivities in healthy virus carriers. *J Virol,* 77**,** 5226-40.

FORREST, C., GOMES, A., REEVES, M. & MALE, V. 2020. NK Cell Memory to Cytomegalovirus: Implications for Vaccine Development. *Vaccines (Basel),* 8.

FOURCADE, J., KUDELA, P., SUN, Z., SHEN, H., LAND, S. R., LENZNER, D., GUILLAUME, P., LUESCHER, I. F., SANDER, C., FERRONE, S., KIRKWOOD, J. M. & ZAROUR, H. M. 2009. PD-1 is a regulator of NY-ESO-1-specific CD8+ T cell expansion in melanoma patients. *J Immunol,* 182**,** 5240-9.

FOURCADE, J., SUN, Z., BENALLAOUA, M., GUILLAUME, P., LUESCHER, I. F., SANDER, C., KIRKWOOD, J. M., KUCHROO, V. & ZAROUR, H. M. 2010. Upregulation of Tim-3 and PD-1 expression is associated with tumor antigen-specific CD8+ T cell dysfunction in melanoma patients. *J Exp Med,* 207**,** 2175-86.

FRANKLIN, C., ROOMS, I., FIEDLER, M., REIS, H., MILSCH, L., HERZ, S., LIVINGSTONE, E., ZIMMER, L., SCHMID, K. W., DITTMER, U.,

SCHADENDORF, D. & SCHILLING, B. 2017. Cytomegalovirus reactivation in patients with refractory checkpoint inhibitor-induced colitis. *European Journal of Cancer,* 86**,** 248-256.
GABOR, F., JAHN, G., SEDMAK, D. D. & SINZGER, C. 2020. In vivo Downregulation of MHC Class I Molecules by HCMV Occurs During All Phases of Viral Replication but Is Not Always Complete. *Front Cell Infect Microbiol,* 10**,** 283.
GABRIELE, M., MASSIMO, P., ALESSANDRO, Z., AMALIA, P., LARA, R., VALERIA, B., ALESSANDRA, O., ATIM, M., MASSIMO, F., TERESA, S. & CARLO, F. 2012. Lack of full CD8 functional restoration after antiviral treatment for acute and chronic hepatitis C virus infection. *Gut,* 61**,** 1076.
GALLIMORE, A., GLITHERO, A., GODKIN, A., TISSOT, A. C., PLÜCKTHUN, A., ELLIOTT, T., HENGARTNER, H. & ZINKERNAGEL, R. 1998. Induction and exhaustion of lymphocytic choriomeningitis virus-specific cytotoxic T lymphocytes visualized using soluble tetrameric major histocompatibility complex class I-peptide complexes. *J Exp Med,* 187**,** 1383-93.
GANESAN, A.-P., CLARKE, J., WOOD, O., GARRIDO-MARTIN, E. M., CHEE, S. J., MELLOWS, T., SAMANIEGO-CASTRUITA, D., SINGH, D., SEUMOIS, G., ALZETANI, A., WOO, E., FRIEDMANN, P. S., KING, E. V., THOMAS, G. J., SANCHEZ-ELSNER, T., VIJAYANAND, P. & OTTENSMEIER, C. H. 2017. Tissue-resident memory features are linked to the magnitude of cytotoxic T cell responses in human lung cancer. *Nature Immunology,* 18**,** 940-950.
GARCÍA-RÍOS, E., NUÉVALOS, M., MANCEBO, F. J. & PÉREZ-ROMERO, P. 2021. Is It Feasible to Use CMV-Specific T-Cell Adoptive Transfer as Treatment Against Infection in SOT Recipients? *Frontiers in Immunology,* 12.
GARON, E. B., RIZVI, N. A., HUI, R., LEIGHL, N., BALMANOUKIAN, A. S., EDER, J. P., PATNAIK, A., AGGARWAL, C., GUBENS, M., HORN, L., CARCERENY, E., AHN, M.-J., FELIP, E., LEE, J.-S., HELLMANN, M. D., HAMID, O., GOLDMAN, J. W., SORIA, J.-C., DOLLED-FILHART, M., RUTLEDGE, R. Z., ZHANG, J., LUNCEFORD, J. K., RANGWALA, R., LUBINIECKI, G. M., ROACH, C., EMANCIPATOR, K. & GANDHI, L. 2015. Pembrolizumab for the Treatment of Non–Small-Cell Lung Cancer. *New England Journal of Medicine,* 372**,** 2018-2028.
GE, Z., ZHOU, G., CAMPOS CARRASCOSA, L., GAUSVIK, E., BOOR, P. P. C., NOORDAM, L., DOUKAS, M., POLAK, W. G., TERKIVATAN, T., PAN, Q., TAKKENBERG, R. B., VERHEIJ, J., ERDMANN, J. I., JNM, I. J., PEPPELENBOSCH, M. P., KRAAN, J., KWEKKEBOOM, J. & SPRENGERS, D. 2021. TIGIT and PD1 Co-blockade Restores ex vivo Functions of Human Tumor-Infiltrating CD8(+) T Cells in Hepatocellular Carcinoma. *Cell Mol Gastroenterol Hepatol,* 12**,** 443-464.
GEBHARDT, T., WAKIM, L. M., EIDSMO, L., READING, P. C., HEATH, W. R. & CARBONE, F. R. 2009. Memory T cells in nonlymphoid tissue that provide enhanced local immunity during infection with herpes simplex virus. *Nature Immunology,* 10**,** 524-530.
GEHRING, A. J., HO, Z. Z., TAN, A. T., AUNG, M. O., LEE, K. H., TAN, K. C., LIM, S. G. & BERTOLETTI, A. 2009. Profile of tumor antigen-specific CD8 T cells in patients with hepatitis B virus-related hepatocellular carcinoma. *Gastroenterology,* 137**,** 682-90.

GHONEUM, A., AFIFY, H., SALIH, Z., KELLY, M. & SAID, N. 2018. Role of tumor microenvironment in ovarian cancer pathobiology. *Oncotarget,* 9**,** 22832-22849.
GIBSON, L., PICCININI, G., LILLERI, D., REVELLO, M. G., WANG, Z., MARKEL, S., DIAMOND, D. J. & LUZURIAGA, K. 2004. Human Cytomegalovirus Proteins pp65 and Immediate Early Protein 1 Are Common Targets for CD8+ T Cell Responses in Children with Congenital or Postnatal Human Cytomegalovirus Infection1. *The Journal of Immunology,* 172**,** 2256-2264.
GILLESPIE, G. M., WILLS, M. R., APPAY, V., O'CALLAGHAN, C., MURPHY, M., SMITH, N., SISSONS, P., ROWLAND-JONES, S., BELL, J. I. & MOSS, P. A. 2000. Functional heterogeneity and high frequencies of cytomegalovirus-specific CD8(+) T lymphocytes in healthy seropositive donors. *J Virol,* 74**,** 8140-50.
GORAL, S. 2011. The three-signal hypothesis of lymphocyte activation/targets for immunosuppression. *Dialysis & Transplantation,* 40**,** 14-16.
GORDON, C. L., MIRON, M., THOME, J. J., MATSUOKA, N., WEINER, J., RAK, M. A., IGARASHI, S., GRANOT, T., LERNER, H., GOODRUM, F. & FARBER, D. L. 2017. Tissue reservoirs of antiviral T cell immunity in persistent human CMV infection. *J Exp Med,* 214**,** 651-667.
GUO, L., LIU, X. & SU, X. 2023. The role of TEMRA cell-mediated immune senescence in the development and treatment of HIV disease. *Frontiers in Immunology,* 14.
GUPTA, P. K., GODEC, J., WOLSKI, D., ADLAND, E., YATES, K., PAUKEN, K. E., COSGROVE, C., LEDDEROSE, C., JUNGER, W. G., ROBSON, S. C., WHERRY, E. J., ALTER, G., GOULDER, P. J. R., KLENERMAN, P., SHARPE, A. H., LAUER, G. M. & HAINING, W. N. 2015. CD39 Expression Identifies Terminally Exhausted CD8+ T Cells. *PLOS Pathogens,* 11**,** e1005177.
HAN, A.-J., XIONG, M. & ZONG, Y.-S. 2000. Association of Epstein-Barr Virus With Lymphoepithelioma-Like Carcinoma of the Lung in Southern China. *American Journal of Clinical Pathology,* 114**,** 220-226.
HAN, Y., LIU, D. & LI, L. 2020. PD-1/PD-L1 pathway: current researches in cancer. *Am J Cancer Res,* 10**,** 727-742.
HANEY, D., QUIGLEY, M. F., ASHER, T. E., AMBROZAK, D. R., GOSTICK, E., PRICE, D. A., DOUEK, D. C. & BETTS, M. R. 2011. Isolation of viable antigen-specific CD8+ T cells based on membrane-bound tumor necrosis factor (TNF)-α expression. *J Immunol Methods,* 369**,** 33-41.
HANLEY, P. J. & BOLLARD, C. M. 2014. Controlling cytomegalovirus: helping the immune system take the lead. *Viruses,* 6**,** 2242-58.
HARARI, A., BELLUTTI ENDERS, F., CELLERAI, C., BART, P. A. & PANTALEO, G. 2009. Distinct profiles of cytotoxic granules in memory CD8 T cells correlate with function, differentiation stage, and antigen exposure. *J Virol,* 83**,** 2862-71.
HAY, Z. L. Z. & SLANSKY, J. E. 2022. Granzymes: The Molecular Executors of Immune-Mediated Cytotoxicity. *Int J Mol Sci,* 23.
HE, Q.-F., XU, Y., LI, J., HUANG, Z.-M., LI, X.-H. & WANG, X. 2018. CD8+ T-cell exhaustion in cancer: mechanisms and new area for cancer immunotherapy. *Briefings in Functional Genomics,* 18**,** 99-106.

HE, R., HOU, S., LIU, C., ZHANG, A., BAI, Q., HAN, M., YANG, Y., WEI, G., SHEN, T., YANG, X., XU, L., CHEN, X., HAO, Y., WANG, P., ZHU, C., OU, J., LIANG, H., NI, T., ZHANG, X., ZHOU, X., DENG, K., CHEN, Y., LUO, Y., XU, J., QI, H., WU, Y. & YE, L. 2016. Follicular CXCR5- expressing CD8(+) T cells curtail chronic viral infection. *Nature,* 537**,** 412-428.

HE, X. & XU, C. 2020. PD-1: A Driver or Passenger of T Cell Exhaustion? *Molecular Cell,* 77**,** 930-931.

HE, X.-H., JIA, Q.-T., LI, F.-Y., SALTIS, M., LIU, Y., XU, L.-H. & ZHA, Q.-B. 2008. CD8+ T cells specific for both persistent and non-persistent viruses display distinct differentiation phenotypes but have similar level of PD-1 expression in healthy Chinese individuals. *Clinical Immunology,* 126**,** 222-234.

HERTOGHS, K. M., MOERLAND, P. D., VAN STIJN, A., REMMERSWAAL, E. B., YONG, S. L., VAN DE BERG, P. J., VAN HAM, S. M., BAAS, F., TEN BERGE, I. J. & VAN LIER, R. A. 2010. Molecular profiling of cytomegalovirus-induced human CD8+ T cell differentiation. *J Clin Invest,* 120**,** 4077-90.

HOSIE, L., PACHNIO, A., ZUO, J., PEARCE, H., RIDDELL, S. & MOSS, P. 2017. Cytomegalovirus-Specific T Cells Restricted by HLA-Cw*0702 Increase Markedly with Age and Dominate the CD8+ T-Cell Repertoire in Older People. *Frontiers in Immunology,* 8.

HOUGHTON, A. N. & GUEVARA-PATIÑO, J. A. 2004. Immune recognition of self in immunity against cancer. *J Clin Invest,* 114**,** 468-71.

HUANG, H., WANG, Y., RUDIN, C. & BROWNE, E. P. 2022. Towards a comprehensive evaluation of dimension reduction methods for transcriptomic data visualization. *Communications Biology,* 5**,** 719.

HUANG, J., FOGG, M., WIRTH, L. J., DALEY, H., RITZ, J., POSNER, M. R., WANG, F. C. & LORCH, J. H. 2017. Epstein-Barr virus-specific adoptive immunotherapy for recurrent, metastatic nasopharyngeal carcinoma. *Cancer,* 123**,** 2642-2650.

HUANG, J., ZENG, X., SIGAL, N., LUND, P. J., SU, L. F., HUANG, H., CHIEN, Y.-H. & DAVIS, M. M. 2016. Detection, phenotyping, and quantification of antigen-specific T cells using a peptide-MHC dodecamer. *Proceedings of the National Academy of Sciences,* 113**,** E1890-E1897.

HUDRY, D., LE GUELLEC, S., MEIGNAN, S., BÉCOURT, S., PASQUESOONE, C., EL HAJJ, H., MARTÍNEZ-GÓMEZ, C., LEBLANC, É., NARDUCCI, F. & LADOIRE, S. 2022. Tumor-Infiltrating Lymphocytes (TILs) in Epithelial Ovarian Cancer: Heterogeneity, Prognostic Impact, and Relationship with Immune Checkpoints. *Cancers (Basel),* 14.

HUNG, A. L., MAXWELL, R., THEODROS, D., BELCAID, Z., MATHIOS, D., LUKSIK, A. S., KIM, E., WU, A., XIA, Y., GARZON-MUVDI, T., JACKSON, C., YE, X., TYLER, B., SELBY, M., KORMAN, A., BARNHART, B., PARK, S. M., YOUN, J. I., CHOWDHURY, T., PARK, C. K., BREM, H., PARDOLL, D. M. & LIM, M. 2018. TIGIT and PD-1 dual checkpoint blockade enhances antitumor immunity and survival in GBM. *Oncoimmunology,* 7**,** e1466769.

HUTCHINSON, J. A., KRONENBERG, K., RIQUELME, P., WENZEL, J. J., GLEHR, G., SCHILLING, H.-L., ZEMAN, F., EVERT, K., SCHMIEDEL, M., MICKLER, M., DREXLER, K., BITTERER, F., CORDERO, L., BEYER, L., BACH, C., KOESTLER, J., BURKHARDT, R., SCHLITT, H. J., HELLWIG, D., WERNER, J. M., SPANG, R., SCHMIDT, B., GEISSLER, E. K. & HAFERKAMP, S. 2021.

Virus-specific memory T cell responses unmasked by immune checkpoint blockade cause hepatitis. *Nature Communications,* 12**,** 1439.
HUTCHISON, S. & PRITCHARD, A. L. 2018. Identifying neoantigens for use in immunotherapy. *Mammalian Genome,* 29**,** 714-730.
HWANG, W. T., ADAMS, S. F., TAHIROVIC, E., HAGEMANN, I. S. & COUKOS, G. 2012. Prognostic significance of tumor-infiltrating T cells in ovarian cancer: a meta-analysis. *Gynecol Oncol,* 124**,** 192-8.
HYUN, S.-J., SOHN, H.-J., LEE, H.-J., LEE, S.-D., KIM, S., SOHN, D.-H., HONG, C.-H., CHOI, H., CHO, H.-I. & KIM, T.-G. 2017. Comprehensive Analysis of Cytomegalovirus pp65 Antigen-Specific CD8+ T Cell Responses According to Human Leukocyte Antigen Class I Allotypes and Intraindividual Dominance. *Frontiers in Immunology,* 8.
IANNELLO, A. & RAULET, D. H. 2013. Immune surveillance of unhealthy cells by natural killer cells. *Cold Spring Harb Symp Quant Biol,* 78**,** 249-57.
IM, S. J., HASHIMOTO, M., GERNER, M. Y., LEE, J., KISSICK, H. T., BURGER, M. C., SHAN, Q., HALE, J. S., LEE, J., NASTI, T. H., SHARPE, A. H., FREEMAN, G. J., GERMAIN, R. N., NAKAYA, H. I., XUE, H.-H. & AHMED, R. 2016. Defining CD8+ T cells that provide the proliferative burst after PD-1 therapy. *Nature,* 537**,** 417-421.
IM, S. J., KONIECZNY, B. T., HUDSON, W. H., MASOPUST, D. & AHMED, R. 2020. PD-1+ stemlike CD8 T cells are resident in lymphoid tissues during persistent LCMV infection. *Proc Natl Acad Sci U S A,* 117**,** 4292-4299.
IMANI, S., TAGIT, O. & PICHON, C. 2024. Neoantigen vaccine nanoformulations based on Chemically synthesized minimal mRNA (CmRNA): small molecules, big impact. *npj Vaccines,* 9**,** 14.
INGERSLEV, K., HØGDALL, E., SKOVRIDER-RUMINSKI, W., SCHNACK, T. H., LIDANG, M., HØGDALL, C. & BLAAKAER, J. 2019. The prevalence of EBV and CMV DNA in epithelial ovarian cancer. *Infect Agent Cancer,* 14**,** 7.
IVANISENKO, N. V., SHASHKOVA, T. I., SHEVTSOV, A., SINDEEVA, M., UMERENKOV, D. & KARDYMON, O. 2024. SEMA 2.0: web-platform for B-cell conformational epitopes prediction using artificial intelligence. *Nucleic Acids Research,* 52**,** W533-W539.
IWAI, Y., ISHIDA, M., TANAKA, Y., OKAZAKI, T., HONJO, T. & MINATO, N. 2002. Involvement of PD-L1 on tumor cells in the escape from host immune system and tumor immunotherapy by PD-L1 blockade. *Proc Natl Acad Sci U S A,* 99**,** 12293-7.
JABBARI, A. & HARTY, J. T. 2006. Secondary memory CD8+ T cells are more protective but slower to acquire a central-memory phenotype. *J Exp Med,* 203**,** 919-32.
JACKSON, S. E., MASON, G. M., OKECHA, G., SISSONS, J. G. P. & WILLS, M. R. 2014. Diverse Specificities, Phenotypes, and Antiviral Activities of Cytomegalovirus-Specific CD8⁺ T Cells. *Journal of Virology,* 88**,** 10894-10908.
JACKSON, S. E., MASON, G. M. & WILLS, M. R. 2011. Human cytomegalovirus immunity and immune evasion. *Virus Research,* 157**,** 151-160.
JANEWAY, C. A. & MEDZHITOV, R. 2002. Innate Immune Recognition. *Annual Review of Immunology,* 20**,** 197-216.

JANG, D. I., LEE, A. H., SHIN, H. Y., SONG, H. R., PARK, J. H., KANG, T. B., LEE, S. R. & YANG, S. H. 2021. The Role of Tumor Necrosis Factor Alpha (TNF-α) in Autoimmune Disease and Current TNF-α Inhibitors in Therapeutics. *Int J Mol Sci,* 22.
JIANG, Y., LI, Y. & ZHU, B. 2015. T-cell exhaustion in the tumor microenvironment. *Cell Death & Disease,* 6**,** e1792-e1792.
JOFFRE, O. P., SEGURA, E., SAVINA, A. & AMIGORENA, S. 2012. Cross-presentation by dendritic cells. *Nature Reviews Immunology,* 12**,** 557-569.
JOHNSTON, ROBERT J., COMPS-AGRAR, L., HACKNEY, J., YU, X., HUSENI, M., YANG, Y., PARK, S., JAVINAL, V., CHIU, H., IRVING, B., EATON, DAN L. & GROGAN, JANE L. 2014. The Immunoreceptor TIGIT Regulates Antitumor and Antiviral CD8⁺ T Cell Effector Function. *Cancer Cell,* 26**,** 923-937.
JOLLER, N. & KUCHROO, V. K. 2017. Tim-3, Lag-3, and TIGIT. *In:* YOSHIMURA, A. (ed.) *Emerging Concepts Targeting Immune Checkpoints in Cancer and Autoimmunity.* Cham: Springer International Publishing.
KAECH, S. M. & CUI, W. 2012. Transcriptional control of effector and memory CD8+ T cell differentiation. *Nature Reviews Immunology,* 12**,** 749-761.
KALEJTA, R. F. 2008. Tegument proteins of human cytomegalovirus. *Microbiol Mol Biol Rev,* 72**,** 249-65, table of contents.
KALIA, V., YUZEFPOLSKIY, Y., VEGARAJU, A., XIAO, H., BAUMANN, F., JATAV, S., CHURCH, C., PRLIC, M., JHA, A., NGHIEM, P., RIDDELL, S. & SARKAR, S. 2021. Metabolic regulation by PD-1 signaling promotes long-lived quiescent CD8 T cell memory in mice. *Sci Transl Med,* 13**,** eaba6006.
KALLIES, A., ZEHN, D. & UTZSCHNEIDER, D. T. 2020. Precursor exhausted T cells: key to successful immunotherapy? *Nature Reviews Immunology,* 20**,** 128-136.
KAMPHORST, A. O., WIELAND, A., NASTI, T., YANG, S., ZHANG, R., BARBER, D. L., KONIECZNY, B. T., DAUGHERTY, C. Z., KOENIG, L., YU, K., SICA, G. L., SHARPE, A. H., FREEMAN, G. J., BLAZAR, B. R., TURKA, L. A., OWONIKOKO, T. K., PILLAI, R. N., RAMALINGAM, S. S., ARAKI, K. & AHMED, R. 2017. Rescue of exhausted CD8 T cells by PD-1–targeted therapies is CD28-dependent. *Science,* 355**,** 1423-1427.
KANSY, B. A., CONCHA-BENAVENTE, F., SRIVASTAVA, R. M., JIE, H. B., SHAYAN, G., LEI, Y., MOSKOVITZ, J., MOY, J., LI, J., BRANDAU, S., LANG, S., SCHMITT, N. C., FREEMAN, G. J., GOODING, W. E., CLUMP, D. A. & FERRIS, R. L. 2017. PD-1 Status in CD8(+) T Cells Associates with Survival and Anti-PD-1 Therapeutic Outcomes in Head and Neck Cancer. *Cancer Res,* 77**,** 6353-6364.
KARED, H., MARTELLI, S., NG, T. P., PENDER, S. L. & LARBI, A. 2016. CD57 in human natural killer cells and T-lymphocytes. *Cancer Immunol Immunother,* 65**,** 441-52.
KARRER, U., SIERRO, S., WAGNER, M., OXENIUS, A., HENGEL, H., KOSZINOWSKI, U. H., PHILLIPS, R. E. & KLENERMAN, P. 2003. Memory inflation: continuous accumulation of antiviral CD8+ T cells over time. *J Immunol,* 170**,** 2022-9.
KAWAMURA, S., NAKASONE, H., TAKESHITA, J., KIMURA, S. I., NAKAMURA, Y., KAWAMURA, M., YOSHINO, N., MISAKI, Y., YOSHIMURA, K., MATSUMI,

S., GOMYO, A., AKAHOSHI, Y., KUSUDA, M., KAMEDA, K., TANIHARA, A., TAMAKI, M., KAKO, S. & KANDA, Y. 2021. Prediction of Cytomegalovirus Reactivation by Recipient Cytomegalovirus-IgG Titer before Allogeneic Hematopoietic Stem Cell Transplantation. *Transplant Cell Ther,* 27**,** 683.e1-683.e7.

KEIR, M. E., BUTTE, M. J., FREEMAN, G. J. & SHARPE, A. H. 2008. PD-1 and its ligands in tolerance and immunity. *Annu Rev Immunol,* 26**,** 677-704.

KENTER, G. G., WELTERS, M. J., VALENTIJN, A. R., LOWIK, M. J., BERENDS-VAN DER MEER, D. M., VLOON, A. P., ESSAHSAH, F., FATHERS, L. M., OFFRINGA, R., DRIJFHOUT, J. W., WAFELMAN, A. R., OOSTENDORP, J., FLEUREN, G. J., VAN DER BURG, S. H. & MELIEF, C. J. 2009. Vaccination against HPV-16 oncoproteins for vulvar intraepithelial neoplasia. *N Engl J Med,* 361**,** 1838-47.

KERN, F., BUNDE, T., FAULHABER, N., KIECKER, F., KHATAMZAS, E., RUDAWSKI, I. M., PRUSS, A., GRATAMA, J. W., VOLKMER-ENGERT, R., EWERT, R., REINKE, P., VOLK, H. D. & PICKER, L. J. 2002. Cytomegalovirus (CMV) phosphoprotein 65 makes a large contribution to shaping the T cell repertoire in CMV-exposed individuals. *J Infect Dis,* 185**,** 1709-16.

KHAN, N., COBBOLD, M., CUMMERSON, J. & MOSS, P. A. 2010. Persistent viral infection in humans can drive high frequency low-affinity T-cell expansions. *Immunology,* 131**,** 537-48.

KHAN, N., HISLOP, A., GUDGEON, N., COBBOLD, M., KHANNA, R., NAYAK, L., RICKINSON, A. B. & MOSS, P. A. H. 2004. Herpesvirus-Specific CD8 T Cell Immunity in Old Age: Cytomegalovirus Impairs the Response to a Coresident EBV Infection1. *The Journal of Immunology,* 173**,** 7481-7489.

KHAN, N., SHARIFF, N., COBBOLD, M., BRUTON, R., AINSWORTH, J. A., SINCLAIR, A. J., NAYAK, L. & MOSS, P. A. 2002. Cytomegalovirus seropositivity drives the CD8 T cell repertoire toward greater clonality in healthy elderly individuals. *J Immunol,* 169**,** 1984-92.

KHANNA, P., BLAIS, N., GAUDREAU, P.-O. & CORRALES-RODRIGUEZ, L. 2017. Immunotherapy Comes of Age in Lung Cancer. *Clinical Lung Cancer,* 18**,** 13-22.

KIM, J., KIM, A. R. & SHIN, E. C. 2015. Cytomegalovirus Infection and Memory T Cell Inflation. *Immune Netw,* 15**,** 186-90.

KINAN DRAK, A. & DIDIER, M. 2018. Significance of Tumor Microenvironment Scoring and Immune Biomarkers in Patient Stratification and Cancer Outcomes. *In:* SUPRIYA, S. (ed.) *Histopathology.* Rijeka: IntechOpen.

KLEIN, S., GHERSI, D., MANNS, M. P., PRINZ, I., CORNBERG, M. & KRAFT, A. R. M. 2020. PD-L1 Checkpoint Inhibition Narrows the Antigen-Specific T Cell Receptor Repertoire in Chronic Lymphocytic Choriomeningitis Virus Infection. *J Virol,* 94.

KLENERMAN, P. & HILL, A. 2005. T cells and viral persistence: lessons from diverse infections. *Nature Immunology,* 6**,** 873-879.

KLENERMAN, P. & OXENIUS, A. 2016. T cell responses to cytomegalovirus. *Nature Reviews Immunology,* 16**,** 367-377.

KNOBLACH, T., GRANDEL, B., SEILER, J., NEVELS, M. & PAULUS, C. 2011. Human cytomegalovirus IE1 protein elicits a type II interferon-like host cell

response that depends on activated STAT1 but not interferon-γ. *PLoS Pathog,* 7**,** e1002016.
KOH, J., KIM, S., WOO, Y. D., SONG, S. G., YIM, J., HAN, B., LIM, S., AHN, H. K., MUN, S., KIM, J. S., KEAM, B., KIM, Y. A., LEE, S.-H., JEON, Y. K. & CHUNG, D. H. 2022. TCF1+PD-1+ tumour-infiltrating lymphocytes predict a favorable response and prolonged survival after immune checkpoint inhibitor therapy for non-small-cell lung cancer. *European Journal of Cancer,* 174**,** 10-20.
KREIDIEH, F. Y. & TAWBI, H. A. 2023. The introduction of LAG-3 checkpoint blockade in melanoma: immunotherapy landscape beyond PD-1 and CTLA-4 inhibition. *Ther Adv Med Oncol,* 15**,** 17588359231186027.
KRUMMEL, M. F. & ALLISON, J. P. 1995. CD28 and CTLA-4 have opposing effects on the response of T cells to stimulation. *J Exp Med,* 182**,** 459-65.
KUDRYAVTSEV, I. V., ARSENTIEVA, N. A., KOROBOVA, Z. R., ISAKOV, D. V., RUBINSTEIN, A. A., BATSUNOV, O. K., KHAMITOVA, I. V., KUZNETSOVA, R. N., SAVIN, T. V., AKISHEVA, T. V., STANEVICH, O. V., LEBEDEVA, A. A., VOROBYOV, E. A., VOROBYOVA, S. V., KULIKOV, A. N., SHARAPOVA, M. A., PEVTSOV, D. E. & TOTOLIAN, A. A. 2022. Heterogenous CD8+ T Cell Maturation and 'Polarization' in Acute and Convalescent COVID-19 Patients. *Viruses,* 14.
KUMAR, B. V., CONNORS, T. J. & FARBER, D. L. 2018. Human T Cell Development, Localization, and Function throughout Life. *Immunity,* 48**,** 202-213.
KURMAN, R. J. & SHIH IE, M. 2008. Pathogenesis of ovarian cancer: lessons from morphology and molecular biology and their clinical implications. *Int J Gynecol Pathol,* 27**,** 151-60.
KWOK, G., YAU, T. C., CHIU, J. W., TSE, E. & KWONG, Y. L. 2016. Pembrolizumab (Keytruda). *Hum Vaccin Immunother,* 12**,** 2777-2789.
KWON, B. 2015. Is CD137 Ligand (CD137L) Signaling a Fine Tuner of Immune Responses? *Immune Netw,* 15**,** 121-124.
LABIDI-GALY, S. I., PAPP, E., HALLBERG, D., NIKNAFS, N., ADLEFF, V., NOE, M., BHATTACHARYA, R., NOVAK, M., JONES, S., PHALLEN, J., HRUBAN, C. A., HIRSCH, M. S., LIN, D. I., SCHWARTZ, L., MAIRE, C. L., TILLE, J.-C., BOWDEN, M., AYHAN, A., WOOD, L. D., SCHARPF, R. B., KURMAN, R., WANG, T.-L., SHIH, I.-M., KARCHIN, R., DRAPKIN, R. & VELCULESCU, V. E. 2017. High grade serous ovarian carcinomas originate in the fallopian tube. *Nature Communications,* 8**,** 1093.
LAFEMINA, R. L., PIZZORNO, M. C., MOSCA, J. D. & HAYWARD, G. S. 1989. Expression of the acidic nuclear immediate-early protein (IE1) of human cytomegalovirus in stable cell lines and its preferential association with metaphase chromosomes. *Virology,* 172**,** 584-600.
LANFERMEIJER, J., DE GREEF, P. C., HENDRIKS, M., VOS, M., VAN BEEK, J., BORGHANS, J. A. M. & VAN BAARLE, D. 2021. Age and CMV-Infection Jointly Affect the EBV-Specific CD8(+) T-Cell Repertoire. *Front Aging,* 2**,** 665637.
LANG, K. S., MORIS, A., GOUTTEFANGEAS, C., WALTER, S., TEICHGRÄBER, V., MILLER, M., WERNET, D., HAMPRECHT, K., RAMMENSEE, H. G. & STEVANOVIC, S. 2002. High frequency of human cytomegalovirus (HCMV)-

specific CD8+ T cells detected in a healthy CMV-seropositive donor. *Cell Mol Life Sci,* 59**,** 1076-80.
LANGER, C. J., GADGEEL, S. M., BORGHAEI, H., PAPADIMITRAKOPOULOU, V. A., PATNAIK, A., POWELL, S. F., GENTZLER, R. D., MARTINS, R. G., STEVENSON, J. P., JALAL, S. I., PANWALKAR, A., YANG, J. C.-H., GUBENS, M., SEQUIST, L. V., AWAD, M. M., FIORE, J., GE, Y., RAFTOPOULOS, H. & GANDHI, L. 2016. Carboplatin and pemetrexed with or without pembrolizumab for advanced, non-squamous non-small-cell lung cancer: a randomised, phase 2 cohort of the open-label KEYNOTE-021 study. *The Lancet Oncology,* 17**,** 1497-1508.
LARBI, A. & FULOP, T. 2014. From “truly naïve” to “exhausted senescent” T cells: When markers predict functionality. *Cytometry Part A,* 85**,** 25-35.
LAU, S. K., CHEN, Y.-Y., CHEN, W.-G., DIAMOND, D. J., MAMELAK, A. N., ZAIA, J. A. & WEISS, L. M. 2005. Lack of association of cytomegalovirus with human brain tumors. *Modern Pathology,* 18**,** 838-843.
LEARY, A., TAN, D. & LEDERMANN, J. 2021. Immune checkpoint inhibitors in ovarian cancer: where do we stand? *Therapeutic Advances in Medical Oncology,* 13**,** 17588359211039899.
LEE, C. H., YELENSKY, R., JOOSS, K. & CHAN, T. A. 2018. Update on Tumor Neoantigens and Their Utility: Why It Is Good to Be Different. *Trends Immunol,* 39**,** 536-548.
LEE, S.-W., CHOI, H. Y., LEE, G.-W., KIM, T., CHO, H.-J., OH, I.-J., SONG, S. Y., YANG, D. H. & CHO, J.-H. 2021. CD8⁺ TILs in NSCLC differentiate into TEMRA via a bifurcated trajectory: deciphering immunogenicity of tumor antigens. *Journal for ImmunoTherapy of Cancer,* 9**,** e002709.
LENGYEL, E. 2010. Ovarian cancer development and metastasis. *Am J Pathol,* 177**,** 1053-64.
LI, F., LI, C., CAI, X., XIE, Z., ZHOU, L., CHENG, B., ZHONG, R., XIONG, S., LI, J., CHEN, Z., YU, Z., HE, J. & LIANG, W. 2021. The association between CD8+ tumor-infiltrating lymphocytes and the clinical outcome of cancer immunotherapy: A systematic review and meta-analysis. *EClinicalMedicine,* 41**,** 101134.
LI, S., ZHUANG, S., HEIT, A., KOO, S. L., TAN, A. C., CHOW, I. T., KWOK, W. W., TAN, I. B., TAN, D. S. W., SIMONI, Y. & NEWELL, E. W. 2022. Bystander CD4(+) T cells infiltrate human tumors and are phenotypically distinct. *Oncoimmunology,* 11**,** 2012961.
LI, X., WANG, R., FAN, P., YAO, X., QIN, L., PENG, Y., MA, M., ASLEY, N., CHANG, X., FENG, Y., HU, Y., ZHANG, Y., LI, C., FANNING, G., JONES, S., VERRILL, C., MALDONADO-PEREZ, D., SOPP, P., WAUGH, C., TAYLOR, S., MCGOWAN, S., CERUNDOLO, V., CONLON, C., MCMICHAEL, A., LU, S., WANG, X., LI, N. & DONG, T. 2019. A Comprehensive Analysis of Key Immune Checkpoint Receptors on Tumor-Infiltrating T Cells From Multiple Types of Cancer. *Front Oncol,* 9**,** 1066.
LIEBER, S., REINARTZ, S., RAIFER, H., FINKERNAGEL, F., DREYER, T., BRONGER, H., JANSEN, J. M., WAGNER, U., WORZFELD, T., MÜLLER, R. & HUBER, M. 2018. Prognosis of ovarian cancer is associated with effector

memory CD8(+) T cell accumulation in ascites, CXCL9 levels and activation-triggered signal transduction in T cells. *Oncoimmunology,* 7**,** e1424672.
LIU, R., LI, H. F. & LI, S. 2024. PD-1-mediated inhibition of T cell activation: Mechanisms and strategies for cancer combination immunotherapy. *Cell Insight,* 3**,** 100146.
LO NIGRO, C., MACAGNO, M., SANGIOLO, D., BERTOLACCINI, L., AGLIETTA, M. & MERLANO, M. C. 2019. NK-mediated antibody-dependent cell-mediated cytotoxicity in solid tumors: biological evidence and clinical perspectives. *Ann Transl Med,* 7**,** 105.
LONG, H. M., MECKIFF, B. J. & TAYLOR, G. S. 2019. The T-cell Response to Epstein-Barr Virus–New Tricks From an Old Dog. *Frontiers in Immunology,* 10.
LOREGIAN, A., APPLETON, B. A., HOGLE, J. M. & COEN, D. M. 2004. Residues of human cytomegalovirus DNA polymerase catalytic subunit UL54 that are necessary and sufficient for interaction with the accessory protein UL44. *J Virol,* 78**,** 158-67.
LUN, A. T. L., RICHARD, A. C. & MARIONI, J. C. 2017. Testing for differential abundance in mass cytometry data. *Nat Methods,* 14**,** 707-709.
MACKAY, L. K., BRAUN, A., MACLEOD, B. L., COLLINS, N., TEBARTZ, C., BEDOUI, S., CARBONE, F. R. & GEBHARDT, T. 2015. Cutting edge: CD69 interference with sphingosine-1-phosphate receptor function regulates peripheral T cell retention. *J Immunol,* 194**,** 2059-63.
MACKAY, L. K., RAHIMPOUR, A., MA, J. Z., COLLINS, N., STOCK, A. T., HAFON, M.-L., VEGA-RAMOS, J., LAUZURICA, P., MUELLER, S. N., STEFANOVIC, T., TSCHARKE, D. C., HEATH, W. R., INOUYE, M., CARBONE, F. R. & GEBHARDT, T. 2013. The developmental pathway for CD103+CD8+ tissue-resident memory T cells of skin. *Nature Immunology,* 14**,** 1294-1301.
MAHMUD, J., MILLER MICHAEL, J., ALTMAN AARON, M. & CHAN GARY, C. 2020. Human Cytomegalovirus Glycoprotein-Initiated Signaling Mediates the Aberrant Activation of Akt. *Journal of Virology,* 94**,** 10.1128/jvi.00167-20.
MAHNKE, Y. D., BRODIE, T. M., SALLUSTO, F., ROEDERER, M. & LUGLI, E. 2013. The who's who of T-cell differentiation: human memory T-cell subsets. *Eur J Immunol,* 43**,** 2797-809.
MANTEGAZZA, A. R., MAGALHAES, J. G., AMIGORENA, S. & MARKS, M. S. 2013. Presentation of phagocytosed antigens by MHC class I and II. *Traffic,* 14**,** 135-52.
MARCUS, L., FASHOYIN-AJE, L. A., DONOGHUE, M., YUAN, M., RODRIGUEZ, L., GALLAGHER, P. S., PHILIP, R., GHOSH, S., THEORET, M. R., BEAVER, J. A., PAZDUR, R. & LEMERY, S. J. 2021. FDA Approval Summary: Pembrolizumab for the Treatment of Tumor Mutational Burden-High Solid Tumors. *Clin Cancer Res,* 27**,** 4685-4689.
MARIN-ACEVEDO, J. A., KIMBROUGH, E. O. & LOU, Y. 2021. Next generation of immune checkpoint inhibitors and beyond. *Journal of Hematology & Oncology,* 14**,** 45.
MARIUZZA, R. A., SHAHID, S. & KARADE, S. S. 2024. The immune checkpoint receptor LAG3: Structure, function, and target for cancer immunotherapy. *J Biol Chem,* 300**,** 107241.

MASOPUST, D., HA, S.-J., VEZYS, V. & AHMED, R. 2006. Stimulation History Dictates Memory CD8 T Cell Phenotype: Implications for Prime-Boost Vaccination1. *The Journal of Immunology,* 177**,** 831-839.
MATSUZAKI, J., GNJATIC, S., MHAWECH-FAUCEGLIA, P., BECK, A., MILLER, A., TSUJI, T., EPPOLITO, C., QIAN, F., LELE, S., SHRIKANT, P., OLD, L. J. & ODUNSI, K. 2010. Tumor-infiltrating NY-ESO-1–specific CD8⁺ T cells are negatively regulated by LAG-3 and PD-1 in human ovarian cancer. *Proceedings of the National Academy of Sciences,* 107**,** 7875-7880.
MCCOACH, C. E. & BIVONA, T. G. 2018. The evolving understanding of immunoediting and the clinical impact of immune escape. *J Thorac Dis,* 10**,** 1248-1252.
MCLANE, L. M., ABDEL-HAKEEM, M. S. & WHERRY, E. J. 2019. CD8 T Cell Exhaustion During Chronic Viral Infection and Cancer. *Annu Rev Immunol,* 37**,** 457-495.
MIDDLETON, G., BROCK, K., SAVAGE, J., MANT, R., SUMMERS, Y., CONNIBEAR, J., SHAH, R., OTTENSMEIER, C., SHAW, P., LEE, S.-M., POPAT, S., BARRIE, C., BARONE, G. & BILLINGHAM, L. 2020. Pembrolizumab in patients with non-small-cell lung cancer of performance status 2 (PePS2): a single arm, phase 2 trial. *The Lancet Respiratory Medicine,* 8**,** 895-904.
MILIOTOU, A. N. & PAPADOPOULOU, L. C. 2018. CAR T-cell Therapy: A New Era in Cancer Immunotherapy. *Curr Pharm Biotechnol,* 19**,** 5-18.
MILLAR, D. G., RAMJIAWAN, R. R., KAWAGUCHI, K., GUPTA, N., CHEN, J., ZHANG, S., NOJIRI, T., HO, W. W., AOKI, S., JUNG, K., CHEN, I., SHI, F., HEATHER, J. M., SHIGETA, K., MORTON, L. T., SEPULVEDA, S., WAN, L., JOSEPH, R., MINOGUE, E., KHATRI, A., BARDIA, A., ELLISEN, L. W., CORCORAN, R. B., HATA, A. N., PAI, S. I., JAIN, R. K., FUKUMURA, D., DUDA, D. G. & COBBOLD, M. 2020. Antibody-mediated delivery of viral epitopes to tumors harnesses CMV-specific T cells for cancer therapy. *Nat Biotechnol,* 38**,** 420-425.
MITCHELL, D. A., XIE, W., SCHMITTLING, R., LEARN, C., FRIEDMAN, A., MCLENDON, R. E. & SAMPSON, J. H. 2008. Sensitive detection of human cytomegalovirus in tumors and peripheral blood of patients diagnosed with glioblastoma. *Neuro Oncol,* 10**,** 10-8.
MITTAL, D., GUBIN, M. M., SCHREIBER, R. D. & SMYTH, M. J. 2014. New insights into cancer immunoediting and its three component phases--elimination, equilibrium and escape. *Curr Opin Immunol,* 27**,** 16-25.
MOMENIMOVAHED, Z., TIZNOBAIK, A., TAHERI, S. & SALEHINIYA, H. 2019. Ovarian cancer in the world: epidemiology and risk factors. *Int J Womens Health,* 11**,** 287-299.
MOSER, J. C., WEI, G., COLONNA, S. V., GROSSMANN, K. F., PATEL, S. & HYNGSTROM, J. R. 2020. Comparative-effectiveness of pembrolizumab vs. nivolumab for patients with metastatic melanoma. *Acta Oncologica,* 59**,** 434-437.
MOSKOPHIDIS, D., LECHNER, F., PIRCHER, H. & ZINKERNAGEL, R. M. 1993. Virus persistence in acutely infected immunocompetent mice by exhaustion of antiviral cytotoxic effector T cells. *Nature,* 362**,** 758-761.

MOZZI, A., BIOLATTI, M., CAGLIANI, R., FORNI, D., DELL'OSTE, V., PONTREMOLI, C., VANTAGGIATO, C., POZZOLI, U., CLERICI, M., LANDOLFO, S. & SIRONI, M. 2020. Past and ongoing adaptation of human cytomegalovirus to its host. *PLoS Pathog,* 16**,** e1008476.

MÜCKE, K., PAULUS, C., BERNHARDT, K., GERRER, K., SCHÖN, K., FINK, A., SAUER, E. M., ASBACH-NITZSCHE, A., HARWARDT, T., KIENINGER, B., KREMER, W., KALBITZER, H. R. & NEVELS, M. 2014. Human cytomegalovirus major immediate early 1 protein targets host chromosomes by docking to the acidic pocket on the nucleosome surface. *J Virol,* 88**,** 1228-48.

MURATA, T. 2014. Regulation of Epstein–Barr virus reactivation from latency. *Microbiology and Immunology,* 58**,** 307-317.

MURATA, T., SUGIMOTO, A., INAGAKI, T., YANAGI, Y., WATANABE, T., SATO, Y. & KIMURA, H. 2021. Molecular Basis of Epstein-Barr Virus Latency Establishment and Lytic Reactivation. *Viruses,* 13.

NDHLOVU, Z. M., KAMYA, P., MEWALAL, N., KLØVERPRIS, H. N., NKOSI, T., PRETORIUS, K., LAHER, F., OGUNSHOLA, F., CHOPERA, D., SHEKHAR, K., GHEBREMICHAEL, M., ISMAIL, N., MOODLEY, A., MALIK, A., LESLIE, A., GOULDER, P. J., BUUS, S., CHAKRABORTY, A., DONG, K., NDUNG'U, T. & WALKER, B. D. 2015. Magnitude and Kinetics of CD8+ T Cell Activation during Hyperacute HIV Infection Impact Viral Set Point. *Immunity,* 43**,** 591-604.

NEVELS, M., PAULUS, C. & SHENK, T. 2004. Human cytomegalovirus immediate-early 1 protein facilitates viral replication by antagonizing histone deacetylation. *Proceedings of the National Academy of Sciences,* 101**,** 17234-17239.

NEWHOOK, N., FUDGE, N. & GRANT, M. 2017. NK cells generate memory-type responses to human cytomegalovirus-infected fibroblasts. *European Journal of Immunology,* 47**,** 1032-1039.

NOBUOKA, D., YOSHIKAWA, T., TAKAHASHI, M., IWAMA, T., HORIE, K., SHIMOMURA, M., SUZUKI, S., SAKEMURA, N., NAKATSUGAWA, M., SADAMORI, H., YAGI, T., FUJIWARA, T. & NAKATSURA, T. 2013. Intratumoral peptide injection enhances tumor cell antigenicity recognized by cytotoxic T lymphocytes: a potential option for improvement in antigen-specific cancer immunotherapy. *Cancer Immunol Immunother,* 62**,** 639-52.

NOWICKI, T. S., HU-LIESKOVAN, S. & RIBAS, A. 2018. Mechanisms of Resistance to PD-1 and PD-L1 Blockade. *Cancer J,* 24**,** 47-53.

NUTT, S. L., HODGKIN, P. D., TARLINTON, D. M. & CORCORAN, L. M. 2015. The generation of antibody-secreting plasma cells. *Nat Rev Immunol,* 15**,** 160-71.

ODEBERG, J., PLACHTER, B., BRANDÉN, L. & SÖDERBERG-NAUCLÉR, C. 2003. Human cytomegalovirus protein pp65 mediates accumulation of HLA-DR in lysosomes and destruction of the HLA-DR α-chain. *Blood,* 101**,** 4870-4877.

OGANDO-RIVAS, E., CASTILLO, P., JONES, N., TRIVEDI, V., DRAKE, J., DECHKOVSKAIA, A., CANDELARIO, K. M., YANG, C. & MITCHELL, D. A. 2022. Effects of immune checkpoint blockade on antigen-specific CD8+ T cells for use in adoptive cellular therapy. *Microbiology and Immunology,* 66**,** 201-211.

OTT, P. A., HU, Z., KESKIN, D. B., SHUKLA, S. A., SUN, J., BOZYM, D. J., ZHANG, W., LUOMA, A., GIOBBIE-HURDER, A., PETER, L., CHEN, C., OLIVE, O., CARTER, T. A., LI, S., LIEB, D. J., EISENHAURE, T., GJINI, E., STEVENS, J., LANE, W. J., JAVERI, I., NELLAIAPPAN, K., SALAZAR, A. M., DALEY, H., SEAMAN, M., BUCHBINDER, E. I., YOON, C. H., HARDEN, M., LENNON, N., GABRIEL, S., RODIG, S. J., BAROUCH, D. H., ASTER, J. C., GETZ, G., WUCHERPFENNIG, K., NEUBERG, D., RITZ, J., LANDER, E. S., FRITSCH, E. F., HACOHEN, N. & WU, C. J. 2017. An immunogenic personal neoantigen vaccine for patients with melanoma. *Nature,* 547**,** 217-221.

PARADOWSKA, E., JABŁOŃSKA, A., STUDZIŃSKA, M., WILCZYŃSKI, M. & WILCZYŃSKI, J. R. 2019. Detection and genotyping of CMV and HPV in tumors and fallopian tubes from epithelial ovarian cancer patients. *Scientific Reports,* 9**,** 19935.

PARDIECK, I. N., BEYREND, G., REDEKER, A. & ARENS, R. 2018. Cytomegalovirus infection and progressive differentiation of effector-memory T cells. *F1000Res,* 7.

PARRY, H. M., DOWELL, A. C., ZUO, J., VERMA, K., KINSELLA, F. A. M., BEGUM, J., CROFT, W., SHARMA-OATES, A., PRATT, G. & MOSS, P. 2021. PD-1 is imprinted on cytomegalovirus-specific CD4+ T cells and attenuates Th1 cytokine production whilst maintaining cytotoxicity. *PLOS Pathogens,* 17**,** e1009349.

PAUKEN, K. E., GODEC, J., ODORIZZI, P. M., BROWN, K. E., YATES, K. B., NGIOW, S. F., BURKE, K. P., MALERI, S., GRANDE, S. M., FRANCISCO, L. M., ALI, M. A., IMAM, S., FREEMAN, G. J., HAINING, W. N., WHERRY, E. J. & SHARPE, A. H. 2020. The PD-1 Pathway Regulates Development and Function of Memory CD8(+) T Cells following Respiratory Viral Infection. *Cell Rep,* 31**,** 107827.

PENG, T.-R., TSAI, F.-P. & WU, T.-W. 2017. Indirect comparison between pembrolizumab and nivolumab for the treatment of non-small cell lung cancer: A meta-analysis of randomized clinical trials. *International Immunopharmacology,* 49**,** 85-94.

PENNOCK, N. D., WHITE, J. T., CROSS, E. W., CHENEY, E. E., TAMBURINI, B. A. & KEDL, R. M. 2013. T cell responses: naive to memory and everything in between. *Adv Physiol Educ,* 37**,** 273-83.

PEREIRA, B. I., DE MAEYER, R. P. H., COVRE, L. P., NEHAR-BELAID, D., LANNA, A., WARD, S., MARCHES, R., CHAMBERS, E. S., GOMES, D. C. O., RIDDELL, N. E., MAINI, M. K., TEIXEIRA, V. H., JANES, S. M., GILROY, D. W., LARBI, A., MABBOTT, N. A., UCAR, D., KUCHEL, G. A., HENSON, S. M., STRID, J., LEE, J. H., BANCHEREAU, J. & AKBAR, A. N. 2020. Sestrins induce natural killer function in senescent-like CD8+ T cells. *Nature Immunology,* 21**,** 684-694.

PETROVAS, C., CASAZZA, J. P., BRENCHLEY, J. M., PRICE, D. A., GOSTICK, E., ADAMS, W. C., PRECOPIO, M. L., SCHACKER, T., ROEDERER, M., DOUEK, D. C. & KOUP, R. A. 2006. PD-1 is a regulator of virus-specific CD8+ T cell survival in HIV infection. *J Exp Med,* 203**,** 2281-92.

PETTERSEN, F. O., TASKÉN, K. & KVALE, D. 2010. Combined Env- and Gag-specific T cell responses in relation to programmed death-1 receptor and

CD4+ T cell loss rates in human immunodeficiency virus-1 infection. *Clinical and Experimental Immunology,* 161**,** 315-323.
PIERCE, S., GEANES, E. S. & BRADLEY, T. 2020. Targeting Natural Killer Cells for Improved Immunity and Control of the Adaptive Immune Response. *Frontiers in Cellular and Infection Microbiology,* 10.
POLTERMANN, S., SCHLEHOFER, B., STEINDORF, K., SCHNITZLER, P., GELETNEKY, K. & SCHLEHOFER, J. R. 2006. Lack of association of herpesviruses with brain tumors. *Journal of NeuroVirology,* 12**,** 90-99.
POOLE, E., LAU, J., GROVES, I., ROCHE, K., MURPHY, E., CARLAN DA SILVA, M., REEVES, M. & SINCLAIR, J. 2023. The Human Cytomegalovirus Latency-Associated Gene Product Latency Unique Natural Antigen Regulates Latent Gene Expression. *Viruses,* 15.
PRADEU, T., THOMMA, B. P. H. J., GIRARDIN, S. E. & LEMAITRE, B. 2024. The conceptual foundations of innate immunity: Taking stock 30 years later. *Immunity,* 57**,** 613-631.
PUDNEY, V. A., LEESE, A. M., RICKINSON, A. B. & HISLOP, A. D. 2005. CD8+ immunodominance among Epstein-Barr virus lytic cycle antigens directly reflects the efficiency of antigen presentation in lytically infected cells. *J Exp Med,* 201**,** 349-60.
QIAN, X. L., XIA, X. Q., LI, Y. Q., JIA, Y. M., SUN, Y. Y., SONG, Y. M., XUE, H. Q., HAO, Y. F., WANG, J., WANG, X. Z., LIU, C. Y., ZHANG, X. M., ZHANG, L. N. & GUO, X. J. 2023. Effects of tumor-infiltrating lymphocytes on nonresponse rate of neoadjuvant chemotherapy in patients with invasive breast cancer. *Sci Rep,* 13**,** 9256.
QUINTELIER, K., COUCKUYT, A., EMMANEEL, A., AERTS, J., SAEYS, Y. & VAN GASSEN, S. 2021. Analyzing high-dimensional cytometry data using FlowSOM. *Nature Protocols,* 16**,** 3775-3801.
RÅDESTAD, A. F., ESTEKIZADEH, A., CUI, H. L., KOSTOPOULOU, O. N., DAVOUDI, B., HIRSCHBERG, A. L., CARLSON, J., RAHBAR, A. & SÖDERBERG-NAUCLER, C. 2018. Impact of Human Cytomegalovirus Infection and its Immune Response on Survival of Patients with Ovarian Cancer. *Transl Oncol,* 11**,** 1292-1300.
RADZIEWICZ, H., IBEGBU, C. C., FERNANDEZ, M. L., WORKOWSKI, K. A., OBIDEEN, K., WEHBI, M., HANSON, H. L., STEINBERG, J. P., MASOPUST, D., WHERRY, E. J., ALTMAN, J. D., ROUSE, B. T., FREEMAN, G. J., AHMED, R. & GRAKOUI, A. 2007. Liver-infiltrating lymphocytes in chronic human hepatitis C virus infection display an exhausted phenotype with high levels of PD-1 and low levels of CD127 expression. *J Virol,* 81**,** 2545-53.
RAZIORROUH, B., SCHRAUT, W., GERLACH, T., NOWACK, D., GRÜNER, N. H., ULSENHEIMER, A., ZACHOVAL, R., WÄCHTLER, M., SPANNAGL, M., HAAS, J., DIEPOLDER, H. M. & JUNG, M. C. 2010. The immunoregulatory role of CD244 in chronic hepatitis B infection and its inhibitory potential on virus-specific CD8+ T-cell function. *Hepatology,* 52**,** 1934-47.
REITHOFER, M., ROSSKOPF, S., LEITNER, J., BATTIN, C., BOHLE, B., STEINBERGER, P. & JAHN-SCHMID, B. 2021. 4-1BB costimulation promotes bystander activation of human CD8 T cells. *Eur J Immunol,* 51**,** 721-733.
REUBEN, A., ZHANG, J., CHIOU, S.-H., GITTELMAN, R. M., LI, J., LEE, W.-C., FUJIMOTO, J., BEHRENS, C., LIU, X., WANG, F., QUEK, K., WANG, C.,

KHERADMAND, F., CHEN, R., CHOW, C.-W., LIN, H., BERNATCHEZ, C., JALALI, A., HU, X., WU, C.-J., ETEROVIC, A. K., PARRA, E. R., YUSKO, E., EMERSON, R., BENZENO, S., VIGNALI, M., WU, X., YE, Y., LITTLE, L. D., GUMBS, C., MAO, X., SONG, X., TIPPEN, S., THORNTON, R. L., CASCONE, T., SNYDER, A., WARGO, J. A., HERBST, R., SWISHER, S., KADARA, H., MORAN, C., KALHOR, N., ZHANG, J., SCHEET, P., VAPORCIYAN, A. A., SEPESI, B., GIBBONS, D. L., ROBINS, H., HWU, P., HEYMACH, J. V., SHARMA, P., ALLISON, J. P., BALADANDAYUTHAPANI, V., LEE, J. J., DAVIS, M. M., WISTUBA, I. I., FUTREAL, P. A. & ZHANG, J. 2020. Comprehensive T cell repertoire characterization of non-small cell lung cancer. *Nature Communications,* 11**,** 603.

RHA, M.-S. & SHIN, E.-C. 2021. Activation or exhaustion of CD8+ T cells in patients with COVID-19. *Cellular & Molecular Immunology,* 18**,** 2325-2333.

RIBAS, A. & WOLCHOK, J. D. 2018. Cancer immunotherapy using checkpoint blockade. *Science,* 359**,** 1350-1355.

RICKLIN, D., HAJISHENGALLIS, G., YANG, K. & LAMBRIS, J. D. 2010. Complement: a key system for immune surveillance and homeostasis. *Nature Immunology,* 11**,** 785-797.

RIDDELL, S. R., WATANABE, K. S., GOODRICH, J. M., LI, C. R., AGHA, M. E. & GREENBERG, P. D. 1992. Restoration of Viral Immunity in Immunodeficient Humans by the Adoptive Transfer of T Cell Clones. *Science,* 257**,** 238-241.

RIUS, C., ATTAF, M., TUNGATT, K., BIANCHI, V., LEGUT, M., BOVAY, A., DONIA, M., THOR STRATEN, P., PEAKMAN, M., SVANE, I. M., OTT, S., CONNOR, T., SZOMOLAY, B., DOLTON, G. & SEWELL, A. K. 2018. Peptide-MHC Class I Tetramers Can Fail To Detect Relevant Functional T Cell Clonotypes and Underestimate Antigen-Reactive T Cell Populations. *J Immunol,* 200**,** 2263-2279.

ROSATI, E., DOWDS, C. M., LIASKOU, E., HENRIKSEN, E. K. K., KARLSEN, T. H. & FRANKE, A. 2017. Overview of methodologies for T-cell receptor repertoire analysis. *BMC Biotechnology,* 17**,** 61.

ROSATO, P. C., WIJEYESINGHE, S., STOLLEY, J. M., NELSON, C. E., DAVIS, R. L., MANLOVE, L. S., PENNELL, C. A., BLAZAR, B. R., CHEN, C. C., GELLER, M. A., VEZYS, V. & MASOPUST, D. 2019. Virus-specific memory T cells populate tumors and can be repurposed for tumor immunotherapy. *Nature Communications,* 10**,** 567.

ROWSHANRAVAN, B., HALLIDAY, N. & SANSOM, D. M. 2018. CTLA-4: a moving target in immunotherapy. *Blood,* 131**,** 58-67.

RUFER, N., ZIPPELIUS, A., BATARD, P., PITTET, M. J., KURTH, I., CORTHESY, P., CEROTTINI, J.-C., LEYVRAZ, S., ROOSNEK, E., NABHOLZ, M. & ROMERO, P. 2003. Ex vivo characterization of human CD8+ T subsets with distinct replicative history and partial effector functions. *Blood,* 102**,** 1779-1787.

SABATIER, J., URO-COSTE, E., POMMEPUY, I., LABROUSSE, F., ALLART, S., TRÉMOULET, M., DELISLE, M. B. & BROUSSET, P. 2005. Detection of human cytomegalovirus genome and gene products in central nervous system tumours. *Br J Cancer,* 92**,** 747-50.

SAGER, K., ALAM, S., BOND, A., CHINNAPPAN, L. & PROBERT, C. S. 2015. Review article: cytomegalovirus and inflammatory bowel disease. *Alimentary Pharmacology & Therapeutics,* 41**,** 725-733.
SALEH, R., TAHA, R. Z., TOOR, S. M., SASIDHARAN NAIR, V., MURSHED, K., KHAWAR, M., AL-DHAHERI, M., PETKAR, M. A., ABU NADA, M. & ELKORD, E. 2020. Expression of immune checkpoints and T cell exhaustion markers in early and advanced stages of colorectal cancer. *Cancer Immunol Immunother,* 69**,** 1989-1999.
SANDU, I., CERLETTI, D., OETIKER, N., BORSA, M., WAGEN, F., SPADAFORA, I., WELTEN, S. P. M., STOLZ, U., OXENIUS, A. & CLAASSEN, M. 2020. Landscape of Exhausted Virus-Specific CD8 T Cells in Chronic LCMV Infection. *Cell Reports,* 32**,** 108078.
SANTOIEMMA, P. P. & POWELL, D. J., JR. 2015. Tumor infiltrating lymphocytes in ovarian cancer. *Cancer Biol Ther,* 16**,** 807-20.
SARMA, J. V. & WARD, P. A. 2011. The complement system. *Cell Tissue Res,* 343**,** 227-35.
SATO, E., OLSON, S. H., AHN, J., BUNDY, B., NISHIKAWA, H., QIAN, F., JUNGBLUTH, A. A., FROSINA, D., GNJATIC, S., AMBROSONE, C., KEPNER, J., ODUNSI, T., RITTER, G., LELE, S., CHEN, Y. T., OHTANI, H., OLD, L. J. & ODUNSI, K. 2005. Intraepithelial CD8+ tumor-infiltrating lymphocytes and a high CD8+/regulatory T cell ratio are associated with favorable prognosis in ovarian cancer. *Proc Natl Acad Sci U S A,* 102**,** 18538-43.
SAUCE, D., ALMEIDA, J. R., LARSEN, M., HARO, L., AUTRAN, B., FREEMAN, G. J. & APPAY, V. 2007. PD-1 expression on human CD8 T cells depends on both state of differentiation and activation status. *Aids,* 21**,** 2005-13.
SCAPIN, G., YANG, X., PROSISE, W. W., MCCOY, M., REICHERT, P., JOHNSTON, J. M., KASHI, R. S. & STRICKLAND, C. 2015. Structure of full-length human anti-PD1 therapeutic IgG4 antibody pembrolizumab. *Nature Structural & Molecular Biology,* 22**,** 953-958.
SCHEURER, M. E., BONDY, M. L., ALDAPE, K. D., ALBRECHT, T. & EL-ZEIN, R. 2008. Detection of human cytomegalovirus in different histological types of gliomas. *Acta Neuropathol,* 116**,** 79-86.
SCHILLEBEECKX, I., EARLS, J., FLANAGAN, K. C., HIKEN, J., BODE, A., ARMSTRONG, J. R., MESSINA, D. N., ADKINS, D., LEY, J., ALBORELLI, I., JERMANN, P. & GLASSCOCK, J. I. 2022. T cell subtype profiling measures exhaustion and predicts anti-PD-1 response. *Scientific Reports,* 12**,** 1342.
SCHMIDT, F., FIELDS, H. F., PURWANTI, Y., MILOJKOVIC, A., SALIM, S., WU, K. X., SIMONI, Y., VITIELLO, A., MACLEOD, D. T., NARDIN, A., NEWELL, E. W., FINK, K., WILM, A. & FEHLINGS, M. 2023. In-depth analysis of human virus-specific CD8(+) T cells delineates unique phenotypic signatures for T cell specificity prediction. *Cell Rep,* 42**,** 113250.
SECKERT, C. K., GRIESS, M., BÜTTNER, J. K., SCHELLER, S., SIMON, C. O., KROPP, K. A., RENZAHO, A., KÜHNAPFEL, B., GRZIMEK, N. K. A. & REDDEHASE, M. J. 2012. Viral latency drives 'memory inflation': a unifying hypothesis linking two hallmarks of cytomegalovirus infection. *Medical Microbiology and Immunology,* 201**,** 551-566.

SEFRIN, J. P., HILLRINGHAUS, L., MUNDIGL, O., MANN, K., ZIEGLER-LANDESBERGER, D., SEUL, H., TABARES, G., KNOBLAUCH, D., LEINENBACH, A., FRILIGOU, I., DZIADEK, S., OFFRINGA, R., LIFKE, V. & LIFKE, A. 2019. Sensitization of Tumors for Attack by Virus-Specific CD8+ T-Cells Through Antibody-Mediated Delivery of Immunogenic T-Cell Epitopes. *Front Immunol,* 10**,** 1962.

SETTE, A. & CROTTY, S. 2021. Adaptive immunity to SARS-CoV-2 and COVID-19. *Cell,* 184**,** 861-880.

SHANMUGHAPRIYA, S., SENTHILKUMAR, G., VINODHINI, K., DAS, B. C., VASANTHI, N. & NATARAJASEENIVASAN, K. 2012. Viral and bacterial aetiologies of epithelial ovarian cancer. *European Journal of Clinical Microbiology & Infectious Diseases,* 31**,** 2311-2317.

SHARMA, S., MEHTA, N. U., SAUER, T., ROLLINS, L. A., DITTMER, D. P. & ROONEY, C. M. 2024. Cotargeting EBV lytic as well as latent cycle antigens increases T-cell potency against lymphoma. *Blood Advances,* 8**,** 3360-3371.

SHARPE, A. H. & PAUKEN, K. E. 2018. The diverse functions of the PD1 inhibitory pathway. *Nature Reviews Immunology,* 18**,** 153-167.

SHIBUYA, A. & SHIBUYA, K. 2021. DNAM-1 versus TIGIT: competitive roles in tumor immunity and inflammatory responses. *International Immunology,* 33**,** 687-692.

SHIRAVAND, Y., KHODADADI, F., KASHANI, S. M. A., HOSSEINI-FARD, S. R., HOSSEINI, S., SADEGHIRAD, H., LADWA, R., O'BYRNE, K. & KULASINGHE, A. 2022. Immune Checkpoint Inhibitors in Cancer Therapy. *Curr Oncol,* 29**,** 3044-3060.

SHOKOUH, M. R., SAFAEI, A., MOATTARI, A. & SARVARI, J. 2020. Association of Human Papilloma Virus and Epstein-Barr Virus with Ovarian Cancer in Shiraz, Southwestern Iran. *Iran J Pathol,* 15**,** 292-298.

SIERRO, S., ROTHKOPF, R. & KLENERMAN, P. 2005. Evolution of diverse antiviral CD8+ T cell populations after murine cytomegalovirus infection. *European Journal of Immunology,* 35**,** 1113-1123.

SIMEONE, J. C., NORDSTROM, B. L., PATEL, K. & KLEIN, A. B. 2019. Treatment Patterns and Overall Survival in Metastatic Non-Small-Cell Lung Cancer in a Real-World, US Setting. *Future Oncology,* 15**,** 3491-3502.

SIMONI, Y., BECHT, E., FEHLINGS, M., LOH, C. Y., KOO, S.-L., TENG, K. W. W., YEONG, J. P. S., NAHAR, R., ZHANG, T., KARED, H., DUAN, K., ANG, N., POIDINGER, M., LEE, Y. Y., LARBI, A., KHNG, A. J., TAN, E., FU, C., MATHEW, R., TEO, M., LIM, W. T., TOH, C. K., ONG, B.-H., KOH, T., HILLMER, A. M., TAKANO, A., LIM, T. K. H., TAN, E. H., ZHAI, W., TAN, D. S. W., TAN, I. B. & NEWELL, E. W. 2018. Bystander CD8+ T cells are abundant and phenotypically distinct in human tumour infiltrates. *Nature,* 557**,** 575-579.

SINGH, R., KIM, Y.-H., LEE, S.-J., EOM, H.-S. & CHOI, B. K. 2024. 4-1BB immunotherapy: advances and hurdles. *Experimental & Molecular Medicine,* 56**,** 32-39.

SINIGALIA, E., ALVISI, G., MERCORELLI, B., COEN, D. M., PARI, G. S., JANS, D. A., RIPALTI, A., PALÙ, G. & LOREGIAN, A. 2008. Role of homodimerization of human cytomegalovirus DNA polymerase accessory protein UL44 in origin-dependent DNA replication in cells. *J Virol,* 82**,** 12574-9.

SMATTI, M. K., AL-SADEQ, D. W., ALI, N. H., PINTUS, G., ABOU-SALEH, H. & NASRALLAH, G. K. 2018. Epstein-Barr Virus Epidemiology, Serology, and Genetic Variability of LMP-1 Oncogene Among Healthy Population: An Update. *Front Oncol,* 8**,** 211.
SMITH, C. J. & SNYDER, C. M. 2021. Inhibitory Molecules PD-1, CD73 and CD39 Are Expressed by CD8(+) T Cells in a Tissue-Dependent Manner and Can Inhibit T Cell Responses to Stimulation. *Front Immunol,* 12**,** 704862.
SNYDER, C. M. 2011. Buffered memory: a hypothesis for the maintenance of functional, virus-specific CD8+ T cells during cytomegalovirus infection. *Immunologic Research,* 51**,** 195-204.
SNYDER, C. M., CHO, K. S., BONNETT, E. L., VAN DOMMELEN, S., SHELLAM, G. R. & HILL, A. B. 2008. Memory inflation during chronic viral infection is maintained by continuous production of short-lived, functional T cells. *Immunity,* 29**,** 650-9.
STEFANSKI, C. D. & PROSPERI, J. R. 2020. Wnt-Independent and Wnt-Dependent Effects of APC Loss on the Chemotherapeutic Response. *Int J Mol Sci,* 21.
STEVEN, N. M., ANNELS, N. E., KUMAR, A., LEESE, A. M., KURILLA, M. G. & RICKINSON, A. B. 1997. Immediate early and early lytic cycle proteins are frequent targets of the Epstein-Barr virus-induced cytotoxic T cell response. *J Exp Med,* 185**,** 1605-17.
STRAATHOF, K. C. M., BOLLARD, C. M., POPAT, U., HULS, M. H., LOPEZ, T., MORRISS, M. C., GRESIK, M. V., GEE, A. P., RUSSELL, H. V., BRENNER, M. K., ROONEY, C. M. & HESLOP, H. E. 2005. Treatment of nasopharyngeal carcinoma with Epstein-Barr virus–specific T lymphocytes. *Blood,* 105**,** 1898-1904.
SUN, Q., HONG, Z., ZHANG, C., WANG, L., HAN, Z. & MA, D. 2023. Immune checkpoint therapy for solid tumours: clinical dilemmas and future trends. *Signal Transduction and Targeted Therapy,* 8**,** 320.
SYLWESTER, A. W., MITCHELL, B. L., EDGAR, J. B., TAORMINA, C., PELTE, C., RUCHTI, F., SLEATH, P. R., GRABSTEIN, K. H., HOSKEN, N. A., KERN, F., NELSON, J. A. & PICKER, L. J. 2005. Broadly targeted human cytomegalovirus-specific CD4+ and CD8+ T cells dominate the memory compartments of exposed subjects. *J Exp Med,* 202**,** 673-85.
SZABO, P. A., MIRON, M. & FARBER, D. L. 2019. Location, location, location: Tissue resident memory T cells in mice and humans. *Sci Immunol,* 4.
TALHOUNI, S., FADHIL, W., MONGAN, N. P., FIELD, L., HUNTER, K., MAKHSOUS, S., MACIEL-GUERRA, A., KAUR, N., NESTARENKAITE, A., LAURINAVICIUS, A., WILLCOX, B. E., DOTTORINI, T., SPENDLOVE, I., JACKSON, A. M., ILYAS, M. & RAMAGE, J. M. 2023. Activated tissue resident memory T-cells (CD8+CD103+CD39+) uniquely predict survival in left sided "immune-hot" colorectal cancers. *Front Immunol,* 14**,** 1057292.
TAY, K. H., SLAVIN, M. A., THURSKY, K. A., COUSSEMENT, J., WORTH, L. J., TEH, B. W., KHOT, A., TAM, C. S. & YONG, M. K. 2022. Cytomegalovirus DNAemia and disease: current-era epidemiology, clinical characteristics and outcomes in cancer patients other than allogeneic haemopoietic transplantation. *Internal Medicine Journal,* 52**,** 1759-1767.
TESI, R. J. 2019. MDSC; the Most Important Cell You Have Never Heard Of. *Trends Pharmacol Sci,* 40**,** 4-7.

THOM, J. T., WEBER, T. C., WALTON, S. M., TORTI, N. & OXENIUS, A. 2015. The Salivary Gland Acts as a Sink for Tissue-Resident Memory CD8⁺ T Cells, Facilitating Protection from Local Cytomegalovirus Infection. *Cell Reports,* 13**,** 1125-1136.
THOMMEN, D. S., SCHREINER, J., MÜLLER, P., HERZIG, P., ROLLER, A., BELOUSOV, A., UMANA, P., PISA, P., KLEIN, C., BACAC, M., FISCHER, O. S., MOERSIG, W., SAVIC PRINCE, S., LEVITSKY, V., KARANIKAS, V., LARDINOIS, D. & ZIPPELIUS, A. 2015. Progression of Lung Cancer Is Associated with Increased Dysfunction of T Cells Defined by Coexpression of Multiple Inhibitory Receptors. *Cancer Immunology Research,* 3**,** 1344-1355.
THOMMEN, D. S. & SCHUMACHER, T. N. 2018. T Cell Dysfunction in Cancer. *Cancer Cell,* 33**,** 547-562.
THOMPSON, M. P. & KURZROCK, R. 2004. Epstein-Barr virus and cancer. *Clin Cancer Res,* 10**,** 803-21.
TIERNEY, R. J., SHANNON-LOWE, C. D., FITZSIMMONS, L., BELL, A. I. & ROWE, M. 2015. Unexpected patterns of Epstein–Barr virus transcription revealed by a High throughput PCR array for absolute quantification of viral mRNA. *Virology,* 474**,** 117-130.
TIMPERI, E. & BARNABA, V. 2021. CD39 Regulation and Functions in T Cells. *Int J Mol Sci,* 22.
TOMTISHEN, J. P., 3RD 2012. Human cytomegalovirus tegument proteins (pp65, pp71, pp150, pp28). *Virol J,* 9**,** 22.
TOPALIAN, S. L., DRAKE, C. G. & PARDOLL, D. M. 2012. Targeting the PD-1/B7-H1(PD-L1) pathway to activate anti-tumor immunity. *Current Opinion in Immunology,* 24**,** 207-212.
TOPHAM, D. J. & REILLY, E. C. 2018. Tissue-Resident Memory CD8+ T Cells: From Phenotype to Function. *Frontiers in Immunology,* 9.
TORTI, N. & OXENIUS, A. 2012. T cell memory in the context of persistent herpes viral infections. *Viruses,* 4**,** 1116-43.
TOVAR-SALAZAR, A. & WEINBERG, A. 2020. Understanding the mechanism of action of cytomegalovirus-induced regulatory T cells. *Virology,* 547**,** 1-6.
TRAUTMANN, L., JANBAZIAN, L., CHOMONT, N., SAID, E. A., GIMMIG, S., BESSETTE, B., BOULASSEL, M.-R., DELWART, E., SEPULVEDA, H., BALDERAS, R. S., ROUTY, J.-P., HADDAD, E. K. & SEKALY, R.-P. 2006. Upregulation of PD-1 expression on HIV-specific CD8+ T cells leads to reversible immune dysfunction. *Nature Medicine,* 12**,** 1198-1202.
TROMBETTA, E. S. & MELLMAN, I. 2005. CELL BIOLOGY OF ANTIGEN PROCESSING IN VITRO AND IN VIVO. *Annual Review of Immunology,* 23**,** 975-1028.
ULDRICK, T. S., ADAMS, S. V., FROMENTIN, R., ROCHE, M., FLING, S. P., GONÇALVES, P. H., LURAIN, K., RAMASWAMI, R., WANG, C.-C. J., GORELICK, R. J., WELKER, J. L., O'DONOGHUE, L., CHOUDHARY, H., LIFSON, J. D., RASMUSSEN, T. A., RHODES, A., TUMPACH, C., YARCHOAN, R., MALDARELLI, F., CHEEVER, M. A., SÉKALY, R., CHOMONT, N., DEEKS, S. G. & LEWIN, S. R. 2022. Pembrolizumab induces HIV latency reversal in people living with HIV and cancer on antiretroviral therapy. *Science Translational Medicine,* 14**,** eabl3836.

URBANI, S., AMADEI, B., TOLA, D., MASSARI, M., SCHIVAZAPPA, S., MISSALE, G. & FERRARI, C. 2006. PD-1 expression in acute hepatitis C virus (HCV) infection is associated with HCV-specific CD8 exhaustion. *J Virol,* 80**,** 11398-403.

UTZSCHNEIDER, D. T., CHARMOY, M., CHENNUPATI, V., POUSSE, L., FERREIRA, D. P., CALDERON-COPETE, S., DANILO, M., ALFEI, F., HOFMANN, M., WIELAND, D., PRADERVAND, S., THIMME, R., ZEHN, D. & HELD, W. 2016. T Cell Factor 1-Expressing Memory-like CD8+ T Cells Sustain the Immune Response to Chronic Viral Infections. *Immunity,* 45**,** 415-427.

UTZSCHNEIDER, D. T., GABRIEL, S. S., CHISANGA, D., GLOURY, R., GUBSER, P. M., VASANTHAKUMAR, A., SHI, W. & KALLIES, A. 2020. Early precursor T cells establish and propagate T cell exhaustion in chronic infection. *Nature Immunology,* 21**,** 1256-1266.

VAN DEN BERG, S. P. H., PARDIECK, I. N., LANFERMEIJER, J., SAUCE, D., KLENERMAN, P., VAN BAARLE, D. & ARENS, R. 2019. The hallmarks of CMV-specific CD8 T-cell differentiation. *Medical Microbiology and Immunology,* 208**,** 365-373.

VAN DER HEIDEN, P., MARIJT, E., FALKENBURG, F. & JEDEMA, I. 2018. Control of Cytomegalovirus Viremia after Allogeneic Stem Cell Transplantation: A Review on CMV-Specific T Cell Reconstitution. *Biology of Blood and Marrow Transplantation,* 24**,** 1776-1782.

VAN DER WULP, W., REMST, D. F. G., KESTER, M. G. D., HAGEDOORN, R. S., PARREN, P. W. H. I., VAN KASTEREN, S. I., SCHUURMAN, J., HOEBEN, R. C., RESSING, M. E., BLEIJLEVENS, B. & HEEMSKERK, M. H. M. 2024. Antibody-mediated delivery of viral epitopes to redirect EBV-specific CD8+ T-cell immunity towards cancer cells. *Cancer Gene Therapy,* 31**,** 58-68.

VAN GASSEN, S., CALLEBAUT, B., VAN HELDEN, M. J., LAMBRECHT, B. N., DEMEESTER, P., DHAENE, T. & SAEYS, Y. 2015. FlowSOM: Using self-organizing maps for visualization and interpretation of cytometry data. *Cytometry Part A,* 87**,** 636-645.

VAN LEEUWEN, E. M., GAMADIA, L. E., BAARS, P. A., REMMERSWAAL, E. B., TEN BERGE, I. J. & VAN LIER, R. A. 2002. Proliferation Requirements of Cytomegalovirus-Specific, Effector-Type Human CD8+ T Cells1. *The Journal of Immunology,* 169**,** 5838-5843.

VAN LEEUWEN, E. M. M., REMMERSWAAL, E. B. M., HEEMSKERK, M. H. M., TEN BERGE, I. J. M. & VAN LIER, R. A. W. 2006. Strong selection of virus-specific cytotoxic CD4+ T-cell clones during primary human cytomegalovirus infection. *Blood,* 108**,** 3121-3127.

VARANI, S. & LANDINI, M. P. 2011. Cytomegalovirus-induced immunopathology and its clinical consequences. *Herpesviridae,* 2**,** 6.

VIVIER, E., TOMASELLO, E., BARATIN, M., WALZER, T. & UGOLINI, S. 2008. Functions of natural killer cells. *Nature Immunology,* 9**,** 503-510.

VONDERHEIDE, R. H. & JUNE, C. H. 2014. Engineering T cells for cancer: our synthetic future. *Immunol Rev,* 257**,** 7-13.

WALLER, E. C. P., MCKINNEY, N., HICKS, R., CARMICHAEL, A. J., SISSONS, J. G. P. & WILLS, M. R. 2007. Differential costimulation through CD137 (4–1BB)

restores proliferation of human virus-specific “effector memory” (CD28− CD45RAHI) CD8+ T cells. *Blood,* 110**,** 4360-4366.
WANG, F., CHENG, F. & ZHENG, F. 2022. Stem cell like memory T cells: A new paradigm in cancer immunotherapy. *Clinical Immunology,* 241**,** 109078.
WEBB, J. R., MILNE, K., WATSON, P., DELEEUW, R. J. & NELSON, B. H. 2014. Tumor-Infiltrating Lymphocytes Expressing the Tissue Resident Memory Marker CD103 Are Associated with Increased Survival in High-Grade Serous Ovarian Cancer. *Clinical Cancer Research,* 20**,** 434-444.
WEBER, L. M. & ROBINSON, M. D. 2016. Comparison of clustering methods for high-dimensional single-cell flow and mass cytometry data. *Cytometry Part A,* 89**,** 1084-1096.
WEFERS, C., DUIVEMAN-DE BOER, T., YIGIT, R., ZUSTERZEEL, P. L. M., VAN ALTENA, A. M., MASSUGER, L. & DE VRIES, I. J. M. 2018. Survival of Ovarian Cancer Patients Is Independent of the Presence of DC and T Cell Subsets in Ascites. *Front Immunol,* 9**,** 3156.
WEI, J. & ISHIZUKA, J. J. 2021. Going viral: HBV-specific CD8⁺ tissue-resident memory T cells propagate anti-tumor immunity. *Immunity,* 54**,** 1630-1632.
WEISS, S. A., HUANG, A. Y., FUNG, M. E., MARTINEZ, D., CHEN, A. C. Y., LASALLE, T. J., MILLER, B. C., SCHARER, C. D., HEGDE, M., NGUYEN, T. H., ROWE, J. H., OSBORN, J. F., PATTERSON, D. G., SIFNUGEL, N., MEI-AN NOLAN, C., DAVIDSON, R. A., SCHWARTZ, M. A., BALLY, A. P. R., NEELD, D. K., LAFLEUR, M. W., BOSS, J. M., DOENCH, J. G., NICHOLAS HAINING, W., SHARPE, A. H. & SEN, D. R. 2024. Epigenetic tuning of PD-1 expression improves exhausted T cell function and viral control. *Nature Immunology*.
WELTEVREDE, M., EILERS, R., DE MELKER, H. E. & VAN BAARLE, D. 2016. Cytomegalovirus persistence and T-cell immunosenescence in people aged fifty and older: A systematic review. *Experimental Gerontology,* 77**,** 87-95.
WESTERGAARD, M. C. W., ANDERSEN, R., CHONG, C., KJELDSEN, J. W., PEDERSEN, M., FRIESE, C., HASSELAGER, T., LAJER, H., COUKOS, G., BASSANI-STERNBERG, M., DONIA, M. & SVANE, I. M. 2019. Tumour-reactive T cell subsets in the microenvironment of ovarian cancer. *British Journal of Cancer,* 120**,** 424-434.
WHERRY, E. J. 2011. T cell exhaustion. *Nature Immunology,* 12**,** 492-499.
WHERRY, E. J., HA, S.-J., KAECH, S. M., HAINING, W. N., SARKAR, S., KALIA, V., SUBRAMANIAM, S., BLATTMAN, J. N., BARBER, D. L. & AHMED, R. 2007. Molecular Signature of CD8⁺ T Cell Exhaustion during Chronic Viral Infection. *Immunity,* 27**,** 670-684.
WHERRY, E. J., TEICHGRÄBER, V., BECKER, T. C., MASOPUST, D., KAECH, S. M., ANTIA, R., VON ANDRIAN, U. H. & AHMED, R. 2003. Lineage relationship and protective immunity of memory CD8 T cell subsets. *Nature Immunology,* 4**,** 225-234.
WHITESIDE, S. K., SNOOK, J. P., WILLIAMS, M. A. & WEIS, J. J. 2018. Bystander T Cells: A Balancing Act of Friends and Foes. *Trends Immunol,* 39**,** 1021-1035.
WIDMANN, T., SESTER, U., GÄRTNER, B. C., SCHUBERT, J., PFREUNDSCHUH, M., KÖHLER, H. & SESTER, M. 2008. Levels of CMV specific CD4 T cells are

dynamic and correlate with CMV viremia after allogeneic stem cell transplantation. *PLoS One,* 3**,** e3634.
WILLS, M. R., OKECHA, G., WEEKES, M. P., GANDHI, M. K., SISSONS, P. J. G. & CARMICHAEL, A. J. 2002. Identification of Naive or Antigen-Experienced Human CD8+ T Cells by Expression of Costimulation and Chemokine Receptors: Analysis of the Human Cytomegalovirus-Specific CD8+ T Cell Response1. *The Journal of Immunology,* 168**,** 5455-5464.
WOLF, Y., ANDERSON, A. C. & KUCHROO, V. K. 2020. TIM3 comes of age as an inhibitory receptor. *Nature Reviews Immunology,* 20**,** 173-185.
WU, X., GU, Z., CHEN, Y., CHEN, B., CHEN, W., WENG, L. & LIU, X. 2019. Application of PD-1 Blockade in Cancer Immunotherapy. *Comput Struct Biotechnol J,* 17**,** 661-674.
WU, X., ZHANG, H., XING, Q., CUI, J., LI, J., LI, Y., TAN, Y. & WANG, S. 2014. PD-1(+) CD8(+) T cells are exhausted in tumours and functional in draining lymph nodes of colorectal cancer patients. *Br J Cancer,* 111**,** 1391-9.
XIE, N., SHEN, G., GAO, W., HUANG, Z., HUANG, C. & FU, L. 2023. Neoantigens: promising targets for cancer therapy. *Signal Transduct Target Ther,* 8**,** 9.
YAMAMOTO, R., NISHIKORI, M., KITAWAKI, T., SAKAI, T., HISHIZAWA, M., TASHIMA, M., KONDO, T., OHMORI, K., KURATA, M., HAYASHI, T. & UCHIYAMA, T. 2008. PD-1–PD-1 ligand interaction contributes to immunosuppressive microenvironment of Hodgkin lymphoma. *Blood,* 111**,** 3220-3224.
YANG, B., LI, X., ZHANG, W., FAN, J., ZHOU, Y., LI, W., YIN, J., YANG, X., GUO, E., LI, X., FU, Y., LIU, S., HU, D., QIN, X., DOU, Y., XIAO, R., LU, F., WANG, Z., QIN, T., WANG, W., ZHANG, Q., LI, S., MA, D., MILLS, G. B., CHEN, G. & SUN, C. 2022. Spatial heterogeneity of infiltrating T cells in high-grade serous ovarian cancer revealed by multi-omics analysis. *Cell Rep Med,* 3**,** 100856.
YANG, Q., GODING, S. R., HOKLAND, M. E. & BASSE, P. H. 2006. Antitumor activity of NK cells. *Immunologic Research,* 36**,** 13-25.
YANG, S., LIU, F., WANG, Q. J., ROSENBERG, S. A. & MORGAN, R. A. 2011. The shedding of CD62L (L-selectin) regulates the acquisition of lytic activity in human tumor reactive T lymphocytes. *PLoS One,* 6**,** e22560.
YANG, Z. Z., GROTE, D. M., ZIESMER, S. C., XIU, B., NOVAK, A. J. & ANSELL, S. M. 2015. PD-1 expression defines two distinct T-cell sub-populations in follicular lymphoma that differentially impact patient survival. *Blood Cancer Journal,* 5**,** e281-e281.
YE, L., QIAN, Y., YU, W., GUO, G., WANG, H. & XUE, X. 2020. Functional Profile of Human Cytomegalovirus Genes and Their Associated Diseases: A Review. *Front Microbiol,* 11**,** 2104.
YOUNG, L. S. & RICKINSON, A. B. 2004. Epstein–Barr virus: 40 years on. *Nature Reviews Cancer,* 4**,** 757-768.
YU, C., HE, S., ZHU, W., RU, P., GE, X. & GOVINDASAMY, K. 2023. Human cytomegalovirus in cancer: the mechanism of HCMV-induced carcinogenesis and its therapeutic potential. *Front Cell Infect Microbiol,* 13**,** 1202138.
YU, H. & ROBERTSON, E. S. 2023. Epstein-Barr Virus History and Pathogenesis. *Viruses,* 15.

ZANELLA, L., RIQUELME, I., BUCHEGGER, K., ABANTO, M., ILI, C. & BREBI, P. 2019. A reliable Epstein-Barr Virus classification based on phylogenomic and population analyses. *Scientific Reports,* 9**,** 9829.
ZANGGER, N. & OXENIUS, A. 2022. T cell immunity to cytomegalovirus infection. *Current Opinion in Immunology,* 77**,** 102185.
ZANGHELLINI, F., BOPPANA, S. B., EMERY, V. C., GRIFFITHS, P. D. & PASS, R. F. 1999. Asymptomatic primary cytomegalovirus infection: virologic and immunologic features. *J Infect Dis,* 180**,** 702-7.
ZAPPA, C. & MOUSA, S. A. 2016. Non-small cell lung cancer: current treatment and future advances. *Translational Lung Cancer Research,* 5**,** 288-300.
ZHANG, H., SNYDER, K. M., SUHOSKI, M. M., MAUS, M. V., KAPOOR, V., JUNE, C. H. & MACKALL, C. L. 2007. 4-1BB is superior to CD28 costimulation for generating CD8+ cytotoxic lymphocytes for adoptive immunotherapy. *J Immunol,* 179**,** 4910-8.
ZHANG, L., CONEJO-GARCIA, J. R., KATSAROS, D., GIMOTTY, P. A., MASSOBRIO, M., REGNANI, G., MAKRIGIANNAKIS, A., GRAY, H., SCHLIENGER, K., LIEBMAN, M. N., RUBIN, S. C. & COUKOS, G. 2003. Intratumoral T Cells, Recurrence, and Survival in Epithelial Ovarian Cancer. *New England Journal of Medicine,* 348**,** 203-213.
ZHANG, P., ZHANG, L., XU, K., LIN, Y., MA, R., ZHANG, M. & LI, X. 2024. Evaluating the impact of PD-1 inhibitor treatment on key health outcomes for cancer patients in China. *International Journal of Clinical Pharmacy,* 46**,** 429-438.
ZHENG, M. Z. M. & WAKIM, L. M. 2022. Tissue resident memory T cells in the respiratory tract. *Mucosal Immunol,* 15**,** 379-388.